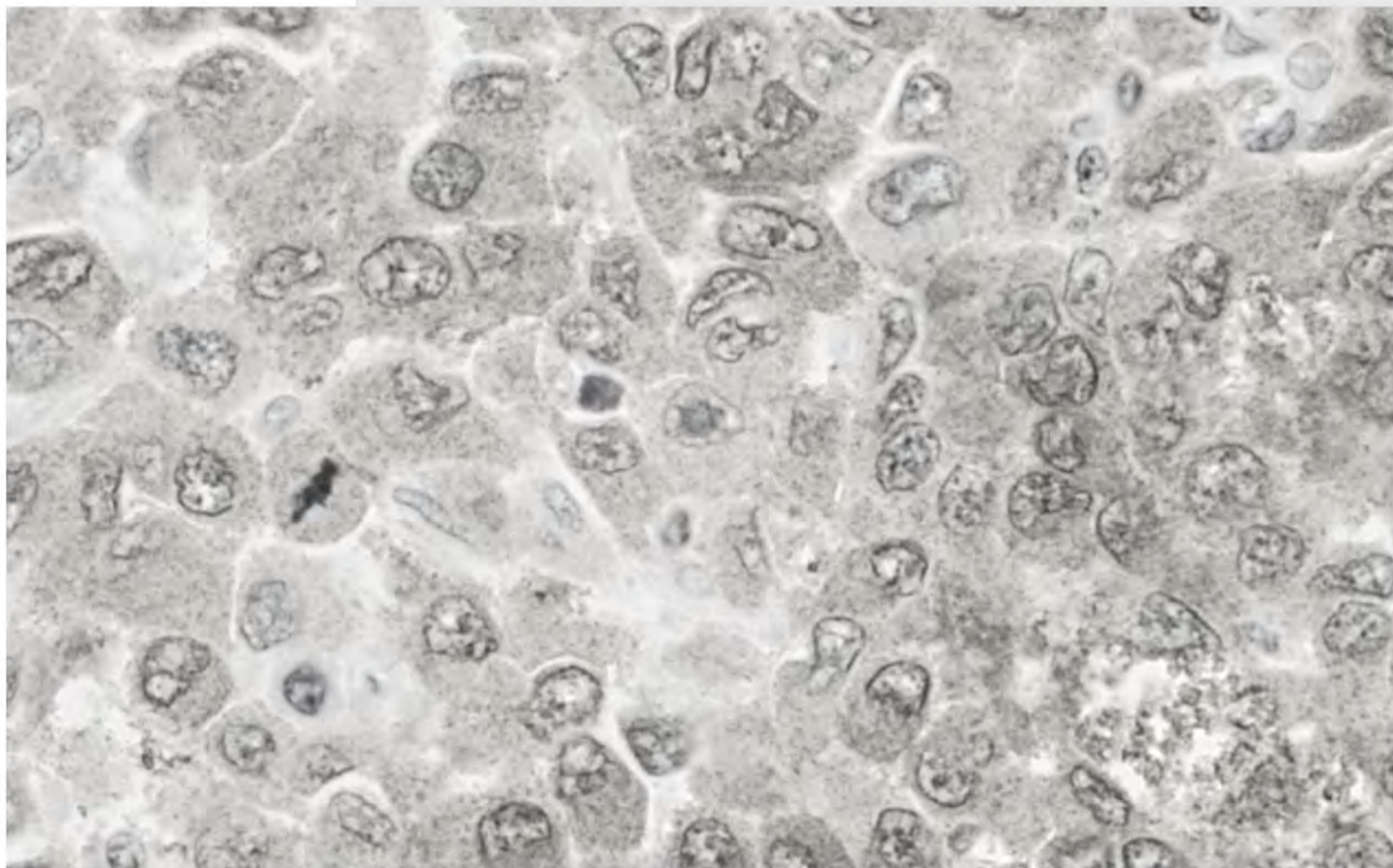


ROLE OF RKIP AND PIRIN IN THE MALIGNANT PROGRESSION OF CUTANEOUS MELANOMA. NEW DIAGNOSIS AND PROGNOSIS BIOMARKERS

CRISTINA PENAS LAGO
LEIOA, 2022



SUPERVISORS

MARIA DOLORES BOYANO LÓPEZ
CARMEN ÁLVAREZ DOMÍNGUEZ



DOCTORAL THESIS

ROLE OF RKIP AND PIRIN IN THE MALIGNANT PROGRESSION OF CUTANEOUS MELANOMA. NEW DIAGNOSIS AND PROGNOSIS BIOMARKERS

CRISTINA PENAS LAGO

LEIOA, 2022

Supervisors:

Maria Dolores Boyano López

Carmen Álvarez Domínguez

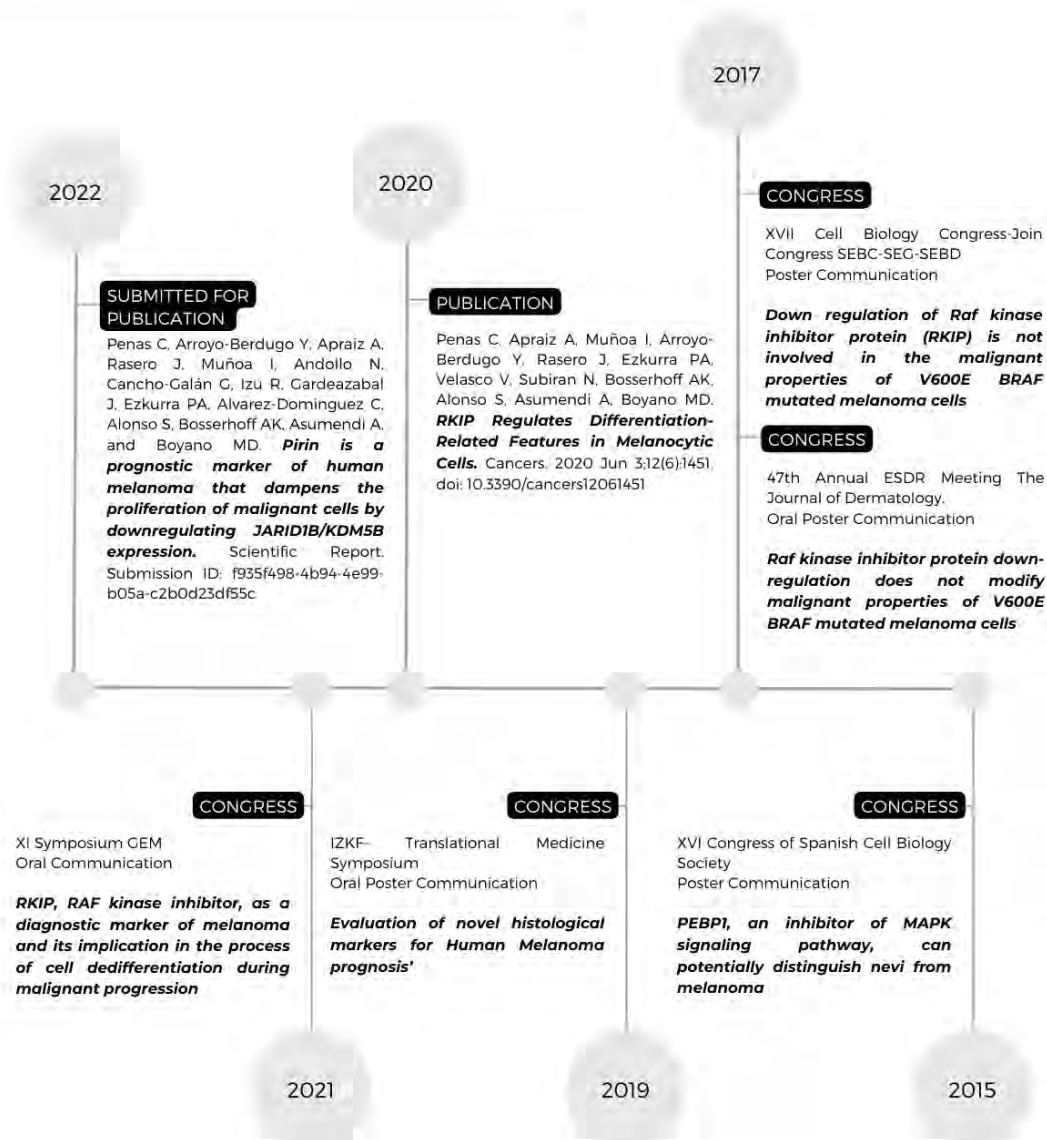
*To my grandparents Angel and Celsa
To my aitite Angel and my amama Maria*



FUNDINGS AND DISSEMINATION OF THE RESEARCH

This doctoral thesis has been supported by grants from the Basque Government (KK2016-036, KK2017-041 and KK2020-00069 to M.D.B.), the UPV/EHU (GIU17/066 to M.D.B.), H2020-ESCEL JTI (15/01 to M.D.B.) and MINECO (PCIN-2015-241 to M.D.B.).

During the completion of this Doctoral Thesis, Cristina Penas Lago was the beneficiary of the Predoctoral Training Program for Non-Doctoral Research Staff from the Basque Government



GRATEFULNESS

A thesis work has great teamwork behind it. As such, I would like to take this opportunity to thank all the people who helped make this project a reality.

To begin with, I would like to extend my gratitude to my supervisors, Dr. Maria Dolores Boyano and Dr. Carmen Alvarez. Thanks, Maria Dolores, for being an inspiration every day, professionally and personally. For mentoring me with such tenderness and kindness. Without you, I would not be where I am today. Carmen, it was always a pleasure to speak with you. You always answered my questions and were kind when I was discouraged. Seeing how you convey your work, I find an example to follow to further my work of scientific dissemination.

To all the colleagues and research group members from the Department of Cellular Biology and Histology: Aintzane, Aintza, Bea, Noe, Aitor,... for always giving me time to ask how things were going and for helping me with technical problems. For all those moments I needed to talk to someone who understood what it is like to do a doctoral thesis, I am grateful to my predoctoral colleagues Andrea, Rocio, Yoana, Maider, Miguel, Maddalen, and everyone else. To Iraia, because without your assistance, the RNA seq data would have consumed me.

I am grateful to Dr. Anja Bosserhoff and her entire team for their warm and friendly reception in their lab in Germany. I greatly appreciate your guidance and support during the months I was there to conduct the study.

In the words of Dr. Tu Youyou, 'I just wanted to do a good job at my job,' so thank you to everyone who has helped, supported, and guided me over the years. I am deeply grateful.

Thank you!

Thanks to my parents, Mertxe and Jose, for laying the foundation for who I am today. Thanks for letting me devote myself to what I liked without any pressure. Thanks for always being available to me.

I am grateful to my brother Gaizka for constantly being a support for me. Thank you for making me feel understood by simple audio whatsapp.

A special thank you to Lorena, Jauna, Salamandrita, Aino, and Nere, my women's network, for forgiving me for all those coffees postponed for science. Thanks for the messages of 'hey, I miss you, and I hope you're doing well' when I've been busy working for weeks. For those funny audios/videos that brightened my bad days even in the distance. Thanks for being there, growing together, and being the support system in good times, but above all, in times of need.

For Maite, for the way she sees the world. Thank you for reaffirming my love of my job on days I wanted to give up. Thank you so much for telling me what I need to hear and, more importantly, for telling me what I should listen to even if I don't like it. Thank you for being there, always.

INDEX



INDEX

Abbreviations	I
Figure Content	VII
Table Content	XI
RESUMEN	XVII
Introducción.....	XVII
Hipótesis y objetivos	XIX
Material y métodos.....	XIX
Resultados y discusión	XX
Conclusiones	XXIV
ABSTRACT.....	XXVII
OVERVIEW	3
The current landscape of melanoma epidemiology.....	3
Etiological factors for malignant melanoma	8
Histopathology of melanoma.....	10
Melanoma development.....	10
Melanoma heterogeneity and plasticity.....	15
An overview of melanoma diagnosis and staging	17
Clinical and molecular classification of melanoma.....	20
HYPOTHESIS AND OBJECTIVES.....	27
Background	27
Hypothesis.....	29
Objectives	30
MATERIAL AND METHODS	33
Patients.....	33
Ethics statement.....	33
Recruitment and managements	33
FFPE tissue samples and immunohistochemistry	34
Data analysis.....	35
Cell cultures.....	36
Maintenance.....	36
Freezing and thawing	36
Mycoplasma detection	37
Modulation of gene expression.....	38

Silencing by transduction with lentiviral particles.....	38
Functional assays	40
Proliferation assays	40
Migration assays	41
Data analysis	42
Molecular analysis.....	42
Protein analysis	42
Gene expression analysis	45
RESULTS	
Chapter 01.....	59
Potential value of RKIP and Pirin proteins as melanoma diagnostic and prognostic markers	
Characteristics of the patients enrolled in the study	59
Differential expression of RKIP protein between nevi and melanoma biopsies...61	
Pirin expression and the Breslow thickness in melanoma biopsies is correlated with the metastatic progression of melanoma.....	66
Chapter 02.....	71
RKIP regulates melanocyte differentiation by modulating the stemness-related transcription factor	
Involvement of RKIP on malignancy-related properties of melanoma cells.....	71
Transcriptome modulation by RKIP downregulation in HEMn-LP cells.....	74
NANOG as a putative transcription factor regulated by RKIP	76
Chapter 03.....	81
Pirin modulates melanoma proliferation by targeting the slow-cycling transcriptional regulator JARID1B	
Pirin expression regulates the proliferation rates of melanoma cell lines	81
Transcriptome modulation in healthy skin melanocytes after PIR down-regulation.....	82
<i>JARID1B</i> , a transcription factor putatively regulated by <i>PIR</i>	85
DISCUSSION	
RKIP and Pirin as biomarkers for melanoma diagnosis and prognosis	89
RKIP Regulates Differentiation-Related Features in Melanocytic Cells.....	91
Pirin dampens the proliferation of malignant cells by downregulating JARID1B/KDM5B expression	93
CONCLUSIONS.....	99
REFERENCES.....	103
ANNEX A	123
ANNEX B	127
ANNEX C	143

ABBREVIATIONS



Abbreviation	Description
ACTB	Actin beta
AJCC	American Joint Committee on Cancer
AJCC	American Joint Committee on Cancer
AKT	Protein Kinase B
ALM	Acral lentigo melanoma
ANOVA	variance analysis
BCL-3	B-cell lymphoma 3-encoded protein
BIC	Bayesian Information Criterion
BPs	Biological Processes
BRAF	B-Raf Proto-Oncogene, Serine/Threonine Kinase
BSA	Bovine Serum Albumin
Cdna	complementary DNA
c-MYC	Myc proto-oncogene, bHLH transcription factor
c-Rel,	REL Proto-Oncogene, NF- κ B Subunit
CSD	Cumulative sun damage
CT	computed tomography
DEGs	Differentially expressed genes
DEPC	diethylpyrocarbonate
DMEM	Dulbecco's Modified Eagle Medium
DMSO	dimethyl sulfoxide
DNA	Deoxyribonucleic acid
DTT	Dithiothreitol
E2F1	E2f transcription factor 1
EAPC	Estimated Annual Percentage Change
ECL	Enhanced chemiluminescence
ECM	Extracellular matrix
EDTA	Ethylenediaminetetraacetic acid
EGFP	Enhanced Green Fluorescent Protein
EMT	Epithelial-to-mesenchymal transition
ERK1	Mitogen-Activated Protein Kinase 3
ERK2	Mitogen-Activated Protein Kinase 1
FBS	Fetal bovine serum
FDR	False discovery rate
FFPE	Formaldehyde Fixed Paraffin Embedded
GAPDH	Glyceraldehyde 3-phosphate dehydrogenase
GEO	Gene expression omnibus
GFP	Green fluorescence protein
GO	Gene Ontology
GPCR	G protein-coupled receptors
GSK3 β	Glycogen synthase kinase-3 beta
H&E	hematoxylin and eosin staining
HEMn-DP	Human epidermal melanocytes, neonatal, darkly pigmented
HEMn-LP	Human epidermal melanocytes, neonatal, lightly pigmented
HEMn-MP	Human epidermal melanocytes, neonatal, moderately pigmented
HMB-45	anti-melanosoma, HMB45
HRP	Horseradish Peroxidase
IGF-1Rs	Insulin-like growth factor I receptor
IHC	immunohistochemistry

IKK	Inhibitor Of Nuclear Factor Kappa B Kinase
JAK	Janus Kinase
JARID1B	Lysine Demethylase 5B gene
KEGG	Kyoto Encyclopedia of Genes and Genomes
KLF4	Kruppel Like Factor 4
KRAS	KRAS Proto-Oncogene, GTPase
LM	Lentigo melanoma
LMM	Lentigo malignant melanoma
LUM	Lumican
MAPK	Mitogen-activated protein kinase
MART-1/Melan-A	Melanoma Antigen Recognized by T Cells
MEK	Mitogen-Activated Protein Kinase Kinase 1
MIB1	MIB E3 Ubiquitin Protein Ligase 1
miR-21	MicroRNA 21
MITF	Melanocyte Inducing Transcription Factor
MOI	Multiplicity of Infection
mRNA	messenger Ribonucleic Acid
NANOG	Nanog homeobox
NCSC	neural-crest stem-cell
NF1	neurofibromin 1
NFKB	nuclear factor-kappaB
NGS	Next Generation Sequencing
NM	Nodular melanoma
NRAS	NRAS Proto-Oncogene, GTPase
NTRK2	Neurotrophic Receptor Tyrosine Kinase 2
OCT4	POU class 5 homeobox 1
OIS	Oncogene-induced senescence
p100/p52	Nuclear Factor Kappa B Subunit 2
p105/p50	Nuclear Factor Kappa B Subunit 1
PBS	Phosphate buffer saline
PCR	Polymerase chain reaction
PI3K	phosphatidylinositol-3-kinases
PIR	Pirin
PKC	Protein Kinase C
PMEL o gp-100	premelanosome protein
PTEN	Phosphatase And Tensin Homolog
RAF	Raf-1 Proto-Oncogene, Serine/Threonine Kinase
RelA (p65)	RELA Proto-Oncogene, NF-KB Subunit
RelB	RELB Proto-Oncogene, NF-KB Subunit
RGP	radial growth proliferation
RIN	RNA Integrity Number
RIPA	Radioimmunoprecipitation assay buffer
RIPA	Radioimmunoprecipitation Assay
RKIP	Raf kinase Inhibitor protein
RNA	ribonucleic acid
RNU6-2	endogenous reference small nuclear ribonucleic acid (snRNA) B
RPKM	Reads per kilobase of exon model
RPMI	Roswell Park Memorial Institute Medium
RPS15	Ribosomal Protein S15 gene
RPS15	Ribosomal Protein S15

RTKs	receptor tyrosine kinases
RT-qPCR	Real time quantitative polymerase chain reaction
S100	S100 Calcium Binding Protein
SDS	Sodium dodecyl sulfate
shRNA	Short hairpin RNA
SNAIL	Snail transcriptional repressor
SOX2	SRY-box transcription factor 2
SRA	Sequence read archive
SRCCA	Spearman's rank correlation coefficient
SSM	Superficial spread melanoma
STAT	Signal Transducer And Activator Of Transcription
TAK1	Mitogen-Activated Protein Kinase Kinase Kinase 7
TBST	Tris-buffered saline with Tween 20
TBST	Tris-buffered saline
THY-1	THY-1 cell surface antigen
TMM	Trimmed mean of M values
TNFR1	TNF Receptor Superfamily Member 1A
TYR	tyrosinase
UV	Ultraviolet
VGP	vertical growth proliferation
WHO	World Health Organization
XTT	2,3-bis-(2-methoxy-4-nitro-5-sulfophenyl)-2H-tetrazolium-5-carboxanilide
ZEB	Zinc Finger E-box-binding homeobox

FIGURE
CONTENT



Figure 1. Temporal incidence/mortality trends of Melanoma

Figure 2. Melanoma incidence

Figure 3. Melanoma mortality

Figure 4. Skin phototypes

Figure 5. Cross-section of skin's layers

Figure 6. Biologic events and molecular changes in the progression of melanoma

Figure 7. Melanoma key signaling pathways

Figure 8. ABCDE criteria for the early detection of melanoma

Figure 9. Histological subtypes of melanoma and clinical-pathological correlations

Figure 10. Distribution of melanoma cell lines and primary cultures of melanocytes analysed in a two-component plot by Varimax orthogonal rotation

Figure 11. RKIP and Pirin expression in cell culture of melanocytic cells by RT-qPCR and Western blot

Figure 12. Immunostaining for Pirin in three representative melanoma biopsies (negative, low and high)

Figure 13. Workflow overview of transduction protocol with lentiviral particles and transfection protocol with lipofectamine and overexpression plasmids.

Figure 14. Workflow overview of wound healing assay

Figure 15. Workflow overview of the protein detection process by western blot

Figure 16. RNA integrity numbers (RINs) obtained with Agilent 2100 Bioanalyzer

Figure 17. Library profile qualification by Agilent High Sensitivity DNA Kit

Figure 18. Mapped reads per contig analysed by bamtool stats bioinformatics tool

Figure 19. Distribution of the samples according to diagnosis, tumour location and histological subtype, AJCC stages, Breslow Index expressed in mm and evolution of patients diagnosed in AJCC I and II stages

Figure 20. RKIP expression pattern distribution according to diagnosis, histological type and progression of melanoma patients

Figure 21. Statistical analyses of Raf Kinase Inhibitor Protein (RKIP) expression in FFPE biopsies from patients

Figure 22. Representative images of manually scored RKIP staining categories in FFPE biopsies from patients

Figure 23. Representative images of Pirin staining in FFPE biopsie from a melanoma hematoxylin-eosin staining and imunohistochemistry of Pirin expression

Figure 24. Pirin expression pattern distribution according to diagnosis, histological type and progresion of melanoma patients

Figure 25. Statistical analyses of Pirin expression in FFPE biopsies from patients

Figure 26. Modulation of RKIP expression in A375 and MelHO primary melanoma cell lines

Figure 27. Modulation of RKIP expression in MeWO and A2058 metastatic melanoma cell lines

Figure 28. RNA Sequencing data quality of RKIP downregulated HEMn-LP

Figure 29. RNA Sequencing data and analysis after RKIP downregulation in HEMn-LP

Figure 30. RKIP as a key regulator of *NANOG* expression in melanoma

Figure 31. Functional assays after Pirin upregulation in melanoma cells

Figure 32. RNA Sequencing data quality of Pirin downregulated HEMn-LP

Figure 33. RNA Sequencing data analysis and validation after Pirin downregulation in HEMn-LP

Figure 34. PIR as a key regulator of *JARID1B* expression in melanoma

TABLE
CONTENT



Table 1. Description of the criteria used to classify the staging of melanoma

Table 2. Staging of melanoma based on TNM system

Table 3. Classification of melanoma based on 2018 world health organization classification

Table 4. Details of sources and concentrations of antibodies used for Immunohistochemistry in this study

Table 5. Melanocyte and melanoma cell lines specifications

Table 6. Lentiviral particles specifications

Table 7. Plasmids specifications

Table 8. Percentage of polyacrylamide used depending on the protein of interest

Table 9. Composition of the stacking and running gel

Table 10. Composition of 1L of the electrophoresis buffer (5X)

Table 11. Composition of 1L of the transfer buffer

Table 12. Details of sources and concentrations of antibodies used for western blot in this study

Table 13. RTqPCR primers' sequences

Table 14. Total RNA quantification with Qubit RNA HS Assay Kit

Table 15. Libraries indexing specifications

Table 16. Raw data from the total number of bases, reads, GC (%), Q20 (%), and Q30 (%) calculated for all the samples

Table 17. Alignment data summary

Table 18. Alignment quality analysis by Picard bioinformatics tool. (A) Control samples, (B) RKIP samples and (C) PIR samples

Table 19. Clinical and pathological data from nevus and melanoma patients

Table S1. Differentially expressed genes after RKIP silencing. The details of Log Fold Change, p-value and False Discovery Rate are specified in each column

Table S2. Differentially after PIR silencing. The details of Log Fold Change, p-value and False Discovery Rate are specified in each column

Table S3. Enriched processes after RKIP silencing, specifying the False Discovery Rate for assignment and the list of genes for each one

Table S4. Most enriched term analysis of differentially expressed gene in HEMn-LP after RKIP silencing, which are potentially targeted by NANOG transcription factor.

Table S5. Genes related with development process, which are potentially targets of NANOG transcription factor.

Table S6. Enriched processes after PIR silencing, specifying the False Discovery Rate for assignment and the list of genes for each one

Table S7. Most enriched term analysis of differentially expressed gene in HEMn-LP after PIR silencing, which are potentially targeted by JARID1B transcriptional regulator



RESUMEN

01

Introducción

02

Hipótesis y objetivos

03

Estrategia
metodológica

04

Resultados y
discusión

05

Conclusiones

Introducción

El melanoma maligno es el cancer de piel que surge como resultado de la transformación maligna de los melanocitos. En los últimos 30 años, la incidencia de esta patología a nivel mundial ha aumentado en mayor proporción que el resto de los cánceres, concretamente, entre el 4-6% anual (1), y muestra disparidades sustanciales entre poblaciones, viendose una mayor incidencia en población de piel y ojos claros que viven en zonas geográficas con alta exposición solar (2).

Los melanocitos son células derivadas de la cresta neural que están ubicados principalmente en la capa basal de la epidermis de la piel, donde permanecen bajo el estricto control de células como los queratinocitos. Bajo condiciones homeostáticas normales, la proliferación de melanocitos ocurre solamente tras ser estimulados por factores paracrinicos secretados por los queratinocitos. En este contexto, estos factores activan o reprimen procesos como el ciclo celular, la diferenciación, la adhesión, la señalización y la apoptosis mediados por la interconexión de las vías MAPK, PI3K/AKT y NFκB, entre otras.

Durante la transformación maligna, este control está desregulado como resultado de una serie de modificaciones moleculares que alteran la función normal de estas vías, bien porque afectan a las proteínas implicadas en la ruta o a los reguladores que controlan su actividad. Entre los genes frecuentemente mutados en melanoma se encuentran BRAF, NRAS, NF1 y PTEN, entre otros. Cualquier alteración en estos genes conlleva, por norma general, una sobre activación de la proliferación y una inhibición de la apoptosis. Respecto a las alteraciones que se pueden dar en los elementos reguladores de estas rutas, la proteína inhibidora de la quinasa Raf (RKIP), también conocida como proteína de unión a fosfatidiletanolamina 1, ha sido descrita como un regulador de la vía MAPK, ya que interrumpe la interacción física entre las proteínas MAPK reduciendo la activación de la vía. Respecto al melanoma, los estudios publicados sugieren que RKIP juega un papel importante en la regulación de la capacidad de proliferación, migración e invasión celular (49-51), mediante mecanismos que conducen a la inhibición de la vía NFκB y MAPK. Sin embargo, poco se conoce sobre las vías reguladas por RKIP en melanocitos normales ni sobre su papel en la transformación maligna de este tipo de células. Por otro lado, algunos estudios (51,52) describen una reducción gradual de la expresión de RKIP en relación a la malignidad en pacientes con melanoma. Sin embargo, estos estudios se realizaron con una pequeña cohorte de pacientes por lo que sería necesario un estudio más amplio para establecer el verdadero valor diagnóstico o pronóstico de este marcador en el melanoma. De igual modo, la Pirina, miembro de la superfamilia de las cupinas, ha sido descrito como un regulador de la vía NFκB, ya que forma un complejo estable que mejora la capacidad de Bcl3-NFκB1 para unirse al ADN, induciendo, así, la transcripción de una variedad de genes diana implicados en la supervivencia celular y la apoptosis

(58). La inhibición de Pirina se ha asociado con la capacidad migratoria de las células de melanoma (122) y también se ha propuesto como un inhibidor de la senescencia celular aunque se sabe poco sobre los mecanismos que subyacen a este efecto (135).

La combinación de todos estos cambios genéticos conduce a que los melanocitos normales adquieran diversos fenotipos malignos. Así, se ha descrito un equilibrio entre los fenotipos proliferativos e invasivos en las células de melanoma, lo cual permite que las células sean capaces de mostrar una plasticidad de, lo que se ha llamado, *fenotipo adaptativo*. De acuerdo con esta propuesta de plasticidad fenotípica, los fenotipos estables de melanoma se definen por transcriptomas de melanocitos diferenciados o melanocitos de ciclo lento o *'slow-cycling cells'* con marcadores de célula madre o *'stem-like cell makers'*. Las propiedades asociadas al perfil *'stem-like cell'* pueden explicar la persistencia de ciertas células tumorales tras el tratamiento con fármacos. Uno de los genes relacionados con la regulación del mantenimiento del estado de indiferenciación es NANOG (70). Así, por ejemplo, durante la formación de esferas en el melanoma, se incrementa la expresión de NANOG (74), y se ha visto su implicación en la regulación de la transición epitelio-mesenquimatoso, proceso clásicamente ligado al aumento de la motilidad de las células cancerosas favoreciendo la diseminación de la enfermedad (75). Por otro lado, el fenotipo asociado a ciclo proliferativo lento o *'slow cycling'* también se ha relacionado con una subpoblación de células que mantiene la supervivencia de las células tumorales (191). Entre los reguladores maestros del ciclo celular retardado se encuentra *JARID1B/KDM5B*, o enzima desmetilasa de histonas específica de lisinas. Varios estudios han proporcionado evidencia de que *JARID1B* es un supresor de tumores en el melanoma maligno, ya que sus niveles de expresión están regulados a la baja e inhibe la proliferación celular de manera dependiente de *Rb* (82-84). Dado que la plasticidad del fenotipo está estrechamente relacionada con el inicio, la progresión y la resistencia a la terapia del melanoma, es de gran interés identificar cómo se generan estas transiciones de fenotipo a fin de identificar nuevos enfoques terapéuticos.

En otro orden de cosas, los melanomas también muestran una amplia variedad a nivel histológico, pudiendo mostrar características epiteliales, hematológicas, mesenquimatosas y neurales, que a menudo pueden dificultar el diagnóstico de la enfermedad (96). De hecho, se ha desarrollado una variedad de marcadores inmunohistoquímicos a fin de facilitar la labor del personal clínico de los servicios de dermatología, como el marcador S-100, que sigue siendo el marcador más sensible para las lesiones melanocíticas. Otros marcadores, como HMB-45, MART-1/Melan-A, tirosinasa y MITF son relativamente sensibles, aunque no tanto como S-100. Actualmente, estos biomarcadores utilizados para facilitar el diagnóstico de melanoma permiten diferenciar tumores melanocíticos de otros tipos de tumores, pero no se ha demostrado que alguno de ellos sea predictivo de supervivencia para pacientes con neoplasias melanocíticas. Con el desarrollo de tratamientos más novedosos y específicos, los biomarcadores tumorales son cada día más importantes de cara a su utilización en nuevas estrategias terapéuticas (106,107).

En estudios de proteómica diferencial previos realizados por nuestro grupo de investigación, observamos que RKIP y Pirina eran dos proteínas cuya expresión difería significativamente entre melanocitos de piel y células de melanoma. Por ello, consideramos que presentaban gran potencial para ser utilizados como biomarcadores del melanoma maligno.

Hipótesis y objetivos

En base a todo lo expuesto anteriormente, en esta tesis se ha mantenido la hipótesis de que RKIP y Pirina son proteínas que pueden ser excelentes biomarcadores para el diagnóstico y pronóstico del melanoma cutáneo además de desempeñar un papel importante en la etiopatogenia del melanoma cutáneo.

Así, para determinar la veracidad de esta hipótesis, nos planteamos los siguientes objetivos específicos:

1. Validar la expresión de RKIP y Pirina como marcadores de diagnóstico y pronóstico en melanoma.
2. Evaluar el papel de RKIP y Pirina en las funciones biológicas de los melanocitos de piel.
3. Determinar en que medida RKIP y Pirina contribuyen a la progresión metastásica del melanoma maligno.

Material y métodos

Nuestra estrategia metodológica para valorar el primer objetivo se basó en un estudio retrospectivo en una cohorte pacientes con melanoma en el que se examinó la expresión de las proteínas RKIP y Pirina en cortes histológicos de biopsias de melanoma mediante inmunohistoquímica (IHC). El seguimiento clínico de los pacientes abarcó de 18 meses a 5 años. Posteriormente, se realizó una correlación con los datos clinicopatológicos y la progresión metastásica.

Para evaluar el segundo objetivo sobre las funciones de las proteínas RKIP y Pirina en la biología de los melanocitos, realizamos una evaluación de los cambios transcripcionales tras el silenciamiento de la expresión de ambos genes de forma independiente en células de melanocitos sanos. Los controles y los melanocitos RKIP o PIR silenciados se examinaron mediante secuenciación de ARN. Luego, los resultados del análisis *in silico* de enriquecimiento de ontología génica se validaron en líneas celulares de melanoma a las que se les ha sobreexpresado RKIP o Pirina, respectivamente.

Para abordar el tercer objetivo, se utilizaron líneas celulares de melanoma humano primario y metastásico. Tanto la expresión de RKIP como la de Pirina fueron moduladas por plásmidos de forma

independiente y se realizaron ensayos funcionales de la capacidad proliferativa, migración e invasión. Además, se determinaron y validaron dianas moleculares de RKIP y Pirina mediante co-transfecciones y determinaciones moleculares.

Resultados y discusión

El melanoma maligno es una forma de cáncer de piel que es extremadamente letal. Para garantizar un tratamiento adecuado y un resultado exitoso, es esencial un diagnóstico oportuno y preciso del melanoma maligno. En este sentido, las alteraciones moleculares en la patogenia del melanoma son objeto de una investigación muy activa, lo que ha llevado a la identificación de oncogenes y genes supresores de tumores asociados a esta enfermedad para desarrollar enfoques terapéuticos que se necesitan con urgencia. Por ello, el primer objetivo de este trabajo ha sido estudiar el valor potencial de RKIP y Pirina como marcadores de melanoma, lo cual se analiza en el **Capítulo 1** de la sección de Resultados a través de un estudio inmunohistoquímico en una cohorte de 314 pacientes (75 nevus y 239 melanoma).

Respecto a RKIP, de manera general, la expresión intramuestra de esta proteína fue homogénea, observándose un marcaje citoplasmático. El análisis univariante de la comparación por grupos, mostró una diferencia estadísticamente significativa entre la alta expresión que mostraban las biopsias de *nevi* (94% de los casos) frente a los melanomas (51% de los casos). Además, mediante un análisis de regresión logística (en el que se incluyeron la edad y el sexo como covariables) se observó una asociación lineal, es decir, mayores niveles de proteína se correlacionaban significativamente con una mayor probabilidad de que las biopsias fuesen identificadas como nevus. Por otro lado, tanto el análisis univariante como el multivariante confirmaron una diferencia significativa entre la expresión de RKIP entre las biopsias de *nevi* y las de melanoma diagnosticados en estadios tempranos (estadios I y II, según AJCC 8ª Ed.). Al analizar su potencial como marcador pronóstico, aunque no se observaron diferencias significativas entre la expresión de RKIP y el desarrollo de metastasis, altos niveles de RKIP se correlacionaron con un grosor de Breslow más bajo en muestras de todos los estadios de melanoma. Según la bibliografía existente, varios estudios han demostrado que los niveles de RKIP son bajos en una gran variedad de cánceres y que, además, apenas se expresa en las metastasis (115,148-150,164). En el caso del melanoma, en concreto, se ha observado una disminución de RKIP en melanoma uveal y una baja expresión en melanomas cutáneos, tanto primarios como metastásicos (52, 165). Aunque estos estudios son interesantes, se realizaron con cohortes pequeñas de pacientes, y, además, comparaban los niveles de expresión de RKIP entre biopsias de tumores primarios y biopsias tomadas en sitios metastásicos (52,134,148). Aún así, estos resultados muestran un claro silenciamiento de RKIP en relación a la malignidad en las células tumorales, aunque no investigaron la posible utilidad de la expresión de RKIP como marcador pronóstico de buena o mala evolución. Según nuestros resultados, parece que la tinción de RKIP mediante inmunohistoquímica tiene utilidad como marcador diagnóstico para pacientes de melanoma.

De forma similar se correlacionó la expresión de Pirina con los datos clínicos. En primer lugar, mencionar que la tinción intramuestra, a diferencia que en el caso de RKIP, fue heterogénea, observándose células con marcaje sólo nuclear, sólo citoplasmático o ambos. Este patron heterogéneo no mostró ninguna relación con el tipo histológico, el estadio tumoral o la progresión del melanoma. Al realizar la comparación por grupos, se observó que el 80% de los nevi mostraban una alta expresión de Pirina frente al 60% de los melanomas. En relación al tipo histológico, los y las pacientes con melanoma de extensión superficial (MES) mostraron una expresión de Pirina similar con independencia de su evolución. Sin embargo, en el caso del melanoma nodular (MN), quienes eventualmente desarrollaron enfermedad metastásica mostraron niveles de pirina más altos en sus biopsias primarias en una proporción significativamente mayor que aquellos que permanecieron libres de enfermedad. Por otro lado, se evaluó la utilidad de Pirina como marcador pronóstico temprano, utilizando únicamente las biopsias de pacientes con melanoma en estadio temprano (estadios I y II, según AJCC 8ª Ed.), sin embargo, no se observó una asociación directa entre la expresión de Pirin y el hecho de permanecer libre de enfermedad o desarrollar metástasis durante el seguimiento. Aún así, dado que nuestros datos de melanomas primarios tempranos eran heterogéneos, se podría esperar que otros factores de riesgo potenciales pudieran estar enmascarando la asociación entre la expresión de Pirin y la probabilidad de metástasis. Por ello, se realizó un análisis de las diferencias en un escenario multivariado que incluía la expresión de Pirin como el efecto de interés, y la edad, el sexo y la profundidad de Breslow como posibles covariantes. En este caso, un nivel alto de Pirina se asoció significativamente con una mayor probabilidad de metástasis según el modelo de regresión logística. Complementariamente se llevó a cabo un análisis de Factores de Bayes, que resultó ser positivo, indicando que la alta expresión de Pirin en una biopsia implica que sea 10 veces más probable que se desarrolle metástasis. Finalmente, un análisis de Cox mostró que pacientes con una expresión más alta de Pirin tenían más del doble de probabilidad de desarrollar metástasis temprana en comparación con aquellos que expresaban bajos niveles de Pirina. Según lo descrito hasta la fecha en relación a Pirina, parece estar involucrada en la regulación de varios procesos celulares, incluida la inhibición proteínas quinasa, funciones antioxidantes y cofactor transcripcional (30,82,116). Además, se ha demostrado que Pirin puede desempeñar un papel en la tumorigénesis a través de su participación en la regulación de la proliferación celular y la progresión maligna (182). Por otro lado, Lucciulli y colaboradores describieron una deslocalización de Pirina desde el núcleo hasta el citoplasma en un subconjunto de muestras de pacientes con melanoma cuando las compararon con las biopsias de nevi. Además, observaron una correlación positiva entre los niveles citoplasmáticos de Pirin y la progresión del melanoma (135). En nuestro caso, hemos podido establecer que su determinación mediante inmunohistoquímica, junto con el índice de Breslow, podría ser útil como un indicador de pronóstico ya que pacientes con altos niveles de expresión mostraron menor tiempo de supervivencia libre de enfermedad.

En otro orden de cosas, hay que tener en cuenta que la incapacidad para comprender los mecanismos que subyacen a la metástasis, la cual conduce a la mayoría de las muertes relacionadas con el cáncer, plantea un problema importante para el desarrollo de métodos de diagnóstico y pronóstico así como de terapias efectivas. Debido a esto, centramos nuestra atención en el papel de RKIP y Pirina en la biología

de los melanocitos normales y malignos. Para ello, se comenzó por el silenciamiento de ambas proteínas de forma independiente en melanocitos primarios sanos y el posterior análisis de su transcriptome mediante Secuenciación de ARN. Se completaron los estudios con análisis moleculares y funcionales en líneas de melanoma.

Los hallazgos relacionados con los cambios transcripcionales producidos por el silenciamiento de RKIP en melanocitos normales se recogen en el **Capítulo 2** de la sección de Resultados. Lo primero que llamó nuestra atención fue que estas células mostraron modificaciones a nivel de expresión génica asociadas a la firma genética del cáncer. Concretamente, se observaron alteraciones de los procesos celulares íntimamente relacionados con la transformación maligna de las células, como el desarrollo y la diferenciación. Esto iría en concordancia con la expresión más alta de RKIP encontrada en melanocitos diferenciados de lesiones de *nevus* cuando se compara con muestras de melanoma en el Capítulo 1. Más específicamente, se encontró que más del 70% de los genes expresados diferencialmente que se incluyeron en esta sección, *desarrollo y diferenciación*, eran dianas putativas de *NANOG*, un factor de transcripción relacionado con la troncalidad o ‘stemness’ (70). Los ensayos de cotransfección de plásmidos para la sobreexpresión de RKIP junto con plásmidos del promotor de *NANOG* asociado a GFP mostraron que la presencia de RKIP produjo una disminución de la activación del promotor *NANOG*, lo cual apunta hacia una relación funcional entre la expresión de RKIP y *NANOG*. En este contexto, también hemos encontrado que la expresión de miR-21, una diana aguas abajo de *NANOG* (78) y relacionado con la transición epitelio-mesénquima, fue significativamente menor en las células que sobreexpresaban RKIP. Estas mismas células mostraron un aumento de la capacidad migratoria tanto en el test de la herida como a través de filtros con matriz de colágeno. En línea con estos resultados, Lee et al. (173) notaron una gran cantidad de interferencias entre las vías reguladas por RKIP y aquellas bajo el control de los principales factores de transcripción de tallo (es decir, *OCT4*, *KLF4*, *SOX2* y *NANOG*) y propusieron RKIP como un regulador del estado de diferenciación de las células. En conjunto, nuestros resultados sugieren que RKIP regula los estados diferenciados en las células melanocíticas a través del factor de transcripción *NANOG*.

Por otro lado, tal y como se observa en el **Capítulo 3** de la sección de Resultados, el transcriptoma de los melanocitos con Pirina silenciada reveló un enriquecimiento de genes involucrados en la transición G1/S, la organización de la matriz extracelular, la proliferación, la migración y diferenciación celular. Uno de los reguladores del ciclo celular es *JARID1B/KDM5B*, una histona desmetilasa específica de Lisina. Aunque las células de melanoma que expresan *JARID1B* representan solo una pequeña proporción de las células en las poblaciones de melanoma primario y metastásico (187), nuestro conjunto de datos de RNA-seq y el análisis *in silico* de enriquecimiento de factores de transcripción encontraron que *JARID1B* podría regular más de 100 de los genes diferencialmente expresados tras el silenciamiento de Pirina en los melanocitos. Así, los experimentos de cotransfección mostraron una disminución de la activación del promotor de *JARID1B* después de la sobreexpresión de Pirina, lo que sugiere una relación funcional entre la expresión de Pirina y *JARID1B*. Además, demostramos que la sobreexpresión de Pirina en las dos líneas celulares de melanoma metastásico estudiadas condujo a una

disminución significativa en la expresión del gen *JARID1B* y de sus genes diana *E2F1* y *c-MYC* (81,141). En relación a esto, se observó una bajada en la proliferación de las líneas de melanoma que sobreexpresaban Pirina, lo cual concuerda con los bajos niveles de expresión de *JARID1B*, *E2F1* y *c-MYC* obtenidos en los ensayos de cotransfección. Así, en el contexto de nuestro estudio, hemos podido determinar que la capacidad proliferativa de las células de melanoma depende de la interacción de Pirina con *JARID1B*, quien está involucrada en la organogénesis, la función de las células madre y el desarrollo del cancer (80,81).

Con todo ello, mantenemos la Tesis de que en la génesis del melanoma cutáneo pueden estar implicados múltiples mecanismos celulares. En nuestro estudio concreto, la expresión de RKIP y Pirina dibujan escenarios distintos en un *nevus* frente al melanoma. La expresión de RKIP en los melanocitos de los *nevi* inhibiría la expresión de *NANOG* y sus dianas moleculares, manteniendo el estado diferenciado de los melanocitos. Además, la expresión de Pirina modularía la proliferación a través de *JARID1B* y sus dianas moleculares como *E2F1*. Por su parte, en el melanoma, la ausencia de RKIP induciría un panorama diferente, ya que la expresión de *NANOG* favorecería la adquisición del fenotipo invasivo y en este contexto, las células tumorales con ciclo lento inducido por *JARID1B* podría actuar como un estímulo para entrar de nuevo en ciclo y favorecer la formación de metastasis.

Conclusiones

En nuestra hipótesis inicial planteábamos que RKIP y Pirina eran proteínas que desempeñaban un papel en la etiopatogenia del melanoma cutáneo, lo que las convertía en excelentes biomarcadores para el diagnóstico y pronóstico del melanoma cutáneo. Para demostrar esto, investigamos su aplicación potencial como marcadores de melanoma y su papel en las células melanocíticas.

En base a los resultados presentados en esta tesis, se pueden extraer las siguientes conclusiones:

1. La detección inmunohistoquímica de RKIP en biopsias de melanoma puede ser una herramienta útil para el diagnóstico de melanoma.
2. La detección inmunohistoquímica de Pirina junto con el índice de Breslow podría usarse como marcador pronóstico en estadios tempranos (I-II) del melanoma.
3. La baja expresión de RKIP en melanocitos humanos condujo a una firma transcripcional asociada con el cáncer, que incluía una desregulación de genes relacionados con la pigmentación y los procesos de desarrollo y diferenciación.
4. RKIP parece estar involucrado en el mantenimiento del estado de diferenciación de los melanocitos al regular negativamente el factor de transcripción *NANOG* y sus dianas moleculares, como miR-21.
5. La baja expresión de Pirina en melanocitos humanos condujo a un perfil transcripcional caracterizado por una desregulación en la organización de la matriz extracelular, la migración, la proliferación y la respuesta a interferón tipo II.
6. Pirina ejerce un efecto antiproliferativo en las células de melanoma a través de la regulación del factor de transcripción *JARID1B* y sus genes diana, incluidos *E2F1* y *c-MYC*.

A partir de estos resultados, en su conjunto, mantenemos la Tesis de la implicación de ambas proteínas RKIP y Pirina en la tumorigénesis y progresión maligna del melanoma cutáneo y podrían ser la base del diseño de nuevas estrategias terapéuticas para el tratamiento de la enfermedad metastásica del melanoma.

ABSTRACT



Melanoma is an extremely lethal skin cancer that arises as a result of the malignant transformation of melanocytes. The incidence of this pathology worldwide has increased in the last 30 years in greater proportion than the rest of the cancer, between 4-6% yearly, and shows substantial disparities between populations. To ensure appropriate treatment and a successful outcome, a timely and accurate diagnosis and prognosis of malignant melanoma is essential. Because of this, molecular alterations in the pathogenesis of melanoma are the subject of more active research. In terms of histology, melanoma show a wide variety of characteristics including epithelial, hematological, mesenchymal, and neural features, which can often make the diagnosis of the disease challenging. As new biomarkers candidates, in this thesis we examined the expression of RKIP (Raf Kinase Inhibitor Protein) and Pirin. RKIP has been extensively reported as an inhibitor of key signaling pathways involved in the aggressive tumor phenotype and shows decreased expression in several types of cancer, and Pirin originally was considered to act as a transcriptional co-factor, but it has recently been reported to play a role in tumorigenesis and the malignant progression of many tumors. However, these studies were performed with a small cohort of patients, so a larger study is required for further evaluation of this marker's diagnostic or prognostic value. In this context, this doctoral thesis' goals were to evaluate the potential value of RKIP and Pirin as melanoma markers and their implication on melanocytic cell biology.

Regarding RKIP, immunohistochemistry analysis revealed a significantly higher expression of RKIP in nevi compared with early-stage (stage I-II, AJCC 8th) melanoma biopsies. Proliferation, wound healing, and collagen-coated transwell assays uncovered the implication of RKIP on the motility but not on the proliferative capacity of melanoma cells as RKIP protein levels were inversely correlated with the migration capacity of both primary and metastatic melanoma cells but did not alter other parameters. As shown by RNA sequencing, endogenous RKIP knockdown in primary melanocytes triggered the deregulation of cellular differentiation-related processes, including genes (i.e., ZEB1, THY-1) closely related to the EMT. Interestingly, NANOG was identified as a putative transcriptional regulator of many of the deregulated genes, and RKIP was able to decrease the activation of the NANOG promoter. In relation to Pirin, the immunohistochemistry multivariate analysis revealed that early melanoma with stronger Pirin expression were more than twice as likely to develop metastases during the follow-up. On the other hand, transcriptome analysis of PIR downregulated melanocytes showed a dampening of genes involved in the G1/S transition, cell proliferation, and cell migration. In addition, an *in silico* approach predicted that JARID1B as a potential transcriptional regulator that lies between PIR and its downstream modulated genes, which was corroborated by co-transfection experiments and functional analysis.

To summarize, the results obtained in this thesis support the diagnostic utility of RKIP staining due to the significantly lower RKIP protein levels in melanoma samples, even at early stages (I–II) of the disease, and the use of Pirin staining along with the Breslow index as a prognostic marker at early stages (I-II) of melanoma. Moreover, we propose that RKIP could play a role in the maintenance of the differentiation state by negatively regulating NANOG gene expression and, that Pirin could play an important role in modulating the proliferative state of melanoma cells by regulating JARID1B gene expression.





OVERVIEW

01

Current landscape of melanoma epidemiology

02

Etiological factors for malignant melanoma

03

Histopathology of melanoma

- Melanoma development
 - Melanoma heterogeneity and plasticity
 - An overview of melanoma diagnosis and staging
 - Clinical and molecular classification of melanoma
-

The current landscape of melanoma epidemiology

Malignant melanoma is the least common but has the highest mortality rate among skin cancer. This tumor arises from the uncontrolled proliferation of melanocytes, cells that produce melanin. According to GLOBOCAN data, both case and death rates will continue to increase uninterruptedly in the future years. By way of illustration, estimates predict an increase in incidence from 18% to 65% between 2025 and 2040 and an increase in mortality for the same period from 20% to 74% (1). These trends should be analyzed by considering the geographical area, sex, age, and ethnicity, factors that affect the epidemiological data of melanoma.

The incidence of this pathology worldwide has increased in the last 30 years in a more significant proportion than the rest of the cancer, between 4-6% yearly. It shows substantial disparities between populations (2). The Estimated Annual Percentage Change (EAPC) estimates the global incidence of melanoma for the next year, considering the past years' tendencies. In the last three decades, this percentage increased in all geographical areas except Central Asia and Oceania. Southeast Asia and Eastern Europe have the most remarkable upward trend (Figure 1). These differences may be due to data collection biases. Thus, for low socio-demographic index regions where the incidence has been reduced or is very low, it may be due to the limited data sources of melanoma. In addition, the increase in incidence rates should be by the national screening programs in different countries, such as South Korea and Germany, which allow early detection and diagnosis (3-4). The intentional sun exposure, in the last years having tanned skin is synonymous with beauty and well-being, could be the leading cause of this continuous increase in incidence. Moreover, this burden of melanoma is expected to continue to rise, with incidence rates rising through 2026 in Northern Europe (5-9).

Globally, in 2020 the highest incidence was observed in regions with high socio-demographic index, especially Australasia, Northern Europe, and North America (Figure 2a), with a remarkable number of cases in New Zealand (46.56/100.000), Australia (42.74/100.000) and the Netherlands (24.77/100.000). Meanwhile, the trend in Europe shows a pronounced north-to-south, west-to-east gradient (10-11).

Linked to this, it is necessary to highlight that the incidence of melanoma is also influenced by sex, age, and ethnicity. In the last 30 years, the risk of suffering this pathology increased 1.38 times for men and only 0.87-times for women (11). Regarding age, it is worth mentioning that among people aged 15-49 years, higher rates were observed among women, whereas for those older than 50 years, higher rates were observed among men (Figure 2b). Regarding ethnicity, specifically, the incidence of melanoma is up to 30 times higher among fair-skinned Caucasians than African Americans (Figure 2c). However,

the second ones have a lower survival rate at five years. Fair-skinned individuals are more likely to be diagnosed earlier since skin lesions are easier to detect. In addition, it has been described that people with darkly pigmented skin develop melanoma in low sun exposure body areas, such as mucous membranes and the acral regions (palms of the hands and feet). It implies a later detection and, consequently, in more advanced stages of the disease at diagnosis.

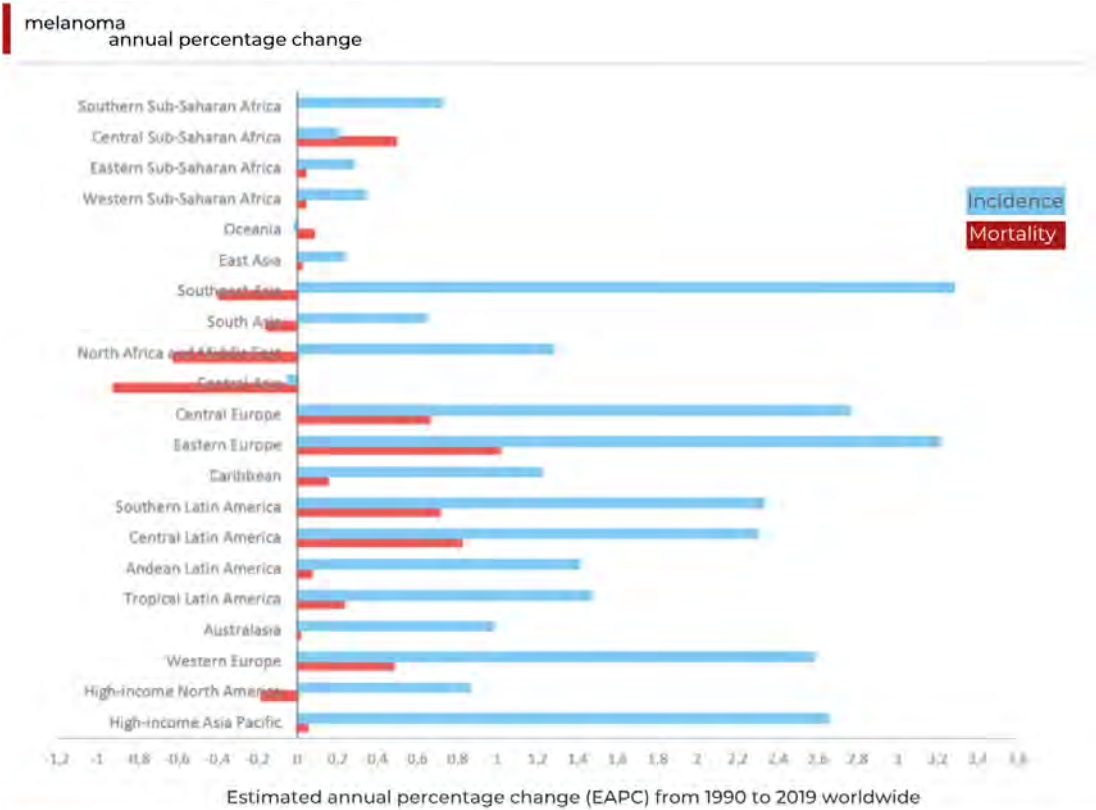


FIGURE 1 Temporal incidence/mortality trends of Melanoma. Estimated annual percentage change of incidence/deaths from 1990 to 2019 worldwide. Data sources: <http://ghdx.healthdata.org/gbd-results-tool>

In the case of mortality, melanoma death rates are leveling off, according to recent studies, and are trending downward in certain regions. Even so, as shown in Figure 3a, the areas with the most significant increase in the probability of dying from melanoma are Central Europe, Eastern Europe, Central Latin America, and South America. However, in regions such as Australia, despite having the highest annual percentage change incidence rate, the population has reduced the mortality trend, primarily due to awareness campaigns against skin cancer and the use of sunscreens.

As in the case of incidence, patient management is also not favorable for men since the risk of death from melanoma, although it has been reduced in recent years, is still higher than in the case of women. Even more, in older adults over 70 years old (Figure 3b-c).

There may be a cultural or social reason behind these unique tendencies of both sexes. It has been shown that more than 80% of melanoma could be attributed to exposure to UV radiation (12). In addition, the damages sustained by the skin can accumulate over time, so the appearance of a tumor would not happen until several decades after the first precancerous lesion appears. Due to this, and considering the age range with the highest incidence, we need to consider the different exposure habits men and women had a few generations ago (13). Women were more likely to avoid the sun and use sunscreen, whereas men spent more time in the sun and wore less UV protection (14).

Although the cosmetics industry has now introduced specific skin care products for men, its market niche has mainly been dominated by women until recently, when social pressure has always been aimed at women. Consequently, they became more aware of small changes or lesions, which could lead to the detection of tumors earlier (15-16). Alcohol consumption and diet have also been considered possible factors were influencing melanoma risk, both of which are influenced by social gender stereotypes (17). With all this in mind, developing prevention and detection campaigns explicitly aimed at men would be necessary.

Despite being one of Europe's lowest melanoma death rates, there has been a worrying rise in mortality among Spanish citizens since the last quarter of the 20th century, representing the highest increase within the Mediterranean region. It has been estimated that the number of new cases in Spain will exceed 10,000 in 2022 (3,377 women and 7,474 men).

melanoma
age-standardized incidence rate per 100,000

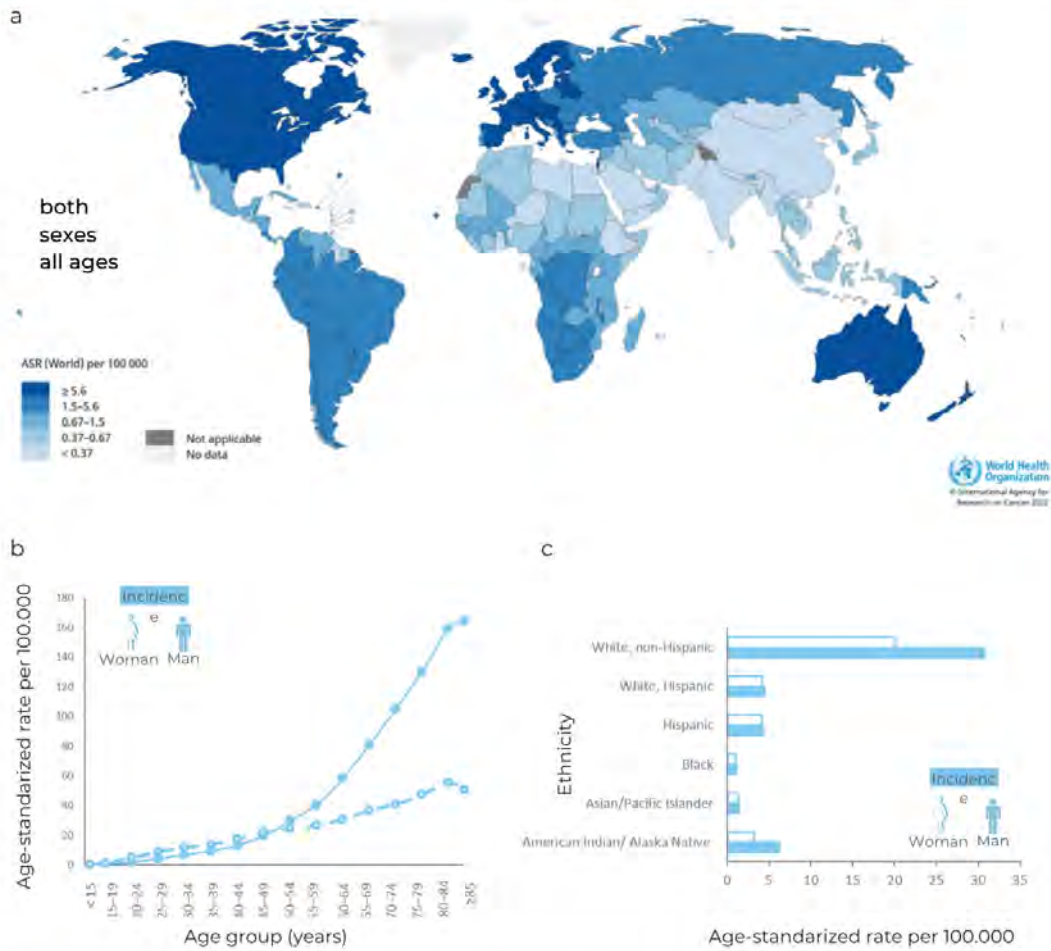


FIGURE 2
Melanoma incidence. (a) map showing estimated age-standardized incidence rate for melanoma of skin worldwide in 2020, both sexes including all ages. Dark blue represents more than 5.6 melanoma cases per 100,000 inhabitants, while light blue represents less than 0.32 melanoma cases per 100,000 inhabitants. Data obtained from globocan, (b) melanoma incidence in united states expressed as age-standardized incidence rate in 2020 by age group and, (c) melanoma incidence in united states expressed as age-standardized incidence rate in 2020 by racial/ethnic group. Data was obtained from national program of cancer registries, and surveillance, epidemiology, and results program

melanoma
age-standardized deaths rate per 100,000

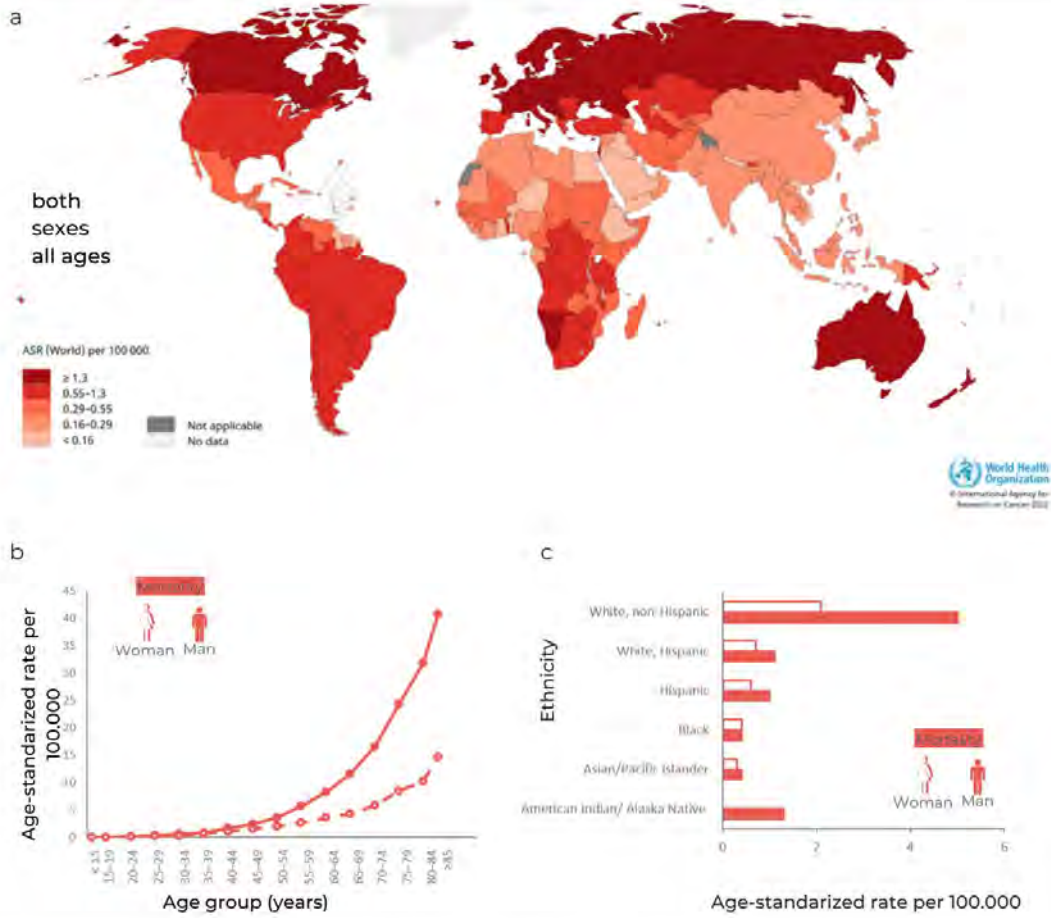


FIGURE 3 Melanoma mortality. (a) map showing estimated age-standardized deaths rate for melanoma of skin worldwide in 2020, both sexes including all ages. Dark red represents more than 1.7 melanoma deaths per 100,000 inhabitants, while light red represents less than 0.12 melanoma deaths per 100,000 inhabitants. Data obtained from globocan, (b) melanoma mortality in united states expressed as age-standardized incidence rate in 2020 by age group and, (c) melanoma mortality in united states expressed as age-standardized incidence rate in 2020 by racial/ethnic group. Data obtained from national program of cancer registries, and surveillance, epidemiology, and results program

Etiological factors for malignant melanoma

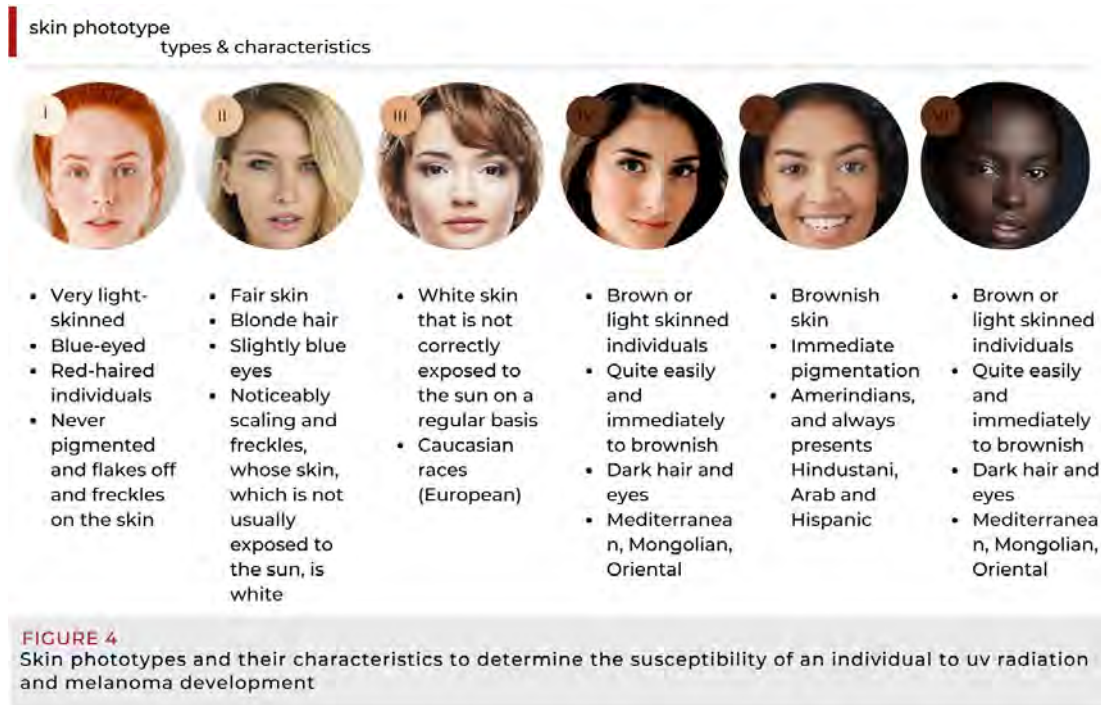
Factors contributing to the development of cutaneous melanoma can be grouped into those specific to the individual (e.g., skin phototype, genetic predisposition) and those specific to the environment.



In terms of grading melanoma risks, ultraviolet radiation would be among the most significant. In addition to sunlight, ultraviolet light can also be produced by artificial lighting systems, such as tanning beds (18). The wavelengths of this light range from 200 to 400nm, with the UVB wavelength being the most carcinogenic to the skin (19-20). By absorbing these waves, the melanocytes are compromised in their ability to repair DNA (21-22). Carcinogenesis is consequently caused by the accumulation of genetic alterations (23-24).

Our ability to tan is one of our natural defenses against solar radiation damages, such as sunburn. Every individual has a unique ability to adjust to the sun, which is determined by their skin phototype. Figure 4 illustrates the six types of skin phototypes.

As a result of their light skin, blond or red hair, freckles, blue eyes, and a light complexion, people with light skin phototypes are at greater risk of developing melanoma. (25,26). Additionally, it may be important to consider the age at which tanning began and the duration of the tanning behavior (27) because prolonged radiation exposure can cause skin burns that cause the genetic changes listed in the previous paragraphs to accumulate over time. Accordingly, there is a direct correlation between sunburns and melanoma development (25, 28).



As described in the epidemiology section, most phenotypic skin characteristics and sun exposure intensity are geographically determined, implying that the incidence of melanoma is also dependent on geographical location (Figure 2). Accordingly, the highest incidence rates have been reported in Australia and New Zealand, followed by Northern Europe (29).

Additionally, people with phototypes I and II tend to have pigmented nevi than those with other phototypes. Pigmented nevi are skin lesions characterized by the benign proliferation of melanocytes. Approximately 15% of melanoma derives from this lesion (30). Therefore, if a person has multiple pigmented nevi that vary in color and shape, they are at a higher risk of melanoma.

It is crucial to consider an individual's personal history in this context. It is essential to evaluate an individual's unique history in this context (31). Melanoma is one of the most immunogenic cancer, with spontaneous remission occurring in roughly 10% to 35% of cases (32). Consequently, immunodeficiency has also been shown to be associated with an increased risk of developing cancer (33). Additionally, almost 15% of melanoma occurs in patients with a family history, and a subgroup of these patients have germline mutations associated with melanoma predisposition (34-35). Despite this, the magnitude of this genetic factor is still unclear, which is why it is recommended that people with a family history maintain a careful examination of their skin and more frequent consultations with dermatologists (36).

Exposure to carcinogenic substances is another risk factor. A study has indicated that herbicides have been associated with a greater likelihood of developing acral melanoma (palms of the hands and feet).

This study revealed a higher incidence of acral melanoma in people who have used these herbicides at home is higher than in people who do not use them (37).

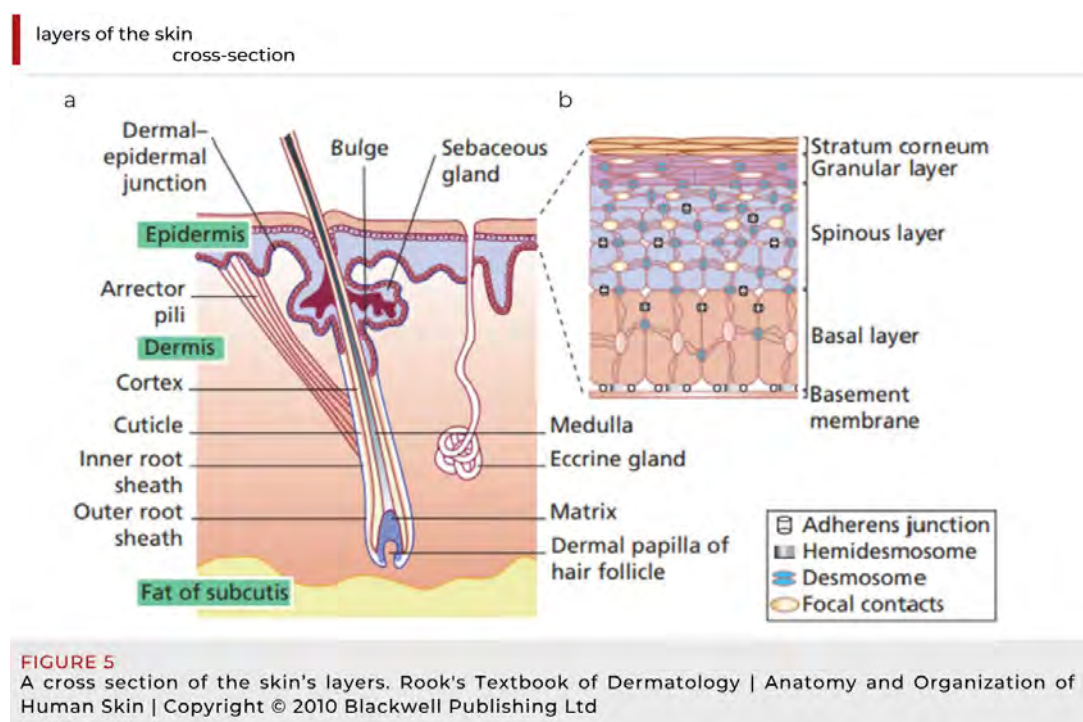
Histopathology of melanoma

Melanoma development

Malignant melanoma develops from melanocytes, melanin-producing cells. In addition to growing in the skin (95% of cases), melanoma can also develop in uvea and mucous membranes due to its embryonic origin at the neural crest.

Skin

Among all the organs of the body, the skin is the largest. As a barrier against physical, chemical, and biological agents, it provides the first level of protection, prevents water loss, and regulates body temperature. The human skin comprises three layers: the epidermis, dermis, and subcutaneous tissue (38) (Figure 5a).



In what has come to be known as the epidermis, the outermost layer is a stratified epithelium made up mainly of keratinocytes (representing 95% of the total cells in this layer), which migrates progressively from the epidermal basement membrane to the skin surface and forms several well-defined layers along the way. In the following order, the basal layer appears followed by the spinous stratum, the granular stratum, and finally, the stratum corneum (Figure 5b).

Another cell type in this layer is Langerhans cells, which function as part of the immune system, looking for antigens within their surroundings to activate an immune response, or Merkel cells, which are closely associated with terminal filaments of cutaneous nerves and are responsible for sensation (39-40).

Besides the epidermis, melanocytes are also present in that basal layer, having a ratio of one melanocyte per ten basal cells. As previously stated, the melanocytes produce the pigment melanin, which is packaged into cellular vesicles known as melanosomes, and delivered into the cytoplasm of the keratinocytes (40) to protect the body from the harmful effects of ultraviolet radiation.

A layer of tissue called the dermis lies beneath the epidermis. Blood vessels, nerves, glands, and hair follicles are found within this thick layer of connective tissue, which is tightly attached to the epidermis by the basement layer. It is connected to the underlying organs, such as bones or muscles, via the subcutaneous layer or hypodermis, which consists of loose connective tissue that contains variable amounts of adipose cells (cells that store fat), depending upon the area of the body and its nutritional requirements.

Melanoma skin cancer

According to the above description, skin melanoma arises from the malignant transformation of melanocytes in the epidermis. Among the molecular alterations, these cells undergo are mutations of genes responsible for regulating the cell cycle, differentiation, adhesion, signaling, and apoptosis. It involves acquiring diverse phenotypic features by normal melanocytes that lead to the development of a malignant phenotype. In the Clark model, one of the most popular, the significance of the histopathological changes related to the progression of melanoma is highlighted (Figure 6). The first phenotypic shift in melanocytes is the development of benign nevi. Despite disrupting the control of growth in these cells, the growth of a nevus is limited, and rarely progress to cancer (41). Oncogenes-induced cell senescence may be responsible for the absence of progression, in which oncogenes stimulate cell growth. From a molecular perspective, excessive activation of the mitogen-activated protein kinase (MAPK) signaling pathway promotes the development of melanoma cells. Activation of this pathway is caused by mutations in *NRAS*, which accounts for approximately 15 percent of melanoma, or mutations in *BRAF*, which account for about 50 percent of melanoma (42).

progression of melanoma

biologic events and molecular changes

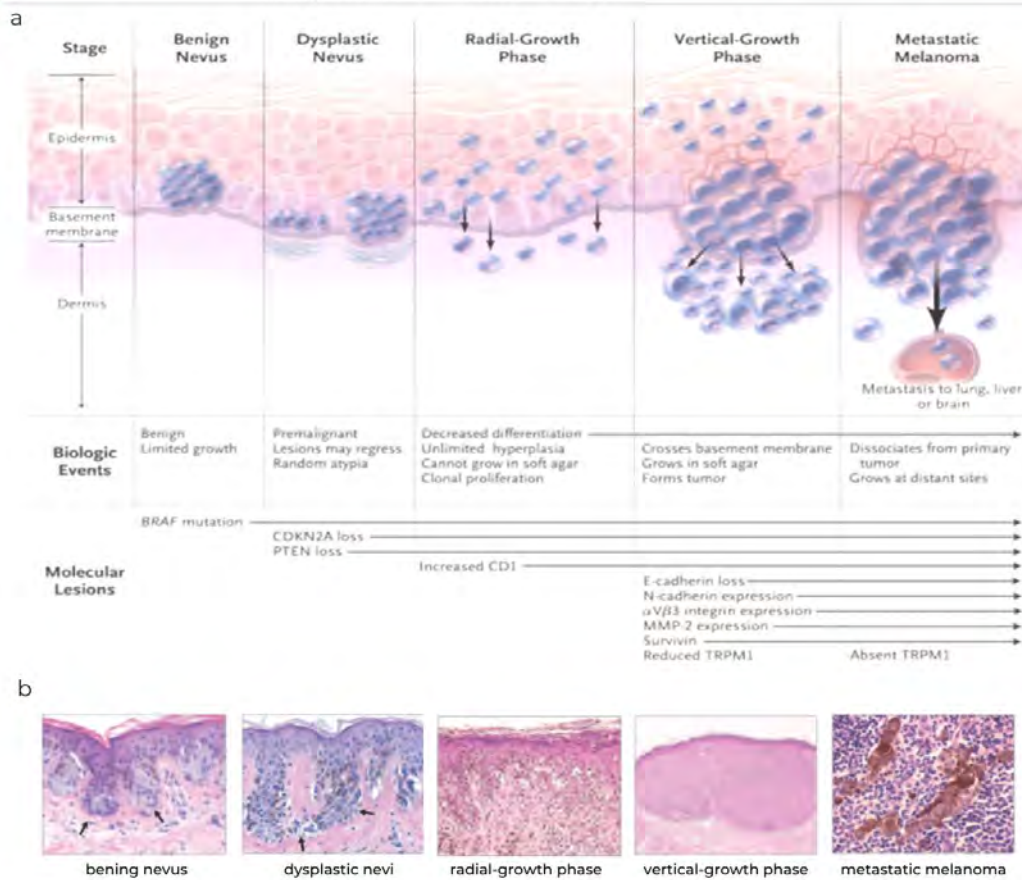
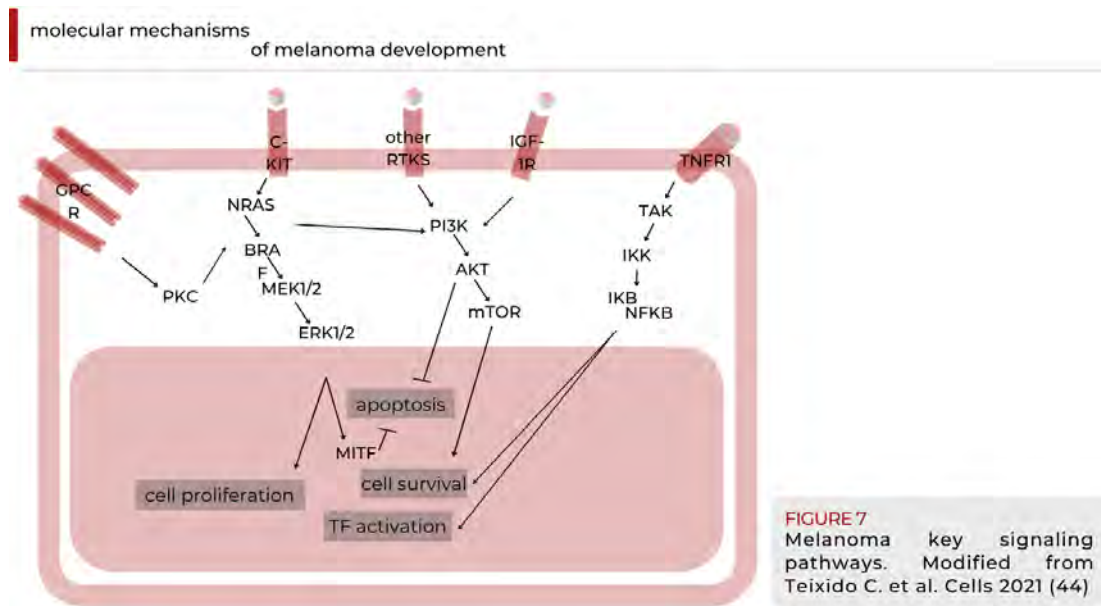


FIGURE 6 Biologic events and molecular changes in the progression of melanoma (a) graphic scheme and (b) histological sections. Arlo J. Miller | Copyright ©2006 The New England Journal of Medicine

Cytologic atypia, which may develop from preexisting benign lesions or as a new tumor, seems to be the next step towards melanoma following the Clark model. This stage of the disease progression involves molecular abnormalities that affect cell growth, DNA repair, and susceptibility to cell death. Next is the radial-growth phase, which refers to tumors that grow laterally along with the epidermis and do not metastatic spread. The condition can last for years, and cancer can be surgically removed with a high success rate. Manifestations of invasive behavior in Clark's model occur in the vertical-growth phase when melanoma cells penetrate the basement membrane and grow intradermally as expanding nodules. Even though this progression model is viewed as a linear stepwise process, many melanoma tumors may not adhere to it in an orderly manner. For example, RGP and VGP melanoma may result from existing nevi lesions or develop spontaneously from normal melanocytes (43).

In both cases, cancer spreads because of the uncontrolled growth of malignant tumor cells due to genetic mutations that cause neoplastic transformation and enable them to escape inhibitory signals. Several hallmarks of cancer characterize this process.

It has been shown that a comprehensive set of molecular pathways is involved in the initiation, proliferation, survival, progression, and invasion of a tumor. In this way, MAPK, PI3K, and NFκB signaling pathways interconnect significantly during melanomagenesis (Figure 7).



Essentially, stimulation of G protein-coupled receptors (GPCR) results in the activation of PKC protein. As a result, activated PKC stimulates the MAPK pathway. Additionally, the receptor tyrosine kinases (RTKs), activated through the binding of extracellular growth factor ligands, also mediate the activation of RAS protein, the top member of the MAPK cascade. Simultaneously, RTK turns on the PI3K path. PI3K may also be activated by GPCRs, IGF-1Rs, and RAS. Briefly, both MAPK and PI3K/AKT pathways mediate cell survival and proliferation. As part of the TNF-alpha pathway (canonical NFκB pathway), binding of the cytokine to its receptor TNFR1 results in activation of TAK1. TAK1 promotes the aggregation of a downstream kinase complex, IKK. In response to the phosphorylation of IκB by the IKK complex, NFκB is released. As a result, this element is translocated to the nucleus, leading to the activation of genes involved in cell survival and anti-apoptosis.

MAPK Pathway

It is well known that mitogen-activated protein kinase (MAPK) is an important signal transduction pathway for various physiological processes, including cell proliferation, differentiation, development, migration, apoptosis, and transformation (45). It is particularly relevant to the development of melanoma. In a normal situation, the MAPK cascade is regulated by scaffolding and regulatory proteins. One of that regulators is Raf Kinase Inhibitor Protein (RKIP), also known as phosphatidylethanolamine binding protein 1 (PEBP1) (46). Raf-1 and MEK are required for the phosphorylation of MEK and the subsequent phosphorylation cascade, and RKIP disrupted the physical interaction of Raf-1 and MEK proteins, reducing the path activation (46). Two mechanisms deregulate the pathway: the gain-of-

function mutations, which make the RAS and RAF proteins consistently present in the cell in their activated state irrespective of external stimuli, and the ineffectiveness of natural inhibitors, such as RKIP.

Concerning the first question, among the mutations most likely to be found in skin cancer is the BRAFV600 mutation of the *BRAF* gene (47). In addition, mutations affect the KRAS protein (mutant KRASQ61) and the neurofibromin 1 (NF1) protein. All of these mutations result in activation of the MAPK pathway and, consequently, in the proliferation and survival of cells (48).

Regarding the second one, it has been described a loss of RKIP expression in melanoma. Published data report the role of RKIP in regulating cell proliferation, migration, and invasion capability (49-51), by mechanisms leading to Ras-ERK1/2 and NFκB pathways inhibition. Nevertheless, there is little known about the pathways regulated by RKIP in normal melanocytes nor its role in the malignant transformation of this type of cell. Some studies (51,52) describe a gradual reduction of malignancy-related RKIP levels in melanoma patients, but these were performed with a small cohort of patients, so it would require a more extensive study to establish the real diagnostic or prognostic value of this marker in melanoma.

PI3K-AKT Pathway

The phosphatidylinositol-3-kinases (PI3Ks) are a family of lipid kinases involved in many cellular processes, including cell survival and growth, differentiation, proliferation, transcription, and translation. Besides transducing signals from growth factors and cytokines, the pathway is a major downstream effector of RTKs and G-protein-coupled receptors (GPCRs) (Figure 9). An essential component of this signaling pathway is AKT, which transmits signals by phosphorylating different downstream effector targets, influencing critical cellular processes, such as apoptosis, DNA repair, cell cycle, glucose metabolism, cell growth, and motility, invasion, and angiogenesis (53).

There are negative regulators to prevent persistent and long-term activation of PI3K-AKT signaling. PTEN is a central regulator of this signaling pathway. When PTEN is missing, AKT is constitutively activated, resulting in malignant melanoma tumor development (54,55).

NFκB Pathway

The nuclear factor-kappaB (NFκB) is a pleiotropic transcription factor that regulates several genes involved in many critical pathways that allow for a wide range of physiological functions such as immune responses, inflammatory responses, development, and cancer initiation and progression (56).

The NFκB family comprises five members identifiable by their conserved Rel homology domains, the part of the proteins that control DNA binding: RelA (p65), RelB, c-Rel, p100/p52, and p105/p50.

Regulation of NFκB family members occurs primarily through binding them by IκB proteins (57). Among the members of the IκB family is the proto-oncoprotein Bcl-3, which is predominantly located in the nucleus. It has been shown that Bcl-3 and Pirin, a member of the cupin superfamily, form a stable complex that enhances Bcl3-p50's ability to bind DNA, inducing transcription of various target genes involved in cell survival and antiapoptosis (58).

The effects of ultraviolet irradiation on skin cells include promoting inflammatory responses and cytokines, many of which have NFκB as a downstream target or effector. If the presence of NFκB is sustained, it may result in the augmentation of pro-inflammatory mediators, which may damage tissues, leading to organ dysfunction and eventually cancer (59). There are different mechanisms through which the activation of NFκB may occur due to upstream deregulation of MAPK and PI3K-AKT signaling pathways. In melanoma cells, these changes increase proliferation and resistance to apoptosis (60).

Melanoma heterogeneity and plasticity

Malignant melanoma is one of the most frequently mutated cancer. However, as described in the preceding section, driver mutations in genes such as *BRAF* or *NRAS* occur early in the course of melanoma development. In contrast, a hierarchical pattern has not been detected between mutations associated with metastasis, suggesting that transcriptional programs are involved in melanoma progression (61).

Two predominant transcriptional programs have been identified in cultured melanoma cells based on gene expression analysis: proliferative' phenotype or 'invasive' phenotype. Interestingly, the two phenotypes are not determined by genetic mutations, and transcriptional activity can reprogramme a phenotype. There is a balance between both phenotypes regulated by transcriptional master regulators, which enable cells to be capable of adaptive phenotype plasticity (61).

One evidence for adaptive phenotype plasticity can be found in single-cell analyses of melanoma biopsies, which have detected populations of cells with invasive or proliferative phenotypic states and single cells with transitional phenotypic forms. Based on this phenotype plasticity hypothesis, stable melanoma phenotypes are defined by transcriptomes relating to differentiated melanocytes or slow-cycling cells with neural-crest stem-cell (NCSC) markers (61). Tumor persistence seems to rely on a particular subset of cells with these acquired "stem cell-like" properties (62,63). Like embryonic stem cells (ESC), this subpopulation of tumor stem-like cells can grow intensively and infiltrate local tissue (52, 62-69). The self-renewal capability of embryonic stem cells is regulated by pluripotency-related transcription factors such as Nanog homeobox (*NANOG*), POU class 5 homeobox 1 (*OCT4*), and SRY-box transcription factor 2 (*SOX2*) (70) which are also aberrantly expressed in many malignant human tumors (71–73).

In melanoma, melanosphere formation has been found to increase *NANOG* expression (74). Moreover, *NANOG* and *OCT4* overexpression increases motility and transmigration of melanoma cells (75). In addition to the well-described role of *NANOG* as a crucial regulator of stemness maintenance, this transcription factor has also been implicated in regulating the epithelial-mesenchymal transition (EMT) (76). The EMT process has been classically linked to increased motility of cancer cells, favoring the disease's dissemination (77). This process, characterized by a cellular reprogramming towards a more mesenchymal phenotype, is often driven by the Snail transcriptional repressor (*SNAIL*), the bHLH transcription factor *TWIST*, and the Zinc Finger E-box-binding homeobox (*ZEB*) families (77). *NANOG* has been described as a direct activator of EMT-associated genes, including *ZEB1*, *ZEB2*, and microRNA-21 (miR-21) (78). Interestingly, the literature describes an intertwined signaling system between *SNAIL* and *RKIP*; *SNAIL* has been shown to repress transcription of *RKIP* while simultaneously, *SNAIL* has also been described as a downstream target of *RKIP* (79). Furthermore, a negative correlation has been found between *RKIP* and the expression of EMT regulators, including *ZEB1*, *ZEB2*, and *SNAIL* (79), although the underlying mechanism remains elusive.

On the other hand, the slow-cycling phenotype has also been associated with a subpopulation of cells that sustain the tumor bulk. One of the master regulators of retarded cell cycle is *JARID1B/KDM5B*, a lysine-specific histone demethylase that belongs to the jumonji/ARID domain-containing family of histone demethylases (80). The post-translational modification of histones plays an essential role in patterning transcriptional activation and repression. *JARID1B* is involved in regulating the G2/M checkpoint and late phases of the M phase. Moreover, *JARID1B* has been found to target genes involved in regulating development and determining cell fate. An earlier study demonstrated that *JARID1B* did not play a critical role in ESC self-renewal but was essential for ESC differentiation into neurons (81). Moreover, there has been evidence that *JARID1B* functions as a tumor suppressor in malignant melanoma since its expression levels are downregulated, and it inhibits cell proliferation in an Rb-dependent manner (82-84). In contrast, *JARID1B* has also been shown to promote melanoma maintenance and metastatic progression in immunodeficient mice (85,86).

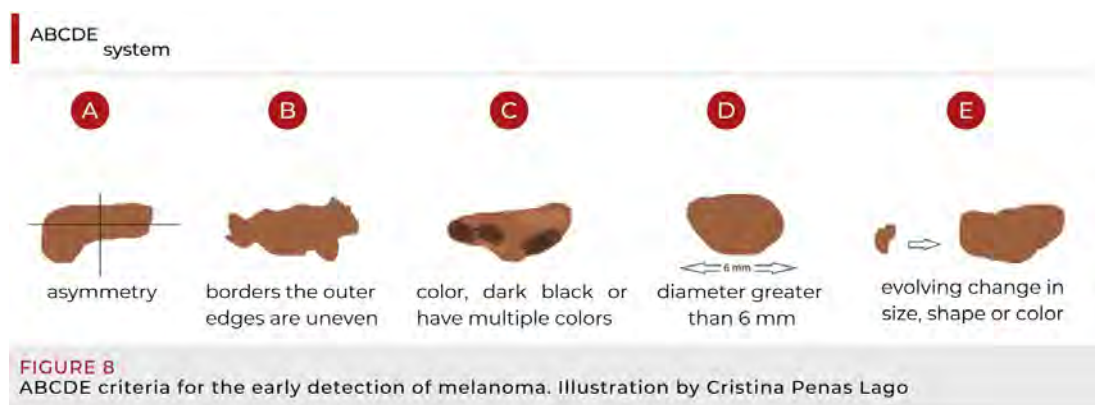
The result is a complex scenario in which melanoma cells can adjust their phenotype to meet external survival requirements. It would appear that while the switch from a proliferative to an invasive phenotype is more common, the pass from an invasive to a proliferative phenotype depends on the particular microenvironment. Therefore, cell reprogramming depends upon the cells integrating multiple signals over a prolonged time to transition from a slow-cycling, invasive state to a proliferating, differentiated state (81). Since phenotype plasticity plays an essential role in the initiation, progression, and resistance to melanoma therapy, it would be necessary to identify which transition represents the obstacle for the metastases for targeting it as a new therapeutic approach.

An overview of melanoma diagnosis and staging

An early diagnosis of the melanoma, can significantly increase the chances of survival. However, if the cancer is not removed surgically in time, it can become one of the deadliest forms of cancer if left untreated. For this reason, resources supporting early detection are very crucial.

ABCDE system

Lesions of melanoma are usually identified incidentally during a routine skin exam utilizing the ABCDE mnemonic. This method has been developed to aid physicians and patients in identifying specific characteristics often associated with melanoma, including asymmetry, border irregularity, color variation, a diameter greater than 6 mm, time of progression, or time of lesion growth (Figure 8). A pigmented lesion with any ABCDE-related characteristics should be considered suspicious for melanoma during a medical examination (87).



This method was initially described in 1985 (88). However, its validity has been questioned because melanomas lack ABCDE characteristics in many instances (35-40%), making their diagnosis difficult and inducing the likelihood that they will progress to more advanced stages. Some authors have attempted to address this issue by proposing to add the "FG rule" with F for firm and G for growth (89,90). Due to this, it is necessary to include additional criteria in managing suspicious melanoma lesions, such as the Clark and Breslow indexes.

Clark index and Breslow thickness

Wallace Clark developed in the 1960s a scale based on the histological evaluation of melanoma, known as Clark levels, taking into account the depth of the tumor and its impact on survival. He also described different types of melanoma and disproved the theory that all melanoma arises from nevi (91). According to W. Clark, there are five levels:

- Level I: melanoma cells are only confined to the epidermis. This condition is also known as melanoma in situ.
- Level II: the cells invade the papillary dermis under the epidermis.
- Level III: melanoma cells invade the papillary and reticular dermis junction.
- Level IV: the melanoma invades the reticular or deep dermis.
- Level V: the tumor grows to the subcutaneous fat beneath the dermis.

On the other hand, Alexander Breslow, a decade later, showed that the thickness of the lesion compromised the prognosis of the disease. This thickness is measured as the deepest penetration in millimeters. This also made it possible to differentiate which would be the population with the most significant benefit from lymph node dissection (92,93).

- Less than 1.00 mm: 5-year survival is 92-97%.
- From 1.01 to 2.00 mm: 5-year survival is 80-92%.
- From 2.01 to 4.00 mm: 5-year survival is 60-75%.
- More than 4.01 mm: 5-year survival is 50%.

With the implementation of the TNM standard staging system, the American Joint Committee on Cancer (AJCC) has solved this remarkable aspect of cancer symptoms a little differently with the ability for clinicians to determine the stage at which a given disease is. This system collects information about primary tumor (T), spread to lymph nodes (N), and the presence of distant metastasis (M). Over the past forty years, even though the Clark classification for cutaneous melanoma has been widely accepted by medical professionals worldwide, there have been observations that the index has limitations. This is especially true regarding histology subtypes such as acral lentiginous melanoma. Accordingly, the current AJCC staging system does not consider the Clark Level.

Before anything else, the TNM system takes into account the size and extent of the primary tumor, which is calculated on the Breslow scale to calculate tumor thickness, and it also considers ulceration. A second factor to consider is whether cancer has spread to nearby lymph nodes and whether a node has microscopic or macroscopic metastasis. Additionally, it allows the identification and classification of in-transit metastases (more than 3 cm away from the primary tumor but have yet to reach a lymph node) and satellite lesions (tumors larger than 0.5 mm found within the same histology section as the primary tumor). And eventually, the presence of distant metastasis (94). Each of these categories consists of several subtypes, as shown in Table 1.

Table 1. Description of the criteria used to classify the staging of melanoma (95)

Stage	Description
Tumor (T)	
Tx	Primary tumor cannot be assessed
T0	No evidence of primary tumor
Tis	Melanoma in situ. Precancerous lesion. Melanoma cells are found between the epidermis and dermis of the skin, and have not invaded yet these layers.
T1	Tumor ≤ 1 mm thick
T1a	Tumor ≤ 1 mm thick, no ulceration and mitotic rate $< 1/\text{mm}^2$
T1b	Tumor ≤ 1 mm thick, either with ulceration or mitotic rate $> 1/\text{mm}^2$
T2	Tumor 1-2 mm thick
T2a	Tumor 1-2 mm thick, no ulceration
T2b	Tumor 1-2 mm thick, with ulceration
T3	Tumor 2-4 mm thick
T3a	Tumor 2-4 mm thick, no ulceration
T3b	Tumor 2-4 mm thick, with ulceration
T4	Tumor > 4 mm thick
T4a	Tumor > 4 mm thick, no ulceration
T4b	Tumor > 4 mm thick, with ulceration
Node (N)	
Nx	Regional lymph nodes cannot be assessed
N0	No melanoma found in regional lymph nodes
N1	Melanoma found in 1 lymph node
N1a	Melanoma found in 1 lymph node, microscopic metastasis
N1b	Melanoma found in 1 lymph node, macroscopic metastasis
N2	Melanoma found in 2-3 lymph nodes
N2a	Melanoma found in 2-3 lymph nodes, microscopic metastasis
N2b	Melanoma found in 2-3 lymph nodes, macroscopic metastasis
N2c	In-transit melanoma or satellite lesions are found, without metastasis to lymph nodes. Melanoma is found in ≥ 4 lymph nodes, or in ≥ 2 lymph nodes that appear to be joined together.
N3	In-transit melanoma or satellite lesions are found, with metastasis to lymph nodes.
Metastasis (M)	
Mx	Metastasis cannot be assessed
M0	No metastasis
M1a	Metastasis to skin, subcutaneous tissues or distant lymph nodes
M1b	Metastasis to lung
M1c	Metastasis to any other distant organs
M1d	Metastasis to nervous system

Once all the information has been collected, a stage can be assigned (Table 2). In the case the tumor growth affects only the outermost layer of the skin, that is, the epidermis, the patient presents a stage 0 or melanoma in situ. These cases have the best prognosis, with surgery as the selected treatment. In addition, in this very fine melanoma, there is 30% of cases of spontaneous remission.

Generally, stage I melanoma invade the dermis layer but have not spread to the lymph nodes. This stage is sub-classified based on the thickness of the tumor mass. Thus, there is stage IA if the tumor is no more than 1 mm thick and with or without ulceration, and stage IB when the cancer is between 1 and 2 mm thick and does not present ulceration.

For its part, a stage II melanoma has invaded the deeper layers of the dermis, which carries more risk, but has not yet spread to the nodes. Stage IIA melanoma is more than 1 mm but not more than 2 mm thick with ulceration, or more than 2 mm but not more than 4 mm thick without ulceration. Stage IIB corresponds to tumors greater than 2 mm but not more than 4 mm thick, with ulceration, or greater than

4 mm thick, without ulceration. There is a third type, stage IIC, with the highest risk of spread among the stage II. In this case, the tumor is more than 4 mm thick and is ulcerated.

Table 2. Staging of melanoma based on TNM system (95)

Stage	T	N	M
0	Tis	N0	M0
IA	T1a	N0	M0
IB	T1b	N0	M0
	T2a		
IIA	T2b	N0	M0
	T3a		
IIB	T3b	N0	M0
	T4a		
IIC	T4b	N0	M0
		N1a	M0
IIIA	T1-T4a	N2a	M0
		N1a	
		N2a	
IIIB	T1-T4b	N1b	M0
		N2b	
		N2c	
IIIC	T1-T4b	N1b	M0
		N2b	
		N2c	
IV	Any T	N3	M1
	Any T	Any N	

The advanced stages of the disease correspond with stages III and IV. A stage III melanoma diagnosis implies that the tumor cells have spread to the nearest lymph nodes, but there are no observable distant metastases. Stage III melanoma is subdivided into IIIA, IIIB, and IIIC. In any of them, the thickness of the tumor is not taken into account, but rather the number of nodes affected (1 node in the case of stage IIA, between 2-3 for stage IIB, and more than 4 for subclassification IIIC). Stage IV would correspond to distant metastasis of both lymph nodes and other organs. The TNM system makes it possible to encode the target organ to which the melanoma has spread, M1A the skin, M1B the lung, M1C other organs, and, the most advanced form, M1D that invades the central nervous system.

Clinical and molecular classification of melanoma

Histological classification

Histopathological diagnosis and classification of melanocytic lesions is probably the most significant conceptual and practical challenge in modern dermatopathology. According to traditional classifications, melanoma can be divided into four clinical types depending on their anatomical localization and evolution (96).

In situ/Superficial Spread Melanoma (SSM) manifests as a pigmented macule of irregular shape that may eventually become a large papule or plaque if invasion occurs. Melanoma in situ is defined as a proliferation of malignant melanocytes in the epidermis, whereas invasive SSM manifests as a proliferation of atypical melanocytes in the superficial dermis. This type of melanoma is most prevalent among Caucasians and represents 70-80% of all cases of melanoma in this ethnic group. The most common presentation site is sun-exposed skin, such as the trunk and back of males' and females' back and lower limbs. About 40% of SSMs are derived from preexisting lesions such as common or dysplastic nevi (Figure 9a-b) (97,98).

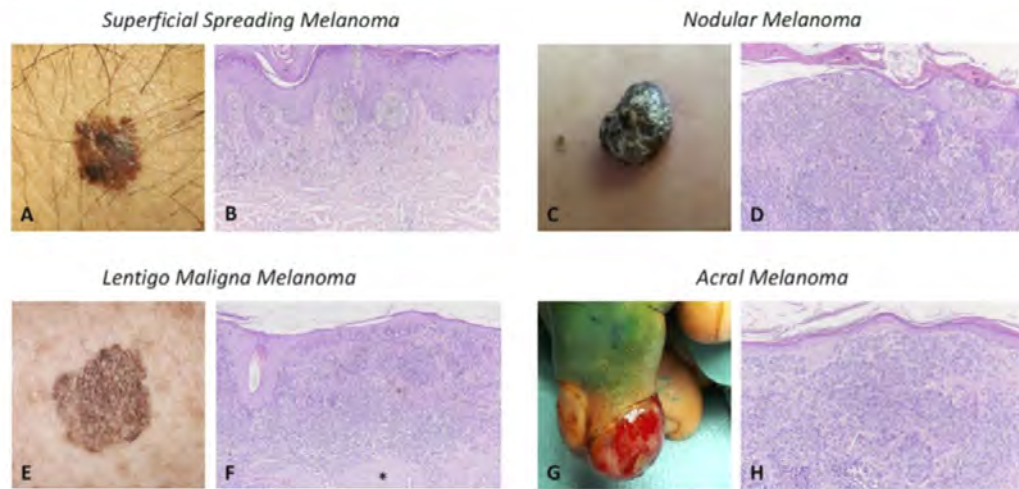


FIGURE 9
Histological subtypes of melanoma and clinical-pathological correlations (a-b) superficial spreading melanoma, (c-d) nodular melanoma, (e-f) lentigo maligna melanoma and (g-h) acral melanoma. Cristian Scatena | Copyright ©2021 Frontiers in Oncology (96)

A **nodular melanoma** (NM) forms a brown-to-black, nodular tumor, often eroding in appearance, characterized by a vertical growth phase. Even though it is the second most prevalent type of melanoma, with an incidence of 15-25%, it is considered the most aggressive because it exhibits rapid growth that begins immediately after the vertical phase. Middle-aged patients usually experience this problem on their head, neck, or trunk, and men are more likely to experience it than women (Figure 9c-d) (99,100).

Located mainly on sun damaged surfaces, such as the face of Caucasian elderly individuals, **Lentigo Malignant Melanoma** (LMM) is an invasive form of melanoma in situ/lentigo maligna. On a histological basis, lentigo maligna is defined as a proliferation of lentiginous spindle melanocytes along the base of the epidermis that usually does not invade the dermis. In this case, the lesion is larger than 3 cm, multicolored (different shades of brown and black), and features elevated areas (Figure 9e-f) (101,102).

Finally, a microscopic examination of the extremities is required to diagnose **Acral Lentigo Melanoma** (ALM). ALM is a slow-growing macule/plaque or nodule present in the subungual or palmoplantar/volar zones with poorly circumscribed pigmentation. It is important to note that ALM occurs more commonly in Black (60-70%) and Asian (35-45%) populations than in individuals with fair skin (<5%). Since they are also large, irregular, and black in appearance, they can be confused with lentigo malignant melanoma (Figure 9g-h) (100,103,104).

It may be worth mentioning that there are many less common variants of melanoma, such as spitzoid melanoma, small cell melanoma, malignant blue nevus, desmoplastic melanoma, and ocular melanoma (conjunctival or uveal) and mucosal melanoma, amongst others (105).

Molecular features of melanocytic lesions

The morphological criteria for determining atypia are often disagreeable and subject to inter-observer variability, particularly in non-conventional diagnoses lesions. Considering these challenges, the World Health Organization (WHO) incorporated known molecular pathways into its latest classification of melanocytic tumors, introducing the concept of "intermediate" lesions (97). This multidimensional classification suggests that the conventional approach of identifying melanocytic tumors as either benign or malignant may no longer be adequate. WHO 2018 identifies nine categories or pathways leading to melanoma, each driven by genetic factors (Table 3).

As a result of these molecular signatures' heterogeneity, two critical implications emerge: first, it emphasizes the need for individualization of melanoma diagnosis, prognosis, and treatment; second, it offers a broad range of potential biomarkers and novel putative therapeutic targets. In dermatology, the following antigens/antibodies are commonly used to diagnose melanoma (106,107):

The frequency of S100 expression in malignant cutaneous melanoma is approximately 95%. Several factors can influence its expression, including too much or too little fixation time, previously frozen tissue, and enzymatic pretreatment with trypsin. Antibodies can be polyclonal or monoclonal, and both identify melanocytosis in a cytoplasmic and nuclear manner. Among the many antigens detected by anti-S100, A6 is expressed by some melanocytotic lesions and may also be helpful when detecting neurotheliomas.

The Melanoma Antigen Recognized by T Cells-1 (MART1) is one of the most important melanocytic markers. Two different antibodies detect the antigen (Melan-A and A-103), expressed by a wide range of benign and malignant melanocytic lesions. Consequently, it is of great value in detecting melanocytic differentiation. On the other hand, a diagnosis of desmoplastic melanoma is unlikely if this marker is highly expressed in a spindle cell melanocytic lesion.

Table 3. Classification of melanoma based on 2018 world health organization classification (97)

UV exposure	Categories	Melanoma subtype	Key molecular genes
Low-CSD melanoma	Pathway I	Superficial spreading melanoma	BRAFV600 mut TERT mut CDKN2A mut PTEN mut NRAS mut TP53 mut
High-CSD melanoma	Pathway II	Lentigo maligna melanoma	NRAS mut TP53 mut KIT mut CDKN2A mut TERT mut PTEN mut BRAFnon-V600Emut
	Pathway III	Desmoplastic melanoma	NF1 mut NRAS mut NFKBIE mut PIK3CA mut
Low or no UV /CSD melanoma	Pathway IV	Spitz melanoma	ALK rearr CDKN2A mut NTRK1 rearr HRAS mut NRTK3 rearr
	Pathway V	Acral melanoma	KIT mut ALK rearr NRTK3 rearr CDKN2A mut CCND1amp TERT mut NRAS or BRAF mut
	Pathway VI	Mucosal melanoma	KIT mut SF3B1 mut CDKN2A mut CCND1 amp CDK4 mut MDM2 amp NRAS or BRAF mut
	Pathway VII	Melanoma arising in congenital nevi	NRAS mut BRAFV600E mut
	Pathway VIII	Melanoma arising in blue nevi	GNA11 mut GNAQ mut CYSLTR2 mut SF3B1 mut BAP1 mut EIFAX mut
	Pathway IX	Uveal melanoma	GNA11 mut GNAQ mut CYSLTR2 mut PLCB4 mut BAP1 mut EIFAX mut SF3B1 mut
May occur in any or most of the pathways		Nodular melanoma	
<i>Abbreviations: amp, amplification CSD, cumulative sun damage mut, mutation rearr, rearrangement</i>			

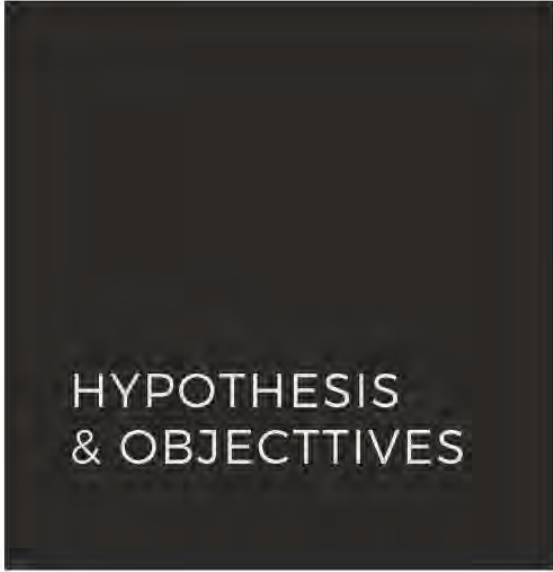
The anti-HMB45 antibody detects the premelanosome protein (PMEL or gp-100) in melanoma and junctional nevi. The expression of gp100 in primary cutaneous melanoma differs from that of nevi since it is often distributed in patchy patterns throughout the dermis. This pattern is also found in nevoid melanoma. It is especially useful in detecting the pattern of nevi maturation. Accordingly, superficial type Amelanocytes (epithelioid cells located within the epithelium or close to the epithelium and predominantly pigmented) express neuronal markers and gp100. In contrast, deeply located type C melanocytes (spindle cells) express schwannian markers. However, it has been proven to be insensitive to desmoplastic malignant melanoma.

Proliferation markers such as MIB1 (detected by anti-Ki67 antibody) are expressed in proliferating cells. Similar to gp100, its pattern of expression indicates whether or not a tissue has matured. A small percentage of cells in both common and dysplastic nevi exhibit reactivity, which is typically located at the dermalepidermal junction or in more superficial dermis compartments. Melanoma, on the other

hand, display a random pattern of immunoreactivity and typically have a proliferative fraction of over 10%, particularly near the edge of the lesion.

The enzyme tyrosinase (TYR) participates in melanogenesis and therefore is relatively specific for the differentiation of melanocytic cells. However, it also exhibits a lower sensitivity to detect desmoplastic melanoma.

In the manner described, the tissue markers S100, MART-1, and gp100/HMB45 can be used to differentiate melanoma from other types of cancer, but none of these markers can accurately distinguish non-malignant melanotic lesions from malignant melanoma, nor are they able to stratify melanoma patients by their risk of progression.



HYPOTHESIS
& OBJECTIVES

01

Background

02

Hypothesis

03

Objectives

04

Methodological
strategy

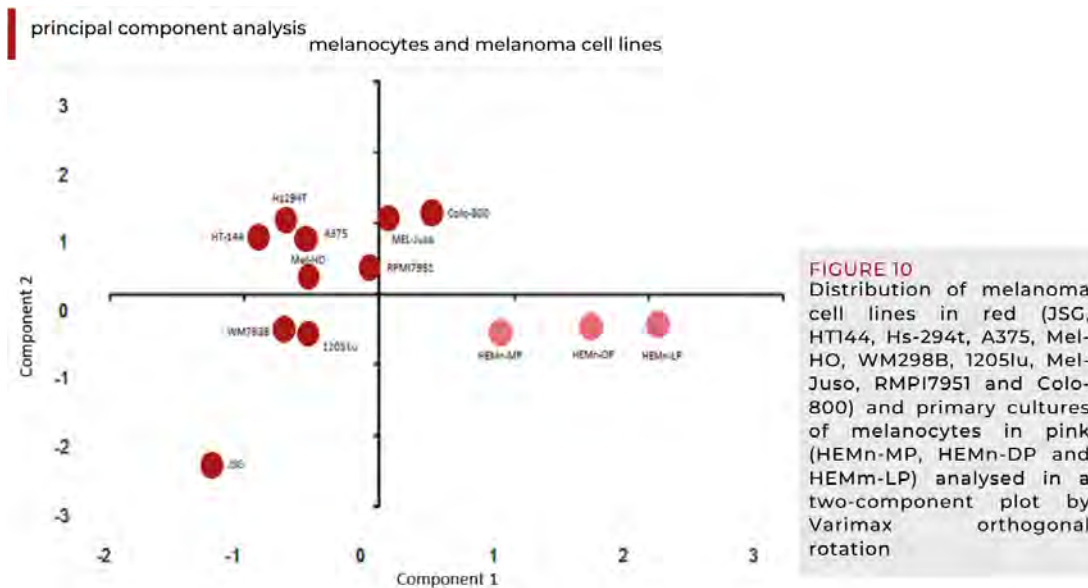
Hypothesis and objectives

Background

Although cutaneous melanoma account for less than 5% of all skin cancer, they are the deadliest due to their propensity to metastasize and a lack of effective treatment at advanced stages. Currently, the diagnosis and prognosis of malignant melanoma are mainly based on the evaluation of biopsies of skin lesions removed from patients. Clinicians determine a melanoma patient's prognosis based mainly on the Breslow and the presence of ulceration and sentinel nodes (108). It has been reported that 10% of melanoma recurrences within five years of follow-up have occurred in the early stages (I and II according to the 8th edition of AJCC) (109). In this context, it has been recently found in a study involving 784 patients that 53.8% of patients with metastatic melanoma had an initial stage of I-II (110). Therefore, it would appear that conventional risk markers are not detecting many early melanoma with the potential to metastasize.

The most critical aspect of reducing melanoma deaths is identifying markers that can be used for early stratification of melanoma, particularly those with a worse course. Related to the latter group, there is a need to understand the biology of thin melanoma that is ultimately lethal.

In previous work by our research group, the differential proteomic analysis that included melanoma and primary melanocyte lines highlighted several novel candidate markers of cutaneous melanoma (111). In the principal component analysis, where mRNAs and proteins of *RKIP* and *PIR* were analyzed showed the highest significance in terms of expression between healthy primary melanocytes (HEMn-MP, HEMn-DP, and HEMm-LP) and melanoma cells (JSG, HT144, Hs-294t, A375, Mel-HO, WM298B, 1205lu, Mel-Juso, RMPI7951, and Colo-800) (Figure 10).



In its original description, RKIP was an inhibitor of MAPK or ERK1/2 pathways. However, later studies revealed its additional role as a regulator of other signaling cascades, such as GPCR, GSK3b, and NF- κ B (46,112). It functions as a signaling switch in essential processes such as differentiation, proliferation, and survival of cells. The deregulation of this protein has been associated with a wide variety of diseases, including cancer (113-115).

As far as *PIR*/Pirin is concerned, it was initially described as a ubiquitously expressed nuclear protein with a putative function as a transcriptional cofactor (116). Over time, several studies have revealed that this protein plays an essential role in processes such as cell cycle regulation (117-119), inflammatory response (120,121), migration regulation, and epithelial-mesenchymal transition regulation (122-126).

Based on our results quantifying mRNA levels by RT-PCR, RKIP expression was generally reduced in melanoma cell lines compared to primary normal melanocytes (Figure 11a). We found that the protein level of RKIP was also consistently reduced in melanoma cell lines with no change in primary cell lines (A375, Colo-800, WM793B, Mel-Ho, and Mel-JUSO) or metastatic cell lines (1205Lu, A2058, Hs294t, HT-144, MeWO, and RPMI7951) (Figure 11b).

A lower expression of the *PIR* gene was also observed in melanoma cell lines compared to melanocytes (Figure 11c). However, comparing melanoma cell lines, it was found that *PIR* mRNA levels were more heterogeneous than in the *RKIP* study. As a result, we observed a much lower amount of Pirin protein in all melanoma cell lines than in melanocytes (Figure 11d). Consequently, these markers were licensed under a European Patent (No. EP3051291. Method of Diagnosis and prognosis of cutaneous melanoma).

RKIP and Pirin expression in cell lines

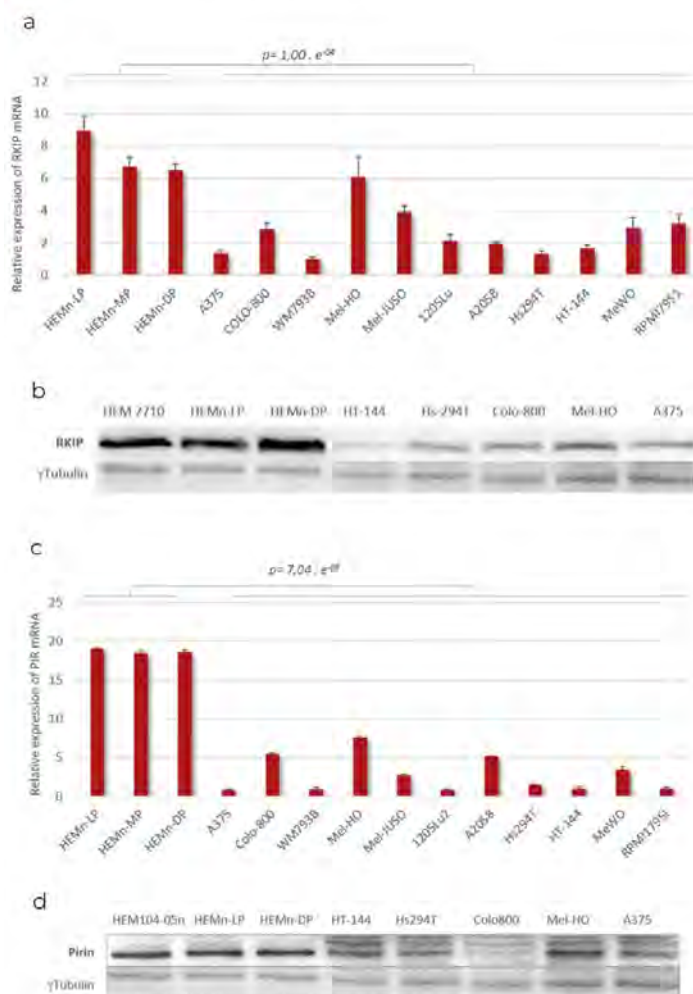


FIGURE 11
 RKIP and Pirin expression in cell culture of melanocytic cells. Using RTqPCR analysis, mRNA expression for RKIP (a) and Pirin (c) were assessed in primary melanocytes (HEMn-MP, HEMn-DP and HEMm-LP), primary melanoma cell lines (A375, Colo-800, WM793B, Mel-HO, Mel-JUSO) and metastatic melanoma (1205Lu, A2058, Hs294t, HT-144, MeWO, RPMI7951) Protein expression was determined by western blot using RKIP antibody (b) and Pirin Antibody (d) in three melanocytes cell lines and five melanoma cell lines. Tubulin expression was used as loading control. Figure is representative of three independent experiments

Hypothesis

According to our previous results, we maintain the hypothesis that RKIP and Pirin are proteins that could play a role in the etiopathogenesis of cutaneous melanoma, making them excellent biomarkers for diagnosis and prognosis of cutaneous melanoma.

Objectives

To achieve the hypothesis, we set the following specific objectives:

OBJECTIVE 01	OBJECTIVE 02	OBJECTIVE 03
Validate the expression of RKIP and Pirin protein as a good diagnostic and prognostic marker of melanoma	Assess the effects of RKIP and Pirin on the biological functions of melanocytes	Determine whether RKIP and Pirin contribute to the progression of melanoma
		
methodological approach	methodological approach	methodological approach
<ul style="list-style-type: none">• Retrospective cohort study• Immunohistochemistry (IHC)• Clinicopathological data correlation analysis	<ul style="list-style-type: none">• Healthy melanocyte cell lines• Down regulation of both <i>RKIP</i> and <i>PIR</i> independently by lentiviral particles• RNA Sequencing• Gene ontology enrichment <i>in silico</i> analysis• Validation of results	<ul style="list-style-type: none">• Melanoma cell lines• Overexpression of both <i>RKIP</i> and <i>Pirin</i> independently by expression plasmids• <i>In vitro</i> functional assays such as proliferation, migration and invasion• Validation of results by cotransfections and molecular determination



MATERIAL
& METHODS

01

Patients

02

Cell cultures

03

Gene modulation

04

Functional analysis

05

Molecular analysis

Material and methods

Patients

Ethics statement

Informed consent was obtained from all subjects, and the Ethics Committee approved the study of the Basque Government. A brief overview of the informed consent includes information regarding the project title, the principal investigator, funding sources, the study's purpose, data processing, and confidentiality, among other details. The full document can be read in *Annex A*.

Recruitment and managements

The patients were diagnosed at the Dermatology Services of Cruces and Basurto University Hospitals (Bizkaia, Spain) and the Oncology Service at the Onkologikoa Hospital (Gipuzkoa, Spain). The inclusion criteria were:

1. A histologically confirmed diagnosis of the nevus or malignant melanoma,
2. No treatment except primary surgery,
3. No infection as judged by clinical evaluation and the absence of any increase in parameters related to infections in the blood

After lesion examination, patients were subjected to surgery, where a tumor biopsy was taken for pathologic examination. Then, the staff of the Biobank proceeded to extract a blood sample. This service was responsible for maintaining blood samples, DNA extracted from blood, serum, and FFPE tumor biopsy in optimal storage conditions. After surgery of the primary tumor, clinical check-ups were scheduled every three months for the first two years of the follow-up and every six months thereafter until a five-year follow-up had been completed. Annual revisions were then scheduled up to the tenth year post-surgery. The patients who developed metastasis during the follow-up period were again examined every three months for two years after their metastasis had been diagnosed. The presence or absence of metastasis was assessed in all patients by physical examination and through laboratory and radiological testing (X-rays and/or computed tomography -CT- scanning). Metastases were detected in 92 of the 239 melanoma patients studied (38%), including those in whom the disease had already spread at the moment of diagnosis. Disease stages were classified according to the AJCC 8th edition [19], and each patient's clinical and diagnostic data was collected retrospectively from centralized electronic and/or paper medical records. For the statistical prediction analysis, only melanoma patients at early disease stages (I and II) were considered (159 subjects in total), and inclusion in the “disease-free” group required a minimum tracking of 2 years.

FFPE tissue samples and immunohistochemistry

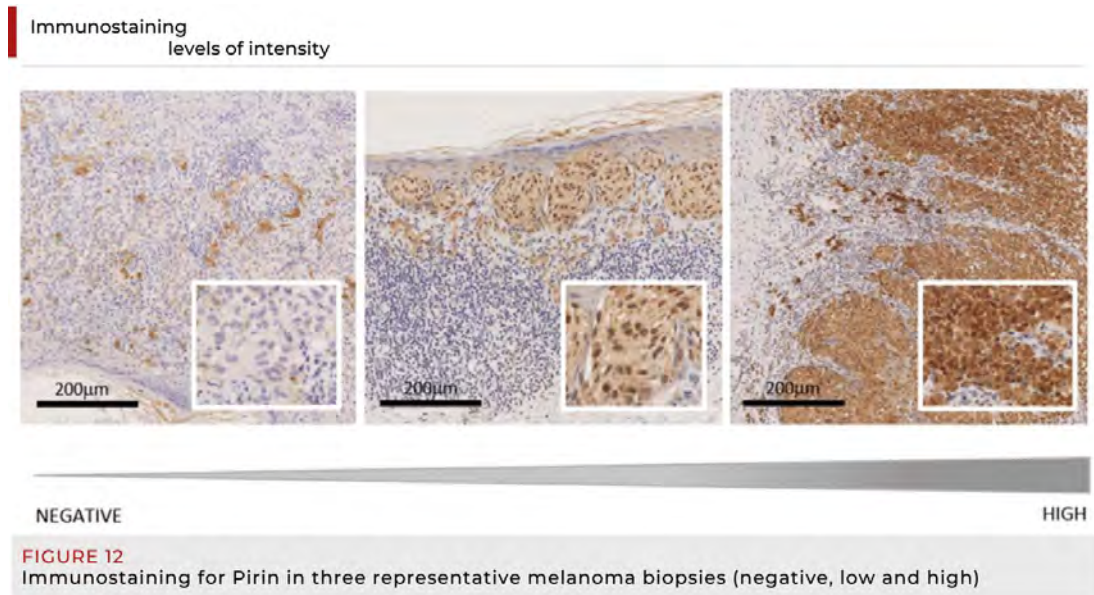
Immunohistochemistry is a methodology based on the reaction between the antigens and antibodies. It is a routine diagnostic method in hospitals, which functions as clinical decision support. A total of 75 nevi and 239 skin melanoma tumor sections (4 µm thick) from formalin-fixed paraffin-embedded (FFPE) blocks were collected on Superfrost plus glass slides (15438060, Thermo Fisher Scientific, USA) for both hematoxylin and eosin staining (H&E) and immunohistochemistry.

The expression of RKIP and Pirin in tissue sections was analyzed by immunohistochemistry (IHC) using the Autostainer Link 48 (Agilent Technologies, Inc, USA) and the reagents comprised in the Dako EnVisionFLEX kit. Before IHC staining, deparaffination and optimized antigen retrieval for each marker (low or high pH) were performed using the PTLINK (Agilent Technologies, Inc, USA) equipment with the manufacturer buffers. Specific antibody references, working dilutions, and antigen retrieval conditions used for each selected marker are detailed in Table 4.

Table 4. Details of sources and concentrations of antibodies used for Immunohistochemistry in this study

Antibody name	Retrieval	Dilution	Reference
Recombinant Anti-RKIP antibody	Low (acid pH)	IHC: 1:250	Abcam, UK ab76582
Anti-Pirin rabbit polyclonal antibody	Low (acid pH)	IHC: 1:500	Thermo Fisher Scientific, USA PA5-29777
Labelled Polymer-HRP		-	Agilent Technologies, Inc, USA K4065

All the sections were counterstained with hematoxylin, and one unit from each biopsy was stained with Haematoxylin- Eosin (H&E) to adequately study the tumor. All involved reagents, except for the specific antibodies, were manufactured by Dako (Agilent Technologies, Inc, USA). Sections were rinsed with EnVision FLEX Wash Buffer after each incubation step until the antibody binding visualization. All procedures were performed at room temperature unless otherwise specified. Heat-induced antigen retrieval was carried out using EnVision FLEX Target Retrieval Solution Low pH for 20 min at 98°C before IHC. After endogenous peroxidase quenching, sections were incubated with specific antibodies and with a secondary reagent (FLEX mouse or rabbit linker) for 15 min each. After a 20 min incubation with HRP-labelled polymer, antibody binding was visualized by incubating with Liquid DAB+ Substrate Chromogen System for 10 min. Sections were counterstained with hematoxylin, dehydrated with alcohol and cytosol, and mounted on glass coverslips. Then, the sections were scanned using Aperio Imagescope software (Leica Biosystems, Spain) or NanoZoomer S210 Digital slide scanner (Hamamatsu Photonics K.K., Japan), and two independent observers determined expression quantification according to staining intensity: (0) negative, (1) low, or (2) high staining (Figure 12).



Data analysis

In all quantitative tests, the SPSS version 26 program was used. Fisher exact test was applied to check the normality of the data. To compare differences between the two groups, Student's t-test was performed. $P < 0.05$ was considered statistically significant, $P < 0.01$ was considered highly statistically significant. Multiple comparisons were made using analysis of variance (ANOVA). Statistically significant differences were considered from $p < 0.05$.

Statistical analysis of RKIP expression data was performed using R 3.4.4. Univariate statistical testing between categorical features (Sex, Melanoma Evolution, and Diagnosis between Melanoma and Nevus) was assessed by a Pearson's chi-squared test. In contrast, the Cochran-Armitage Test was employed when ordinal variables were involved (RKIP and AJCC stage). Likewise, statistical differences between two or more groups were estimated by a two-tailed Kruskal–Wallis test or ANOVA if the normality assumption measured by the Shapiro–Wilk test was satisfied. Finally, a general linear model was employed for multivariate analysis, with an orthogonal polynomial contrast expansion in RKIP, assuming equally spaced levels. All p-values were computed non-parametrically using the R package “coin” (127) and corrected for multiple comparisons using an FDR controlling procedure (128).

On the other hand, the methodology employed for the analysis of Pirin was a bivariate statistical testing of categorical parameters (e.g., sex and melanoma prognosis) with Pearson's chi-squared tests. In contrast, the Cochran-Armitage Test was employed when the Pirin was involved. Statistical differences between two or more groups were estimated with a two-tailed Kruskal-Wallis test or by ANOVA if normality was assumed based on the Shapiro-Wilk test. A logistic regression model was employed to test the association between Pirin and prognosis, adjusting for possible sources of co-variation. For this analysis, marginal effects were also computed (129). Finally, a Cox Proportional-Hazard model was

established to test the association of Pirin with the onset of metastasis (measured in months). All p-values were computed non-parametrically using the R package “coin” (130), controlling for the false discovery rate (FDR) in the case of multiple testing (128), and statistical evidence of the effects was quantified using the BIC (Bayesian Information Criterion) and Bayes factors (131). The Bayes Factors indicate the probability of the alternative hypothesis (in our case, there is an association of Pirin expression with metastasis) relative to the null hypothesis (no association of Pirin expression with metastasis) and vice versa, such that: $BF_{01} = \text{Probability (Null Hypothesis)} / \text{Probability (Alternative Hypothesis)}$; and $BF_{10} = 1 / BF_{01}$ (the inverse). All the analyses were carried out using R version 3.6.1.

Cell cultures

Maintenance

In this work, three primary melanocytes and four melanoma cell lines were used (Table 5). The cells were routinely cultured in T-25 flasks (83.3910, Sarstedt AG & Co., Germany) in a monolayer. They maintained in their corresponding medium supplemented with either 1X Human Melanocyte Growth Supplement or 10% FBS, 2 mM L-Glutamine, and a 100 µg/mL antibiotic solution streptomycin and 100 IU/ml of penicillin. All lines were incubated inside incubators with a humid atmosphere (saturated with 95% water vapor) at 37°C and 5% CO₂. For their subculture, the cells were washed with PBS and trypsinized with a Trypsin-EDTA solution for 1 min at 37°C. After this time, the trypsin was inactivated with SBF, and the solution was centrifuged at 200 xg for 5 min. The supernatant was removed, and the pellet was resuspended with fresh medium. Cell numbers were counted using a Bürker counting chamber (BrandTech® Scientific Inc., Germany) and a 1: 1 ratio of trypan blue (Sigma-Aldrich Quimica, S.A., Spain). Trypan blue is a vital dye capable of crossing the broken membranes of dead cells so that dead cells appear stained blue. In contrast, living cells do not incorporate it and are refractive when viewed under an inverted microscope. Once the total number of cells had been calculated, and the cell viability had always been found to be greater than 95%, the desired number of cells was seeded in a new culture flask for maintenance. Cells in the exponential growth phase were always used for the experiments.

Freezing and thawing

Most primary cells, such as primary melanocytes used in this study, have a limited lifetime, except primary cells isolated from tumors. To avoid problems derived from the uninterrupted cultivation of the cell lines (genetic alterations, contaminations, etc.), they were kept in culture for a certain number of passages (approximately 20 passages, two months). After this period, they were removed and replaced by new cells. For this reason, a stock of frozen cells of each cell type was maintained, allowing us to replenish the line at any time needed.

Freezing

Once trypsinized and counting, the exponentially growing cells were centrifuged at 200 xg for 5 min. Once the supernatant had been removed, the pellet was resuspended at a concentration of 2-3 x 10⁶ cells/mL, depending on the cell line, in SBF with 10% DMSO. After resuspending the cells in the freezing medium, 1 ml of the suspension per cryovial was pipetted, and the cryovials were introduced into a Mr. Frosty™ freezing container (Thermo Fisher Scientific, USA) to keep them at -80°C for 24 hours in a deep freezer. This container holds isopropanol and allows a gradual decrease in temperature until freezing, minimizing the formation of crystals and, therefore, cell damage and death during this process. Finally, after 24 hours at -80°C, the cryovials were stored in liquid nitrogen, where they were kept at -196°C until their new use.

Table 5. Melanocyte and melanoma cell lines specifications

Cell line	Origin	Culture specification	
HEMn-LP	Invitrogen_C-002-5C. Lightly pigmented neonatal foreskin	Medium 254; 1X Human Melanocyte Growth Supplement	
HEMn-MP	Invitrogen_C-102-5C. Moderately pigmented neonatal foreskin	Medium 254; 1X Human Melanocyte Growth Supplement	
HEMn-DP	Invitrogen_C-202-5C. Darkly pigmented neonatal foreskin	Medium 254; 1X Human Melanocyte Growth Supplement	
A375	ATCC_CRL-1619. Human malignant melanoma, primary. Female. BRAF V600E	Innoprot_ACC62. Human malignant melanoma, primary. Female BRAF V600E	DMEM; 10% FBS; 2 mM L-glutamine; 100 UI/mL Penicillin; 100 µg/mL Streptomycin
MelHO	ATCC_CRL-11147. Human malignant melanoma, metastatic lymph node. Male. BRAF V600E	DMEM; 10% FBS; 2 mM L-glutamine; 100 UI/mL Penicillin; 100 µg/mL Streptomycin	
A2058	ATCC HTB-65. Human malignant melanoma, metastatic lymph node. Male. BRAF WT	RPMI 1640 GlutaMAX™; 10% FBS; 100 UI/mL Penicillin; 100 µg/mL Streptomycin	

Thawing

Thawing should be as fast as possible. The cryovials were placed in a bath at 37°C until the content had thawed. The vial contents were then seeded in a T-25 flask with fresh medium and appropriate supplementation. As the cells were adherent, it should have been waited for 3-5 hours to check if the cells had adhered to the bottom of the flask. If positive, the medium was changed to remove the DMSO content and the remains of dead cells.

Mycoplasma detection

Cell culture contamination is a severe problem that is not only limited to bacterial or fungal infections, which are easily detectable during subcultures due to the size of the cells. Some infections, such as those caused by mycoplasma, are not evident during routine monitoring of cell culture at the macroscopic or microscopic level. However, this contamination entails a series of consequences, such as alterations in

the proliferative rate and cell viability and chromosomal and metabolic alterations, which can generate disturbances in the analyses carried out. Therefore, cell cultures were tested for mycoplasma every three months to eliminate any contaminated cultures. The commercial Venor® GeM One-Step Test (11-8025, Minerva Biolabs, USA) was used, which detects ten mycoplasma species by PCR. For the analysis, the supernatant of culture media that has been in culture for at least 48 hours was used.

Modulation of gene expression

Gene expression analysis studies how genes are transcribed to synthesize functional gene products: RNA or proteins. The study of the regulation of these pathways provides information on normal cellular processes, such as cell differentiation, or pathological processes, such as tumorigenesis.

Silencing by transduction with lentiviral particles

Lentiviral vectors are a high transduction efficacy and safe method for gene delivery into hard-to-transfer cells, such as primary melanocytes. Moreover, lentiviral particles can be employed in standard Biosafety Level 2 tissue culture facilities, as they are replication-incompetents.

Table 6. Lentiviral particles specifications

Gene	Reference	Supplier
Transduction efficiency control	copGFP Control Lentiviral Particles (sc-108084)	Santa Cruz Biotechnology Inc., USA
Transduction scramble control	Control shRNA Lentiviral Particles (sc-108080)	Santa Cruz Biotechnology Inc., USA
RKIP PEBP1	PEBP1 shRNA Lentiviral Particles (sc-36430-V)	Santa Cruz Biotechnology Inc., USA
PIR	PIR shRNA Lentiviral Particles (sc-61359-V)	Santa Cruz Biotechnology Inc., USA

Normal primary melanocyte cell line HEMn-LP was transduced with lentiviral particles for gene silencing following the manufacturer's instruction with minor modifications (Figure 13a). Briefly, 24 hours before viral infection, cells were seeded in a 6-well plate. In our case, we did not use polybrene® because it was toxic for our primary cells. Polybrene® is a polycation that neutralizes charge interactions to increase the binding between the pseudoviral capsid and the cellular membrane.

The ratio of the number of transducing lentiviral particles to the number of cells (Multiplicity of Infection, MOI) used in these experiments was of 2 MOI of lentiviral particles, directly added to each well and were incubated overnight. Specifically, the shRNA specified in Table 6 was used. The day after, the medium with the lentiviral particles was replaced, and a fresh medium was added. Two days after that, the cells were selected with 5 µg/mL of Puromicine (P8833, Sigma-Aldrich Quimica, S.A., Spain) to get stable cell lines.

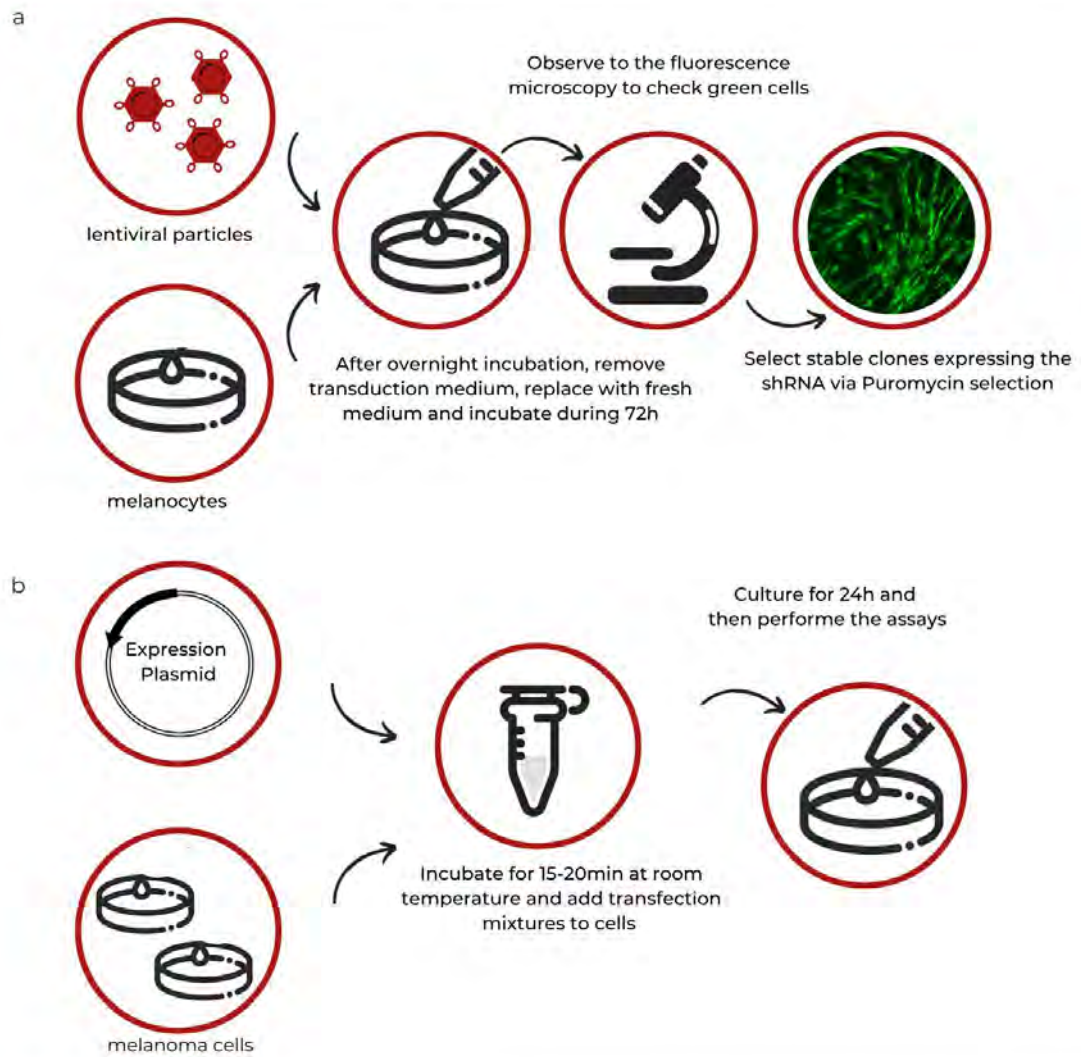


FIGURE 13 Workflow overview of (a) transduction protocol with lentiviral particles and (b) transfection protocol with lipofectamine and overexpression plasmids.

Overexpression by transfection with plasmid

Transfection plasmid is widely used to achieve efficient gene transfer in easy-to-transfer cells, such as melanoma cells. Due to that, A2058 and MeWO metastatic melanoma cell lines were transfected with overexpressing plasmid for RKIP or PIR using Lipofectamine 2000 (11668019, Thermo Fisher Scientific, USA) according to the manufacturer's instructions (Figure 13b).

Table 7. Plasmids specifications

Gene	Reference	Supplier
scramble	pCMV-myc-DKK	OriGene Technologies, Inc, USA
RKIP PEBP1	pCMV-PEBP1-myc-DDK	OriGene Technologies, Inc, USA
PIR	pCMV-PIR-myc-DKK	OriGene Technologies, Inc, USA
Nanog promoter	PL-SIN-Nanog-EGFP #21321 EW1024-FP	Addgene, USA
Jarid1B promoter	pLU-JARID1B1B promoter-EGFP	Kerafast Inc., USA

Briefly, after seeding cells were 70–90% confluent the transfection reagent mix was added. This mix included Opti-MEM® Medium, Lipofectamine 2000 and plasmid of interest. The Table 7 includes the information of the plasmid used in this study. All of the transfection experiments were performed with 500 ng of each plasmid. The mix was incubated during 15-20 min and then was transferred to the seeded cells. All the experimental assays were performed at least after 24 hours of transfection and a scramble plasmid was used as control.

Functional assays

Proliferation assays

Cell proliferation can be used to assess normal cell health, to measure responses to toxic insult, or as a prognostic and diagnostic tool in several cancer. The cell viability was determined using the standardized XTT kit (Roche Molecular Biochemicals, USA). This assay is based on the ability of viable cells to transform the yellow XTT tetrazolium salt into orange formazan in the presence of a reducing reagent. The process occurs only in viable, metabolically active cells. The amount of formazan and the orange dye formed is easily quantifiable using a plate spectrophotometer by measuring the absorbance at 490 nm.

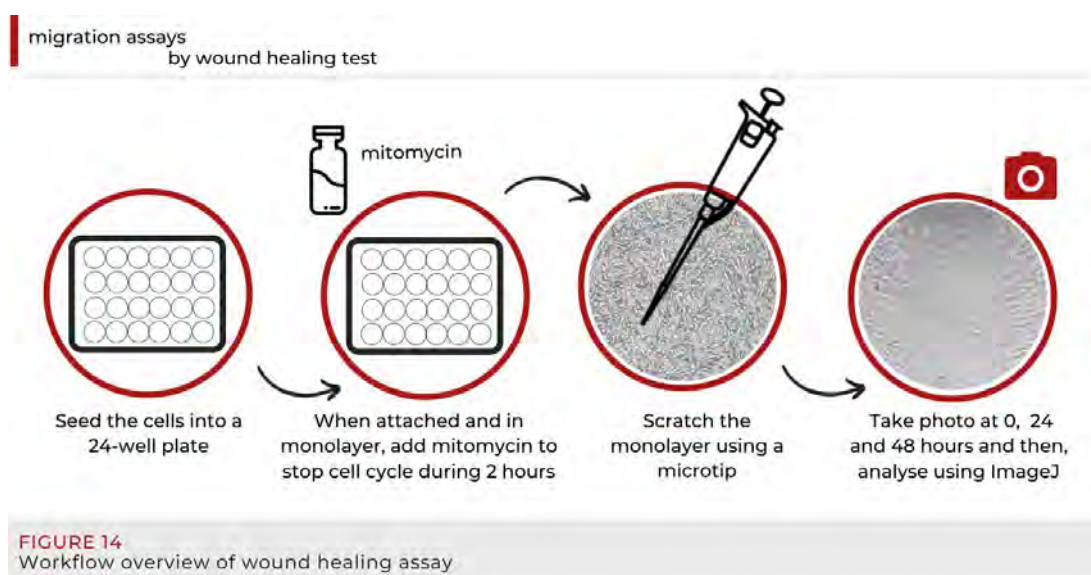
For this assay, cells were seeded in flat-bottomed 96-well plates with the appropriate density according to the cell line in 100 µL of culture medium and left overnight in the oven to adhere to the well. After adding the reducing reagent and XTT mixture to the wells in a 1:50 ratio, the plate was incubated for 4 hours in the incubator. The absorbances were read at 490 nm utilizing a plate spectrophotometer BioTek

Synergy HTX (Agilent Technologies, Inc, USA). Cell viability was calculated as the percentage of cell viability with respect to control cells as follows: (sample absorbance/control absorbance) * 100.

Migration assays

Cell migration occurs during critical physiological processes and is dysregulated in pathological situations, such as cancer metastasis and inflammation. For migration capacity assays (Figure 14), after seeding the cells in 24-well plates, the monolayers were incubated with 0.5 µg/mL of Mitomycin C for 2 hours. Then they were scraped with a sterile plastic micropipette tip. The wound closure was observed over 48 hours, and the photos were taken at 0, 24, and 48 hours with a light microscope. Then, each group's migration percentage was calculated according to the control.

Moreover, the transwell active migration assay was performed using Type I-Collagen coated inserts with 6.5-mm-diameter polycarbonate filters (8-µm pore size). Cells (1×10^4) suspended in 200 µL of DMEM without FBS were seeded in the top chambers. The bottom chambers were filled with 300 µL of DMEM containing 10% FBS (as a chemoattractant). Cells were allowed to migrate overnight. The non-migrated cells on the upper surface of the filter were carefully and thoroughly removed with cotton swabs. Migrated cells were fixed with a mix of cold 4% paraformaldehyde plus 2% ethanol and stained with crystal violet. Five images per insert were taken using a compound optical microscope, and migrated cells were quantified by ImageJ software. Results were expressed as the average number of migrated cells per well obtained from three separate experiments done in triplicate.



Data analysis

In all quantitative tests performed (proliferation and migration assays), the SPSS version 26 program was used. Fisher exact test was applied to check the normality of the data. To compare differences between the two groups, Student's t-test was performed. $P < 0.05$ was considered statistically significant, $P < 0.01$ was considered highly statistically significant, and $P > 0.05$ was considered statistically insignificant.

Molecular analysis

Protein analysis

Protein extraction

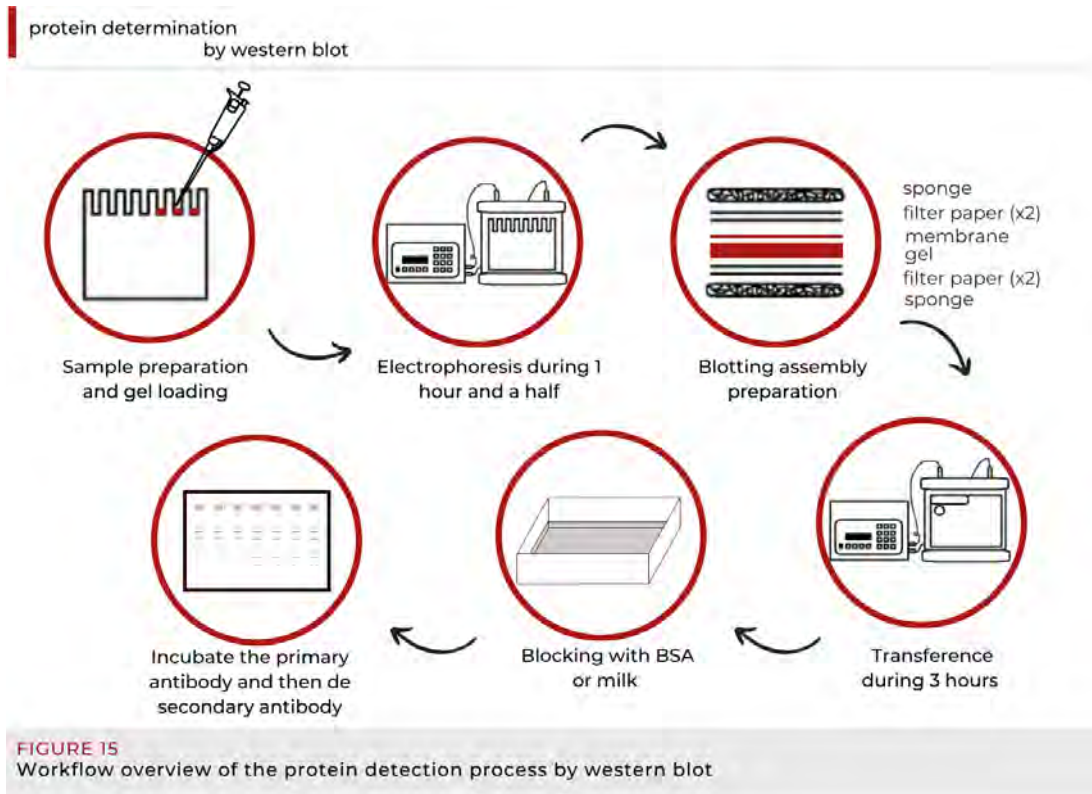
Melanoma cells and primary melanocytes were harvested by trypsinization, washed with PBS and lysed in RIPA lysis buffer (80 mM Tris-HCl pH 8, 150 mM NaCl, 1% NP 40, 0.5% sodium deoxycholate, 0.1% SDS) containing Protease Inhibitor Cocktail (Sigma-Aldrich Quimica S.A., Spain) for 15 minutes on ice. Lysates were then cleared by centrifugation at 1500 xg for 5 minutes. Total protein concentration was determined using the bicinchoninic acid assay.

Protein quantification

Protein quantification was performed by preparing a straight standard with increasing known concentrations of Bovine Serum Albumin (BSA). To prepare the samples, each eppendorf was adequately named and mixed 5 μ L of each sample with 45 μ L of Milli-Q H₂O. Then, knowing that the relation between bicinchoninic acid and cupric sulfate had to be 50:1, 1 mL of this mix was poured into each eppendorf, and all samples were incubated at 37°C in darkness for about 30 minutes. Finally, the absorbance was measured at 562 nm in a spectrophotometer.

Protein detection by western blotting

Western blot is a widely used analytical technique for the study of proteins. This method allows the detection of a single protein within a biological sample, specifically with an antibody that recognizes a unique epitope on the protein of interest. Protein detection using this technique involves a first step in separating the proteins based on their molecular weight, transferring them to a membrane, and subsequently labeling them with the antibody of interest.



SDS polypolyacrylamide gel electrophoresis

The SDS polypolyacrylamide gel electrophoresis technique (SDS-PAGE) allows the separation of denatured proteins on gels with a polypolyacrylamide matrix. The gels were prepared by polymerization of polyacrylamide, taking into account the percentage of this polymer concentration. The higher the percentage of polyacrylamide, the smaller the pore size and the better the resolution of low molecular mass proteins. On the contrary, if a protein with high molecular weight is to be detected, the percentage of polyacrylamide must be lowered to obtain larger pores that allow a better resolution of large proteins. In this study, 12% of polyacrylamide concentration was used.

Table 8. Percentage of polypolyacrylamide used depending on the protein of interest

% polyacrylamide	15%	10%	7.5%	5%
KDa range	12-43	16-68	36-94	57-212

The gels are composed of two different parts (Table 9):

- Stacking gel: It has large pores that allow the proteins to migrate freely and get stacked at the interface between stacking and running gel. The purpose is that proteins start migrating at the same time.
- Running gel: The resolving part of the gel, in which proteins run according to their molecular weight.

Table 9. Composition of the stacking and running gel

Stacking gel		Running gel				
	4%		7.5%	10%	12%	15%
30% Acry-bis	1 mL	30% Acry-bi	3.8 mL	5 mL	6 mL	7.5 mL
0.5M Tris-HCL (pH6.8)	0.75 mL	2M Tris-HCL (pH8.8)	3 mL	3 mL	3 mL	3 mL
H2O miliQ	5.75 mL	H2O miliQ	9 mL	7 mL	6 mL	4.5 mL
20% SDS	37.5 mL	20%SDS	75 mL	75 mL	75 mL	75 mL
10%APS	62.5 mL	10%APS	75 mL	75 mL	75 mL	75 mL
TEMED	6.25 mL	TEMED	5 mL	5 mL	5 mL	5 mL

Every sample contained 2 μ L of Dithiothreitol (DTT, which breaks down hydrogen bonds) and 4 μ L of Laemmli 1X loading buffer (60 mM Tris-HCl pH 6.8, 2% p/v SDS, 10% glycerol, 0.002% blue bromophenol, 1mM DTT and bidistilled water up to 20 μ L). Then, samples were boiled at 95°C for 5 minutes and loaded with 7 μ L of molecular weight ladder Precision Plus Protein™ Dual Colors Standards of BioRad and 20 μ L of each sample. The assembly was covered with the electrophoresis buffer (Table 10). Then, electrophoresis was at 100 V for 10 minutes; and then at 180 V for around 45 minutes.

Table 10. Composition of 1L of the electrophoresis buffer (5X)

Tris (tris(hydroxymethyl)aminomethane)	15.15 g
Glycine	72.1 g
Sodium dodecyl sulphate	5 g
Milli-Q H2O	Up to 1L

Transference

This step involves transferring the proteins from the gel to a nitrocellulose membrane (Whatman GmbH-GE Healthcare, Dassel, Germany) by applying voltage. For that, an electroblotting cassette containing a small pillow, two thin filters, the gel with proteins, the nitrocellulose membrane, and another two filters plus a small pad was assembled and placed on the electrodes in the blotting unit with transfer buffer (Table 11). The transference conditions were 3 hours at 300 mA. To verify a successful transfer, the nitrocellulose membrane was incubated for 2 minutes in Ponceau red solution. This stain binds reversibly to the positively charged functional groups of the protein (amino group) and the non-polar regions. After checking the transference, the membrane was washed extensively in water until the dye was gone.

Table 11. Composition of 1L of the transfer buffer

Tris (tris(hydroxymethyl)aminomethane)	5.8 g
Glycine	29 g
Sodium dodecyl sulphate	1 g
Metanol	200 mL
Milli-Q H ₂ O	Up to 1 L

Immunostaining

The blots were incubated with PBS containing 5% Bovine Serum Albumin and 0.1% Tween-20 for 1 hour to block nonspecific binding and then incubated with an appropriate dilution of primary antibody at 4°C overnight (Table 12). The membrane was washed with TBST three times (10 min/each time), then incubated with goat anti-mouse Horseradish Peroxidase (HRP) conjugated secondary antibody for 2 hours at room temperature. Finally, proteins were visualized by enhanced chemiluminescence using the SuperSignal® West Pico Chemiluminescent Substrate (Thermo Fisher Scientific, USA). The following table includes the antibody details used in this study.

Table 12. Details of sources and concentrations of antibodies used for western blot in this study

Antibody name	Dilution	Reference
Recombinant Anti-RKIP antibody	1:5000	Abcam, UK ab76582
Anti-Pirin rabbit polyclonal antibody	1:1000	Thermo Fisher Scientific, USA PA5-29777
Anti-gamma Tubulin antibody	1:1000	Abcam, UK ab 11321
Goat F(ab') ₂ Anti-Mouse IgG(H+L), Human ads-HRP	1:8000	SouthernBiotech, USA 1032-05
Goat anti-Rabbit IgG (H+L) Secondary Antibody, HRP	1:10000	Abcam, UK ab6721

Gene expression analysis

RNA extraction and quantification

Total RNA from cultured cells was isolated using the RNeasy Mini kit (Qiagen Inc, Germany). The entire process was carried out on the ice and with sterile material. After collecting the cells, the number of cells was counted, and 1×10^7 cells were separated since RNA extraction was performed from 1×10^7 cells. They were centrifuged at 300 xg for 5 minutes, and the PBS was removed. The pellet was resuspended with 600 μ L of a solution consisting of 1 ml of RLT buffer and 10 μ L of β -mercaptoethanol. The sample was passed ten times through a syringe with a 20G needle for complete and homogeneous cell lysis. Then, the 70% ethanol addition step is followed by the transfer of 700 μ L of the sample to an RNeasy separation column. After centrifuging it at 1500 xg for 15 seconds, the eluate was discarded, and the column was placed in the same collecting tube. This step was repeated as often as necessary until the entire sample was collected. Then 700 μ L of RW1 buffer was added to the

column to clean it, and it was centrifuged at 1500 xg for 15 seconds. The eluate was again discarded, and the treatment with DNase was carried out, for which 80 μ L of a solution containing 10 μ L of DNase and 70 μ L of RDD buffer were added. It was incubated for 15 minutes at room temperature (20-30°C), and then 700 μ L of buffer RW1 was added and centrifuged for 15 seconds at 1500 xg. The eluate was discarded, and the column was transferred to a new collecting tube. Two washes were then carried out with 500 μ L of RPE buffer each, centrifuging at 1500 xg for 15 seconds in the first wash and 2 minutes in the second. Finally, the column was transferred to a 1.5 mL Eppendorf tube, and the RNA was eluted by adding 50 μ L of DEPC water (Ambion Inc., USA) by centrifugation at 1500 xg for 1 minute. Samples were correctly labeled, quantified by NanoDrop (Thermo Fisher Scientific, USA), and stored at -80°C until use to ensure RNA integrity.

Real Time quantitative Polimerase Chain Reaction (RTqPCR)

For each sample, cDNA was synthesized from 1 μ g total RNA using the iScript™ cDNA Synthesis kit (Bio-Rad, USA) according to the manufacturer's instruction. The reaction mixture contained 0.1 μ L cDNA from the reverse transcription reaction, together with forward and reverse specific primers and iQ™ SYBR® Green Supermix (Bio-Rad, USA) in a final reaction volume of 20 μ L. Quantitative real-time RT-PCR assays were carried out using an iCycler PCR platform (Bio-Rad, USA). The PCR reaction began with heating at 95°C for 10 min, followed by 45 cycles of desnaturation at 95°C for 30 sec, annealing at the corresponding temperature for each gene (56-61°C) for 20 sec and extension at 72°C for 30 sec. Each assay included a negative control consisting of the absence of cDNA. Expression data were generated from 2 amplification reactions with samples and controls run in triplicate. Optical data obtained by real-time PCR were analyzed using the MyiQ Single-Color Real-Time PCR Detection System Software v.1.0 (Bio-Rad, USA). The expression of three different housekeeping genes (ACTB, GAPDH, and RPS15) also was analyzed to normalize expression data using the Gene Expression Macro Software Version 1.1 (Bio-Rad Laboratories, Hercules, CA, USA), where the relative expression values were computed by the comparative Ct method (132,133). The sequences of primers used are specified in the following Table 13.

Table 13. RTqPCR primers' sequences

Gene name	Forward primer	Reverse primer
<i>ACTB</i>	5'-AGATGACCCAGATCATGTTTGAG-3'	5'-GTCACCGGAGTCCATCACG-3'
<i>c-MYC</i>	5'-GCTCCTGGCAAAGGTCAG-3'	5'-GTTGTGCTGATGTGTGGAGAC-3'
<i>E2F1</i>	5'-TGACATCACCAACGTCCTTGA-3'	5'-CTGTCCGAGGTCCTGGGTC-3'
<i>GAPDH</i>	5'-CCTGTTTCGACAGTCAGCCG-3'	5'-CGACCAAATCCGTTGACTCC-3'
<i>JARID1B</i>	5'-GACTGGGACAACAGAACCT-3'	5'-TGGACTAACACCATGGAGG-3'
<i>LUM</i>	5'-AACTGCCCTGAAAGCTACCC-3'	5'-AGCCACTGCAGATCAGTTACA-3'
<i>NTRK2</i>	5'-CTCCCGGAATTGGGTTGGAG-3'	5'-GGGGCCGAGATTCCTTGTA-3'
<i>PIR</i>	5'-GGAGCCTCAGTACCAGAACT-3'	5'-CTTGGACTTTATTCCCAGGGC-3'
<i>RKIP</i>	5'-AATAGACCCACCAGCATTTG-3'	5'-TGCCACTGCTGATGTCATTG-3'
<i>RPS15</i>	5'-CGACCAAATCCGTTGACTCC-3'	5'-CGGGCCGGCCATGCTTTACG-3'
<i>THY-1</i>	5'-GTTTGACCAGGAAAGCAGCG-3'	5'-CTCTTGGGAGCTTGGGACAG-3'
<i>ZEB1</i>	5'-GTGCAGTTACACCTTTGCA-3'	5'-CACATGTCTTTGATCTTCTCT-3'
<i>Has-miR-21-5p</i>	-	5'-UAGCUUAUCAGACUGAUGUUGA-3'
<i>Has_RNU6-2</i>	-	5'-CGCTTCGGCAGCACATATACTA-3'

Gene expression levels results were analysed using the SPSS version 26 program. Fisher exact test was applied to check the normality of the data. To compare differences between two groups, Student's t-test was performed. $P < 0.05$ was considered statistically significant, $P < 0.01$ was considered highly statistically significant, and $P > 0.05$ was considered statistically insignificant.

For detection of mature miRNA, cDNA was prepared in a reverse transcription reaction using miScript HiSpec Buffer from the miScript II RT Kit (Qiagen Inc, Hilden, Germany). Oncogene *miR-21* was detected by RT-qPCR. The primers used were Has-miR-21-5p (MS00009079, Qiagen Inc, Hilden, Germany) and Has-RNU6-2 (MS00033740, Qiagen Inc, Hilden, Germany) as reference mature miRNA. The RT-qPCR assay was conducted under the following conditions: Stage 1: 15 min at 95 °C; Stage 2: 60 cycles of 15 s at 94 °C, 30 s at 55 °C, 30 s at 70 °C, 1 s at 72; and Stage 3: 5 s at 95 °C, 1 min at 65 °C. The real-time fluorescence intensity was monitored at each cycle of the third stage. Light Cycler® 480 II Real-Time PCR System (Roche, Basilea, Switzerland) was used to perform the reaction.

RNA sequencing analysis

Second generation sequencing (Next Generation Sequencing or NGS) is used to analyze the presence of genes as well as the quantification of their expression globally throughout the entire transcriptome. The complete protocol included an RNA extraction step, followed by its quantification as well as its purity and integrity analysis. Subsequently, libraries were prepared and bioinformatic analysis was carried out after sequencing.

Platform for Genome Analyses of Center for Cooperative Research in Biosciences- CIC bioGUNE (member of the Basque Research and Technology Alliance) lead by the Dr. Ana Maria Aransay was in charge of carrying on both libraries and sequencing steps. The statistical analysis was made thanks to the invaluable technical support of Dr. Iraia Muñoa, Assistant Professor of the Faculty of Medicine and Nursing of the University of the Basque Country. After determining the strength of association between samples and the robustness of sequencing raw data, the Katramila server of the ARINA platform of the University of the Basque Country / Euskal Herriko Unibertsitatea and its calculation nodes were used for extract the biological information from the sequenced samples.

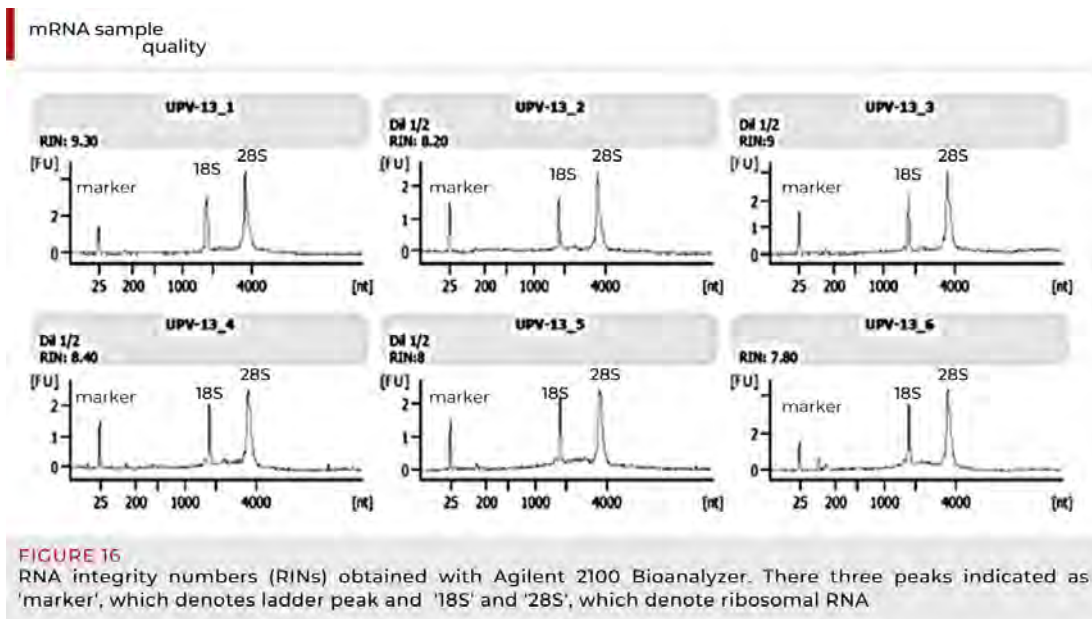
RNA extraction, quantification and purity and integrity analysis

The RNA concentration measured in Qubit 2.0 RNA assay Kit (Q32855, Invitrogen, USA) showed to be enough to start the experiment (Table 14).

Table 14. Total RNA quantification with Qubit RNA HS Assay Kit

Gap_ID	Sample name	Sample name recoded	Sample group	Stock conc. (ng/μL)
UPV-13_1	P6_shCTR	shCTR_P6	1	82.4
UPV-13_2	P6_shRKIP	shRKIP_P6	1	108
UPV-13_3	P6_shPIR	shPIR_P6	1	92
UPV-13_4	P8_shCTR	shCTR_P8	2	92.4
UPV-13_5	P8_shRKIP	shRKIP_P8	2	108
UPV-13_6	P8_shPIR	shPIR_P8	2	71.4

An optical density measurement of RNA obtained from the Bioanalyzer Agilent 6000 Nano Chip (5067-1511, Agilent Technologies, Inc, USA) was used to assess RNA quality and yield. An electropherogram of good-quality RNA is shown in Figure 16, where it can be see the three significant peaks: the ladder peak labeled as ‘marker’ and the 18S and 28S peaks, which denote ribosomal RNA.



Libraries preparation and sequencing analysis

Starting from 400 ng of total RNA, mRNA was purified, fragmented and primed for cDNA synthesis. cDNA first strand was synthesized with SuperScript-II Reverse Transcriptase (18064-014, Thermo Fisher Scientific, USA) for 10 min at 25°C, 15 min at 42°C, 15 min at 70°C and pause at 4°C. cDNA second strand was synthesized with Illumina reagents at 16°C for 1 hour.

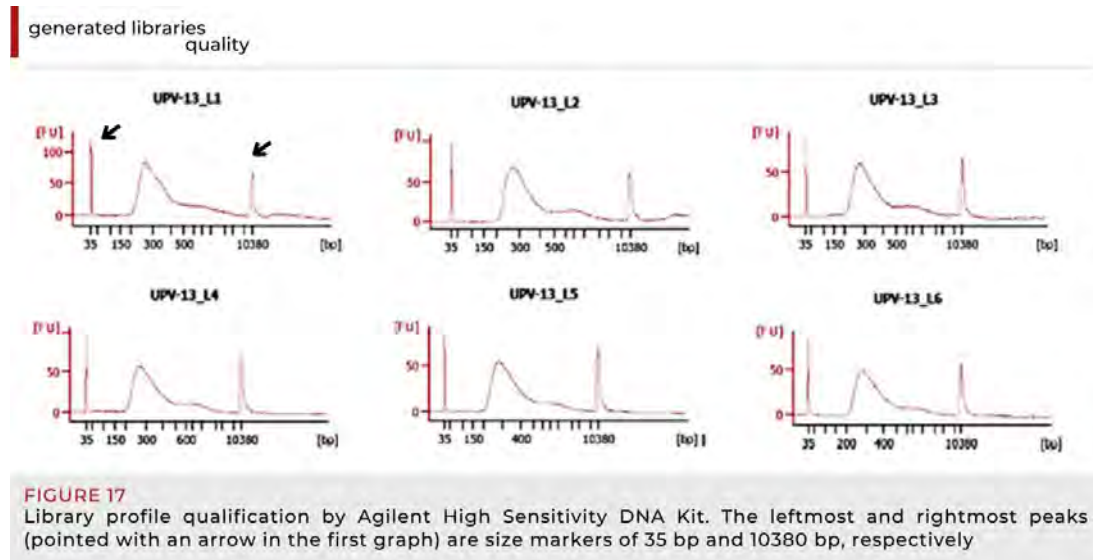
Then, sequencing libraries were prepared following TruSeq Stranded mRNA Sample Preparation Guide with the corresponding kit (RS-122-2101 or RS-122-2102, Illumina Inc., USA). First, A-tailing and adaptor ligation were performed (Table 15). Then, enrichment of libraries was achieved by PCR: 30 sec at 98°C; 15 cycles of 10 sec at 98°C, 30 sec at 60°C, 30 sec at 72°C; 5 min at 72°C and pause at 4°C.

Table 15. Libraries indexing specifications

Gap_ID	Sample name recorded	Sample group	Index	Sequence	Set
UPV-13_1	shCTR_P6	1	A001	ATCACG	B
UPV-13_2	shRKIP_P6	1	A002	CGATGT	A
UPV-13_3	shPIR_P6	1	A003	TTAGGC	B
UPV-13_4	shCTR_P8	2	A004	TGACCA	A
UPV-13_5	shRKIP_P8	2	A005	ACAGTG	A
UPV-13_6	shPIR_P8	2	A006	GCCAAT	A

Afterward, amplified libraries concentration was determined with Qubit fluorometer using the Qubit®dsDNA HS assay kit (Q32854, Invitrogen, USA), and their size distribution was assessed running an aliquot on an Agilent Technologies 2100 Bioanalyzer using an Agilent High Sensitivity DNA Chip (5067-4626, Agilent Technologies Inc., USA). In Figure 17 it can be seen the size

distribution analysis. The leftmost and rightmost peaks (pointed with an arrow) are size markers of 35 bp and 10380 bp, respectively. The fragmented DNA's average length is 150 bp, whereas the average length of the library fragments is estimated to be 300 bp. The obtained libraries seem to have the expected size (average size: 306 bp), and their concentration was appropriate for sequencing.



Sequencing was performed on the Illumina platform HiSeq2500 (resulting in 51bp reads after discarding the final base). The images taken during the sequencing reactions were processed using Illumina's sequencing control software for system control and base calling through an integrated primary analysis software called RTA (Real Time Analysis). The base calls (BCL) binary was converted into FASTQ utilizing Illumina Inc.'s package bcl2fastq. Adapters were not trimmed away from the reads. Briefly, the first step was to collect the data from the sequences and perform a general quality control on the .fastq files to assess their quality and to be able to trust the results that would be obtained from the sequences. For this we use FastQC, to broadly represent quality control. For its FastQC reports, it analyzes a subset of all the data and extrapolates its results to the entire data set. With the information in the reports, you can determine if there have been any technical problems in the sequencing process. Then, the next step was to remove the adapters used to amplify the library. For that, the program used was the Trim Galore! The raw data including total number of bases, GC content, Q20 and Q30 for all samples analysed are detailed in the following Table 16.

Table 16. Raw data from the total number of bases, reads, GC (%), Q20 (%), and Q30 (%) calculated for all the samples

Sample	Size (pb)	Total bases	Read count	GC	AT	Q20(%)	Q30(%)
shCTR_P6	306	2.886.978.573	56.607.423	49.34	50.66	97.61	95.04
shRKIP_P6	306	2.809.608.870	55.090.370	49.32	50.68	97.74	95.25
shPIR_P6	306	2.714.641.362	53.228.262	49.49	50.51	97.77	95.29
shCTR_P8	306	2.719.746.564	53.328.364	49.25	50.75	97.83	95.42
shRKIP_P8	306	2.603.630.019	52.052.569	49.24	50.76	97.83	95.41
shPIR_P8	306	2.577.028.470	50.529.970	49.17	50.83	97.75	95.26

Bioinformatic analysis

The first step before performing the alignment is to create the reference genome index against which we are going to compare our sequences. For this step, the latest version of the human genome offered by the UCSC genome browser was chosen: Human GRCh38 / hg38. The genome was extracted from the archive using the tool “twoBitToFa. Then, we used the specific Hisat2-build tool (from the general Hisat2 tool), to index the genome.

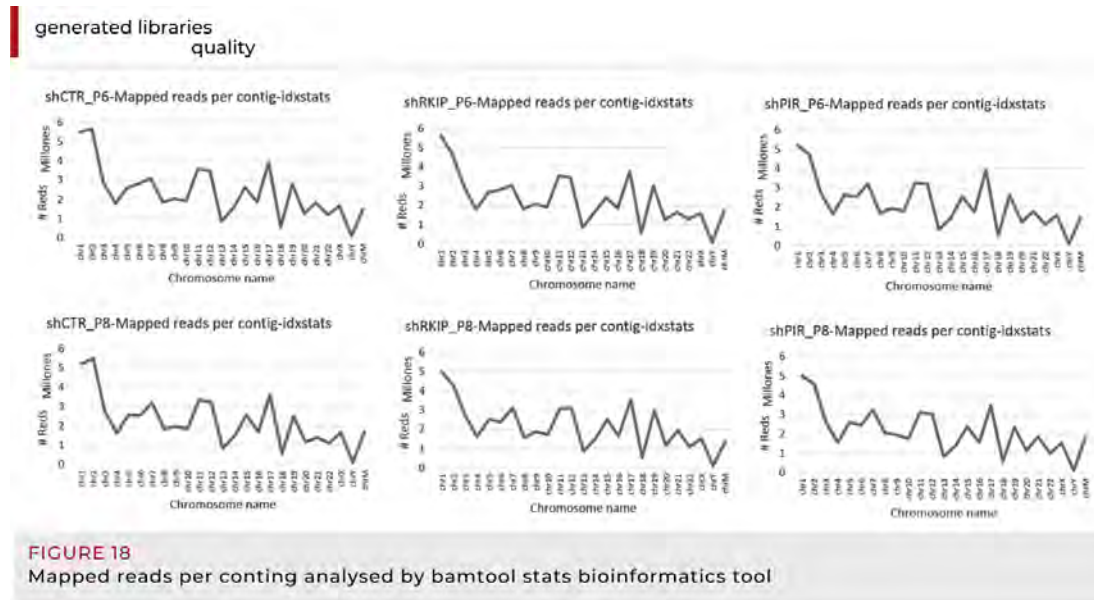
Sequence alignment involves using the reference genome, which was constructed in the previous step, to identify the coordinates of the reads of our sequences. As can be seen in Table 17, in the column "overall alignment rate", very high alignment percentages were obtained, more than 96% for all samples.

Table 17. Alignment data summary

Sample	Total reads	Aligned 0 times	Aligned 1 time	Aligned >1 time	Overall alignment rate
shCTR_P6	54725047	2068423 (3.78%)	47479395 (86.76%)	5177229 (9.46%)	96.22%
shCTR_P8	51653256	1931105 (3.74%)	44875055 (86.88%)	4847096 (9.38%)	96.26%
shPIR_P6	51588814	1888684 (3.66%)	44879696 (87.00%)	4820434 (9.34%)	96.34%
shPIR_P8	48942059	1772039 (3.62%)	42282676 (86.39%)	4887344 (9.99%)	96.38%
shRKIP_P6	53365721	1920512 (3.60%)	46201675 (86.58%)	5243534 (9.83%)	96.40%
shRKIP_P8	49490946	1775255 (3.59%)	42965564 (86.81%)	4750127 (9.60%)	96.41%

The alignment files were later converted to smaller files (.bam and .bai) to make it easier to work with them in the next steps of the analysis. For this, samtools view specific bioinformatic tool was used. Previous to biological information extraction, two bioinformatics tools were used to verify that in the

transformation of the files to sorted.bam and sorted.bai, the information was still correctly maintained: bamtools stats and picard. With the data from the bamtools stats tool, it can see how many reads are mapped per chromosome, in this case it was talking about millions of reads per chromosome. As it can be seen in the Figure 18, it was also a pattern that was maintained in all sequenced samples.



As it mentioned before, another tool to analyse the quality of alignment is Picard, which is a command line tools for manipulating high-throughput sequencing (HTS) data. This analysis provided information about the total number of reads, the percentage of PF reads that aligned to the reference sequence and the rate of bases mismatching the reference for all bases aligned to the reference sequence, among others. In the Table 18 all raw data form Picard analysis is specified. The 100% of reads were passed the Illumina’s quality filter. In addition, more than 96% of reads aligned with the reference genome and the rate of bases mismatching the reference for all bases aligned to the reference sequence was less than 0.001.

Futhermore, the plotCorrelation, a tool included in Deeptools, was used for the analysis and visualization of sample correlations. It was used to visualize the Spearman correlation between the replicas of each sample.

Prior to the analysis of the differential expression of the genes, the information of the reads of each gene is compiled for each replica analysed using the stringtie program. With this information a general library is made with all the values. Subsequently, the featurecounts program is used to finish extracting the values that are used for the final statistics. Then, to quantify and compare the gene expression level within and between the control and the virus-infected groups, we calculated and normalized the expression level of the genes through reads per kilobase of exon model per million mapped reads (RPKM).

Table 18. Alignment quality analysis by Picard bioinformatics tool. (A) Control samples, (B) RKIP samples and (C) PIR samples

(A)	shCTR_P6	shCTR_P8
Total reads	54725047	51653256
Total reads which pass Illumina's quality filter	54725047	51653256
Total reads which aligned with the reference genome	52656624	49722151
Reads mismatched	0.001043	0.001023
Number of insertion and deletion events per 100 aligned bases	0.000018	0.000016
(B)	shRKIP_P6	shRKIP_P8
Total reads	53365721	49490946
Total reads which pass Illumina's quality filter	53365721	49490946
Total reads which aligned with the reference genome	51445209	47715691
Reads mismatched	0.001006	0.001001
Number of insertion and deletion events per 100 aligned bases	0.000017	0.000016
(C)	shPIR_P6	shPIR_P8
Total reads	51588814	48942059
Total reads which pass Illumina's quality filter	51588814	48942059
Total reads which aligned with the reference genome	49700130	47170020
Reads mismatched	0.001006	0.001032
Number of insertion and deletion events per 100 aligned bases	0.000016	0.000016

Differentially expressed genes (DEGs) were identified by means of edgeR package in R-studio, by implementing a negative binomial distribution for the statistical significance. Normalization was performed using the trimmed mean of M values (TMM) method. Reads per kilobase of exon model per million mapped reads (RPKM) for each gene were transformed to log₂-fold changes using R version 3.1.0. The analysis of variance ($p < 0.05$) and false discovery rate ($FDR < 0.05$) tests were performed using the R program (version 3.1.0) to select genes exhibiting significantly different expression patterns.

Finally, these datasheets were used to performe an enrichment analysis to extract the biological significance of detected gene expression alterations. Enrichment results were generated by analyzing the upregulated and downregulated gene sets using BioJupies (Torre D et al., 2018) and EnrichR (Kuleshov MV et al., 2016), which are freely available at <https://amp.pharm.mssm.edu/biojupies/> and <http://amp.pharm.mssm.edu/Enrichr/> respectively. KEGG pathway enrichment analysis of differentially expressed genes (DEG) was performed using the KOBAS online analysis database (available online: <http://kobas.cbi.pku.edu.cn/>). The raw data files of this analysis have been deposited in NCBI Bioproject, with accession number PRJNA636405 for RKIP, aaccession numer PRJNA843921 for PIR.



RESULTS

01

Potential value of RKIP and Pirin proteins as melanoma diagnostic and prognostic markers

02

RKIP regulates melanocyte differentiation by modulating the stemness-related transcription factor *NANOG*

03

Pirin modulates melanoma proliferation by targeting the slow-cycling transcriptional regulator *JARID1B*

A grayscale electron micrograph showing a dense field of melanoma cells. The cells exhibit characteristic features such as large, electron-dense nuclei with prominent nucleoli, and numerous melanosomes (pigment granules) of varying sizes and stages of maturation. The cytoplasm is filled with organelles and fine granular material.

Chapter 01

Potential value of RKIP and Pirin proteins as melanoma diagnostic and prognostic markers

Part of this chapter has been published in *Cancers*:

Penas C, Apraiz A, Muñoa I, Arroyo-Berdugo Y, Rasero J, Ezkurra PA, Velasco V, Subiran N, Bosserhoff AK, Alonso S, Asumendi A, Boyano MD. **RKIP Regulates Differentiation-Related Features in Melanocytic Cells.** *Cancers*. 2020 Jun 3;12(6):1451. doi: 10.3390/cancers12061451

Another part of this chapter has been submitted to be published in *Scientific Report*:

Penas C, Arroyo-Berdugo Y, Apraiz A, Rasero J, Muñoa I, Andollo N, Cancho-Galán G, Izu R, Gardeazabal J, Ezkurra PA, Alvarez-Dominguez C, Alonso S, Bosserhoff AK, Asumendi A, and Boyano MD. **Pirin is a prognostic marker of human melanoma that dampens the proliferation of malignant cells by downregulating JARID1B/KDM5B expression.** Submission ID: f935f498-4b94-4e99-b05a-c2b0d23df55c

Chapter 01

Potential value of RKIP and Pirin proteins as melanoma diagnostic and prognostic markers

Characteristics of the patients enrolled in the study

During this project, a total of 314 patients (154 females and 160 males) were enrolled who had been diagnosed by pathologists with a nevus or malignant melanoma. The clinicopathological features of the group are shown in Table 19. Our collection included 75 nevi and 239 melanoma. Regardless of the diagnosis, the incidence of nevi and melanoma was equal among men and women (Figure 19a). Patients diagnosed with nevus ranged in age from 24 to 78 years old, with the median age being 50 years old, while those diagnosed with melanoma ranged in age from 23 to 87 years old, with the median age being 57 years old (Table 19).

Table 19. Clinical and pathological data from nevus and melanoma patients

	N (%)		N (%)
NEVUS	75	HISTOLOGICAL SUBTYPE	
Age at diagnosis (years, range)	56 (24-78)	SSM	102 (43)
Sex		NM	53(22)
- Male	28 (37)	ALM	21(9)
- Female	47 (63)	LMM	9(4)
		LM	3 (1)
		Others	12 (5)
		ND	39 (16)
MELANOMA	239	AJCC STAGES AT DIAGNOSIS	
Age at diagnosis (years)	57 (23-87)	In situ	34 (14)
Sex		IA	46 (19)
- Male	131 (55)	IB	54 (23)
- Female	108 (45)	IIA	32 (13)
		IIB	15 (6)
		IIC	24 (10)
		IIIA	9 (4)
		IIIB	11 (5)
		IIIC	6 (3)
		IV	8 (3)
LOCALIZATION		DISEASE EVOLUTION	
Head and neck	43(18)	Disease-free	147 (62)
Trunk	74(31)	Metastasis	92 (38)
Upper limb	24 (01)		
Lower limb	69 (29)		
Acral	21 (9)		
Others	5 (2)		
ND	3 (1)		

Analyzing data according to the body location of the tumors, the subgroup of women had a higher incidence of tumors associated with the lower extremities. In contrast, the subset of men had more melanoma attributed to the head and neck and the trunk (Figure 19b).

There were also collected data concerning the subtype of melanoma. As shown in Figure 19c, the superficial spreading melanoma proved to be the most frequent subtype across both sexes (43%), followed by the nodular melanoma, which accounted for 22% of all cases. The remaining samples were diagnosed as lentigo maligna (1%), lentigo malignant melanoma (5%), and acral melanoma (9%). Under the category "others" (12%), low-frequency melanoma, such as those of mucosal origin, were grouped.

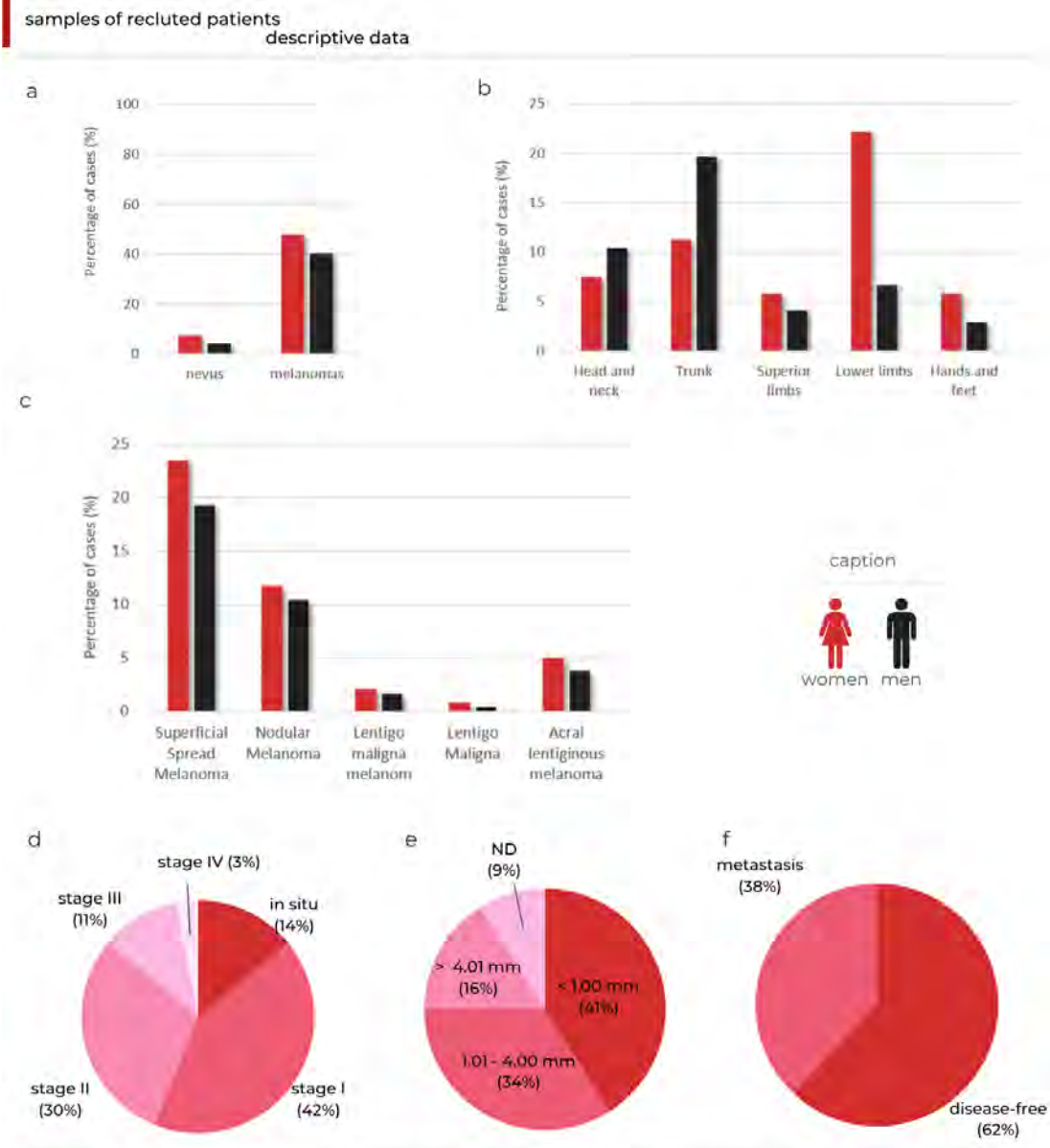


FIGURE 19 Distribution of the samples according to (a) diagnosis, (b) tumour location and (c) histological subtype, (d) AJCC stages, (e) Breslow Index expressed in mm and (f) evolution of patients diagnosed in AJCC I and II stages. All bar charts show the characteristics of the melanoma samples included in this study according to sex

A notable aspect of this study is how many patients included in it were diagnosed at an early stage of their disease (86%) according to AJCC's staging system (8th edition). As shown in Figure 19d, melanoma were found in 14% of cases as in situ melanoma, 42% as stage I melanoma, and 30% as stage II melanoma. Patients diagnosed in stages III and IV constituted 14% of the total.

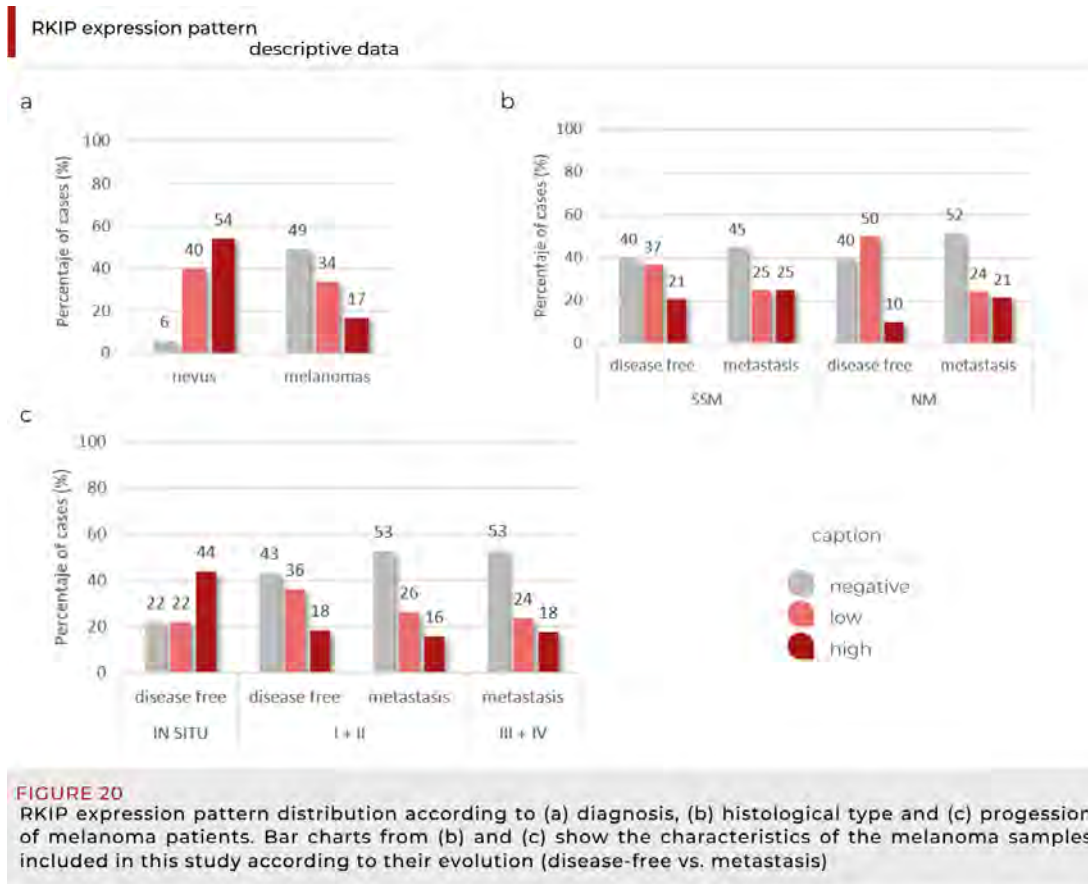
In connection with that, the samples according to the Breslow index, which is used to determine the thickness of tumors, was 41% for tumors that had a thickness of less than a millimeter and 30% for tumors with a thickness between 1 millimeter and 4 millimeters (Figure 19e).

Furthermore, 62% of all melanoma cases analyzed in this study remained disease-free. In comparison, 38% of patients were diagnosed at an advanced stage or developed metastasis during follow-up (the inclusion criteria for this group required a minimum tracking period of two years). This study did not observe a difference in sex-related outcomes, with the same number of men and women in the two groups (Figure 19f).

Differential expression of RKIP protein between nevi and melanoma biopsies

Two independent reviewers evaluated RKIP staining at negative, low, and high expression. A high proportion of nevus samples expressed RKIP, whereas a large number of melanoma samples lost this protein expression (Figure 20a).

Among those with melanoma, most samples analyzed correspond to the histological subtypes of superficial spreading melanoma and nodular melanoma. As shown in Figure 20b, the pattern of RKIP expression does not differ between the groups based on histology and malignant progression. When analyzing the distribution based on the stage at diagnosis, more samples are marked as negative in patients with stages I and II who have metastasized, as well as in those with stages III and IV (Figure 20c).



Representative IHC images of most common lesions (compound nevus, superficial spreading melanoma, and nodular melanoma) are shown in Figure 21a, while the statistical analyses are summarized in Figure 21b–e. Nevi samples exhibited higher positivity for RKIP staining compared with the whole cohort of melanoma samples (Figure 21b); 94% of nevi samples were positive for RKIP whereas only 51% of melanoma cases presented positive staining. Interestingly enough, in situ melanoma, characterized by an excellent prognosis upon surgical removal, exhibited a strong positive RKIP expression in almost 80% of cases. Of note, RKIP staining displayed minimum intrasample variation and a cytoplasmic localization. Univariate analysis confirmed the statistical significance of observed differences among nevi and the entire set of melanoma samples ($q < 0.001$) (Figure 21b) and both, univariate and multivariate analysis, provided statistical evidence for a different level of expression of RKIP in nevi and melanoma at early stages (AJCC 8th I/II) (Figure 21c). Moreover, by means of a logistic regression analysis (Nevus = 0, Melanoma = 1) to control for age and sex as covariates (Figure 21c), a polynomial contrast expansion in RKIP demonstrates that this association is linear ($\beta = -2.288$, $q < 0.001$), i.e., linear increments in protein levels correlate significantly with a larger probability of the biopsies of being identified as nevus, while quadratic effects tend to be moderate and non-significant ($\beta = 0.465$, $q = 0.218$).

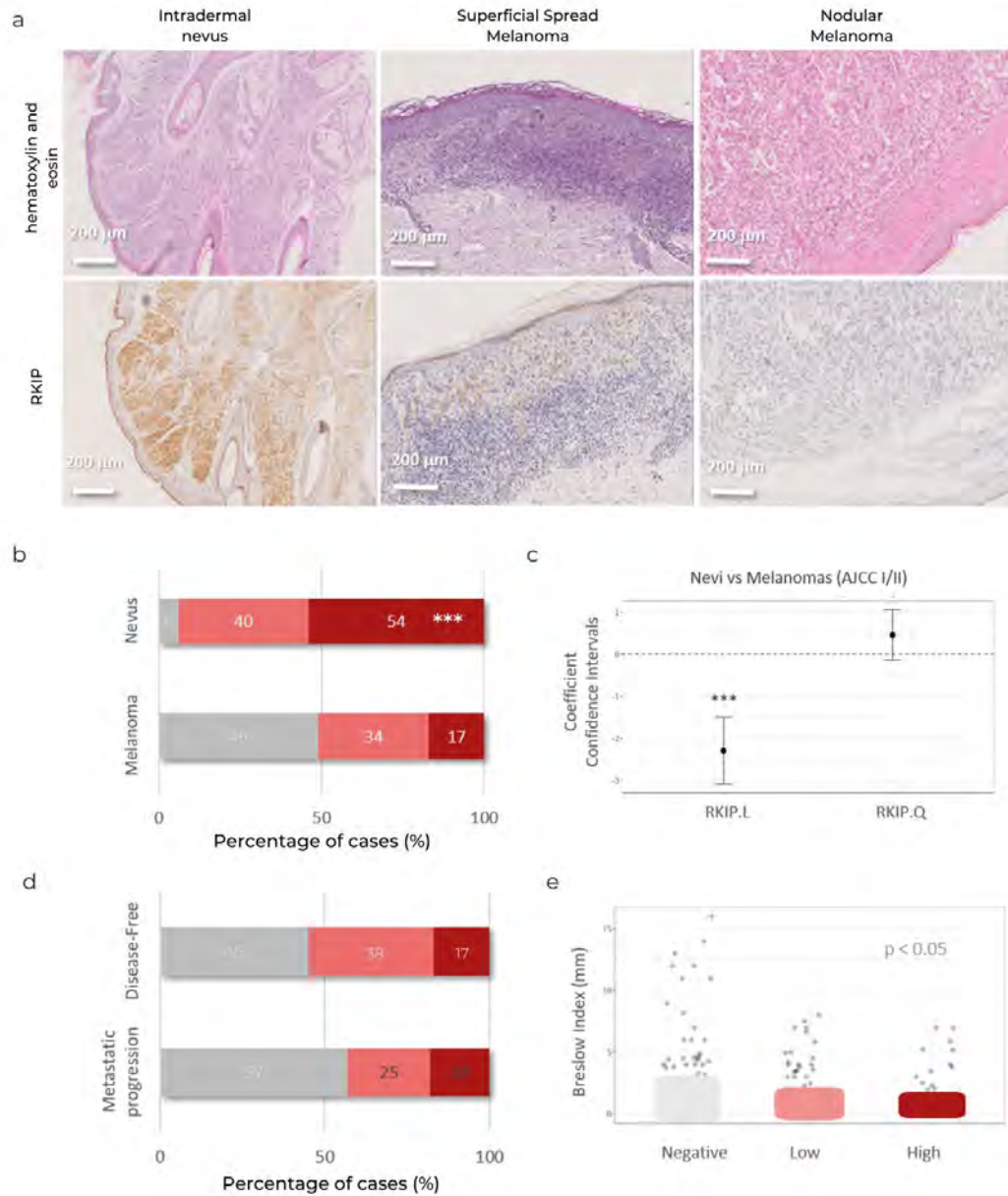


FIGURE 21 Raf Kinase Inhibitor Protein (RKIP) expression in FFPE biopsies from patients. (a) Upper section of picture: Hematoxylin-Eosin staining. Lower section of picture: IHC analysis of RKIP in normal melanocytes from a compound nevus, superficial spreading melanoma and nodular melanoma, (b) RKIP staining distribution on nevus and melanoma tissue, (c) Coefficient confidence intervals for RKIP protein expression between nevus and melanoma samples, (d) RKIP staining distribution on histological sections of melanoma in stages I and II from patients who remained disease-free during follow-up versus patients who developed metastasis, (e) Kruskal-Wallis one-way analysis of Breslow index with respect to RKIP expression. * $q < 0.05$, *** $q < 0.001$

On the other hand, changes in the levels of RKIP did not statistically associate with metastasis development either when including the whole spectrum of melanoma staging ($q = 0.132$), or if we only consider the clinical-risk subset of melanoma subjects (AJCC I + II) ($q = 0.499$) (Figure 21d). Likewise, no significant pattern-differences in this protein were observed between AJCC stages I and II ($q = 0.520$). Nonetheless, we observed an association among RKIP staining and Breslow thickness as melanoma biopsies with higher RKIP protein level tended to display significantly lower values of Breslow thickness ($q = 0.014$) across all AJCC stages (Figure 21e).

An immunohistochemical panel showing the expression of RKIP in relation to malignant progression is shown in Figure 22. In order to illustrate this, a sample of dysplastic nevus is viewed first, followed by a sample of melanoma in situ, and finally melanoma exhibiting an increasing Breslow index. Generally, RKIP expression levels decline with increasing malignant progression, with high levels observed in dysplastic nevi and a progressive loss in tumors with higher Breslow index

In summary, clear RKIP staining differences were observed among benign (nevi) and early stage (I–II) melanoma. In addition, RKIP staining could not predict disease progression but high RKIP level correlated with lower Breslow thickness in samples of all melanoma stages (Figure 22).

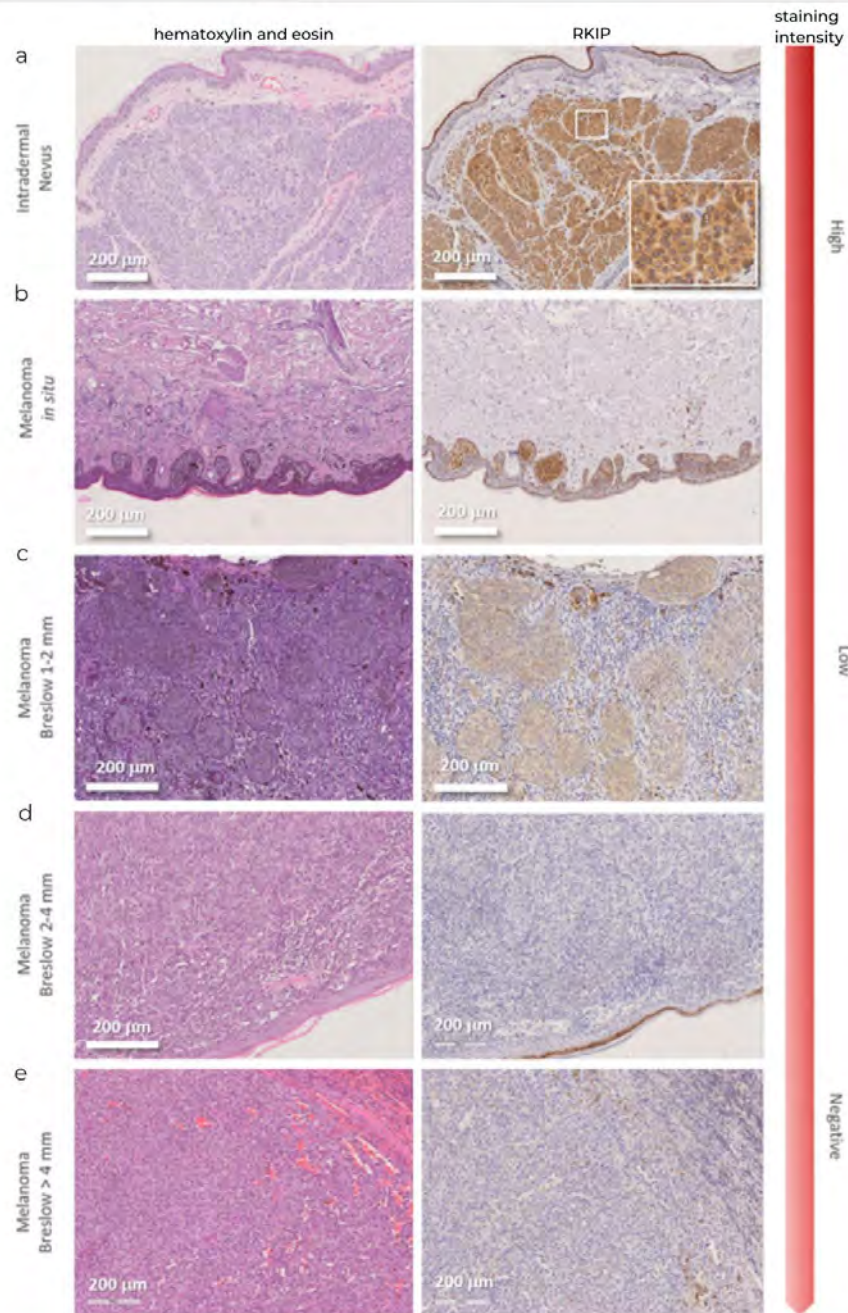
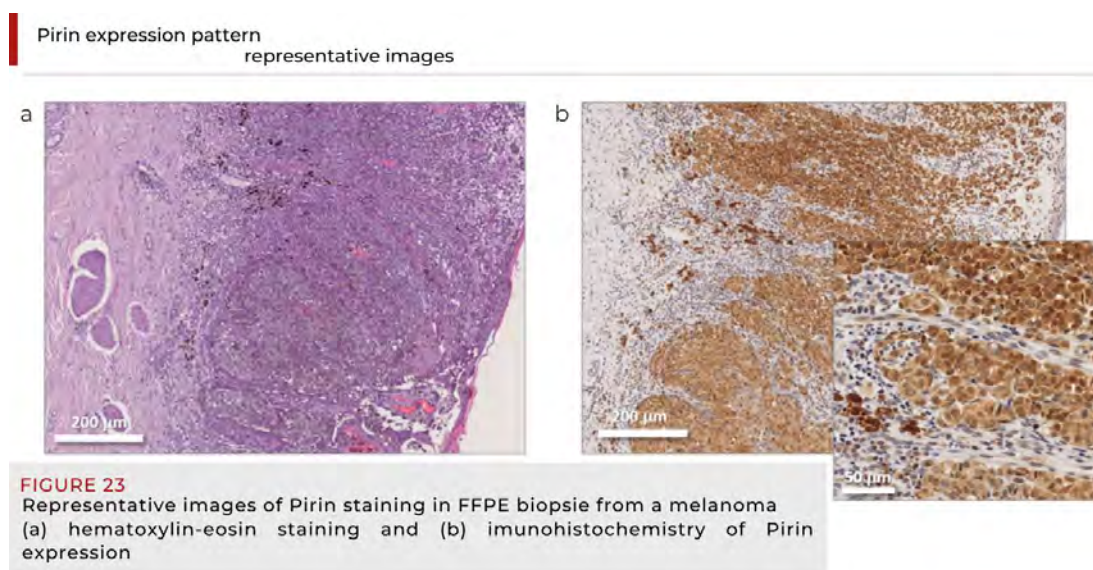


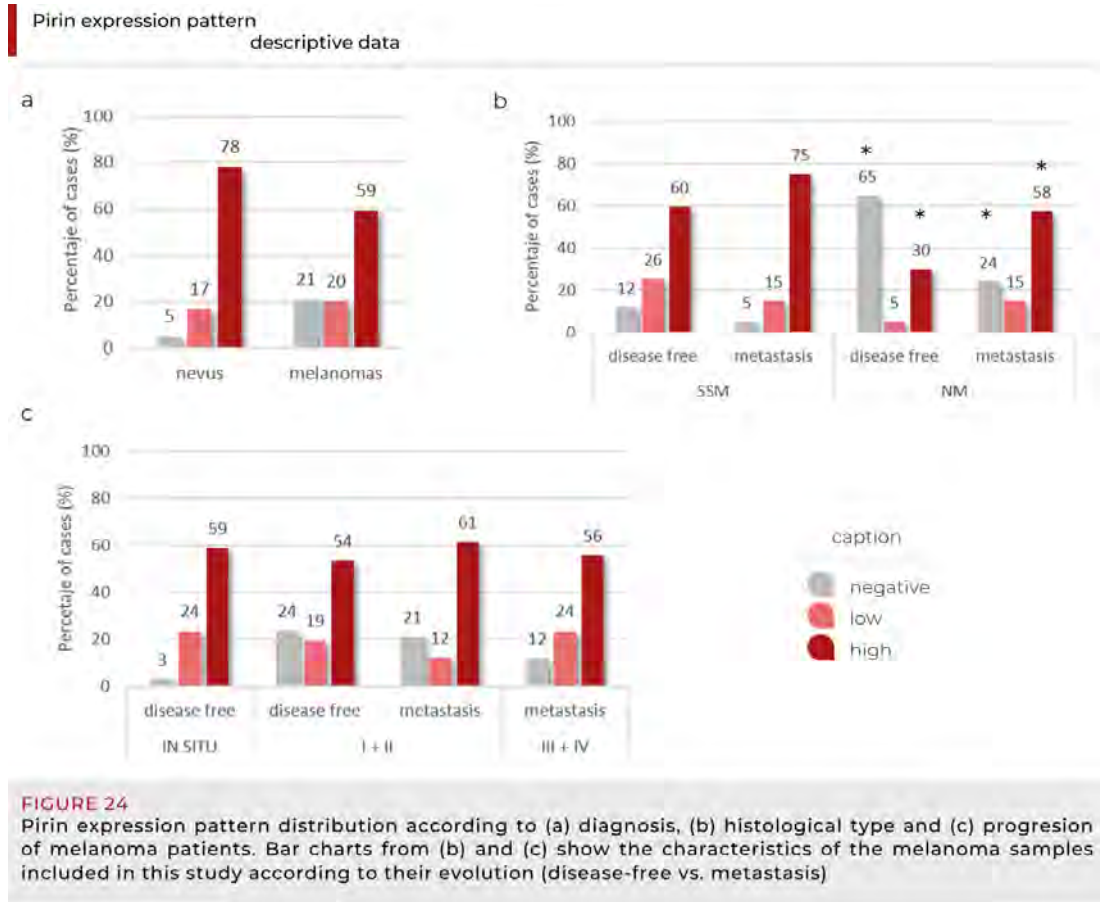
FIGURE 22
Representative images of manually scored RKIP staining categories in FFPE biopsies from patients. At the left: Hematoxylin-Eosin staining (H-E). At the right: Immunohistochemistry (IHC) of RKIP for increasing Breslow Index. (a-b) Strong staining for intradermal nevus and in situ melanoma, respectively; (c) weak staining for a melanoma with Breslow Index between 1 and 2 mm; (d-e) negative staining for melanomas thicker than 2 mm

Pirin expression and the Breslow thickness in melanoma biopsies is correlated with the metastatic progression of melanoma

The determination of Pirin expression levels in melanoma biopsies was conducted in the same manner and with the consecutive sample slides as that which was described previously for RKIP IHC. Pirin immunostaining was observed in some cells in both nuclear and cytoplasmic regions and others only cytoplasmic. There was no correlation between the expression location and the histology type of melanoma, stage, or melanoma progression (Figure 23).



When comparing Pirin expression in nevi and melanoma, we first observed that 80% of the nevi biopsies were strongly stained for Pirin, which was significantly more than in the cohort of melanoma samples, in which strong Pirin expression was seen in 60% of the histological sections ($p < 0.05$; Figure 24a, Figure 25a). Surprisingly, the analysis by histological type revealed a differentiation in the expression pattern between superficial spreading and nodular melanoma (SSM and NM, respectively). SSM patients had similar expressions of Pirin regardless of their evolution. However, in the case of nodular melanoma, patients that eventually developed metastatic disease had the highest levels of Pirin expression in their primary melanoma in a more significant proportion than patients who remained disease-free (Figure 24b). As shown in Figure 24c, no differences between patients who developed metastasis and remained disease-free during follow-up were found.



The usefulness of Pirin expression as an early prognostic marker was evaluated, only using the biopsies from early stage melanoma patients (stages I and II, according to AJCC 8th) and classifying them according to their clinical progression (metastasis or not: Figure 25b). We did not observe a direct association between Pirin expression and the patients who remained disease-free or those who developed metastases during the follow-up (Cochran-Armitage $\chi^2 = 1.372$, $p = 0.271$). However, since our data from early primary melanoma was heterogeneous, one might expect that other potential risk factors might be masking the association between Pirin expression and the probability of metastasis. For example, both age and Breslow depth appeared to be statistically higher in the metastatic group ($Z = -3.965$, $P < 0.001$) than in the disease-free group ($Z = -8.0526$, $P < 0.001$), the latter serving as an indicator of melanoma stage.

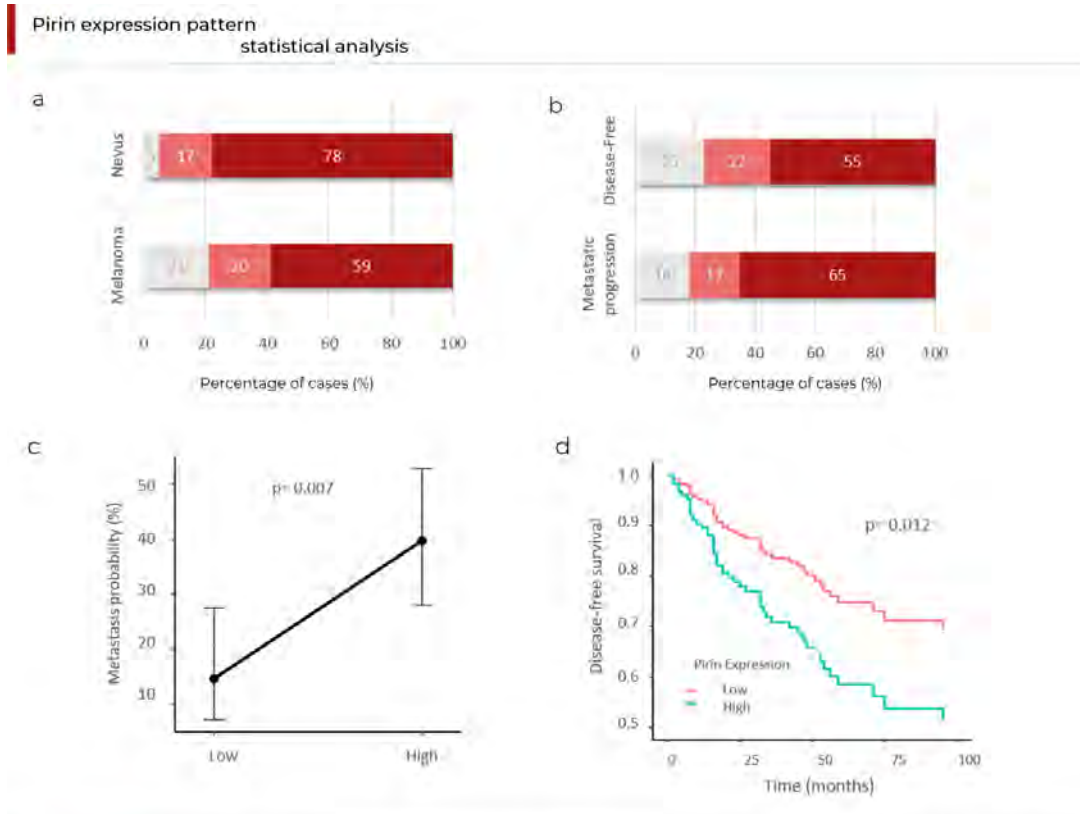


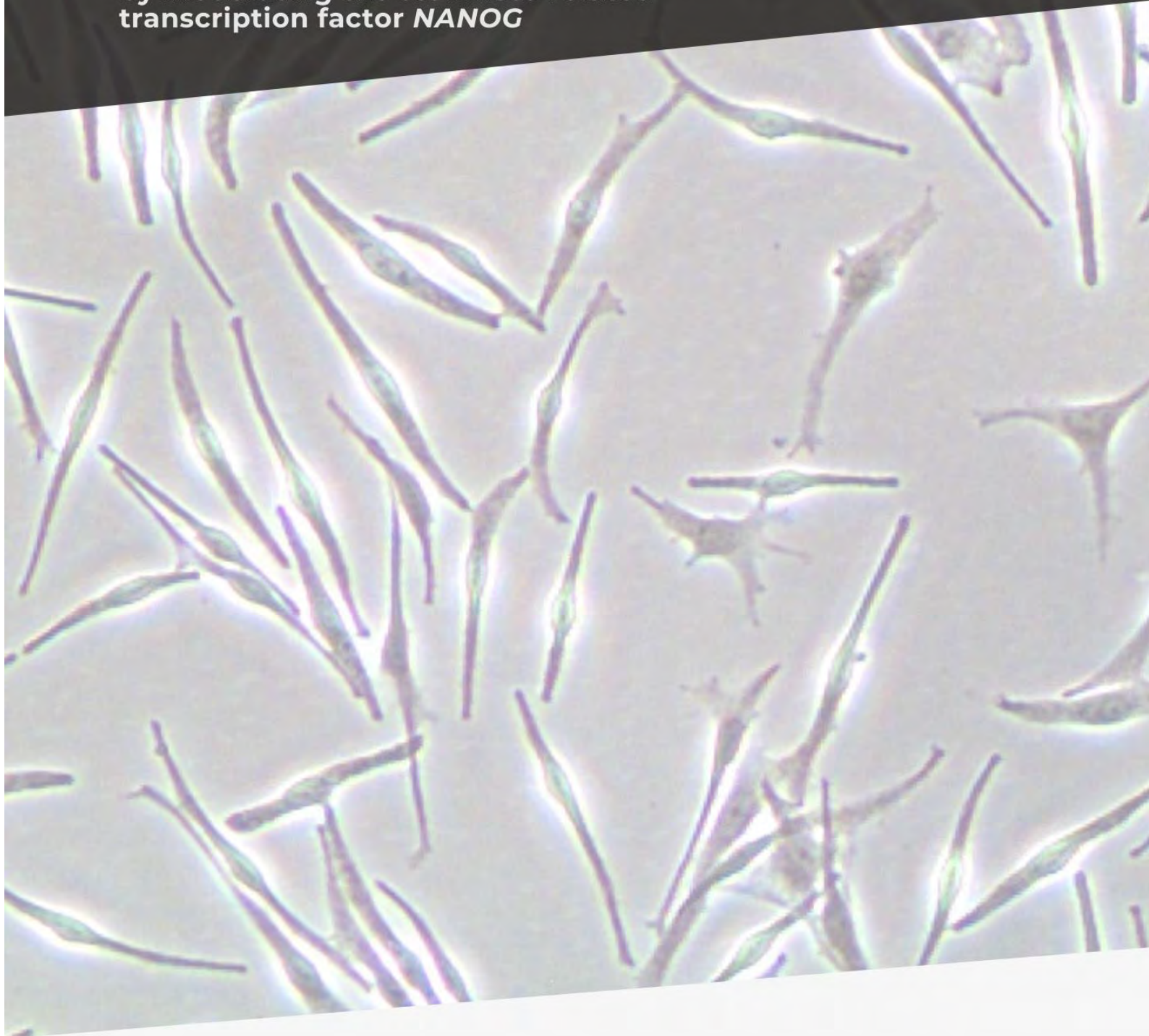
FIGURE 25

Pirin expression in FFPE biopsies from melanoma patients. (a) Comparative analysis of the proportion of cases with each level of Pirin expression between nevi and melanoma cases, (b) Comparative analysis of patients with early stage melanomas (I and II stages, AJCC 8th) who remained disease-free or developed metastasis during the follow-up and the proportion of cases with each level of Pirin expression, (c) The marginalized metastatic probability with respect to Pirin expression (Low and High) from a Logistic Regression model, which also included the Breslow Index, age and sex as co-variates and, (d) Adjusted survival curves in terms of Pirin expression using a Cox Proportional-Hazard model: * $p < 0.05$

Consequently, we set out to test the differences in a multivariate scenario that included Pirin expression as our effect of interest, and age, sex and Breslow depth as possible co-variants. We further simplified our procedure by comparing the intense expression of Pirin (“High”) with the merged low levels of negative and low expression (“Low”). Stronger Pirin expression was significantly associated with an increased probability of metastasis as witnessed in a logistic regression model ($p=0.007$, $OR=3.851$, $95\% CI [1.453, 10.213]$; Figure 25c). Furthermore, we performed a Bayes factors analysis to determine the probability of the alternative hypothesis, i.e.: the existence of an association between strong Pirin expression and metastasis. The result turned out to be positive, with a $BF_{01}=0.090$ and a $BF_{10}=11.097$, which implies that the existence of a relationship between strong Pirin expression and metastasis is 10 times more likely than the existence of no such effect. Finally, a Cox analysis showed that patients with stronger Pirin expression have more than twice the probability of developing early metastasis compared to those expressing Pirin weakly ($p=0.012$, $HR=2.305$, $95\% CI [1.203, 4.417]$), $BF_{01}=0.189$, $BF_{10}=5.28$; Figure 25d).

Chapter 02

RKIP regulates melanocyte differentiation by modulating the stemness-related transcription factor *NANOG*



This chapter has been published in *Cancers*:

Penas C, Apraiz A, Muñoa I, Arroyo-Berdugo Y, Rasero J, Ezkurra PA, Velasco V, Subiran N, Bosserhoff AK, Alonso S, Asumendi A, Boyano MD. **RKIP Regulates Differentiation-Related Features in Melanocytic Cells.** *Cancers (Basel)*. 2020 Jun 3;12(6):1451. doi: 10.3390/cancers12061451. PMID: 32503139; PMCID: PMC7352799.

Chapter 02

RKIP regulates melanocyte differentiation by modulating the stemness-related transcription factor

As a signaling switch, RKIP plays a role in essential processes such as differentiation, proliferation, and cell survival. Moreover, deregulation of *RKIP* expression has been associated with a wide variety of disorders such as neurological diseases, diabetes, altered spermiogenesis and cancer (113-115). With a general loss of *RKIP* expression in tumor tissues and its demonstrated ability to influence pathways leading to tumor cell proliferation or an invasive phenotype (65-67, 134), a more comprehensive analysis of RKIP-dependent pathways on primary cells is necessary to determine profile alterations that may influence cellular transformation or promote an aggressive phenotype. Thus, in this work, we examined the role of RKIP in the biology of primary melanocytes and malignant melanoma cells.

Involvement of RKIP on malignancy-related properties of melanoma cells

To study the involvement of RKIP in the pathogenesis of melanoma, we modified the endogenous *RKIP* levels expression on A375 and MelHo primary melanoma cell lines and A2058 and MeWo metastatic melanoma cell lines. Downregulation of endogenous RKIP was accomplished by RKIP shRNA lentiviral particles, while RKIP-overexpressing plasmids were used to increase cellular RKIP levels.

Downregulation by shRNA led to a decrease of up to the 70-80% on the endogenous *RKIP* mRNA level on selected primary melanoma cells lines (Figure 26a) which was also consistent with a reduction on the protein percentage (Figure 26b). Reduction of endogenous RKIP by lentiviral silencing did not alter proliferation capability of A375 and MelHO cells (Figure 26c). By contrast, the RKIP-downregulated primary melanoma cells showed a significantly increase in motility, assessed both by wound healing and collagen-coated transwell assays (Figure 26d-e).

modulation of RKIP expression in primary melanoma cell lines
functional assays

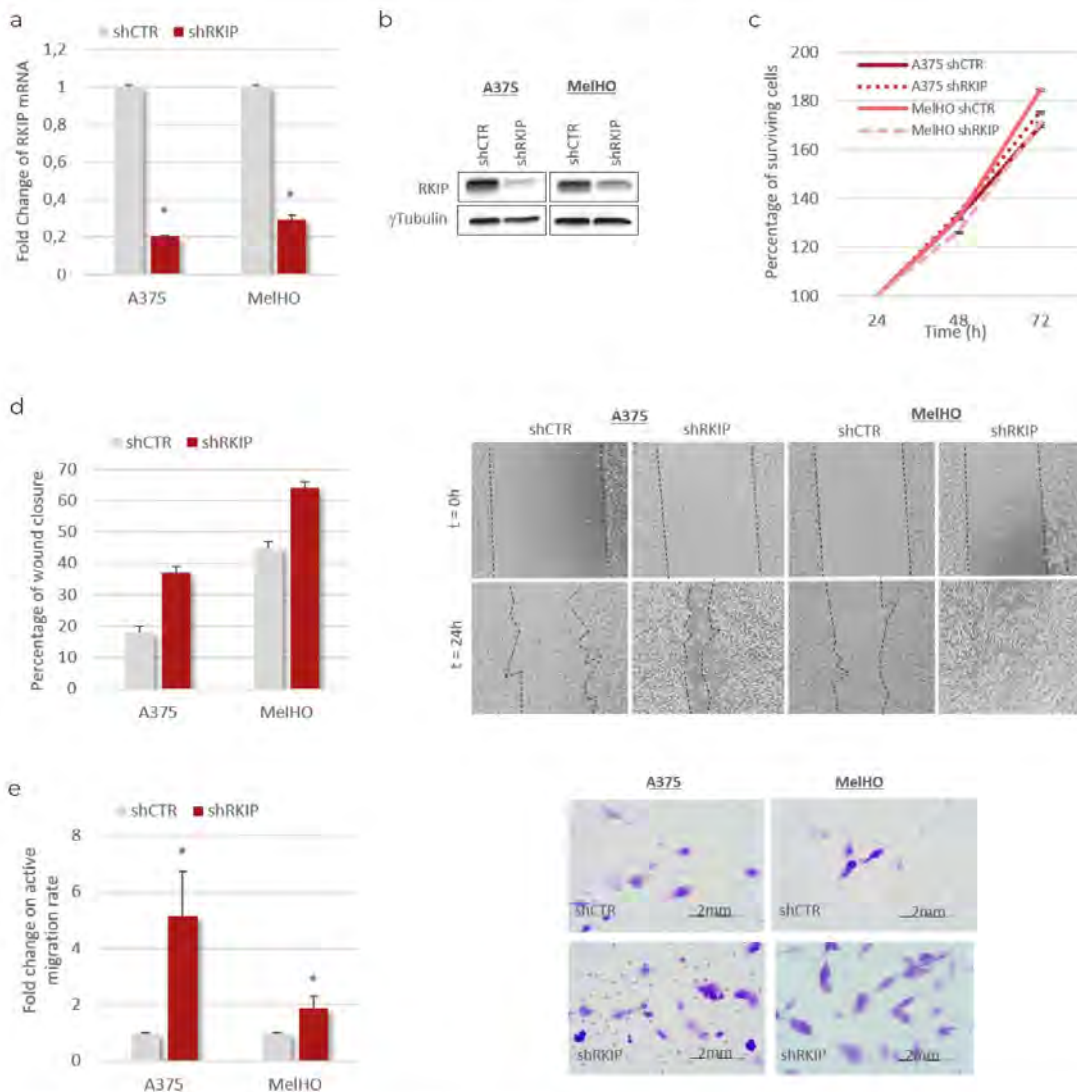
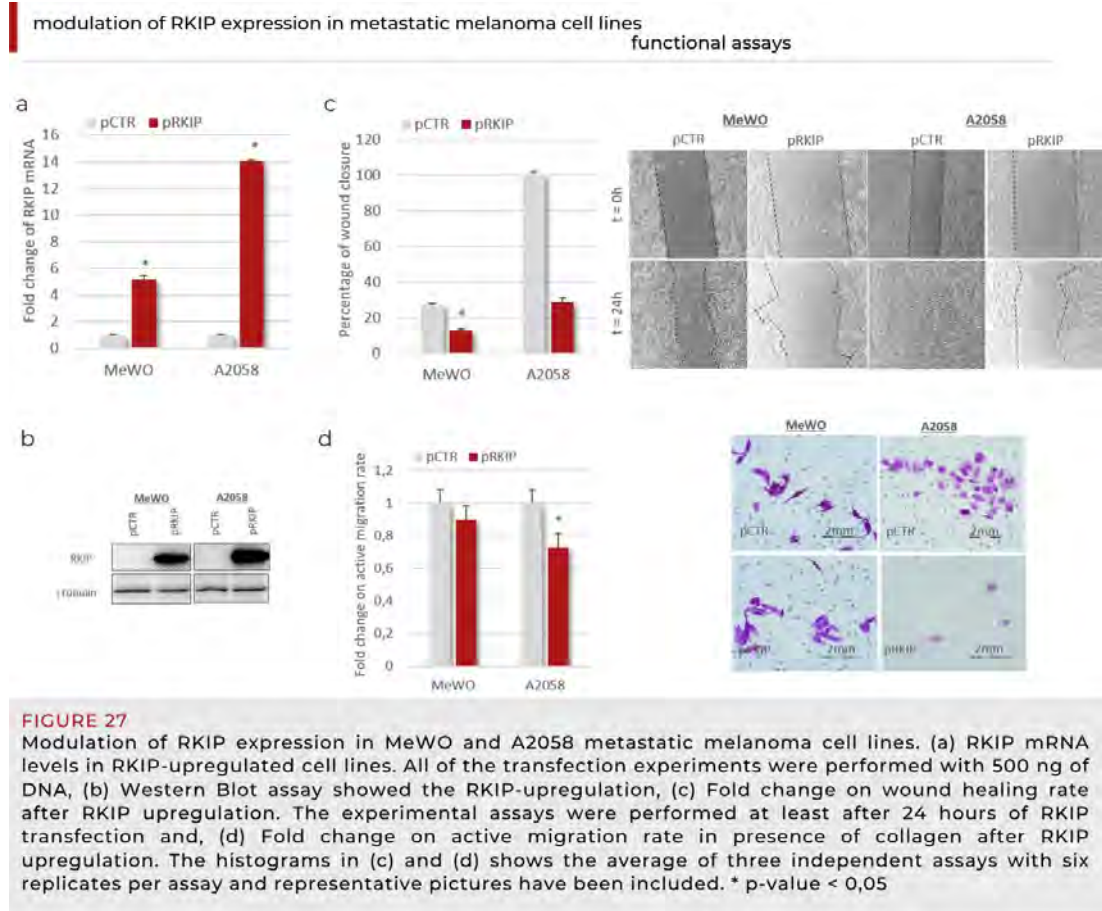


FIGURE 26
Modulation of RKIP expression in A375 and MelHO primary melanoma cell lines. (a) RKIP mRNA levels in RKIP-downregulated, (b) Western Blot assay showed the RKIP-downregulation, (c) Proliferation rate after RKIP downregulation determined by XTT assay. Results of each experiment are expressed related to the values obtained for the transfection control. Data as given as a mean \pm SD of at least three experiments of different transfection; (d) Fold change on wound healing rate after RKIP downregulation, (e) Fold change on active migration rate in presence of collagen after RKIP downregulation. The histograms in (d) and (e) shows the average of three independent assays with six replicates per assay and representative pictures have been included. * p-value < 0,05

To reinforce our data regarding the involvement of RKIP expression in melanoma cell motility, MeWO and A2058 metastatic melanoma cell lines were transfected with a RKIP-overexpressing plasmid resulting in a 5 and 15-fold increase of *RKIP*-mRNA level, respectively (Figure 27a). In addition, we detected a concomitant elevation of intracellular RKIP-protein percentage (Figure 27b).

Consistent with our previous results in primary melanoma, the increase on cellular RKIP expression level led to a decrease in the migration capability of melanoma cells (Figure 27c). Surprisingly, both

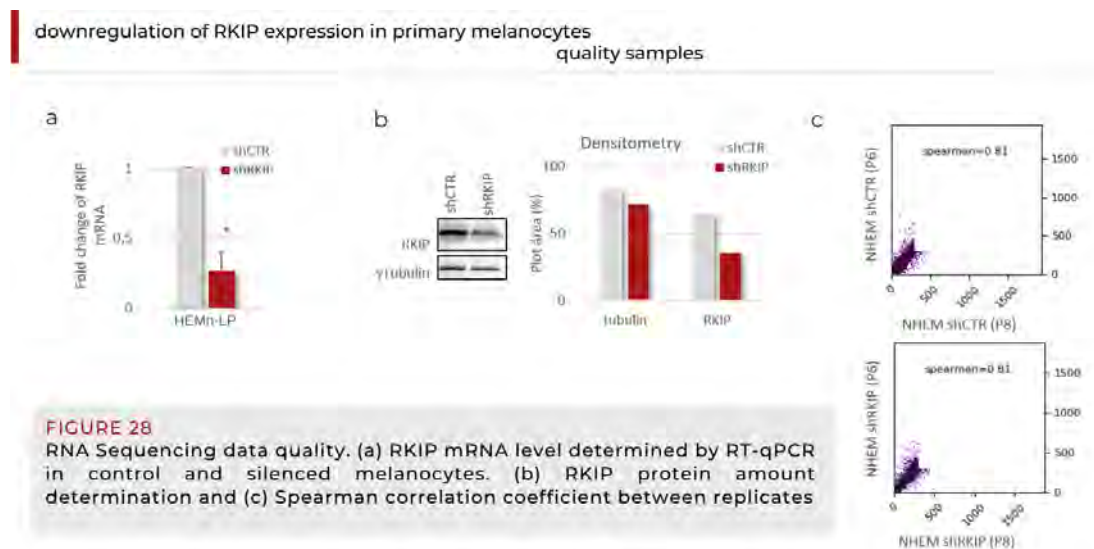
analyzed cell lines showed different behavior on the active migration assay (Figure 27d); thus, while no differences were observed in MeWO cells, RKIP overexpression clearly diminished the capacity of A2058 cells to pass through a collagen-based barrier. Of note, basal collagen-through migration activity of MeWO cells was significantly lower than that of A2058 cells (data not shown).



Briefly, cellular RKIP levels were inversely correlated to the migration capability of both, primary and metastatic melanoma cell lines, while no major effect was detected on cellular proliferation.

Transcriptome modulation by RKIP downregulation in HEMn-LP cells

With the aim of elucidating the molecular mechanisms whereby RKIP could modulate processes related to cellular malignancy, *RKIP* was downregulated in primary melanocytes (HEMn-LP) by the above described shRNA lentiviral particles. Infection resulted in a 70-80% reduction of *RKIP* mRNA and 40% of protein level (Figure 28).



Two independent replicates of control (shCTRL) and RKIP knockdown (shRKIP) HEMn-LP samples were subjected to RNA sequencing. The first part of the analysis focused on the identification of a set of differentially expressed genes between shCTRL and shRKIP HEMn-LP based on standard threshold $\text{Log}_2\text{FC} \geq 1$, $p\text{-value} \leq 0.05$ and False Discovery Rate (FDR) ≤ 0.05 . The resulting 224 differentially expressed genes were used for monitoring the functions and pathways that were mainly affected in melanocytes due to the decreased *RKIP* expression. The set of genes with modified expression were roughly equally divided into over- (113) and under-expressed genes (111). The Log_2FC , p-values and FDR for each gene are detailed in *Annex B*: Table S1.

In order to gain insight into the functional characteristics of detected changes, over- and under-expressed genes after RKIP silencing were subjected to pathway (Kyoto Encyclopedia of Genes and Genomes, KEGG) (Figure 29a) and Gene Ontology (GO) (Figure 29b) enrichment analyses. RKIP knockdown on HEMn-LP cells displayed a transcriptional misregulation in the GO term ‘cancer gene signature’ ($p\text{-value} < 0.001$).

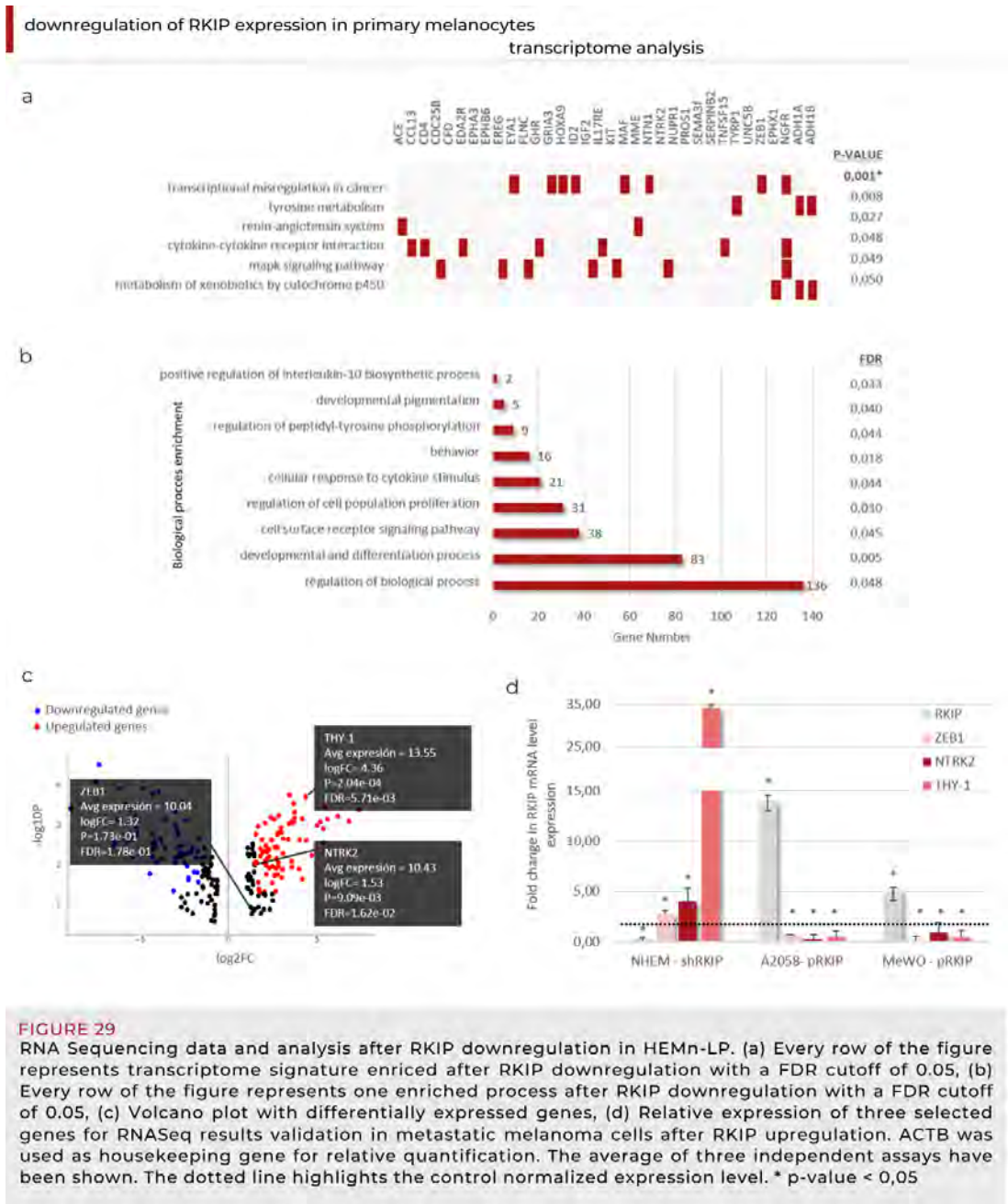


FIGURE 29
 RNA Sequencing data and analysis after RKIP downregulation in HEMn-LP. (a) Every row of the figure represents transcriptome signature enriched after RKIP downregulation with a FDR cutoff of 0.05, (b) Every row of the figure represents one enriched process after RKIP downregulation with a FDR cutoff of 0.05, (c) Volcano plot with differentially expressed genes, (d) Relative expression of three selected genes for RNASeq results validation in metastatic melanoma cells after RKIP upregulation. ACTB was used as housekeeping gene for relative quantification. The average of three independent assays have been shown. The dotted line highlights the control normalized expression level. * p-value < 0,05

Moreover, the set of genes with altered expression upon endogenous RKIP reduction showed an enrichment in a variety of essential processes including developmental pigmentation, proliferation and developmental and cell differentiation (p-value < 0.05; Figure 29b, Annex C: Table S3). Interestingly, RKIP knockdown led to the downregulation of essential melanocyte-pigmentation genes such as *PMEL* (Melanocytic lineage-specific antigen, 2-fold decrease, p value 0.0003, FDR 0.04), *MLANA* (Melanoma Antigen recognized by T-cells, 8-fold decrease, p value 0.001, FDR 0.02), *GPRI43* (G-Protein Coupled Receptor 143, 11-fold decrease, p value 10⁻⁵, FDR 0.01) and *TYRP1* (Tyrosinase-related protein 1, 5-fold decrease, p value 10⁻⁶, FDR 0.007). On the other hand, only *KIT* (proto-oncogene KIT,) was upregulated among the deregulated genes belonging to the developmental pigmentation group (2.3-fold increase, p value 0.0001, FDR 0.02).

Development and differentiation showed the best FDR value among significantly enriched biological processes. This signature encompassed 83 genes which represented 37% of the total altered gene-set and included HOX family members, proto-oncogene *KIT*, proto-oncogene *MYC*, *ZEB1* and Thy-1 cell surface antigen (*THY-1*), among others (*Annex C*: Table S3). We focused on genes belonging to this process due to the statistical robustness of this group on our data set as well as to the intimate link among this particular process and the cellular migration-capability. As shown in Figure 29c-d, downregulation of endogenous RKIP led to an increase on the expression of selected genes, validating the RNA Seq data.

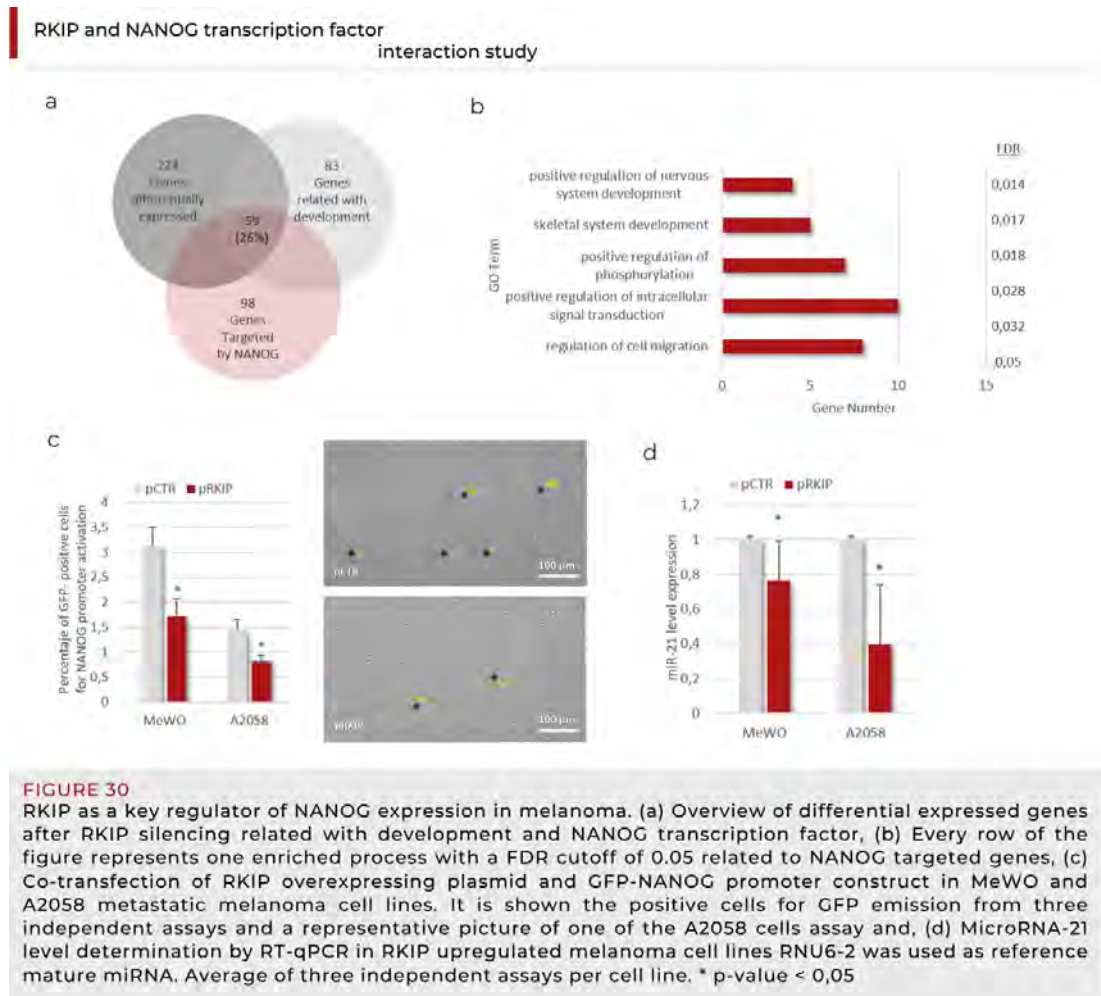
Interestingly, neurotrophic receptor tyrosine kinase 2 (*NTRK2*), *ZEB1* and *THY-1* are not only implicated in developmental processes, as they also known regulators of cellular migration. Based on our previous results that implicated RKIP on the migration capability of melanoma cells, we made use of RKIP overexpression to analyze the effect on *ZEB1*, *NTRK2* and *THY-1* transcription. RKIP-driven transcriptional repression was confirmed by RT-qPCR for *ZEB1* and *THY-1* in both cell lines (A2058 and MeWO) while *NTRK2* revealed a cell type-dependent response (Figure 29d). Taking together, RKIP revealed the capacity to modulate genes involved in essential processes (e.g. Development and differentiation) and to repress genes with described roles in cellular migration.

NANOG as a putative transcription factor regulated by RKIP

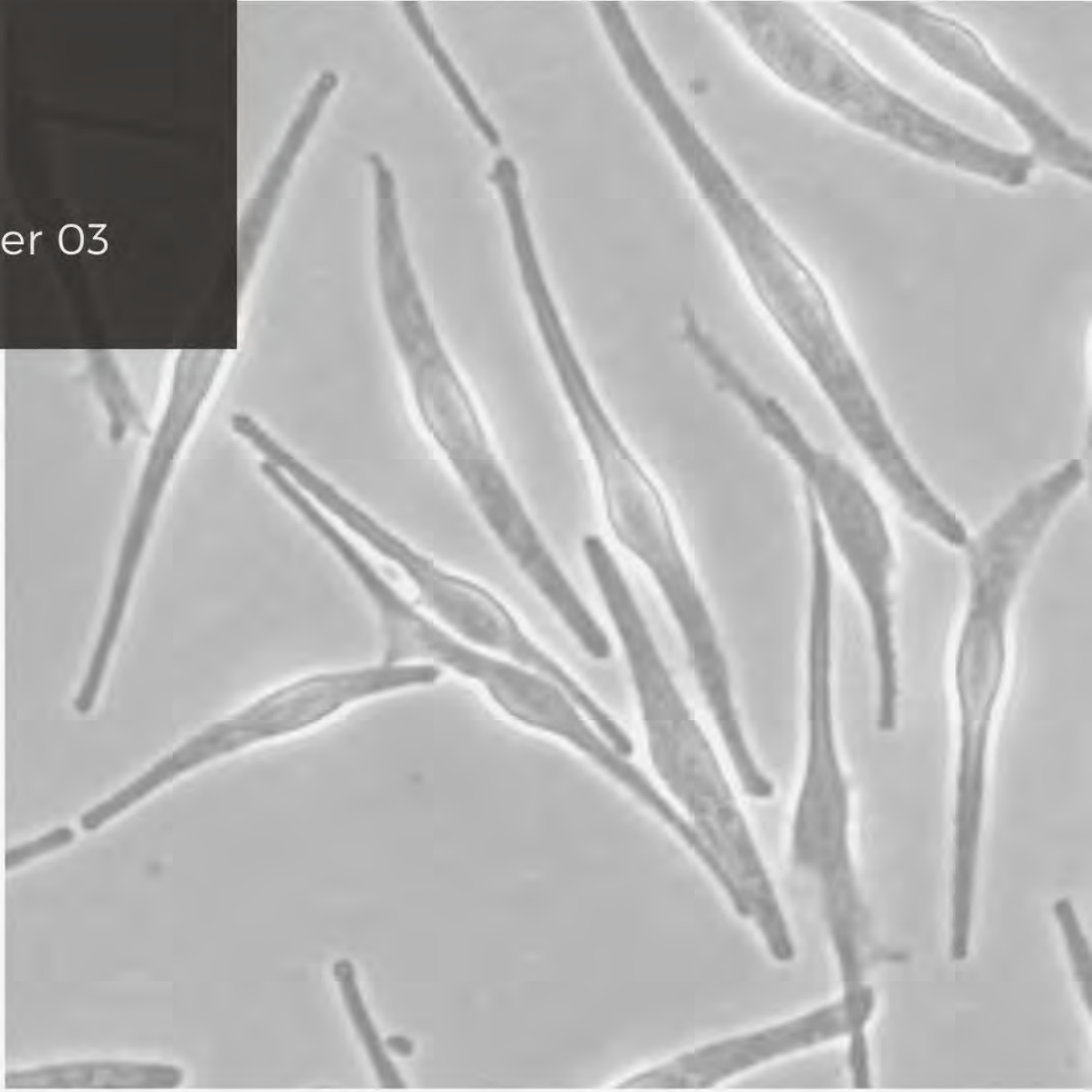
RKIP has no described function as a direct transcriptional regulator. Thus, observed transcriptional alterations imply the presence of yet unknown transcription factors or regulators downstream RKIP. We focused on deregulated genes belonging to development and differentiation and conducted an in silico approach in order to detect potential transcription factors acting between RKIP and its downstream modulated genes. Seventy-one percent of genes in this category were putative targets of NANOG transcription factor (Figure 30a, *Annex C*: Table S4, Table S5). *NANOG* is a transcription factor involved in the maintenance of stemness and often linked to cancer aggressiveness (Figure 30b). Therefore, we wonder whether RKIP could somehow modulate *NANOG* expression. To analyze this point, we made use of a construct encoding the *NANOG* promoter attached to the Enhanced Green Fluorescent Protein (EGFP) coding sequence, and cells were cotransfected with either empty plasmid (pCTR) or RKIP-coding plasmid (pRKIP). Activation of *NANOG* promoter was determined as the percentage of cells expressing EGFP. As shown in Figure 30c, increased RKIP expression led to a significant decrease on *NANOG* promoter activation; a similar effect was observed in both cell lines.

The gene miR-21 is a described target for NANOG (78). To further validate the implication of RKIP in *NANOG* regulation, we determined miR-21 transcription level upon RKIP overexpression. As shown in Figure 30d, the expression of miR-21 was significantly lower on RKIP-overexpressing cells.

These findings point towards the involvement of NANOG downstream RKIP in the regulation of gene expression.



Chapter 03



Pirin modulates melanoma proliferation by targeting the slow-cycling transcriptional regulator JARID1B

This chapter has been submitted to be published in Scientific Report:

Penas C, Arroyo-Berdugo Y, Apraiz A, Rasero J, Muñoa I, Andollo N, Cancho-Galán G, Izu R, Gardeazabal J, Ezkurra PA, Alvarez-Dominguez C, Alonso S, Bosserhoff AK, Asumendi A, and Boyano MD. **Pirin is a prognostic marker of human melanoma that dampens the proliferation of malignant cells by downregulating JARID1B/KDM5B expression.** Submission ID: f935f498-4b94-4e99-b05a-c2b0d23df55c

Chapter 03

Pirin modulates melanoma proliferation by targeting the slow-cycling transcriptional regulator JARID1B

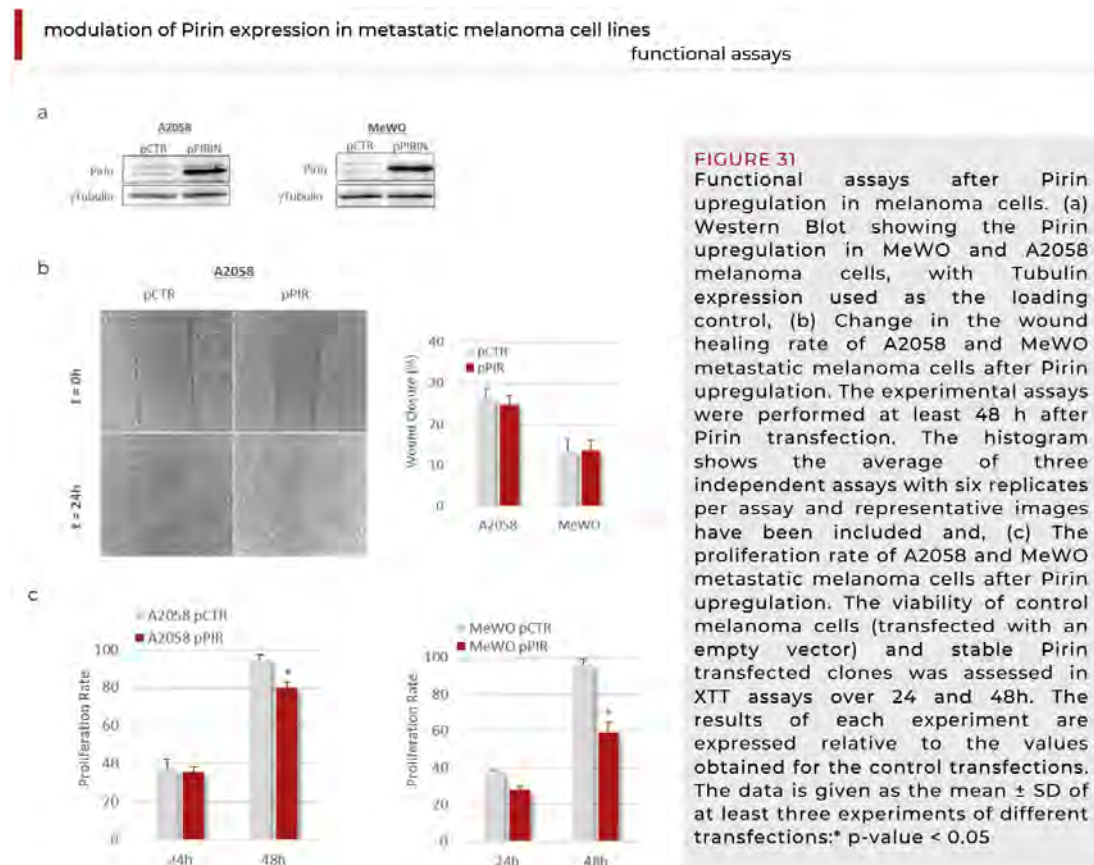
Several studies revealed the implication of Pirin in a wide range of processes, including cell cycle control (117-119), inflammatory responses (120,121), migration and the EMT (121-127). Similarly, to other cupin proteins, Pirin also displays enzymatic properties and functions as a nuclear transcriptional regulator (123). Moreover, Pirin inhibition has been related to weaker migratory capacity of melanoma cells (122), and it has been proposed to inhibit cellular senescence (135). Due to that, in recent years, speculation regarding its oncogenesis potential has increased (118, 119, 122).

Pirin expression regulates the proliferation rates of melanoma cell lines

To further study the role of Pirin in the pathogenesis of melanoma, we evaluated the expression of Pirin in melanocytes and in eleven melanoma cell lines by RT-qPCR and in Western Blots. The relative Pirin mRNA levels reflected the generalized weaker expression of the PIR gene in melanoma cell lines relative to the melanocytes from neonatal foreskin ($p\text{-value}=7.04\text{E}^{-08}$: see Figure 11c, *Hypothesis and Objectives section*). Notably, heterogeneous mRNA levels were detected among the melanoma cell lines. Accordingly, when we analysed the amounts of Pirin protein (see Figure 11d, *Hypothesis and Objectives section*), less Pirin was evident in all the melanoma cell lines analysed relative to the melanocytes.

These results were consistent with the generally stronger Pirin expression observed in benign nevi relative to the melanoma biopsies. However, the significant heterogeneity found in the melanoma biopsies and the melanoma cell lines, and the relationship between Pirin expression and melanoma progression, led us to study the involvement of Pirin in the proliferation and migration of two metastatic melanoma cell lines. The differences in Pirin expression observed between benign and malignant lesions, as well as in the cell lines, suggested a need to assess the biological processes regulated by Pirin in the context of melanoma. As such, MeWo and A2058 melanoma cells were transfected with a plasmid to overexpress PIR, and the proliferation and migration of these cells was analyzed.

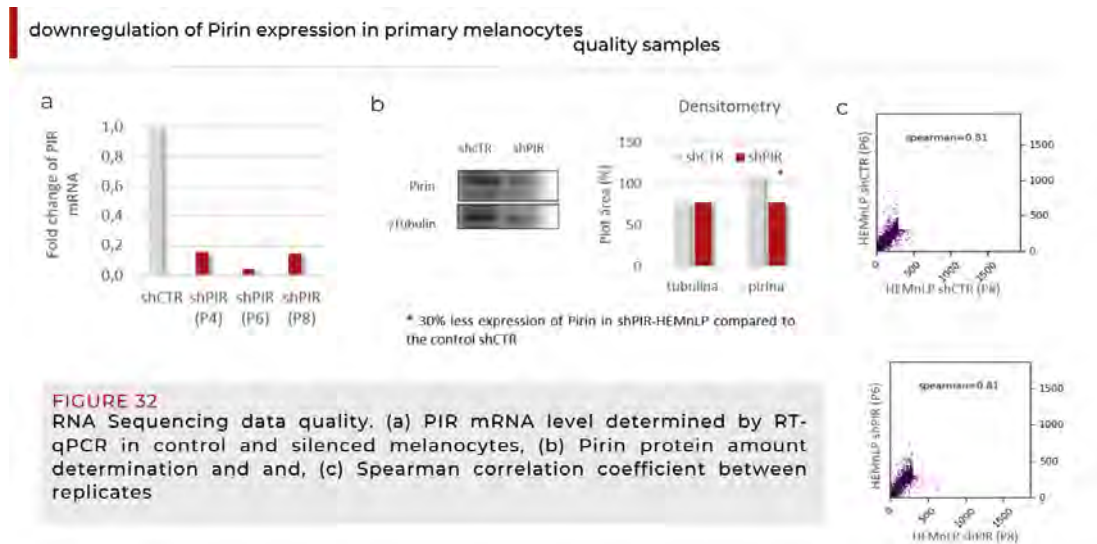
The overexpression of PIR-mRNA was correlated with more protein in Western Blots of these cells, showing a 5 to 15-fold increase in Pirin protein relative to the parental A2058 and MeWO melanoma cell lines, respectively (Figure 31a). When the wound-healing and proliferation of these cells was assessed, no significant differences were detected in the migration capacity between the control cells and those that overexpress Pirin (Figure 31b). By contrast, a significantly lower proliferation rate was seen in the pPIR transfected cells relative to the parental controls. This effect was evident after 48 hours in culture for both the Pirin-overexpressing-melanoma cell lines (Figure 31c).



Transcriptome modulation in healthy skin melanocytes after PIR down-regulation

Having assessed the capacity of Pirin to regulate basic tumour-related processes like proliferation, and in order to reveal the molecular mechanisms regulated by this protein, we performed a RNA-seq analysis. The strong Pirin expression observed in melanocytes and the lack of information regarding the role of Pirin in non-transformed cells led us to select this cell model to downregulate Pirin gene

expression and to determine the transcriptomic alterations provoked. Pirin-specific shRNA expression induced a 90% reduction in PIR mRNA and a 30% loss of Pirin protein in HEMn-LP melanocytes (Figure 32a-b). Two independent replicates of control (shCTR) and PIR knockdown (shPIR) HEMn-LP samples were subjected to RNA sequencing. Initial quality control showed strong congruence of the biological replicates, with Spearman correlation values for all replicates of $r = 0.81$ (Figure 32c). This demonstrated the reliability of the data produced and illustrated transcriptional changes were consistent in each condition.

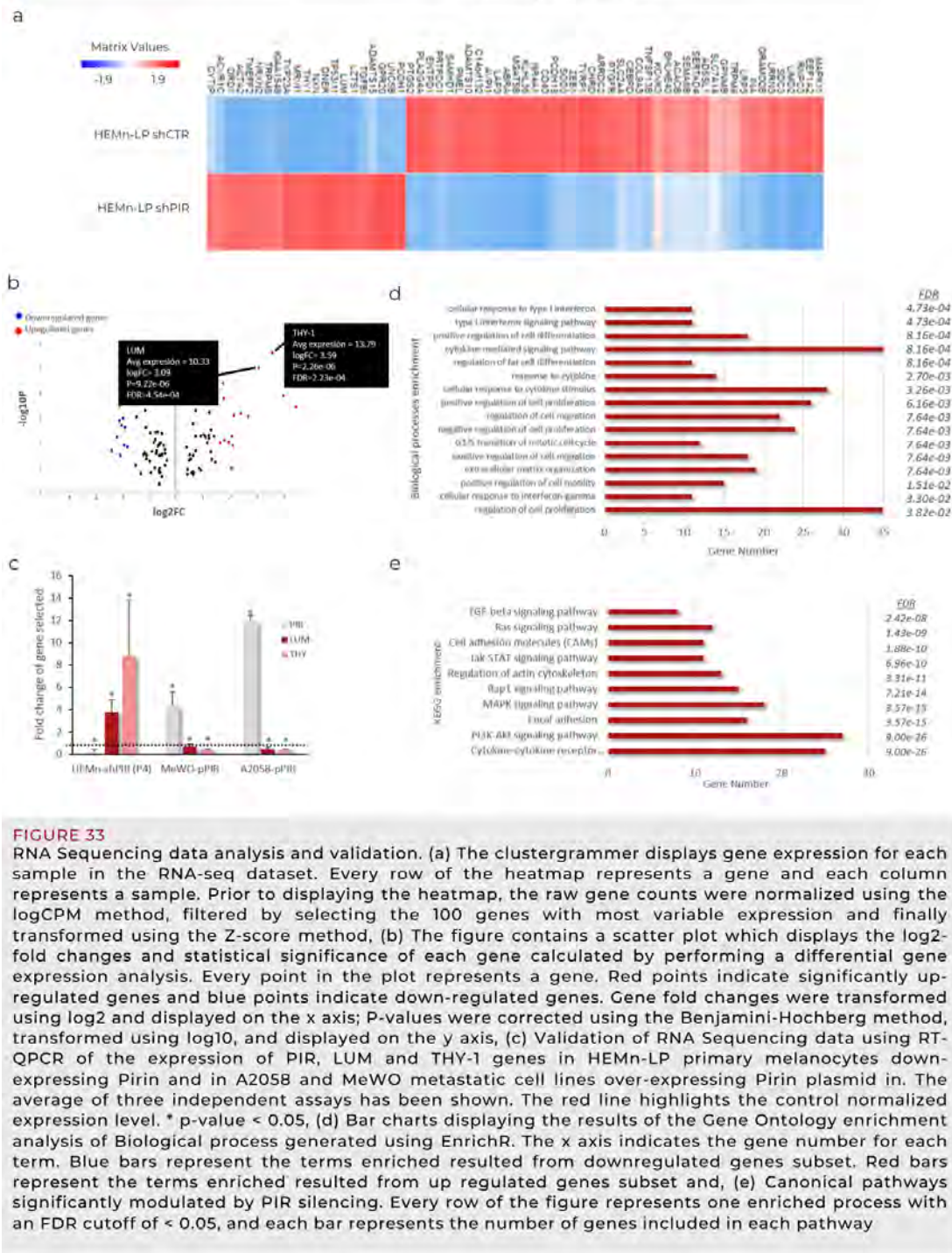


A set of DEGs was identified when shCTR and shPIR HEMn-LP were compared based on standard threshold $p\text{-value} \leq 0.05$ and a $FDR \leq 0.05$. In total, 824 DEGs were identified, of which 446 were downregulated and 374 were upregulated (*Annex B*: Table S2). The Figure 33a shows the genes with most variable expression after applying the $\logFC > (2)$ and $\logFC < (-2)$ filter).

To validate the sequencing results, we focused on two genes linked to the malignant properties of melanoma cells, both of which underwent a significant increase in their mRNA levels in our dataset (Figure 33b): Lumican (*LUM*), a gene related to growth and metastasis (136-138); and THY-1, a cell surface antigen (*Thy-1/CD90*) that acts as an adhesion molecule for the extravasation of endothelial tissues and as a tumor suppressor (139,140). We analyzed the expression of these two genes by RT-qPCR in HEMn-LP PIR-silenced cells, and in MeWO and A2058 metastatic melanoma cells overexpressing Pirin (Figure 33c). The reduction in *PIR* mRNA was correlated with higher levels of *LUM* and *THY-1* mRNA. Conversely, overexpression of *PIR* mRNA was associated with weaker *LUM* and *THY-1* gene expression in transfected melanoma cells relative to the control cells. Together, *PIR* modulation appears to modify the transcriptome of cells, provoking the up and down-regulation of different genes.

downregulation of Pirin expression in primary melanocytes

transcriptome analysis



To identify the biological processes that might be modified in response to *PIR* silencing, a functional enrichment analysis was performed on RNA sequencing datasets using the BioJupies Interactive Notebook, obtaining the Biological Processes (BPs) of that Gene Ontology (GO) analysis (Figure 33d, Annex C: Table S6). Among the upregulated genes the BPs were mainly associated with extracellular matrix (ECM) organization, the regulation of migration, the regulation of proliferation and the cell cycle, and cell responses to type II interferon. For the downregulated genes, cell differentiation,

cytokine-mediated signaling and innate immune response were the BPs predominantly altered. The GO annotation results (overlapping genes, p-value and FDR) of the DEGs after PIR silencing are summarized in Table S1, and the top ten pathways in the pathway-enrichment analysis included: cytokine-cytokine receptor interaction, PI3K-AKT signaling pathway, focal adhesion, MAPK-signaling pathway, and JAK-STAT-signaling pathway (Figure 33e). PI3K-AKT and cytokine-cytokine receptor interaction pathways were the most significantly enriched terms, both with an FDR= $9.00e^{-26}$.

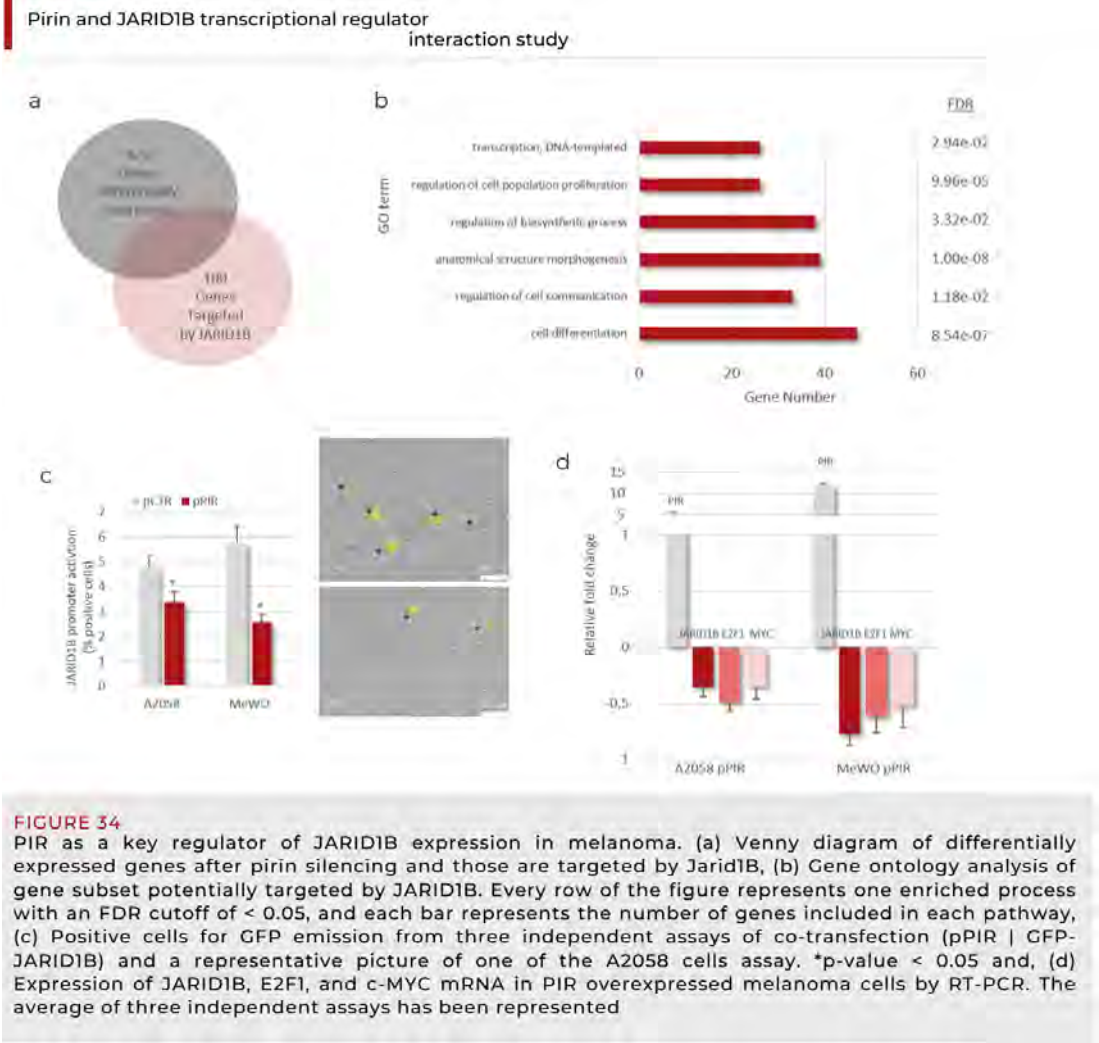
JARID1B, a transcription factor putatively regulated by *PIR*

Due to the fact that Pirin acts as a transcriptional co-regulator with NF1 and NFkB (82), we set out to determine whether Pirin modulated the expression of genes targeted by other transcription factors in melanocytes. A computational analysis of transcription factors likely to be associated with Pirin and its target genes was performed using the Biojupies Interactive Notebook, which significantly predicted that *JARID1B* could be one such transcriptional regulator working between *PIR* and its downstream modulated genes. *JARID1B* was recently described to be a slow cycling gene involved in the epigenetic regulation and malignant reprogramming of melanoma cells (83-85). In our data, more than 100 DEGs were putative targets of this protein (Figure 34a) and significantly, the most strongly enriched GO terms for this subset of genes included regulatory processes related to transcription, proliferation, metabolism, morphogenesis, communication and differentiation (Figure 34b, Annex C: Table S7). It is also interesting to note that an association between *JARID1B* regulation and the PI3K-AKT pathway has been described, which was enriched in response to *PIR* silencing (86). Therefore, we wondered whether *PIR* could somehow modulate *JARID1B* expression. To address this possibility, melanoma cells were co-transfected with a *PIR*-coding plasmid (pPIR) or an empty plasmid (pCTR) and a plasmid in which eGFP expression was driven by the *JARID1B* promoter. Activation of the *JARID1B* promoter was determined through the proportion of cells expressing GFP and significantly, an increase in Pirin expression in MeWO and A2058 melanoma cells led to a significant decrease in *JARID1B* promoter activation in both metastatic melanoma cell lines (Figure 34c).

Based on our findings regarding the DEGs detected following *PIR* silencing in melanocytes, and the significant increase in *E2F1* (p value 5×10^{-4} , FDR 0.022) and *c-MYC* (p value 7.8×10^{-5} , FDR 0.006) expression observed, and given that these are target genes of *JARID1B* (81,141), their expression was evaluated in Pirin overexpressing melanoma cells by RT-qPCR. Significantly weaker expression of the *JARID1B*, *E2F1* and *c-MYC* genes was clearly seen in melanoma cells that overexpressed Pirin relative to the control cells (Figure 34d). Accordingly, it should be noted that the *THY-1* and *LUM* genes (whose expression is shown in Figure 34c) are also targeted by *JARID1B*, and both genes are down-regulated in the metastatic melanoma cells overexpressing *PIR*. Moreover, the rates of proliferation assayed

(Figure 31c) were in agreement with this molecular analysis, since both c-MYC and E2F1 are proteins involved in cell proliferation and cell cycle regulation. In that case, the cells overexpressing Pirin showed a decreased proliferation compared to control cells. These data are consistent with the downregulation of *JARID1B* gene expression.

Together, these results suggest that *PIR* might modulate melanoma proliferation by targeting the slow-cycling transcriptional regulator *JARID1B*.



DISCUSSION



RKIP and Pirin as biomarkers for melanoma diagnosis and prognosis

Melanoma is an extremely lethal form of skin cancer. A timely and accurate diagnosis of malignant melanoma is fundamental to ensuring appropriate treatment and a successful outcome. However, histologically, melanoma exhibits a wide range of features, which include epithelial, hematologic, mesenchymal, and neural characteristics (96). In some cases, this makes the diagnosis of the disease difficult.

Classically, IHC-mediated routine identification of melanocytic lesions include the use of melanocyte and melanoma markers, like tyrosinase (TYR) and tyrosinase-related proteins (TYRP1 and DCT), gp100 and Melan-A (142); nonetheless, the utility of a combined immunohistochemical analysis including Bcl-2, nuclear S100A4, Ki67 and MITF to improve the risk stratification of early-stage malignant melanoma patients has been recently reported (143).

Due to that, the molecular alterations involved in the pathogenesis of melanoma represent a topic of active research, which has enabled the identification of disease-associated key, oncogenes, and tumor suppressor genes providing a scientific foundation for urgently needed therapeutic approaches (144,147).

Based on our previous results from a comparative proteomic analysis between melanocytes and melanoma cell lines results, we selected RKIP and Pirin as candidates for melanoma biomarkers. As a consequence, in this thesis, we focused on the analysis of RKIP and Pirin expression by immunohistochemistry in melanoma patient biopsies.

Regarding RKIP, several studies have shown this protein exhibits low expression levels in various tumors and it is often absent in metastases (115,134, 148,149, 150-164). In agreement, decreased RKIP expression has been associated with metastatic uveal melanoma while low levels of RKIP were detected on both metastatic as well as non-metastatic cutaneous melanoma biopsies (52,165). These studies, although interesting, were carried out with small cohorts of patients. In addition, in those studies claiming the association among low RKIP expression and metastasis, decreased RKIP expression was assessed by comparison of primary tumors and biopsies at metastatic sites (52,134,148). Results obtained from the aforementioned works revealed a clear malignancy-related silencing of RKIP on tumor cells, although they did not analyze the possible predictive role of RKIP. Our study, including 75 nevi and 239 samples of malignant melanoma, allowed deepening on the diagnostic and prognostic

value of this protein. Of note, all melanoma biopsies were obtained from the primary lesion, which may explain the lack of statistical RKIP-staining differences among stage I–IV melanoma. Also, the cohort size of stage III and IV melanoma patients was small (when compared to stage I–II patients) and we cannot discharge its effect when analyzing all stages together.

In relation to Pirin expression, it seems to participate in the regulation of different cellular processes, acting as a protein kinase inhibitor, antioxidant or putative transcriptional co-factor (143,147,165-167). Some evidence has implicated Pirin in tumorigenesis by promoting cell proliferation and malignant progression of several cancer (168,169). As RKIP, to evaluate the impact of Pirin on melanoma tumorigenesis, we first analyzed the expression of Pirin by immunohistochemistry in the consecutive slides and in the same way as in RKIP study. In both nevus and melanoma groups, strong Pirin expression was observed and significant differences were detected among benign and malignant lesions, with homogeneously strong Pirin expression in benign melanocytes from nevi relative to the heterogeneous expression in malignant melanoma.

Looking for new metastatic biomarkers we focused on early stage melanoma (stage I–II according to AJCC 8th edition) in order to evaluate RKIP and Pirin usefulness to discriminate among patients with good and bad evolution of the disease. Here, our results agree with previous studies on the diagnostic capability of RKIP staining, as melanoma samples exhibited an overall decrease in staining when compared with benign lesions (i.e., nevi). Unfortunately, RKIP staining was not able to distinguish stage I–II patients with a favorable evolution of the disease from those who eventually developed metastasis. Nevertheless, it is worth mentioning the association among strong RKIP staining and lower Breslow index across all melanoma stages (stage I–IV) suggesting that RKIP may not determine tumor malignancy but may be related to the primary tumor position or progress through the skin. In the case of Pirin staining, based on multivariate analyses by Logistic Regression and Cox models, including age and the Breslow index as co-variables, strong Pirin expression was significantly associated with a risk of metastasis, suggesting its importance as a prognostic marker.

To summarize, our study supports the diagnostic utility of RKIP staining due to the significantly lower RKIP protein levels in melanoma samples, even at early stages (I–II) of the disease. Additionally, Pirin staining along with the Breslow index seem to be a prognostic marker at early stages (I–II) of melanoma, since high Pirin protein levels are associated with a more significant probability of metastasis, as well as a shorter time until this clinical end-point.

RKIP Regulates Differentiation-Related Features in Melanocytic Cells

Delving into the study of RKIP protein as regards the pathogenesis of melanoma, we carried out molecular and functional assays using melanocytes and melanoma cell lines. In accordance with our histopathological results and previously published studies (51, 152), we found that both RKIP mRNA and protein expression were significantly lower in melanoma cell lines than in primary cultures of melanocytes with the exception of the Mel-HO cell line; this cell line exhibited *RKIP* mRNA level similar to that observed on melanocytes but a reduced protein content that suggests the involvement of a post-transcriptional mechanism limiting translation. Of note, *RKIP* has been described as a target for several microRNAs able to regulate cellular protein level (112).

Several authors have suggested that RKIP may not have a significant role in primary tumors but that instead, this protein could play an important role as a metastatic suppressor (115,134, 148,149, 150-164). In this sense, and despite the described role for RKIP in the regulation of the MAPK/ERK pathway, RKIP has been implicated on the invasive behavior of malignant melanoma cells but not on their proliferative capability (51). Moreover, Schoentgen and Jonic (68) described the involvement of RKIP on the cortical actin organization during the membrane changes that happen during tumor cell migration. In agreement with previous studies, we confirmed the implication of RKIP on the motility of malignant melanoma cells as *RKIP* expression was inversely correlated with the migration capability of both, primary and metastatic melanoma cell lines. Nevertheless, modulation of the cellular RKIP level did not show an influence on the proliferative activity of melanoma cells. Therefore, considering the relevance of cellular motility on tumor metastasis, these results support a role for RKIP loss in melanoma dissemination.

To define the cellular mechanisms regulated by RKIP that could explain the selective force favoring a decreased presence of this protein on melanoma when comparing with benign lesions (i.e., nevi), *RKIP* gene was silenced using lentivirus in primary melanocytes and RNA sequencing were performed to analyze the transcriptome changes derived from *RKIP* modulation. The transcriptome of melanocytes after *RKIP* silencing revealed a transcriptional misregulation in cancer gene signature. Among others, this signature included altered expression pattern of the oncogenes *KIT*, *BCL3*, *MAF*, *MYC*, *MYCL*, *HOXA9*, *CDC25B*, and *PIMI*. In our data, all of them showed a two to five-fold increase, supporting the role for *RKIP* like a tumor suppressor gene (170). Interestingly enough, downregulation of RKIP expression on melanocytes resulted in the alteration of cellular processes intimately linked to malignant transformation of cells, such as development and differentiation. Moreover, developmental pigmentation, a process specifically linked to the melanocytic

lineage, was also enriched. According to our RNA-seq data, RKIP would be a repressor of *KIT* and an inducer of *TYRP1*, *MLANA*, and *PMEL* gene expression, among others. *TYRP1*, *MLANA*, and *PMEL* are among the best-known transcriptional targets of the master melanogenic regulator microphthalmia-associated transcription factor (*MITF*) (171) and it would be of interest to further analyze the possible crosstalk among RKIP and MITF. In addition, data indicate that RKIP represents a brake for the EMT process, by regulating the expression of genes such as *ZEB1*, *THY-1* and *NTRK2*.

Scientific evidence demonstrates that in a heterogeneous tumor mass, those cells responsible for drug-resistance, recurrence and metastasis contain characteristics of stem cells, that is, the ability to self-renew and differentiate in any cell type of the tumor mass (172). In this work, after silencing of RKIP in HEMn-LP melanocytes, more than 70% of the differential expression genes belonging to development and differentiation were found to be putative targets of *NANOG*. *NANOG* has been identified as one of the crucial inducers of this stem cell-like state type (70) and is aberrantly expressed in many types of tumors (71-73). We observed that transient forced-increase of RKIP expression in metastatic melanoma cells led to the decrease of *NANOG* promoter activation pointing towards a functional relationship among RKIP and *NANOG* expression. In line with these results, Lee et al. (173) noticed a high amount of crosstalks between pathways regulated by RKIP and those under the control of main stemness transcription factors (i.e., *OCT4*, *KLF4*, *SOX2*, and *NANOG*) and proposed RKIP as a regulator of the differentiation state of cells. This hypothesis would be in agreement with the stronger RKIP expression found in differentiated melanocytes from nevi lesions when comparing with melanoma samples.

In addition to the maintenance of the stemness, *NANOG* has been also implicated in the EMT (69,76) and by regulating the expression of *ZEB1* and *THY-1* among other genes (78). In fact, EMT and development of stemness properties are often closely related processes (174). As previously mentioned, these two genes are among those with deregulated expression in our RNA-seq study. *ZEB1* is one of the major activators of the EMT program and increasing evidence places *ZEB1* also as an important regulator of differentiation, proliferation, DNA damage response and cell survival (175). Interestingly, *ZEB1* is among the transcription factors driving the early hybrid EMT state and hybrid EMT states (i.e., states with intermediate characteristics among fully epithelial and fully mesenchymal cells) have been linked to collective cells migration and highest metastatic potential (174). This result, together with the observed modulation of the cellular migration capacity driven by RKIP, are in line with the rapid RKIP diminution observed on malignant lesions, even at early stages, as well as the association among low Breslow index and presence of RKIP. In fact, capacity of a tumor to deepen on the skin requires the acquisition of characteristics as those blocked by RKIP. On the other hand, *THY-1* is a protein implicated in the endothelium transvasation of melanoma cells during metastasis spreading (139). These results could be indicating the implication of RKIP loss in the plasticity required for the intra- and extravasation during melanoma metastasis. In this context, we have also found that the expression of miR-21 was significantly lower on RKIP-overexpressing cells. miR-21 is a known target for *NANOG* (78) and an important inducer of EMT affecting migration and invasion capability (176-178) suggesting

a possible role for this onco-miRNA in melanoma malignancy (78,179). These results point towards the involvement of NANOG downstream RKIP in the regulation of gene expression related to malignant phenotype of melanoma cells.

To summarize, we propose that RKIP could play a role in the maintenance of the differentiation state by negatively regulating *NANOG* gene expression although further research would be required for a better description of the underlying mechanism.

Pirin dampens the proliferation of malignant cells by downregulating JARID1B/KDM5B expression

The cellular activity of Pirin has mainly been studied in terms of extracellular matrix (ECM) tumorigenicity (82,125,180) and thus, despite its broad distribution, there is little information regarding the role of Pirin in non-transformed cells and tissues (116,181). To better understand the role of Pirin in a melanocytic context, we firstly studied *PIR*/Pirin expression in primary melanocytes and melanoma cell lines by RT-qPCR and in Western Blots, demonstrating that primary melanocytes exhibit generally stronger and more homogenous Pirin expression than melanoma cell lines, which had significantly lower expression and more heterogeneity among the different cell lines analyzed. We studied proliferation and migration of metastatic melanoma cells in which Pirin was overexpressed and we found this upregulation did not modify migration but rather, it did induce a significant decrease in the proliferation rate of both the melanoma cell lines studied. In this context, controversial results have been found in different tumors. For example, in DLD1 colorectal cancer cells Pirin does not affect viability or migration (126), whereas knocking down Pirin in breast cancer cells was seen to significantly dampen in vitro proliferation and decrease xenograph tumor growth in mice (182). In melanoma, Pirin has been related to an inhibition of migration (122), and it has been proposed to be an inhibitor of melanocyte senescence (135) and a malignant biomarker (183).

In accordance with the antiproliferative activity observed when Pirin is overexpressed in melanoma cells, the transcriptomic analysis following PIR-silencing in primary melanocytes here revealed an enrichment of genes involved in the negative regulation of cell proliferation, the G1/S transition and extracellular matrix organization and positive regulation of cell migration (*Annex C*: Table S6). Furthermore, deleterious mutations in the *PIR* gene were recently identified in breast cancer that could affect protein structure, stability and function (182). These results could explain the discrepancies found when studying different cancer or different tumor cell lines. On the other hand, melanoma heterogeneity was recently proposed to be due to the co-existence of different melanoma cell phenotypes and adaptive phenotype plasticity given that transcriptional reprogramming could drive melanoma progression (184).

Transcriptional reprogramming has been detected at different stages of melanoma, with enhanced mesenchymal traits in circulating melanoma cells and proliferative features in metastatic tumors (184). Hence, cells with different phenotypes may interact in a cooperative manner and contribute to successful metastatic progression (61,185).

In recent years, attention is being paid to epigenetic regulation in melanoma (85), which led to the description of *JARID1B* as an epigenetic regulator implicated in the transcriptional reprogramming of several tumor cells and in tumor heterogeneity (186). Although *JARID1B* expressing melanoma cells represent only a small proportion of the cells in the primary and metastatic melanoma populations (187), the RNA-seq dataset and the transcription factor enrichment analysis found that *JARID1B* could target more than 100 of the DEGs identified. Furthermore, co-transfection experiments showed a decrease of *JARID1B* promoter activation after Pirin overexpression, pointing to a functional relationship between Pirin and *JARID1B* expression. In addition, we demonstrated that the overexpression of Pirin in both the metastatic melanoma cell lines studied led to a significant decrease in *JARID1B* gene expression, and that of its target genes *E2F1* and *c-MYC* (81,141). These results may explain the antiproliferative effect of Pirin observed in melanoma cell lines. Indeed, in canine oral melanoma cell lines *JARID1B*-inhibitors drive anti-proliferative activity and overcame cisplatin resistance (188).

From our data, we believe that in normal melanocytes Pirin expression could regulate the rate of proliferation through *JARID1B* and the *E2F1* pathway, although the expression of other genes favors melanoma tumors acquiring an invasive phenotype through the expression of genes related to the epithelial-mesenchymal transition (69,76,78,189). Indeed, Pirin is functionally associated with several proteins involved in cytoskeleton reorganization, such as *WASF2* and *NCKAP1*, which could explain the link between Pirin overexpression and malignant progression (122, 190). In this cell context, the delay in cell cycle progression produced by *JARID1B* downregulation could stimulate tumor cells to re-enter the cell cycle, increasing proliferation. Tumor cells with a slow-cycling phenotype may be metabolically active and highly aggressive, with increased potential to grow and metastasize (84,191,192).

We propose that Pirin could play an important role in modulating the proliferative state of melanoma cells by regulating *JARID1B* gene expression. However, further research will be necessary to better understand the mechanisms underlying this phenomenon, which could shed light on useful therapeutic strategies for these tumors.

Finally, if we approach all the results obtained from this thesis as a whole, we can think that both systems *RKIP/NANOG* and *Pirin/JARID1B* could be working together, so it would be facing two scenarios. On the one hand, benign melanocytes from nevus, in which the high expression *RKIP* maintenance the differentiation state blocking the stemness transcription factor *NANOG*. Additionally, high Pirin expression may be regulating the cell cycle through *JARID1B* and *E2F1* expression. In the other hand, melanoma cells, in which the absent of *RKIP* expression produces a different panorama. The expression

of *NANOG* favors the acquisition of invasive phenotype through the expression of genes related to the mesenchymal epithelial transition (69,76,78). In this cellular context, the delay in the cell cycle progression produced for *JARID1B* downregulation could acts a stimulus for the tumor cell to re-enter in the cell cycle and metastasize. Melanoma cells could be able to adjust their phenotype to meet external survival requirements (86).

CONCLUSIONS



Conclusions

In our initial hypothesis, we arose that RKIP and Pirin were proteins that played a role in the etiopathogenesis of cutaneous melanoma, making them excellent biomarkers for the diagnosis and prognosis of cutaneous melanoma. In order to demonstrate this, we investigated their potential application as melanoma markers and their role in melanocytic cells.

Based on the results presented in this thesis, the following conclusions can be drawn:

1. Immunohistochemical detection of RKIP in primary melanoma biopsies can be a useful tool for melanoma diagnosis.
2. Immunohistochemical detection of Pirin along with the Breslow index could be used as a prognostic marker at early stages (I-II) of melanoma.
3. *RKIP* down expression in human neonatal epidermal melanocytes led to a transcriptional signature associated with cancer, including misregulation of genes related to pigmentation and development and differentiation processes.
4. RKIP appears to be involved in the maintenance of the differentiation state of melanocytes by negatively regulating *NANOG* transcription factor and its downstream targets such as miR-21.
5. A low presence of Pirin in human neonatal epidermal melanocytes led to a transcriptional profile characterized by a dysregulation in extracellular matrix organization, migration, proliferation, and interferon type II responses.
6. Pirin exerts an antiproliferative effect on melanoma cells through regulation of the *JARID1B* transcription factor and its target genes, including *E2F1* and *c-MYC*.

Based on the present findings, we maintain the thesis that both RKIP and Pirin are involved in tumorigenesis and the malignant progression of cutaneous melanoma. Therefore, this research could lead to the development of new therapeutic strategies for the treatment of metastatic disease melanoma.

REFERENCES



References

1. Sung H, Ferlay J, Siegel R.L, et al. Global cancer statistics 2020: GLOBOCAN estimates of incidence and mortality worldwide for 36 cancers in 185 countries. *CA. Cancer J. Clin.* 2021, 71: 209–249. DOI: 10.3322/caac.21660
2. Lin L, Yan L, Liu Y, et al. Incidence and death in 29 cancer groups in 2017 and trend analysis from 1990 to 2017 from the Global Burden of Disease Study. *J Hematol Oncol.* 2019, 12:96. DOI: 10.1186/s13045-019-0783-9
3. Park S.J, Oh C.M, Kim B.W, et al. Nationwide incidence of ocular melanoma in South Korea by using the national cancer registry database (1999–2011). *Invest. Ophthalmol. Vis. Sci.* 2015, 56: 4719–24. DOI: 10.1167/iovs.15-16532
4. Katalinic A, Eisemann N, Waldmann A. Skin cancer screening in Germany. Documenting melanoma incidence and mortality from 2008 to 2013. *Dtsch. Arztebl. Int.* 2015, 112:629–34. DOI: 10.3238/arztebl.2015.0629
5. Pilleron S, Soto-Perez-de-Celis E, Vignat J, et al. Estimated global cancer incidence in the oldest adults in 2018 and projections to 2050. *Int J Cancer.* 2021, 148:601-608. DOI: 10.1002/ijc.33232
6. Rahib L, Wehner M.R, Matrisian L.M, et al. Estimated Projection of US Cancer Incidence and Death to 2040. *JAMA Netw Open.* 2021, 4:e214708. DOI: 10.1001/jamanetworkopen.2021.4708
7. Smittenaar R, Petersen K.A, Stewart K, et al. Cancer incidence and mortality projections in the UK until 2035. *Br J Cancer.* 2016, 115:1147-1155. DOI: 10.1038/bjc.2016.304
8. Weir H.K, Thompson T.D, Stewart S.L, et al. Cancer Incidence Projections in the United States Between 2015 and 2050. *Prev Chronic Dis.* 2021, 18:E59. DOI: 10.5888/pcd18.210006
9. Singh G.K, Jemal A. Socioeconomic and Racial/Ethnic Disparities in Cancer Mortality, Incidence, and Survival in the United States, 1950-2014: Over Six Decades of Changing Patterns and Widening Inequalities. *J Environ Public Health.* 2017, 2017:2819372. DOI: 10.1155/2017/2819372
10. Saginala K, Barsouk A, Aluru J.S, et al. Epidemiology of Melanoma. *Med. Sci.* 2021, 9:63. DOI: 10.3390/medsci9040063
11. Li Z, Fang Y, Chen H, et al. Spatiotemporal trends of the global burden of melanoma in 204 countries and territories from 1990 to 2019: Results from the 2019 global burden of disease study. *Neoplasia.* 2022, 24:12-21. DOI: 10.1016/j.neo.2021.11.013
12. Jones O.T, Ranmuthu C.K.I, Hall P.N, et al. Recognising Skin Cancer in Primary Care. *Adv Ther.* 2020, 37:603-616. DOI: 10.1007/s12325-019-01130-1
13. Liu-Smith F, Farhat A.M, Arce A, et al. Sex differences in the association of cutaneous melanoma incidence rates and geographic ultraviolet light exposure. *Journal of the American Academy of Dermatology.* 2017, 76: 499–505.e3. DOI: 10.1016/j.jaad.2016.08.027

14. Sideris E, Thomas S.J. Patients' sun practices, perceptions of skin cancer and their risk of skin cancer in rural Australia. *Health Promot J Austr.* 2020, 31:84-92. DOI: 10.1002/hpja.253
15. Wright C.Y, Kapwata T, Singh E, et al. Trends in Melanoma Mortality in the Population Groups of South Africa. *Dermatology.* 2019, 235:396-399. DOI: 10.1159/000500663
16. Miller K.D, Nogueira L, Mariotto A.B, et al. Cancer treatment and survivorship statistics, 2019. *CA Cancer J Clin.* 2019, 69:363-385. DOI: 10.3322/caac.21565
17. Yang D.D, Salciccioli J.D, Marshall D.C, et al. Trends in malignant melanoma mortality in 31 countries from 1985 to 2015. *Br J Dermatol.* 2020, 183:1056-1064. DOI: 10.1111/bjd.19010
18. Kozmin S.G, Slezak G, Reynaud-Angelin A, et al. Ultraviolet A radiation is highly mutagenic in cells that are unable to repair 7,8-dihydro-8-oxoguanine in *Saccharomyces cerevisiae*. *Proc. Natl. Acad. Sci. USA.* 2005, 102:538–543. DOI: 10.1073/pnas.0504497102
19. Ichihashi M, Ueda M, Budiyo A, et al. UV-induced skin damage. *Toxicology.* 2003, 189:21-39. DOI: 10.1016/s0300-483x(03)00150-1
20. Carr S, Smith C, Wernberg J. Epidemiology and Risk Factors of Melanoma. *Surg. Clin. North Am.* 2020, 100:1–12. DOI: 10.1016/j.suc.2019.09.005
21. Obrador E, Liu-Smith F, Dellinger R.W, et al. Oxidative stress and antioxidants in the pathophysiology of malignant melanoma. *Biol. Chem.* 2019, 400: 589–612. DOI: 10.1515/hsz-2018-0327
22. Douki, T. Oxidative Stress and Genotoxicity in Melanoma Induction: Impact on Repair Rather Than Formation of DNA Damage? *Photochem. Photobiol.* 2020, 96, 962–972.
23. Khan, A.Q.; Travers, J.B.; Kemp, M.G. Roles of UVA radiation and DNA damage responses in melanoma pathogenesis. *Environ. Mol. Mutagenesis.* 2018, 59, 438–460.
24. Trucco, L.D.; Mundra, P.A.; Hogan, K.; Garcia-Martinez, P.; Viros, A.; Mandal, A.; Macagno, N.; Gaudy-Marqueste, C.; Allan, D.; Baenke, F.; et al. Ultraviolet radiation–induced DNA damage is prognostic for outcome in melanoma. *Nat. Med.* 2019, 25, 221–224.
25. Raimondi, S.; Suppa, M.; Gandini, S. Melanoma Epidemiology and Sun Exposure. *Acta Derm. Venereol.* 2020, 100, 250–258.
26. Bishop, J. Lentigos, Melanocytic Naevi and Melanoma. In *Rook's Textbook of Dermatology*, 8th ed.; Blackwell publishing: Oxford, UK, 2010; Volume 54, pp. 32–56. *Int. J. Mol. Sci.* 2021, 22, 6395 12 of 14
27. Djavid, A.R.; Stonesifer, C.; Fullerton, B.T.; Wang, S.W.; Tartaro, M.A.; Kwinta, B.D.; Grimes, J.M.; Geskin, L.J.; Saenger, Y.M. Etiologies of Melanoma Development and Prevention Measures: A Review of the Current Evidence. *Cancers* 2021, 13, 4914. <https://doi.org/10.3390/cancers13194914>
28. Hausauer, A.; Swetter, S.; Cockburn, M.; Clarke, C. Increases in melanoma among

- adolescent girls and young women in California: Trends by socioeconomic status and UV radiation exposure. *Arch. Dermatol.* 2011, 147, 783–789.
29. Trakatelli, M.; Bylaite-Bucinskiene, M.; Correia, O.; Cozzio, A.; De Vries, E.; Medenica, L.; Nagore, E.; Paoli, J.; Stratigos, A.J.; Del Marmol, V.; et al. Clinical assessment of skin phototypes: Watch your words! *Eur. J. Dermatol.* 2017, 27, 615–619.
 30. von Schuckmann LA, Hughes MCB, Ghiasvand R, et al. Risk of Melanoma Recurrence After Diagnosis of a High-Risk Primary Tumor. *JAMA Dermatol.* 2019;155(6):688–693. doi:10.1001/jamadermatol.2019.0440
 31. Botella-Estrada R, Traves V, Requena C, Guillen-Barona C, Nagore E. Correlation of histologic regression in primary melanoma with sentinel node status. *JAMA Dermatol.* 2014 Aug;150(8):828-35. doi: 10.1001/jamadermatol.2013.9856. PMID: 24898614.
 32. Escandell I, Martín JM, Jordá E. Novel Immunologic Approaches to Melanoma Treatment. *Actas Dermosifiliogr.* 2017 Oct;108(8):708-720. English, Spanish. doi: 10.1016/j.ad.2017.01.017. Epub 2017 May 18. PMID: 28527857
 33. Toussi, A., Mans, N., Welborn, J., & Kiuru, M. (2020). Germline mutations predisposing to melanoma. *Journal of cutaneous pathology*, 47(7), 606–616. <https://doi.org/10.1111/cup.13689>
 34. Damsky, W.; Bosenberg, M. Melanocytic nevi and melanoma: Unraveling a complex relationship. *Oncogene* 2017, 36, 5771–5792.
 35. Zocchi, L.; Lontano, A.; Merli, M.; Dika, E.; Nagore, E.; Quaglino, P.; Puig, S.; Ribero, S. Familial Melanoma and Susceptibility Genes: A Review of the Most Common Clinical and Dermoscopic Phenotypic Aspect, Associated Malignancies and Practical Tips for Management. *J. Clin. Med.* 2021, 10, 3760. <https://doi.org/10.3390/jcm10163760>
 36. Stanganelli, I.; De Felici, M.B.; Mandel, V.D.; Caini, S.; Raimondi, S.; Corso, F.; Bellerba, F.; Quaglino, P.; Sanlorenzo, M.; Ribero, S.; et al. The association between pesticide use and cutaneous melanoma: A systematic review and meta-analysis. *J. Eur. Acad. Dermatol. Venereol.* 2020, 34, 691–708
 37. Kanitakis J. Anatomy, histology and immunohistochemistry of normal human skin. *Eur J Dermatol.* 2002 Jul-Aug;12(4):390-9; quiz 400-1. PMID: 12095893.
 38. Anatomy and Physiology of the Skin, *Journal of the Dermatology Nurses' Association: November/December 2011 - Volume 3 - Issue 6 - p 366* doi: 10.1097/JDN.0b013e31823cccbe
 39. Lawton S (2019) Skin 1: the structure and functions of the skin. *Nursing Times* [online]; 115, 12, 30-33.
 40. Clark WH Jr, Elder DE, Guerry D IV, Epstein MN, Greene MH, Van Horn M.A study of tumor progression: the precursor lesions of superficial spreading and nodular melanoma. *Hum Pathol* 1984;15:1147-65

41. Leonardi GC, Falzone L, Salemi R, Zanghi A, Spandidos DA, Mccubrey JA, Candido S, Libra M. Cutaneous melanoma: From pathogenesis to therapy (Review). *Int J Oncol.* 2018 Apr;52(4):1071-1080. doi: 10.3892/ijo.2018.4287. Epub 2018 Feb 27. PMID: 29532857; PMCID: PMC5843392.
42. Miller AJ, Mihm MC. Melanoma. *New England Journal of Medicine.* 2006;355(1):51-65. doi:10.1056/NEJMra052166
43. Marghoob, Nadeem G., Liopyris, Konstantinos and Jaimes, Natalia. "Dermoscopy: A Review of the Structures That Facilitate Melanoma Detection" *Journal of Osteopathic Medicine*, vol. 119, no. 6, 2019, pp. 380-390. <https://doi.org/10.7556/jaoa.2019.067>
44. Teixido C, Castillo P, Martinez-Vila C, Arance A, Alos L. Molecular Markers and Targets in Melanoma. *Cells.* 2021 Sep 5;10(9):2320. doi: 10.3390/cells10092320. PMID: 34571969; PMCID: PMC8469294.
45. Raman, M.; Chen, W.; Cobb, M.H. Differential regulation and properties of MAPKs. *Oncogene* 2007, 26, 3100-3112.
46. Yeung K., Seitz T., Li S., Janoschk P., McFerrank B., Kaiser C., Feek F., Katsanakisk K.D., Rose D.W., Mischak H., et al. Suppression of Raf-1 kinase activity and MAP kinase signalling by RKIP. *Nature.* 1999;401:e173. doi: 10.1038/43686.
47. Davies, H.; Bignell, G.R.; Cox, C.; Stephens, P.; Edkins, S.; Clegg, S.; Teague, J.; Woffendin, H.; Garnett, M.J.; Bottomley, W.; et al. Mutations of the BRAF gene in human cancer. *Nature* 2002, 417, 949-954.
48. Nissan, M.H.; Pratilas, C.A.; Jones, A.M.; Ramirez, R.; Won, H.; Liu, C.; Tiwari, S.; Kong, L.; Hanrahan, A.J.; Yao, Z.; et al. Loss of NF1 in cutaneous melanoma is associated with RAS activation and MEK dependence. *Cancer Res.* 2014, 74, 2340-2350.
49. Beshir A.B., Ren G., Magpusao A.N., Barone L.M., Yeung K.C., Fenteany G. Raf kinase inhibitor protein suppresses nuclear factor- κ B-dependent cancer cell invasion through negative regulation of matrix metalloproteinase expression. *Cancer Lett.* 2010;299:137-149. doi: 10.1016/j.canlet.2010.08.012.
50. Jilaveanu L.B., Zito C.R., Aziz S.A., Conrad P.J., Schmitz J.C., Sznol M., Camp R.L., Rimm D.L., Kluger H.M. C-Raf is associated with disease progression and cell proliferation in a subset of melanomas. *Clin. Cancer Res.* 2009;15:5704-5713. doi: 10.1158/1078-0432.CCR-09-0198.
51. Schuierer M.M., Bataille F., Hagan S., Kolch W., Bosserhoff A.-K. Reduction in Raf Kinase Inhibitor Protein Expression Is Associated with Increased Ras-Extracellular Signal-Regulated Kinase Signaling in Melanoma Cell Lines. *Cancer Res.* 2004;64:5186. doi: 10.1158/0008-5472.CAN-03-3861.
52. Cardile V., Malaponte G., Loreto C., Libra M., Caggia S., Trovato F.M., Musumeci G. Raf kinase inhibitor protein (RKIP) and phospho-RKIP expression in melanomas. *Acta*

- Histochem. 2013;115:795–802.
doi: 10.1016/j.acthis.2013.03.003.
53. Scheid, M.P.; Woodgett, J.R. PKB/AKT: Functional insights from genetic models. *Nat. Rev. Mol. Cell Biol.* 2001, 2, 760–768.
54. Stahl, J.M.; Cheung, M.; Sharma, A.; Trivedi, N.R.; Shanmugam, S.; Robertson, G.P. Loss of PTEN promotes tumour development in malignant melanoma. *Cancer Res.* 2003, 63, 2881–2890.
55. Lito, P.; Pratilas, C.A.; Joseph, E.W.; Tadi, M.; Halilovic, E.; Zubrowski, M.; Huang, A.; Wong, W.L.; Callahan, M.K.; Merghoub, T. et al. Relief of profound feedback inhibition of mitogenic signaling by RAF inhibitors attenuates their activity in BRAFV600E melanomas. *Cancer Cell* 2012, 22, 668–682.
56. Ben-Neriah Y, Karin M. Inflammation meets cancer, with NF- κ B as the matchmaker. *Nat Immunol.* 2011 Jul 19;12(8):715-23. doi: 10.1038/ni.2060. PMID: 21772280.
57. Baldwin AS. Control of oncogenesis and cancer therapy resistance by the transcription factor NF-kappaB. *J Clin Invest.* 2001 Feb;107(3):241-6. doi: 10.1172/JCI11991. PMID: 11160144; PMCID: PMC199203.
58. Dechend R, Hirano F, Lehmann K, Heissmeyer V, Ansieau S, Wulczyn FG, Scheidereit C, Leutz A. The Bcl-3 oncoprotein acts as a bridging factor between NF-kappaB/Rel and nuclear co-regulators. *Oncogene.* 1999 Jun 3;18(22):3316-23. doi: 10.1038/sj.onc.1202717. PMID: 10362352.
59. George J, Lim JS, Jang SJ, et al. Comprehensive genomic profiles of small cell lung cancer. *Nature.* 2015 Aug 6;524(7563):47-53. doi: 10.1038/nature14664. Epub 2015 Jul 13. PMID: 26168399; PMCID: PMC4861069.
60. Dhawan P, Richmond A. A novel NF-kappa B-inducing kinase-MAPK signaling pathway up-regulates NF-kappa B activity in melanoma cells. *J Biol Chem.* 2002 Mar 8;277(10):7920-8. doi: 10.1074/jbc.M112210200. Epub 2001 Dec 28. PMID: 11773061; PMCID: PMC2668260.
61. Arozarena I, Wellbrock C. Phenotype plasticity as enabler of melanoma progression and therapy resistance. *Nat Rev Cancer.* 2019 Jul;19(7):377-391. doi: 10.1038/s41568-019-0154-4. Epub 2019 Jun 17. PMID: 31209265.
62. Friedmann-Morvinski D, Verma IM. Dedifferentiation and reprogramming: origins of cancer stem cells. *EMBO Rep.* 2014 Mar;15(3):244-53. doi: 10.1002/embr.201338254. Epub 2014 Feb 14. PMID: 24531722; PMCID: PMC3989690.
63. Gabriela-Freitas M, Pinheiro J, Raquel-Cunha A, Cardoso-Carneiro D, Martinho O. RKIP as an Inflammatory and Immune System Modulator: Implications in Cancer. *Biomolecules.* 2019 Nov 22;9(12):769. doi: 10.3390/biom9120769. PMID: 31766768; PMCID: PMC6995551.

64. Martinho O., Granja S., Jaraquemada T., Caeiro C., Miranda-Gonçalves V., Honavar M., Costa P., Damasceno M., Rosner M.R., Lopes J.M., et al. Downregulation of RKIP is associated with poor outcome and malignant progression in gliomas. *PLoS ONE*. 2012;7:e30769. doi: 10.1371/journal.pone.0030769.
65. Beshir A.B., Ren G., Magpusao A.N., Barone L.M., Yeung K.C., Fenteany G. Raf kinase inhibitor protein suppresses nuclear factor- κ B-dependent cancer cell invasion through negative regulation of matrix metalloproteinase expression. *Cancer Lett*. 2010;299:137–149. doi: 10.1016/j.canlet.2010.08.012.
66. Jilaveanu L.B., Zito C.R., Aziz S.A., Conrad P.J., Schmitz J.C., Sznol M., Camp R.L., Rimm D.L., Kluger H.M. C-Raf is associated with disease progression and cell proliferation in a subset of melanomas. *Clin. Cancer Res*. 2009;15:5704–5713. doi: 10.1158/1078-0432.CCR-09-0198.
67. Schuierer M.M., Bataille F., Hagan S., Kolch W., Bosserhoff A.-K. Reduction in Raf Kinase Inhibitor Protein Expression Is Associated with Increased Ras-Extracellular Signal-Regulated Kinase Signaling in Melanoma Cell Lines. *Cancer Res*. 2004;64:5186. doi: 10.1158/0008-5472.CAN-03-3861.
68. Schoentgen F, Jonic S. PEBP1/RKIP behavior: a mirror of actin-membrane organization. *Cell Mol Life Sci*. 2020 Mar;77(5):859-874. doi: 10.1007/s00018-020-03455-5. Epub 2020 Jan 20. PMID: 31960115.
69. Yadav AK, Desai NS. Cancer Stem Cells: Acquisition, Characteristics, Therapeutic Implications, Targeting Strategies and Future Prospects. *Stem Cell Rev Rep*. 2019 Jun;15(3):331-355. doi: 10.1007/s12015-019-09887-2. PMID: 30993589.
70. Molofsky AV, Pardal R, Morrison SJ. Diverse mechanisms regulate stem cell self-renewal. *Curr Opin Cell Biol*. 2004 Dec;16(6):700-7. doi: 10.1016/j.ceb.2004.09.004. PMID: 15530784.
71. Watanabe M, Ohnishi Y, Inoue H, Wato M, Tanaka A, Kakudo K, Nozaki M. NANOG expression correlates with differentiation, metastasis and resistance to preoperative adjuvant therapy in oral squamous cell carcinoma. *Oncol Lett*. 2014 Jan;7(1):35-40. doi: 10.3892/ol.2013.1690. Epub 2013 Nov 19. PMID: 24348816; PMCID: PMC3861537.
72. Ling GQ, Chen DB, Wang BQ, Zhang LS. Expression of the pluripotency markers Oct3/4, Nanog and Sox2 in human breast cancer cell lines. *Oncol Lett*. 2012 Dec;4(6):1264-1268. doi: 10.3892/ol.2012.916. Epub 2012 Sep 13. PMID: 23197999; PMCID: PMC3506717.
73. Zhang Y, Wang Z, Yu J, Shi Jz, Wang C, Fu Wh, Chen Zw, Yang J. Cancer stem-like cells contribute to cisplatin resistance and progression in bladder cancer. *Cancer Lett*. 2012 Sep 1;322(1):70-7. doi: 10.1016/j.canlet.2012.02.010. Epub 2012 Feb 15. PMID: 22343321.

74. Perego M, Tortoreto M, Tragni G, Mariani L, Deho P, Carbone A, Santinami M, Patuzzo R, Mina PD, Villa A, Pratesi G, Cossa G, Perego P, Daidone MG, Alison MR, Parmiani G, Rivoltini L, Castelli C. Heterogeneous phenotype of human melanoma cells with in vitro and in vivo features of tumor-initiating cells. *J Invest Dermatol*. 2010 Jul;130(7):1877-86. doi: 10.1038/jid.2010.69. Epub 2010 Apr 8. PMID: 20376064.
75. Borrull A, Ghislin S, Deshayes F, Lauriol J, Alcaide-Loridan C, Middendorp S. Nanog and Oct4 overexpression increases motility and transmigration of melanoma cells. *J Cancer Res Clin Oncol*. 2012 Jul;138(7):1145-54. doi: 10.1007/s00432-012-1186-2. Epub 2012 Mar 11. PMID: 22406932.
76. Sun C, Sun L, Jiang K, Gao DM, Kang XN, Wang C, Zhang S, Huang S, Qin X, Li Y, Liu YK. NANOG promotes liver cancer cell invasion by inducing epithelial-mesenchymal transition through NODAL/SMAD3 signaling pathway. *Int J Biochem Cell Biol*. 2013 Jun;45(6):1099-108. doi: 10.1016/j.biocel.2013.02.017. Epub 2013 Mar 7. Erratum in: *Int J Biochem Cell Biol*. 2018 Dec;105:144. PMID: 23474366.
77. Brabletz T, Kalluri R, Nieto MA, Weinberg RA. EMT in cancer. *Nat Rev Cancer*. 2018 Feb;18(2):128-134. doi: 10.1038/nrc.2017.118. Epub 2018 Jan 12. PMID: 29326430.
78. Palla A.R., Piazzolla D., Alcazar N., Cañamero M., Graña O., Gómez-López G., Dominguez O., Dueñas M., Paramio J.M., Serrano M. The pluripotency factor NANOG promotes the formation of squamous cell carcinomas. *Sci Rep*. 2015;5 doi: 10.1038/srep10205.
79. Yesilkanal AE, Rosner MR. Targeting Raf Kinase Inhibitory Protein Regulation and Function. *Cancers (Basel)*. 2018 Sep 4;10(9):306. doi: 10.3390/cancers10090306. PMID: 30181452; PMCID: PMC6162369.
80. Harmeyer KM, Facompre ND, Herlyn M, Basu D. JARID1 Histone Demethylases: Emerging Targets in Cancer. *Trends Cancer*. 2017 Oct;3(10):713-725. doi: 10.1016/j.trecan.2017.08.004. Epub 2017 Sep 12. PMID: 28958389; PMCID: PMC5679451.
81. Han M, Xu W, Cheng P, Jin H, Wang X. Histone demethylase lysine demethylase 5B in development and cancer. *Oncotarget*. 2017 Jan 31;8(5):8980-8991. doi: 10.18632/oncotarget.13858. PMID: 27974677; PMCID: PMC5352456.
82. Perez-Dominguez F, Carrillo-Beltrán D, Blanco R, Muñoz JP, León-Cruz G, Corvalan AH, Urzúa U, Calaf GM, Aguayo F. Role of Pirin, an oxidative stress sensor protein, in epithelial carcinogenesis. *Biology (Basel)*. 2021 Feb 4;10(2):116. doi: 10.3390/biology10020116. PMID: 33557375; PMCID: PMC7915911.
83. Xhabija B, Kidder BL. KDM5B is a master regulator of the H3K4-methylome in stem cells, development and cancer. *Semin Cancer Biol*. 2019 Aug;57:79-85. doi: 10.1016/j.semcancer.2018.11.001. Epub 2018 Nov 16. PMID: 30448242; PMCID: PMC6522339.

84. Vogel FCE, Bordag N, Zügner E, Trajkovic-Arsic M, Chauvistré H, Shannan B, Váraljai R, Horn S, Magnes C, Thomas Siveke J, Schadendorf D, Roesch A. Targeting the H3K4 demethylase KDM5B Reprograms the metabolome and phenotype of melanoma cells. *J Invest Dermatol.* 2019 Dec;139(12):2506-2516.e10. doi: 10.1016/j.jid.2019.06.124. Epub 2019 Jun 21. PMID: 31229500.
85. Giunta EF, Arrichiello G, Curvietto M, Pappalardo A, Bosso D, Rosanova M, Diana A, Giordano P, Petrillo A, Federico P, Fabozzi T, Parola S, Riccio V, Mucci B, Vanella V, Festino L, Daniele B, Ascierio PA, Ottaviano M, On Behalf Of Scito Youth. Epigenetic regulation in melanoma: facts and hopes. *Cells.* 2021 Aug 11;10(8):2048. doi: 10.3390/cells10082048. PMID: 34440824; PMCID: PMC8392422.
86. Facompre ND, Harmeyer KM, Sole X, Kabraji S, Belden Z, Sahu V, Whelan K, Tanaka K, Weinstein GS, Montone KT, Roesch A, Gimotty PA, Herlyn M, Rustgi AK, Nakagawa H, Ramaswamy S, Basu D. JARID1B enables transit between distinct states of the stem-like cell population in oral cancers. *Cancer Res.* 2016 Sep 15;76(18):5538-49. doi: 10.1158/0008-5472.CAN-15-3377. Epub 2016 Aug 3. Erratum in: *Cancer Res.* 2017 Dec 15;77(24):7136. PMID: 27488530; PMCID: PMC5026599.
87. Marghoob, Nadeem G., Liopyris, Konstantinos and Jaimes, Natalia. "Dermoscopy: A Review of the Structures That Facilitate Melanoma Detection" *Journal of Osteopathic Medicine*, vol. 119, no. 6, 2019, pp. 380-390. <https://doi.org/10.7556/jaoa.2019.067>
88. FriedmanRJ, RigelDS, KopfAW. Early detection of malignant melanoma: the role of physician examination and self-examination of the skin. *CA Cancer J Clin.* 1985;35(3):130-151.10.3322/canjclin.35.3.130
89. ChamberlainAJ, Fritschil, KellyJW. Nodular melanoma: patients' perceptions of presenting features and implications for earlier detection. *J Am Acad Dermatol.* 2003;48(5):694-701. doi:10.1067/mjd.2003.216
90. KellyJW. Nodular melanoma: how current approaches to early detection are failing. *J Drugs Dermatol.* 2005;4(6):790-793
91. Clark WH, From L, Bernardino EA, Mihm MC. The Histogenesis and Biologic Behavior of Primary Human Malignant Melanomas of the Skin. *Cancer Res.*1969;29(3):705-27.
92. Breslow A. Thickness, cross-sectional areas and depth of invasion in the prognosis of cutaneous melanoma. *Ann Surg.* 1970;172(5):902-8.
93. Tejera-Vaquerizo A, Ribero S, Puig S, Boada A, Paradela S, Moreno-Ramírez D, Cañueto J, de Unamuno B, Brinca A, Descalzo-Gallego MA, Osella-Abate S, Cassoni P, Carrera C, Vidal-Sicart S, Bennáassar A, Rull R, Alos L, Requena C, Bolumar I, Traves V, Pla Á, Fernández-Orland A, Jaka A, Fernández-Figueres MT, Hilari JM, Giménez-Xavier P, Vieira R, Botella-Estrada R, Román-Curto C,

- Ferrándiz L, Iglesias-Pena N, Ferrándiz C, Malveyh J, Quaglino P, Nagore E; SENTIMEL group. Survival analysis and sentinel lymph node status in thin cutaneous melanoma: A multicenter observational study. *Cancer Med.* 2019 Aug;8(9):4235-4244. doi: 10.1002/cam4.2358. Epub 2019 Jun 18. PMID: 31215168; PMCID: PMC6675713.
94. Dai Ogata, Kenjiro Namikawa, Akira Takahashi, Naoya Yamazaki, A51 review of the AJCC melanoma staging system in the TNM classification (eighth edition), *Japanese Journal of Clinical Oncology*, Volume 51, Issue 5, May 2021, Pages 671–674, <https://doi.org/10.1093/jjco/hyab022>
95. Keung, E. Z., & Gershenwald, J. E. (2018). The eighth edition American Joint Committee on Cancer (AJCC) melanoma staging system: implications for melanoma treatment and care. *Expert review of anticancer therapy*, 18(8), 775–784.
96. Scatena, C., Murtas, D., & Tomei, S. (2021). Cutaneous Melanoma Classification: The Importance of High-Throughput Genomic Technologies. *Frontiers in oncology*, 11, 635488.
97. Elder DE, Bastian BC, Cree IA, Massi D, Scolyer RA. The 2018 World Health Organization Classification of Cutaneous, Mucosal, and Uveal Melanoma: Detailed Analysis of 9 Distinct Subtypes Defined by Their Evolutionary Pathway. *Arch Pathol Lab Med* 2020;144:500–22.
98. Elder DE, Massi D, Scolyer RA, Willemze R, editors. *WHO Classification of Skin Tumours*. Fourth ed. Lyon, France: IARC; 2018.
99. Busam KJ, Gerami P, Scolyer RA. *Pathology of Melanocytic Tumors*. Elsevier; 2019.
100. Plaza JA, Prieto VG. *Pathology of Pigmented Skin Lesions*. Springer; 2017.
101. Busam KJ, Gerami P, Scolyer RA. *Pathology of Melanocytic Tumors*. Elsevier; 2019.
102. Massi G, Leboit PE. *Histological Diagnosis of Nevi and Melanoma*. Springer; 2014.
103. Basurto-Lozada P, Molina-Aguilar C, Castaneda-Garcia C, Vázquez-Cruz ME, Garcia-Salinas OI, Álvarez-Cano A, et al. Acral lentiginous melanoma: basic facts, biological characteristics and research perspectives of an understudied disease. *Pigment Cell Melanoma Res* 2021;34:59–71.
104. Fernandez-Flores A, Cassarino DS. Histopathological diagnosis of acral lentiginous melanoma in early stages. *Ann Diagn Pathol* 2017;26:64–9.
105. Bobos M. Histopathologic classification and prognostic factors of melanoma: a 2021 update. *Ital J Dermatol Venerol.* 2021 Jun;156(3):300-321. doi: 10.23736/S2784-8671.21.06958-3. Epub 2021 May 13. PMID: 33982546.
106. Prieto VG, Shea CR. Immunohistochemistry of melanocytic proliferations. *Arch Pathol Lab Med.* 2011 Jul;135(7):853-9. doi: 10.5858/2009-0717-RAR.1. PMID: 2173

107. Dinehart MS, Dinehart SM, Sukpraprut-Braaten S, High WA. Immunohistochemistry utilization in the diagnosis of melanoma. *J Cutan Pathol*. 2020 May;47(5):446-450. doi: 10.1111/cup.13648. Epub 2020 Jan 27. PMID: 31955450.
108. Michielin O, van Akkooi ACJ, Ascierto PA, Dummer R, Keilholz U; ESMO Guidelines Committee. Electronic address: clinicalguidelines@esmo.org. Cutaneous melanoma: ESMO Clinical Practice Guidelines for diagnosis, treatment and follow-up†. *Ann Oncol*. 2019 Dec 1;30(12):1884-1901. doi: 10.1093/annonc/mdz411. PMID: 31566661.
109. Bajaj S, Donnelly D, Call M, Johannet P, Moran u, polsky d, shapiro r, berman r, pavlick a, weber j, zhong j, osman i. melanoma prognosis: accuracy of the american joint committee on cancer staging manual eighth edition. *J Natl Cancer Inst*. 2020 Sep 1;112(9):921-928. doi: 10.1093/jnci/djaa008. PMID: 31977051; PMCID: PMC7492758.
110. Ertekin SS, Podlipnik S, Riquelme-Mc Loughlin C, Barreiro-Capurro A, Arance A, Carrera C, Malvey J, Puig S. Initial Stage of Cutaneous Primary Melanoma Plays a Key Role in the Pattern and Timing of Disease Recurrence. *Acta Derm Venereol*. 2021 Jul 15;101(7):adv00502. doi: 10.2340/00015555-3832. PMID: 34003298.
111. Arroyo-Berdugo Y, (2013). Identification of diagnostic, prognostic and susceptibility biomarkers in cutaneous malignant melanoma. (unpublished thesis). University of the Basque Country.
112. Zaravinos A, Bonavida B, Chatzaki E, Baritaki S. RKIP: A Key Regulator in Tumor Metastasis Initiation and Resistance to Apoptosis: Therapeutic Targeting and Impact. *Cancers (Basel)*. 2018 Aug 24;10(9):287. doi: 10.3390/cancers10090287. PMID: 30149591; PMCID: PMC6162400.
113. Rajkumar K, Nichita A, Anoor PK, Raju S, Singh SS, Burgula S. Understanding perspectives of signalling mechanisms regulating PEBP1 function. *Cell Biochem Funct*. 2016 Aug;34(6):394-403. doi: 10.1002/cbf.3198. Epub 2016 Jul 7. PMID: 27385268.
114. Lamiman K, Keller JM, Mizokami A, Zhang J, Keller ET. Survey of Raf kinase inhibitor protein (RKIP) in multiple cancer types. *Crit Rev Oncog*. 2014;19(6):455-68. doi: 10.1615/critrevoncog.2014011987. PMID: 25597355.
115. Escara-Wilke J, Yeung K, Keller ET. Raf kinase inhibitor protein (RKIP) in cancer. *Cancer Metastasis Rev*. 2012 Dec;31(3-4):615-20. doi: 10.1007/s10555-012-9365-9. PMID: 22684368.
116. Wendler WM, Kremmer E, Förster R, Winnacker EL. Identification of pirin, a novel highly conserved nuclear protein. *J Biol Chem*. 1997 Mar 28;272(13):8482-9. doi: 10.1074/jbc.272.13.8482. PMID: 9079676.
117. Yoshikawa R, Yanagi H, Hashimoto-Tamaoki T, Morinaga T, Nakano Y, Noda M, Fujiwara Y, Okamura H, Yamamura T. Gene expression in response to anti-

- tumour intervention by polysaccharide-K (PSK) in colorectal carcinoma cells. *Oncol Rep.* 2004 Dec;12(6):1287-93. PMID: 15547752.
118. Panchal HD, Vranizan K, Lee CY, Ho J, Ngai J, Timiras PS. Early anti-oxidative and anti-proliferative curcumin effects on neuroglioma cells suggest therapeutic targets. *Neurochem Res.* 2008 Sep;33(9):1701-10. doi: 10.1007/s11064-008-9608-x. Epub 2008 Feb 26. PMID: 18299980.
119. Qiao Z, Wang D, Hahn J, Ai J, Wang Z. Pirin down-regulates the EAF2/U19 protein and alleviates its growth inhibition in prostate cancer cells. *Prostate.* 2014 Feb;74(2):113-20. doi: 10.1002/pros.22729. Epub 2013 Nov 23. PMID: 24272884; PMCID: PMC4827099.
120. Woodruff PG, Ellwanger A, Solon M, Cambier CJ, Pinkerton KE, Koth LL. Alveolar macrophage recruitment and activation by chronic second hand smoke exposure in mice. *COPD.* 2009 Apr;6(2):86-94. doi: 10.1080/15412550902751738. PMID: 19378221; PMCID: PMC2873864.
121. Tien CP, Chen CH, Lin WY, Liu CS, Liu KJ, Hsiao M, Chang YC, Hung SC. Ambient particulate matter attenuates Sirtuin1 and augments SREBP1-PIR axis to induce human pulmonary fibroblast inflammation: molecular mechanism of microenvironment associated with COPD. *Aging (Albany NY).* 2019 Jul 12;11(13):4654-4671. doi: 10.18632/aging.102077. PMID: 31299012; PMCID: PMC6660058.
122. Miyazaki I, Simizu S, Okumura H, Takagi S, Osada H. A small-molecule inhibitor shows that pirin regulates migration of melanoma cells. *Nat Chem Biol.* 2010 Sep;6(9):667-73. doi: 10.1038/nchembio.423. Epub 2010 Aug 15. PMID: 20711196.
123. Komai K, Niwa Y, Sasazawa Y, Simizu S. Pirin regulates epithelial to mesenchymal transition independently of Bcl3-Slug signaling. *FEBS Lett.* 2015 Mar 12;589(6):738-43. doi: 10.1016/j.febslet.2015.01.040. Epub 2015 Feb 11. PMID: 25680527.
124. Lisabeth EM, Kahl D, Gopallawa I, Haynes SE, Misesk SA, Campbell PL, Dexheimer TS, Khanna D, Fox DA, Jin X, Martin BR, Larsen SD, Neubig RR. Identification of Pirin as a molecular target of the CCG-1423/CCG-203971 series of antifibrotic and antimetastatic compounds. *ACS Pharmacol Transl Sci.* 2019 Apr 12;2(2):92-100. doi: 10.1021/acspsci.8b00048. Epub 2019 Mar 18. PMID: 32039344; PMCID: PMC7006939.
125. Aedo-Aguilera V, Carrillo-Beltrán D, Calaf GM, Muñoz JP, Guerrero N, Osorio JC, Tapia JC, León O, Contreras HR, Aguayo F. Curcumin decreases epithelial-mesenchymal transition by a Pirin-dependent mechanism in cervical cancer cells. *Oncol Rep.* 2019 Nov;42(5):2139-2148. doi: 10.3892/or.2019.7288. Epub 2019 Aug 21. PMID: 31436299.
126. Zhang Y, Knatko EV, Higgins M, Dayalan Naidu S, Smith G, Honda T, de la Vega L, Dinkova-Kostova AT. Pirin, an Nrf2-regulated protein, is overexpressed

- in human colorectal tumors. *Antioxidants* (Basel). 2022 Jan 28;11(2):262. doi: 10.3390/antiox11020262. PMID: 35204145; PMCID: PMC8868368.
127. Hothorn T., Hornik K., Wien W., Van De Wiel M.A., Zeileis A. Implementing a Class of Permutation Tests: The coin Package. *J. Stat. Softw.* 2008; 28:1–23. doi: 10.18637/jss.v028.i08.
128. Benjamini Y., Hochberg Y. Controlling the False Discovery Rate: A Practical and Powerful Approach to Multiple Testing. *J. R. Stat. Soc. Ser. B.* 1995;57:289–300. doi: 10.1111/j.2517-6161.1995.tb02031.x.
129. Lüdtke, (2018). ggeffects: Tidy data frames of marginal effects from regression models. *Journal of Open Source Software*, 3(26), 772, <https://doi.org/10.21105/joss.00772>
130. Zeileis A, van deWiel MA, Hornik Kurt, Hothorn T. Implementing a class of permutation tests: the coin package. *Journal of Statistical Software*, 2008; 28 (8)1-23. ISSN 1548-7660
131. Wagenmakers EJ, Brown S. On the linear relation between the mean and the standard deviation of a response time distribution. *Psychol Rev.* 2007 Jul;114(3):830-41. doi: 10.1037/0033-295X.114.3.830. PMID: 17638508.
132. Pfaffl MW. A new mathematical model for relative quantification in real-time RT-PCR. *Nucleic Acids Res.* 2001 May 1;29(9):e45. doi: 10.1093/nar/29.9.e45. PMID: 11328886; PMCID: PMC55695.
133. Vandesompele J, De Preter K, Pattyn F, Poppe B, Van Roy N, De Paepe A, Speleman F. Accurate normalization of real-time quantitative RT-PCR data by geometric averaging of multiple internal control genes. *Genome Biol.* 2002 Jun 18;3(7):RESEARCH0034. doi: 10.1186/gb-2002-3-7-research0034. Epub 2002 Jun 18. PMID: 12184808; PMCID: PMC126239.
134. Fu Z., Smith P.C., Zhang L., Rubin M.A., Dunn R.L., Yao Z., Keller E.T. Effects of Raf Kinase Inhibitor Protein Expression on Suppression of Prostate Cancer Metastasis. *J. Natl. Cancer Inst.* 2003;95:878–889. doi: 10.1093/jnci/95.12.878.
135. Licciulli S, Luise C, Scafetta G, Capra M, Giardina G, Nuciforo P, Bosari S, Viale G, Mazzarol G, Tonelli C, Lanfrancone L, Alcalay M. Pirin inhibits cellular senescence in melanocytic cells. *Am J Pathol.* 2011 May;178(5):2397-406. doi: 10.1016/j.ajpath.2011.01.019. PMID: 21514450; PMCID: PMC3081152.
136. Chen L, Zhang Y, Zuo Y, Ma F, Song H. Lumican expression in gastric cancer and its association with biological behavior and prognosis. *Oncol Lett.* 2017 Nov;14(5):5235-5240. doi: 10.3892/ol.2017.6842. Epub 2017 Aug 28. PMID: 29098025; PMCID: PMC5652231.
137. Jeanne A, Untereiner V, Perreau C, Proult I, Gobinet C, Boulagnon-Rombi C, Terryn C, Martiny L, Brézillon S, Dedieu S. Lumican delays melanoma growth in mice and drives tumor molecular assembly as well as response to matrix-targeted TAX2 therapeutic peptide. *Sci Rep.* 2017 Aug 9;7(1):7700. doi: 10.1038/s41598-017-07043-9. PMID: 28794454; PMCID: PMC5550434.

138. Pietraszek K, Brézillon S, Perreau C, Malicka-Błaszkiwicz M, Maquart FX, Wegrowski Y. Lumican-derived peptides inhibit melanoma cell growth and migration. *PLoS One*. 2013 Oct 2;8(10):e76232. doi: 10.1371/journal.pone.0076232. PMID: 24098450; PMCID: PMC3788744.
139. Schubert K, Gutknecht D, Köberle M, Anderegg U, Saalbach A. Melanoma cells use Thy-1 (CD90) on endothelial cells for metastasis formation. *Am J Pathol*. 2013 Jan;182(1):266-76. doi: 10.1016/j.ajpath.2012.10.003. Epub 2012 Nov 16. PMID: 23159525.
140. Lung HL, Cheung AK, Cheng Y, Kwong FM, Lo PH, Law EW, Chua D, Zabarovsky ER, Wang N, Tsao SW, Stanbridge EJ, Lung ML. Functional characterization of THY1 as a tumor suppressor gene with antiinvasive activity in nasopharyngeal carcinoma. *Int J Cancer*. 2010 Jul 15;127(2):304-12. doi: 10.1002/ijc.25047. PMID: 19921696.
141. Kuo KT, Huang WC, Bamodu OA, Lee WH, Wang CH, Hsiao M, Wang LS, Yeh CT. Histone demethylase JARID1B/KDM5B promotes aggressiveness of non-small cell lung cancer and serves as a good prognostic predictor. *Clin Epigenetics*. 2018 Aug 9;10(1):107. doi: 10.1186/s13148-018-0533-9. PMID: 30092824; PMCID: PMC6085612.
142. Davis LE, Shalin SC, Tackett AJ. Current state of melanoma diagnosis and treatment. *Cancer Biol Ther*. 2019;20(11):1366-1379. doi: 10.1080/15384047.2019.1640032. Epub 2019 Aug 1. PMID: 31366280; PMCID: PMC6804807.
143. Jurmeister P, Bockmayr M, Treese C, Stein U, Lenze D, Jöhrens K, Friedling F, Dietel M, Klauschen F, Marsch W, Fiedler E, von Laffert M. Immunohistochemical analysis of Bcl-2, nuclear S100A4, MITF and Ki67 for risk stratification of early-stage melanoma - A combined IHC score for melanoma risk stratification. *J Dtsch Dermatol Ges*. 2019 Aug;17(8):800-808. doi: 10.1111/ddg.13917. PMID: 31437373.
144. van den Hurk K., Niessen H.E.C., Veeck J., van den Oord J.J., van Steensel M.A.M., zur Hausen A., van Engeland M., Winnepenninckx V.J.L. Genetics and epigenetics of cutaneous malignant melanoma: A concert out of tune. *Biochim. Biophys. Acta Rev. Cancer*. 2012;1826:89–102. doi: 10.1016/j.bbcan.2012.03.011.
145. Kunz M., Löffler-Wirth H., Dannemann M., Willscher E., Doose G., Kelso J., Kottek T., Nickel B., Hopp L., Landsberg J., et al. RNA-seq analysis identifies different transcriptomic types and developmental trajectories of primary melanomas. *Oncogene*. 2018;37:6136–6151. doi: 10.1038/s41388-018-0385-y
146. Su Y., Bintz M., Yang Y., Robert L., Ng A.H.C., Liud V., Ribas A., Heath J.R., Wei W. Phenotypic heterogeneity and evolution of melanoma cells associated with targeted therapy resistance. *PLoS Comput. Biol*. 2019;15 doi: 10.1371/journal.pcbi.1007034.

147. Shain A.H., Joseph N.M., Yu R., Benhamida J., Liu S., Prow T., Ruben B., North J., Pincus L., Yeh I., et al. Genomic and Transcriptomic Analysis Reveals Incremental Disruption of Key Signaling Pathways during Melanoma Evolution. *Cancer Cell*. 2018;34:45–55.e4. doi: 10.1016/j.ccell.2018.06.005. [PMC free article] [PubMed] [CrossRef] [Google Scholar]
148. Hagan S., Al-Mulla F., Mallon E., Oien K., Ferrier R., Gusterson B., Curto García J.J., Kolch W. Reduction of Raf-1 kinase inhibitor protein expression correlates with breast cancer metastasis. *Clin. Cancer Res*. 2005;11:7392–7397. doi: 10.1158/1078-0432.CCR-05-0283
149. Kim H.S., Kim G.Y., Lim S.J., Kim Y.W. Raf-1 kinase inhibitory protein expression in thyroid carcinomas. *Endocr. Pathol*. 2010;21:253–257. doi: 10.1007/s12022-010-9131-x.
150. Al-Mulla F., Hagan S., Behbehani A.I., Bitar M.S., George S.S., Going J.J., Curto García J.J., Scott L., Fyfe N., Murray G.I., et al. Raf kinase inhibitor protein expression in a survival analysis of colorectal cancer patients. *J. Clin. Oncol*. 2006;24:5672–5679. doi: 10.1200/JCO.2006.07.5499.
151. Xu Y.-F., Yi Y., Qiu S.-J., Gao Q., Li Y.-W., Dai C.-X., Cai M.-Y., Ju M.-J., Zhou J., Zhang B.-H., et al. PEBP1 downregulation is associated to poor prognosis in HCC related to hepatitis B infection. *J. Hepatol*. 2010;53:872–879. doi: 10.1016/j.jhep.2010.05.019
152. Park S., Yeung M.L., Beach S., Shields J.M., Yeung K.C. RKIP downregulates B-Raf kinase activity in melanoma cancer cells. *Oncogene*. 2005;24:3535–3540. doi: 10.1038/sj.onc.1208435.
153. Gimenez M., de Oliveira Souza V.C., Izumi C., Barbieri M.R., Chammas R., Oba-Shinjo S.M., Uno M., Marie S.K.N., Rosa J.C. Proteomic analysis of low- to high-grade astrocytomas reveals an alteration of the expression level of raf kinase inhibitor protein and nucleophosmin. *Proteomics*. 2010;10:2812–2821. doi: 10.1002/pmic.200900722.
154. Wang J., Yang Y.H., Wang A.Q., Yao B., Xie G., Feng G., Zhang Y., Cheng Z.S., Hui L., Dai T.Z., et al. Immunohistochemical detection of the Raf kinase inhibitor protein in nonneoplastic gastric tissue and gastric cancer tissue. *Med. Oncol*. 2010;27:219–223. doi: 10.1007/s12032-009-9194-z.
155. Kim H.-S., Kim G.Y., Lim S.-J., Kim Y.W. Loss of Raf-1 kinase inhibitory protein in pancreatic ductal adenocarcinoma. *Pathology*. 2010;42:655–660. doi: 10.3109/00313025.2010.522172.
156. Shenxiu L., Kuangbiao Z., Liyong Z., Leye H. Expression of Raf Kinase Inhibitor Protein and E-cadherin in Prostate Cancer Tissues. *Zhong Nan Da Xue Xue Bao Yi Xue Ban*. 2009;34:892–897.
157. Birner P., Jesch B., Schultheis A., Schoppmann S.F. RAF-kinase inhibitor protein (RKIP) downregulation in esophageal cancer and its metastases. *Clin.*

- Exp. Metastasis. 2012;29:551–559. doi: 10.1007/s10585-012-9470-8.
158. Zebisch A., Wölfler A., Fried I., Wolf O., Lind K., Bodner C., Haller M., Drasche A., Pirkebner D., Matallanas D., et al. Frequent loss of RAF kinase inhibitor protein expression in acute myeloid leukemia. *Leukemia*. 2012;26:1842–1849. doi: 10.1038/leu.2012.61.
159. Zebisch A., Haller M., Hiden K., Goebel T., Hoefler G., Troppmair J., Sill H. Loss of RAF kinase inhibitor protein is a somatic event in the pathogenesis of therapy-related acute myeloid leukemias with C-RAF germline mutations. *Leukemia*. 2009;23:1049–1053. doi: 10.1038/leu.2009.68.
160. Takemura T., Nakamura S., Yokota D., Hirano I., Ono T., Shigeno K., Fujisawa S., Ohnishi K. Reduction of raf kinase inhibitor protein expression by Bcr-Abl contributes to chronic myelogenous leukemia proliferation. *J. Biol. Chem*. 2010;285:6585–6594. doi: 10.1074/jbc.M109.075788.
161. Jia B., Liu H., Kong Q., Li B. RKIP expression associated with gastric cancer cell invasion and metastasis. *Tumour Biol*. 2012;33:919–925. doi: 10.1007/s13277-012-0317-3.
162. Cheng X.-K., Yu G.-Z., Li X.-D., Ren X.-Q. Molecular mechanism of hepatitis B virus (HBV) on suppression of raf kinase inhibitor protein (RKIP) expression. *Oncotarget*. 2017;8:1132. doi: 10.18632/oncotarget.13586
163. Kim G.-E., Kim N.I., Lee J.S., Park M.H., Yoon J.H. Reduced RKIP Expression is Associated With Breast Neoplastic Progression and is Correlated With Poor Outcomes and Aberrant Methylation in Breast Carcinoma. *Appl. Immunohistochem. Mol. Morphol*. 2017;25:467–474. doi: 10.1097/PAI.0000000000000323.
164. Caltabiano R., Puzzo L., Barresi V., Cardile V., Loreto C., Ragusa M., Russo A., Reibaldi M., Longo A. Expression of Raf Kinase Inhibitor Protein (RKIP) is a predictor of uveal melanoma metastasis. *Histol. Histopathol*. 2014;29:1325–1334. doi: 10.14670/HH-29.1325.
165. Pitcovski J., Shahar E., Aizenshtein E., Gorodetsky R. Melanoma antigens and related immunological markers. *Crit. Rev. Oncol. Hematol*. 2017;115:36–49. doi: 10.1016/j.critrevonc.2017.05.001.
166. Kim H.-S., Won K.Y., Kim G.Y., Kim S.C., Park Y.-K., Kim Y.W. Reduced expression of Raf-1 kinase inhibitory protein predicts regional lymph node metastasis and shorter survival in esophageal squamous cell carcinoma. *Pathol. Res. Pract*. 2012;208:292–299. doi: 10.1016/j.prp.2012.02.011
167. Zhang L, Fu Z, Binkley C, Giordano T, Burant CF, Logsdon CD, Simeone DM. Raf kinase inhibitory protein inhibits beta-cell proliferation. *Surgery*. 2004 Sep;136(3):708-15. doi: 10.1016/j.surg.2003.12.013. PMID: 15349122.
168. Bement WM. A role for RKIP in cell motility. *Chem Biol*. 2005 Sep;12(9):953-4. doi: 10.1016/j.chembiol.2005.08.012. PMID: 16183016.

169. al-Mulla F, Bitar MS, Taqi Z, Rath O, Kolch W. RAF kinase inhibitory protein (RKIP) modulates cell cycle kinetics and motility. *Mol Biosyst.* 2011 Mar;7(3):928-41. doi: 10.1039/c0mb00208a. Epub 2010 Dec 23. PMID: 21180766.
170. Farooqi AA, Li Y, Sarkar FH. The biological complexity of RKIP signaling in human cancers. *Exp Mol Med.* 2015 Sep 25;47(9):e185. doi: 10.1038/emm.2015.70. PMID: 26403261; PMCID: PMC4650930.
171. Goding CR, Arnheiter H. MITF-the first 25 years. *Genes Dev.* 2019 Aug 1;33(15-16):983-1007. doi: 10.1101/gad.324657.119. Epub 2019 May 23. PMID: 31123060; PMCID: PMC6672050.
172. Lee J, Abdeen AA, Hedhli J, Wycislo KL, Dobrucka IT, Fan TM, Dobrucki LW, Kilian KA. Melanoma topology reveals a stem-like phenotype that promotes angiogenesis. *Sci Adv.* 2017 Oct 25;3(10):e1701350. doi: 10.1126/sciadv.1701350. PMID: 29075670; PMCID: PMC5656422.
173. Lee S, Wottrich S, Bonavida B. Crosstalks between Raf-kinase inhibitor protein and cancer stem cell transcription factors (Oct4, KLF4, Sox2, Nanog). *Tumour Biol.* 2017 Apr;39(4):1010428317692253. doi: 10.1177/1010428317692253. PMID: 28378634.
174. Pastushenko I, Blanpain C. EMT Transition States during Tumor Progression and Metastasis. *Trends Cell Biol.* 2019 Mar;29(3):212-226. doi: 10.1016/j.tcb.2018.12.001. Epub 2018 Dec 26. PMID: 30594349.
175. Caramel J, Ligier M, Puisieux A. Pleiotropic Roles for ZEB1 in Cancer. *Cancer Res.* 2018 Jan 1;78(1):30-35. doi: 10.1158/0008-5472.CAN-17-2476. Epub 2017 Dec 18. PMID: 29254997.
176. Sahay D, Leblanc R, Grunewald TG, Ambatipudi S, Ribeiro J, Clézardin P, Peyruchaud O. The LPA1/ZEB1/miR-21-activation pathway regulates metastasis in basal breast cancer. *Oncotarget.* 2015 Aug 21;6(24):20604-20. doi: 10.18632/oncotarget.3774. PMID: 26098771; PMCID: PMC4653029.
177. Mao XH, Chen M, Wang Y, Cui PG, Liu SB, Xu ZY. MicroRNA-21 regulates the ERK/NF- κ B signaling pathway to affect the proliferation, migration, and apoptosis of human melanoma A375 cells by targeting SPRY1, PDCD4, and PTEN. *Mol Carcinog.* 2017 Mar;56(3):886-894. doi: 10.1002/mc.22542. Epub 2016 Sep 22. PMID: 27533779.
178. Zhang HL, Si LB, Zeng A, Long F, Qi Z, Zhao R, Bai M. MicroRNA-21 antisense oligonucleotide improves the sensitivity of A375 human melanoma cell to Cisplatin: An in vitro study. *J Cell Biochem.* 2018 Apr;119(4):3129-3141. doi: 10.1002/jcb.26455. Epub 2018 Jan 4. Retraction in: *J Cell Biochem.* 2021 Nov;122 Suppl 1:S76. PMID: 29058784.
179. Melnik BC. MiR-21: an environmental driver of malignant melanoma? *J Transl Med.* 2015 Jun 27;13:202. doi: 10.1186/s12967-015-0570-5. PMID: 26116372; PMCID: PMC4482047.

180. Arai T, Kojima S, Yamada Y, Sugawara S, Kato M, Yamazaki K, Naya Y, Ichikawa T, Seki N. Pirin: a potential novel therapeutic target for castration-resistant prostate cancer regulated by miR-455-5p. *Mol Oncol*. 2019 Feb;13(2):322-337. doi: 10.1002/1878-0261.12405. Epub 2018 Dec 21. PMID: 30444038; PMCID: PMC6360383.
181. Protein Atlas.org [Internet]. Sweden. The Human Protein Atlas program [updated 2021; cited sept 23rd, 2021] Gene data available at: <https://www.proteinatlas.org/ENSG0000087842-PIR/tissue>
182. Suleman M, Chen A, Ma H, Wen S, Zhao W, Lin D, Wu G, Li Q. PIR promotes tumorigenesis of breast cancer by upregulating cell cycle activator E2F1. *Cell Cycle*. 2019 Nov;18(21):2914-2927. doi: 10.1080/15384101.2019.1662259. Epub 2019 Sep 10. PMID: 31500513; PMCID: PMC6791709.
183. Licciulli S, Luise C, Zanardi A, Giorgetti L, Viale G, Lanfranccone L, Carbone R, Alcalay M. Pirin delocalization in melanoma progression identified by high content immuno-detection based approaches. *BMC Cell Biol*. 2010 Jan 20;11:5. doi: 10.1186/1471-2121-11-5. PMID: 20089166; PMCID: PMC2823719.
184. Rowling EJ, Miskolczi Z, Nagaraju R, Wilcock DJ, Wang P, Telfer B, Li Y, Lasheras-Otero I, Redondo-Muñoz M, Sharrocks AD, Arozarena I, Wellbrock C. Cooperative behaviour and phenotype plasticity evolve during melanoma progression. *Pigment Cell Melanoma Res*. 2020 Sep;33(5):695-708. doi: 10.1111/pcmr.12873. Epub 2020 Mar 20. PMID: 32145051; PMCID: PMC7496243.
185. Chapman A, Fernandez del Ama L, Ferguson J, Kamarashev J, Wellbrock C, Hurlstone A. Heterogeneous tumor subpopulations cooperate to drive invasion. *Cell Rep*. 2014 Aug 7;8(3):688-95. doi: 10.1016/j.celrep.2014.06.045. Epub 2014 Jul 24. PMID: 25066122; PMCID: PMC4542310
186. Lee JE, Kim MY. Cancer epigenetics: Past, present and future. *Semin Cancer Biol*. 2021 Mar 31:S1044-579X(21)00075-4. doi: 10.1016/j.semcancer.2021.03.025. Epub ahead of print. PMID: 33798724.
187. Roesch A, Fukunaga-Kalabis M, Schmidt EC, Zabierowski SE, Brafford PA, Vultur A, Basu D, Gimotty P, Vogt T, Herlyn M. A temporarily distinct subpopulation of slow-cycling melanoma cells is required for continuous tumor growth. *Cell*. 2010 May 14;141(4):583-94. doi: 10.1016/j.cell.2010.04.020. PMID: 20478252; PMCID: PMC2882693.
188. Tobin SJ, Chang H, Kent MS, Davies AE. JARID1-targeted histone H3 demethylase inhibitors exhibit anti-proliferative activity and overcome cisplatin resistance in canine oral melanoma cell lines. *Vet Comp Oncol*. 2021 Sep;19(3):518-528. doi: 10.1111/vco.12691. Epub 2021 Mar 23. PMID: 33715247; PMCID: PMC8455080.

189. Penas C, Apraiz A, Muñoa I, Arroyo-Berdugo Y, Rasero J, Ezkurra PA, Velasco V, Subiran N, Bosserhoff AK, Alonso S, Asumendi A, Boyano MD. RKIP regulates differentiation-related features in melanocytic cells. *Cancers (Basel)*. 2020 Jun 3;12(6):1451. doi: 10.3390/cancers12061451. PMID: 32503139; PMCID: PMC7352799.
190. Carrillo-Beltrán D, Muñoz JP, Guerrero-Vásquez N, Blanco R, León O, de Souza Lino V, Tapia JC, Maldonado E, Dubois-Camacho K, Hermoso MA, Corvalán AH, Calaf GM, Boccardo E, Aguayo F. Human papillomavirus 16 E7 promotes EGFR/PI3K/AKT1/NRF2 signaling pathway contributing to PIR/NF-κB activation in oral cancer cells. *Cancers (Basel)*. 2020 Jul 15;12(7):1904. doi: 10.3390/cancers12071904. PMID: 32679705; PMCID: PMC7409273.
191. Ahn A, Chatterjee A, Eccles MR. The slow cycling phenotype: a growing problem for treatment resistance in melanoma. *Mol Cancer Ther*. 2017 Jun;16(6):1002-1009. doi: 10.1158/1535-7163.MCT-16-0535. PMID: 28576947.
192. Bristot IJ, Kehl Dias C, Chapola H, Parsons RB, Klamt F. Metabolic rewiring in melanoma drug-resistant cells. *Crit Rev Oncol Hematol*. 2020 Sep;153:102995. doi: 10.1016/j.critrevonc.2020.102995. Epub 2020 May 24. PMID: 32569852.

ANNEX A

Informed consent provided to patients who participated in this project

Consent for the conduct of the investigation project

Researcher / Clinical manager:**PROJECT TITLE:**

I.....
 with NID... .. I declare under my responsibility that I have read the Patient Information Sheet, of which a copy has been delivered to me. The characteristics and objective of the study have been explained to me, as well as the possible benefits and risks that I can expect, the rights that I can exercise, and the provisions on the treatment of data and samples. I have been given time and opportunity to ask questions, which have been answered to my satisfaction.

I know that my identity will be kept secret and that my samples will be identified with a coding system. I am free to revoke my consent at any time and for any reason, without having to give an explanation and without having a negative impact on any present or future medical treatment.

I consent to the use of my samples and associated data as part of this research project. I agree to participate voluntarily and I decline to claim any financial benefit for my participation in the study.

I hereby affirm that I have been warned about the possibility of receiving information regarding my health derived from the genetic analyzes carried out on my biological sample.

I request information

I do not want to receive information

once the research on the study results was completed.

If there was a surplus of the sample, I affirm that I was warned about the destination options at the end of the research project.

In this sense:

a) I request the destruction of the excess sample

b) I request that the excess sample be deposited at the Basque Biobank for Research-o + ehun

Date Signature of the patient

Date: Signature of legal representative (if applicable)

Legal representative name:

Relationship with the patient:

I confirm that I have explained the characteristics of the research project and the conservation and security conditions that will be applied to the sample and the conserved data.

Name of the Investigator or the person designated to provide the information:

Signature date.....

ANNEX B

Data from RNA sequencing
analysis

Table S1. Differentially expressed genes after RKIP silencing. The details of Log Fold Change, p-value and False Discovery Rate are specified in each column

Gene Symbol	logFC	p-value	FDR	Gene Symbol	logFC	p-value	FDR
<i>AC008105.3</i>	-1.935	0.001	0.049	<i>CDON</i>	1.526	0.000	0.024
<i>AC025125.1</i>	-3.192	0.000	0.006	<i>CECR7</i>	-0.932	0.001	0.049
<i>AC025594.1</i>	-2.906	0.000	0.024	<i>CENPF</i>	1.176	0.000	0.041
<i>AC079949.2</i>	-5.287	0.000	0.015	<i>CES4A</i>	1.919	0.000	0.041
<i>AC115090.1</i>	5.285	0.000	0.013	<i>CFD</i>	-2.226	0.000	0.024
<i>AC244153.1</i>	5.285	0.000	0.013	<i>CHODL</i>	-4.067	0.000	0.020
<i>ACE</i>	-2.512	0.001	0.048	<i>CHRD1</i>	3.451	0.000	0.014
<i>ADAMTS12</i>	1.076	0.000	0.031	<i>CHRFAM7A</i>	2.553	0.000	0.041
<i>ADAMTS15</i>	2.391	0.000	0.032	<i>CLDN1</i>	-2.065	0.001	0.049
<i>ADAP1</i>	-1.024	0.000	0.041	<i>CLSTN2</i>	2.887	0.000	0.006
<i>ADD3</i>	-1.340	0.001	0.048	<i>CNTN4</i>	-5.823	0.000	0.010
<i>ADH1A</i>	2.779	0.000	0.006	<i>COL22A1</i>	-5.561	0.000	0.019
<i>ADH1B</i>	2.784	0.000	0.014	<i>COL8A1</i>	1.850	0.000	0.040
<i>AL359258.1</i>	-2.534	0.000	0.038	<i>CPED1</i>	-1.193	0.000	0.019
<i>AL390038.1</i>	-2.551	0.000	0.038	<i>CSPG4P13</i>	-0.995	0.000	0.040
<i>AL512329.2</i>	4.490	0.000	0.036	<i>CTSW</i>	3.543	0.000	0.040
<i>ALPL</i>	1.145	0.000	0.041	<i>DIO2</i>	1.512	0.000	0.027
<i>ANLN</i>	0.857	0.000	0.046	<i>EDA2R</i>	-0.967	0.000	0.040
<i>APOL1</i>	-4.465	0.000	0.006	<i>EEF1A2</i>	-3.087	0.000	0.018
<i>ARHGAP26</i>	-1.144	0.000	0.038	<i>EFEMP1</i>	1.972	0.000	0.014
<i>ARHGEF28</i>	-1.141	0.000	0.038	<i>EGLN3</i>	2.434	0.000	0.031
<i>ARHGEF6</i>	-1.208	0.000	0.027	<i>EHBP1L1</i>	-0.830	0.001	0.047
<i>ATP10A</i>	-2.236	0.000	0.031	<i>EPHA3</i>	-6.092	0.000	0.007
<i>AURKC</i>	-3.040	0.000	0.022	<i>EPHB6</i>	5.366	0.000	0.016
<i>BCL3</i>	1.156	0.000	0.024	<i>EPHX1</i>	-0.928	0.000	0.033
<i>BST2</i>	-1.184	0.001	0.049	<i>EREG</i>	-1.663	0.000	0.027
<i>C1orf216</i>	-1.123	0.000	0.033	<i>EYA1</i>	-2.306	0.000	0.034
<i>C1orf54</i>	-3.151	0.000	0.040	<i>FAM167A</i>	1.166	0.000	0.031
<i>C1QTNF7</i>	-3.849	0.000	0.038	<i>FAM171A1</i>	2.078	0.000	0.013
<i>C21orf91-OT1</i>	-1.106	0.000	0.041	<i>FAM180A</i>	7.677	0.000	0.014
<i>C2CD6</i>	2.086	0.000	0.028	<i>FAM198B</i>	1.690	0.000	0.022
<i>C8orf31</i>	1.990	0.000	0.037	<i>FAM198B-AS1</i>	2.419	0.000	0.040
<i>CAPG</i>	2.620	0.000	0.022	<i>FAM43A</i>	-1.285	0.000	0.042
<i>CCDC3</i>	2.572	0.000	0.041	<i>FBXO32</i>	0.937	0.000	0.040
<i>CCL13</i>	1.650	0.001	0.048	<i>FILIP1L</i>	-1.272	0.000	0.023
<i>CD302</i>	1.620	0.000	0.023	<i>FLNC</i>	-2.706	0.000	0.006
<i>CD4</i>	-5.673	0.000	0.017	<i>FMNL1</i>	-1.727	0.000	0.023
<i>CDC25B</i>	1.247	0.000	0.038	<i>FMO6P</i>	2.394	0.000	0.031
<i>CDK18</i>	2.649	0.000	0.013	<i>FRG1BP</i>	-1.537	0.000	0.041

Gene Symbol	logFC	p-value	FDR	Gene Symbol	logFC	p-value	FDR
<i>CDO1</i>	2.221	0.000	0.024	<i>FRG1CP</i>	-0.831	0.001	0.049
<i>FRMD3</i>	2.286	0.000	0.021	<i>LRRC32</i>	2.404	0.000	0.014
<i>FRZB</i>	-2.818	0.000	0.008	<i>LRRN3</i>	-1.662	0.000	0.022
<i>GALNT16</i>	-1.693	0.000	0.031	<i>LYPD6B</i>	1.944	0.000	0.038
<i>GHR</i>	-2.038	0.000	0.025	<i>LZTS1</i>	0.911	0.001	0.049
<i>GLB1L</i>	-1.573	0.000	0.014	<i>MAF</i>	2.860	0.000	0.013
<i>GLP2R</i>	5.737	0.000	0.041	<i>MAL</i>	-4.804	0.000	0.023
<i>GPR143</i>	-5.630	0.000	0.014	<i>MCHR1</i>	2.283	0.000	0.024
<i>GPRC5A</i>	-0.951	0.001	0.049	<i>MCOLN3</i>	-3.064	0.000	0.014
<i>GREB1L</i>	1.464	0.000	0.038	<i>MCTP2</i>	-6.413	0.000	0.035
<i>GRIA3</i>	3.504	0.000	0.006	<i>MEG3</i>	3.478	0.000	0.014
<i>GRID1</i>	-7.459	0.000	0.014	<i>MEG9</i>	3.475	0.000	0.018
<i>H19</i>	3.804	0.000	0.023	<i>MFAP4</i>	2.901	0.000	0.014
<i>HAGLR</i>	-3.058	0.000	0.028	<i>MGP</i>	2.503	0.000	0.038
<i>HCAR1</i>	3.204	0.000	0.019	<i>MID2</i>	-1.467	0.000	0.044
<i>HDAC9</i>	-1.629	0.000	0.032	<i>MKI67</i>	0.842	0.000	0.041
<i>HOXA9</i>	1.258	0.000	0.040	<i>MLANA</i>	-4.031	0.000	0.023
<i>HOXB13</i>	-9.156	0.000	0.007	<i>MME</i>	0.926	0.000	0.032
<i>HOXD9</i>	-4.882	0.000	0.038	<i>MOK</i>	1.034	0.000	0.045
<i>HS3ST3A1</i>	2.829	0.000	0.020	<i>MS4A6E</i>	-2.580	0.000	0.007
<i>HS3ST3B1</i>	2.865	0.000	0.006	<i>MTSS1</i>	-3.194	0.000	0.040
<i>HSPB6</i>	-3.068	0.000	0.041	<i>MT-TS1</i>	0.892	0.000	0.042
<i>HSPB7</i>	-4.167	0.000	0.018	<i>MYCL</i>	2.101	0.001	0.048
<i>ID2</i>	1.884	0.000	0.023	<i>NAPIL3</i>	-3.186	0.000	0.032
<i>IGDCC4</i>	-1.672	0.000	0.041	<i>NAV3</i>	-1.016	0.000	0.046
<i>IGF2</i>	3.920	0.000	0.016	<i>NBPF22P</i>	-2.582	0.000	0.042
<i>IGFN1</i>	6.423	0.000	0.014	<i>NBPF4</i>	-2.891	0.000	0.033
<i>IL17RE</i>	2.597	0.000	0.036	<i>NCEH1</i>	-0.994	0.000	0.038
<i>IRF4</i>	-4.794	0.000	0.023	<i>NDRG4</i>	-1.637	0.000	0.041
<i>KCNA3</i>	-4.644	0.000	0.032	<i>NGFR</i>	-4.556	0.000	0.038
<i>KCNK2</i>	3.263	0.001	0.049	<i>NOSIP</i>	1.342	0.000	0.022
<i>KIAA1217</i>	-7.795	0.000	0.006	<i>NPTX2</i>	-7.594	0.000	0.006
<i>KIAA1324L</i>	3.482	0.000	0.013	<i>NTN1</i>	-3.269	0.000	0.023
<i>KIAA1549</i>	1.842	0.000	0.034	<i>NTRK2</i>	1.311	0.000	0.038
<i>KIAA1755</i>	-1.303	0.000	0.041	<i>NUPR1</i>	2.203	0.000	0.014
<i>KIF20A</i>	1.127	0.000	0.040	<i>NXPH4</i>	2.261	0.000	0.027
<i>KIT</i>	1.170	0.000	0.024	<i>OLFM1</i>	3.534	0.000	0.018
<i>KLF4</i>	-1.204	0.000	0.028	<i>OLFML2B</i>	1.869	0.000	0.014
<i>L3MBTL4</i>	-2.143	0.000	0.028	<i>OLFML3</i>	-1.520	0.000	0.040
<i>LANCL3</i>	3.901	0.000	0.023	<i>ORIE1</i>	-8.410	0.001	0.048
<i>LINC00987</i>	2.001	0.000	0.042	<i>PAX9</i>	-6.157	0.000	0.032
<i>LINC01597</i>	-6.389	0.000	0.035	<i>PAXIP1-AS2</i>	-1.964	0.000	0.022
<i>LINGO1</i>	-1.950	0.000	0.028	<i>PCBP3</i>	1.488	0.000	0.024
<i>LRP5</i>	-1.804	0.000	0.032	<i>PCDH17</i>	-5.334	0.000	0.006

Gene Symbol	logFC	p-value	FDR	Gene Symbol	logFC	p-value	FDR
<i>PDE1C</i>	1.617	0.000	0.014	<i>THY1</i>	4.169	0.000	0.006
<i>PEAR1</i>	-4.338	0.000	0.006	<i>TLE2</i>	1.298	0.000	0.042
<i>PID1</i>	-2.732	0.000	0.025	<i>TM4SF18</i>	-5.520	0.000	0.034
<i>PIM1</i>	1.074	0.001	0.049	<i>TMEM132D</i>	5.580	0.000	0.014
<i>PIP</i>	8.716	0.000	0.040	<i>TMEM200C</i>	-2.842	0.000	0.038
<i>PMEL</i>	-0.962	0.000	0.040	<i>TMEM204</i>	1.071	0.000	0.034
<i>PODNL1</i>	2.274	0.000	0.023	<i>TNFSF15</i>	-1.394	0.000	0.022
<i>PPP1R1C</i>	-4.739	0.000	0.038	<i>TP53I11</i>	1.271	0.000	0.037
<i>PRELP</i>	1.823	0.000	0.033	<i>TYRP1</i>	-2.472	0.000	0.008
<i>PROS1</i>	-0.843	0.000	0.045	<i>UNC5B</i>	3.350	0.000	0.006
<i>PTGDS</i>	-4.541	0.000	0.012	<i>VSTM4</i>	1.824	0.000	0.027
<i>PTGFRN</i>	2.563	0.000	0.018	<i>ZBED6CL</i>	2.645	0.000	0.040
<i>PTGS1</i>	5.011	0.000	0.006	<i>ZEB1</i>	1.143	0.001	0.049
<i>PTP4A3</i>	2.422	0.000	0.016	<i>ZNF558</i>	-4.988	0.000	0.006
<i>PTPRD</i>	-4.112	0.000	0.034	<i>ZNF560</i>	3.943	0.000	0.032
<i>RAP2A</i>	0.884	0.000	0.039				
<i>RARB</i>	-2.438	0.000	0.019				
<i>RARRES2</i>	1.863	0.000	0.029				
<i>RCAN2</i>	-1.365	0.000	0.034				
<i>S100B</i>	-3.243	0.000	0.027				
<i>SEMA3F</i>	1.252	0.000	0.034				
<i>SERPINB2</i>	-2.816	0.000	0.034				
<i>SHANK2</i>	1.726	0.000	0.038				
<i>SHISAL1</i>	2.629	0.000	0.024				
<i>SIX2</i>	1.927	0.000	0.032				
<i>SLC15A3</i>	-6.289	0.000	0.012				
<i>SLC1A3</i>	1.194	0.000	0.034				
<i>SLC38A5</i>	3.235	0.000	0.016				
<i>SLCO4A1</i>	1.574	0.000	0.018				
<i>SLFN11</i>	-1.501	0.000	0.018				
<i>SNTB1</i>	-0.834	0.000	0.042				
<i>SOBP</i>	1.792	0.000	0.037				
<i>SOD3</i>	-1.719	0.000	0.040				
<i>SORCS1</i>	-2.492	0.000	0.040				
<i>SOX11</i>	4.833	0.000	0.028				
<i>ST8SIA2</i>	-0.834	0.000	0.045				
<i>STAMBPL1</i>	0.946	0.000	0.041				
<i>STEAP4</i>	2.175	0.000	0.006				
<i>SYNE2</i>	1.476	0.000	0.028				
<i>TAC1</i>	4.640	0.000	0.013				
<i>TDRD9</i>	-3.793	0.000	0.012				
<i>TEX11</i>	-2.812	0.000	0.023				
<i>THBS2</i>	1.280	0.001	0.049				

Table S2. Differentially after PIR silencing. The details of Log Fold Change, p-value and False Discovery Rate are specified in each column

Gene Symbol	logFC	p-value	FDR	Gene Symbol	logFC	p-value	FDR
<i>A2M</i>	-0.92	0.001	0.032	<i>ACAN</i>	1.35	0.000	0.001
<i>A4GALT</i>	-0.58	0.000	0.008	<i>ACE</i>	-1.09	0.002	0.048
<i>ABCA1</i>	-0.95	0.000	0.002	<i>ACKR4</i>	2.69	0.000	0.001
<i>ABCA6</i>	-0.83	0.001	0.023	<i>ACTA2</i>	1.76	0.000	0.000
<i>ABCA7</i>	-0.74	0.001	0.028	<i>ACTG2</i>	4.26	0.000	0.002
<i>ABCB4</i>	-0.53	0.002	0.046	<i>ACVRC</i>	1.34	0.000	0.018
<i>ABCC1</i>	0.40	0.001	0.034	<i>ADAM19</i>	0.99	0.000	0.005
<i>ABCC4</i>	-0.64	0.000	0.012	<i>ADAM28</i>	-1.32	0.001	0.040
<i>ABCG1</i>	-1.37	0.000	0.014	<i>ADAM8</i>	-0.92	0.001	0.023
<i>ABI3BP</i>	1.22	0.001	0.032	<i>ADAMDEC1</i>	-2.30	0.000	0.000
<i>ABRA</i>	-2.13	0.000	0.006	<i>ADAMTS10</i>	-1.13	0.000	0.004
<i>AC006970.1</i>	-0.54	0.000	0.016	<i>ADAMTS12</i>	2.98	0.000	0.000
<i>AC008105.3</i>	-1.62	0.000	0.011	<i>ADAMTS15</i>	1.42	0.000	0.007
<i>AC008397.2</i>	-1.13	0.000	0.008	<i>ADAMTS2</i>	1.62	0.001	0.034
<i>AC010894.1</i>	4.97	0.001	0.024	<i>ADAMTS6</i>	0.98	0.000	0.012
<i>AC010980.1</i>	-1.30	0.001	0.022	<i>ADAMTS9</i>	-0.44	0.001	0.037
<i>AC010980.2</i>	-1.39	0.000	0.004	<i>ADAMTSL1</i>	1.45	0.001	0.038
<i>AC013565.1</i>	2.14	0.000	0.019	<i>ADAP1</i>	-0.71	0.000	0.008
<i>AC013652.1</i>	0.62	0.001	0.026	<i>ADCY3</i>	0.76	0.000	0.002
<i>AC020916.1</i>	-0.46	0.000	0.019	<i>ADCY4</i>	-0.98	0.000	0.011
<i>AC022034.1</i>	1.07	0.000	0.011	<i>ADD3</i>	-0.89	0.000	0.005
<i>AC022239.1</i>	1.14	0.001	0.037	<i>ADGRE2</i>	-1.36	0.000	0.001
<i>AC023157.1</i>	-0.46	0.002	0.044	<i>ADGRE5</i>	-0.47	0.001	0.026
<i>AC037487.4</i>	-0.55	0.000	0.010	<i>ADGRG1</i>	-0.85	0.001	0.035
<i>AC063965.1</i>	-3.58	0.000	0.004	<i>ADGRL3</i>	-0.77	0.002	0.045
<i>AC068775.1</i>	-0.58	0.001	0.035	<i>ADGRL4</i>	-0.78	0.000	0.004
<i>AC073130.1</i>	1.82	0.000	0.015	<i>ADORA2B</i>	0.57	0.002	0.043
<i>AC079780.1</i>	1.52	0.000	0.019	<i>ADRA2A</i>	-2.02	0.000	0.006
<i>AC083837.2</i>	-1.29	0.000	0.018	<i>ADSSL1</i>	-0.63	0.001	0.026
<i>AC087564.1</i>	-1.86	0.001	0.039	<i>AEBP1</i>	-0.75	0.000	0.015
<i>AC091806.1</i>	-1.23	0.000	0.016	<i>AF201337.1</i>	0.40	0.001	0.041
<i>AC093772.1</i>	-1.91	0.000	0.012	<i>AFAP1</i>	0.47	0.001	0.030
<i>AC100793.2</i>	-0.64	0.000	0.014	<i>AGAP2</i>	-1.19	0.002	0.044
<i>AC103703.1</i>	9.80	0.000	0.000	<i>AGT</i>	-1.04	0.000	0.008
<i>AC107959.4</i>	1.02	0.001	0.034	<i>AGTRAP</i>	-0.52	0.000	0.019
<i>AC108134.3</i>	5.25	0.000	0.005	<i>AK5</i>	1.33	0.000	0.000
<i>AC115090.1</i>	4.45	0.000	0.001	<i>AKAP12</i>	1.01	0.000	0.004
<i>AC116049.1</i>	-0.62	0.000	0.015	<i>AKAP13</i>	-0.44	0.001	0.025
<i>AC139783.2</i>	2.65	0.000	0.017	<i>AL109741.2</i>	-3.15	0.001	0.033
<i>AC141557.1</i>	-2.41	0.000	0.008	<i>AL355312.2</i>	-0.36	0.002	0.046
<i>AC244153.1</i>	4.45	0.000	0.001	<i>AL365361.1</i>	-2.18	0.000	0.021
<i>ACACB</i>	-0.63	0.001	0.038	<i>AL391261.3</i>	-0.64	0.000	0.015

Gene Symbol	logFC	p-value	FDR	Gene Symbol	logFC	p-value	FDR
<i>ACAD10</i>	-0.65	0.000	0.008	<i>ALPK2</i>	0.98	0.000	0.001
<i>AMOTL1</i>	0.51	0.002	0.049	<i>BIN1</i>	0.48	0.000	0.016
<i>AMPH</i>	-1.29	0.001	0.026	<i>BMF</i>	-0.76	0.000	0.015
<i>AMZ1</i>	0.66	0.002	0.042	<i>BMP2</i>	-1.06	0.001	0.023
<i>ANGPTL2</i>	-0.81	0.000	0.017	<i>BMP2K</i>	0.55	0.001	0.033
<i>ANKH</i>	-0.48	0.002	0.047	<i>BMP4</i>	-0.85	0.001	0.033
<i>ANKRD29</i>	1.28	0.000	0.009	<i>BMP8B</i>	1.83	0.000	0.015
<i>ANKRD6</i>	0.95	0.001	0.022	<i>BNC1</i>	1.57	0.000	0.001
<i>ANLN</i>	0.94	0.001	0.022	<i>C11orf87</i>	3.37	0.000	0.000
<i>ANO4</i>	1.03	0.000	0.014	<i>C14orf132</i>	-1.18	0.000	0.003
<i>ANO5</i>	-0.73	0.000	0.008	<i>C1QTNF1</i>	-0.54	0.001	0.032
<i>AOX1</i>	0.43	0.001	0.041	<i>C1QTNF7</i>	-1.73	0.000	0.019
<i>AP000808.1</i>	-2.05	0.000	0.004	<i>C1R</i>	-0.74	0.001	0.029
<i>AP000892.3</i>	2.01	0.001	0.039	<i>C22orf15</i>	-1.34	0.001	0.028
<i>APCDD1L</i>	0.85	0.000	0.019	<i>C2CD6</i>	1.49	0.000	0.006
<i>APLP1</i>	-1.49	0.000	0.004	<i>CA12</i>	-0.77	0.000	0.005
<i>APOL1</i>	-1.97	0.000	0.013	<i>CAB39L</i>	0.54	0.001	0.034
<i>APOL6</i>	-0.41	0.001	0.039	<i>CACNA1A</i>	-1.48	0.000	0.001
<i>AR</i>	-0.51	0.001	0.037	<i>CADM3</i>	1.03	0.000	0.005
<i>ARHGAP18</i>	0.42	0.001	0.035	<i>CADM3-AS1</i>	1.16	0.002	0.045
<i>ARHGAP26</i>	-0.93	0.000	0.005	<i>CALD1</i>	1.14	0.000	0.003
<i>ARHGEF4</i>	2.19	0.000	0.007	<i>CAPN12</i>	-1.40	0.002	0.044
<i>ARRDC2</i>	-0.74	0.000	0.009	<i>CARMN</i>	1.80	0.000	0.001
<i>ARRDC3</i>	-0.63	0.001	0.024	<i>CARNS1</i>	-1.22	0.002	0.046
<i>ARRDC4</i>	0.58	0.000	0.008	<i>CCDC151</i>	-1.02	0.002	0.045
<i>ARSJ</i>	1.21	0.000	0.008	<i>CCDC68</i>	-1.03	0.000	0.003
<i>ASIC1</i>	0.93	0.001	0.040	<i>CCDC80</i>	0.85	0.000	0.011
<i>ATG16L2</i>	-0.38	0.002	0.043	<i>CCL13</i>	-1.36	0.001	0.029
<i>ATOH8</i>	-0.79	0.001	0.038	<i>CCL7</i>	-0.70	0.001	0.038
<i>ATP13A3</i>	0.64	0.001	0.035	<i>CCL8</i>	-1.37	0.000	0.001
<i>ATP2B4</i>	0.52	0.002	0.049	<i>CCNB1</i>	0.48	0.001	0.039
<i>ATP8B4</i>	-2.54	0.000	0.000	<i>CCNL1</i>	-0.50	0.000	0.018
<i>AVPI1</i>	-0.54	0.002	0.045	<i>CCR7</i>	-0.81	0.002	0.047
<i>AVPRIA</i>	-1.13	0.002	0.046	<i>CCRL1P1</i>	2.75	0.000	0.003
<i>B4GALT5</i>	0.40	0.002	0.044	<i>CD40</i>	-0.69	0.000	0.008
<i>BATF</i>	-1.43	0.001	0.042	<i>CD81</i>	-0.58	0.002	0.048
<i>BATF2</i>	-0.82	0.000	0.009	<i>CD9</i>	-1.10	0.000	0.001
<i>BCAM</i>	-0.67	0.000	0.014	<i>CDC6</i>	1.06	0.000	0.019
<i>BCAT1</i>	1.41	0.000	0.000	<i>CDCA5</i>	0.72	0.002	0.046
<i>BCL2</i>	-1.05	0.001	0.037	<i>CDH13</i>	0.77	0.000	0.008
<i>BCL7A</i>	0.95	0.000	0.006	<i>CDK1</i>	0.53	0.001	0.038
<i>BCOR</i>	-0.45	0.001	0.029	<i>CDK18</i>	2.71	0.000	0.000
<i>BEX1</i>	1.00	0.000	0.002	<i>CEBPD</i>	-0.99	0.000	0.001
<i>BHLHE22</i>	-2.04	0.001	0.026	<i>CEMIP2</i>	0.73	0.000	0.019
<i>BHLHE40</i>	-0.82	0.000	0.016	<i>CENPF</i>	0.49	0.001	0.031
<i>BICC1</i>	-0.51	0.001	0.031	<i>CENPU</i>	0.67	0.002	0.047

Gene Symbol	logFC	p-value	FDR	Gene Symbol	logFC	p-value	FDR
<i>CEP250</i>	0.60	0.000	0.012	<i>CXXC4</i>	-1.87	0.000	0.013
<i>CES4A</i>	1.00	0.001	0.022	<i>CYP27A1</i>	-0.60	0.000	0.011
<i>CGREF1</i>	0.76	0.001	0.023	<i>CYP27C1</i>	1.06	0.000	0.017
<i>CHCHD7</i>	0.42	0.001	0.025	<i>CYP4X1</i>	-1.41	0.000	0.001
<i>CHL1</i>	-3.27	0.000	0.000	<i>CYP7B1</i>	-1.01	0.000	0.002
<i>CHRD</i>	-1.85	0.000	0.009	<i>CYTIP</i>	2.09	0.000	0.001
<i>CHRD1</i>	1.92	0.002	0.044	<i>DAB2IP</i>	0.67	0.000	0.009
<i>CHRNE</i>	-1.08	0.001	0.038	<i>DCBLD2</i>	0.97	0.000	0.003
<i>CHST1</i>	-0.78	0.002	0.047	<i>DDAH1</i>	0.58	0.000	0.019
<i>CHSY3</i>	0.56	0.001	0.036	<i>DDIAS</i>	0.88	0.001	0.039
<i>CIITA</i>	0.72	0.000	0.007	<i>DEPDC1</i>	0.80	0.001	0.024
<i>CLCNKA</i>	-1.64	0.000	0.004	<i>DEPTOR</i>	0.90	0.002	0.049
<i>CLTCL1</i>	-0.52	0.001	0.041	<i>DHFR</i>	0.45	0.001	0.033
<i>CLVS2</i>	-1.50	0.000	0.008	<i>DHX58</i>	-0.45	0.001	0.038
<i>CMKLR1</i>	0.52	0.001	0.025	<i>DIAPH3</i>	0.82	0.000	0.013
<i>CMPK2</i>	-0.57	0.002	0.045	<i>DLG1</i>	0.39	0.002	0.044
<i>CMTM4</i>	0.39	0.001	0.036	<i>DMD</i>	0.83	0.001	0.024
<i>CNN1</i>	1.69	0.000	0.017	<i>DNER</i>	4.04	0.000	0.013
<i>CNNM1</i>	0.81	0.000	0.019	<i>DOCK4</i>	-0.55	0.002	0.047
<i>CNTN4</i>	-2.14	0.000	0.002	<i>DPP4</i>	-0.72	0.000	0.015
<i>COA1</i>	0.49	0.002	0.048	<i>DPP7</i>	-0.46	0.001	0.038
<i>COBLL1</i>	0.83	0.002	0.044	<i>DPYSL3</i>	-0.61	0.000	0.013
<i>COL10A1</i>	1.67	0.000	0.004	<i>DRD1</i>	2.72	0.000	0.010
<i>COL13A1</i>	0.79	0.001	0.024	<i>DSG2</i>	-1.76	0.000	0.000
<i>COL21A1</i>	-1.91	0.001	0.026	<i>DSP</i>	1.41	0.000	0.002
<i>COL4A1</i>	1.39	0.001	0.031	<i>DTL</i>	0.95	0.000	0.014
<i>COL4A2</i>	0.88	0.001	0.038	<i>DTWD1</i>	-0.74	0.000	0.003
<i>COL8A1</i>	2.37	0.000	0.001	<i>DUSP5</i>	0.90	0.000	0.011
<i>COL9A3</i>	-2.12	0.000	0.004	<i>DVL2</i>	0.56	0.000	0.013
<i>COTL1</i>	0.42	0.002	0.045	<i>E2F1</i>	0.77	0.001	0.022
<i>COX7A1</i>	0.63	0.001	0.034	<i>EBF4</i>	-1.31	0.000	0.015
<i>CPNE7</i>	-0.84	0.000	0.002	<i>EBPL</i>	0.55	0.002	0.046
<i>CPPED1</i>	0.68	0.000	0.004	<i>EDA2R</i>	0.70	0.000	0.018
<i>CPTIA</i>	-0.49	0.001	0.028	<i>EDIL3</i>	0.46	0.001	0.038
<i>CPTIB</i>	-0.37	0.002	0.045	<i>EEF1A2</i>	-2.11	0.000	0.014
<i>CR786580.1</i>	-1.04	0.002	0.043	<i>EFEMP2</i>	-0.46	0.001	0.025
<i>CREB5</i>	1.34	0.000	0.003	<i>EFNA1</i>	-1.60	0.000	0.010
<i>CRIP2</i>	-0.53	0.001	0.041	<i>EFNB3</i>	-0.97	0.000	0.019
<i>CSGALNACT1</i>	-1.05	0.000	0.002	<i>EGR3</i>	-1.43	0.001	0.026
<i>CSRP2</i>	-0.96	0.001	0.026	<i>EIF4EBP1</i>	0.61	0.002	0.049
<i>CTHRC1</i>	-0.87	0.000	0.009	<i>EMG1</i>	-0.71	0.001	0.026
<i>CTIF</i>	0.46	0.001	0.033	<i>EMILIN1</i>	-0.86	0.000	0.003
<i>CTPS1</i>	0.55	0.001	0.022	<i>EML1</i>	0.59	0.000	0.007
<i>CTSC</i>	1.96	0.000	0.000	<i>EML2</i>	-0.43	0.001	0.039
<i>CXCL6</i>	0.88	0.000	0.002	<i>ENPP2</i>	1.13	0.001	0.030

Gene Symbol	logFC	p-value	FDR	Gene Symbol	logFC	p-value	FDR
<i>ENPP4</i>	-0.51	0.002	0.043	<i>GALNT5</i>	-0.82	0.000	0.008
<i>ENTPDI</i>	-0.78	0.000	0.004	<i>GAS6</i>	0.55	0.002	0.043
<i>EPHA3</i>	-3.35	0.001	0.037	<i>GBP4</i>	2.64	0.000	0.001
<i>EPHX1</i>	-0.49	0.000	0.019	<i>GCH1</i>	-1.03	0.001	0.025
<i>EPOR</i>	-0.72	0.000	0.008	<i>GCLM</i>	0.39	0.002	0.046
<i>ERCC2</i>	0.65	0.000	0.006	<i>GCNT1</i>	0.71	0.001	0.029
<i>ERMP1</i>	-0.55	0.000	0.017	<i>GFPT2</i>	0.66	0.002	0.047
<i>EXO1</i>	0.82	0.002	0.044	<i>GFRA1</i>	1.13	0.002	0.045
<i>EYA1</i>	-1.27	0.000	0.002	<i>GHDC</i>	-0.65	0.000	0.013
<i>EYA4</i>	-1.99	0.000	0.004	<i>GINS4</i>	0.91	0.001	0.036
<i>FABP5P2</i>	1.03	0.001	0.038	<i>GJA1</i>	-0.42	0.002	0.044
<i>FABP5P3</i>	1.51	0.002	0.043	<i>GJA4</i>	2.58	0.000	0.004
<i>FAM107B</i>	0.54	0.000	0.012	<i>GLB1L</i>	-0.57	0.000	0.019
<i>FAM167A</i>	0.64	0.000	0.017	<i>GLIPR1</i>	0.64	0.000	0.006
<i>FAM171A1</i>	1.98	0.000	0.001	<i>GLIS1</i>	0.59	0.001	0.028
<i>FARSB</i>	0.41	0.001	0.039	<i>GLT8D2</i>	-0.56	0.002	0.043
<i>FBLIM1</i>	0.40	0.002	0.049	<i>GMPR</i>	-0.53	0.000	0.011
<i>FBLN1</i>	-0.96	0.000	0.006	<i>GPC4</i>	-1.82	0.001	0.026
<i>FBLN2</i>	-1.40	0.000	0.001	<i>GPD2</i>	-0.61	0.000	0.006
<i>FBXO2</i>	-0.86	0.000	0.017	<i>GPER1</i>	0.92	0.001	0.039
<i>FBXO32</i>	-0.62	0.000	0.009	<i>GPNMB</i>	-0.62	0.000	0.021
<i>FCGRT</i>	-0.50	0.000	0.019	<i>GPR143</i>	-3.54	0.000	0.002
<i>FCMR</i>	-0.53	0.000	0.015	<i>GPR20</i>	2.30	0.002	0.046
<i>FERMT2</i>	0.48	0.001	0.031	<i>GPR3</i>	1.00	0.002	0.043
<i>FERMT3</i>	-0.50	0.001	0.022	<i>GPR78</i>	4.39	0.000	0.000
<i>FGF1</i>	1.77	0.001	0.035	<i>GPRC5A</i>	-0.97	0.000	0.003
<i>FIBIN</i>	-0.72	0.001	0.029	<i>GPRC5C</i>	-0.88	0.000	0.015
<i>FILIP1L</i>	0.58	0.000	0.018	<i>GPT2</i>	0.72	0.002	0.046
<i>FIP1L1</i>	-0.70	0.001	0.041	<i>GRAMD1B</i>	0.62	0.000	0.018
<i>FJX1</i>	0.57	0.002	0.044	<i>GRAMD2B</i>	-0.77	0.000	0.004
<i>FLI1</i>	0.78	0.001	0.039	<i>GREB1L</i>	2.06	0.000	0.007
<i>FLNC</i>	0.84	0.000	0.002	<i>GRID1</i>	-3.09	0.002	0.050
<i>FLRT3</i>	-1.38	0.001	0.024	<i>GTSE1</i>	0.80	0.002	0.047
<i>FMNL1</i>	-1.34	0.001	0.024	<i>GUCY1A2</i>	0.97	0.000	0.012
<i>FNDC1</i>	1.45	0.000	0.018	<i>GYG2</i>	0.53	0.001	0.041
<i>FOSL1</i>	0.52	0.000	0.018	<i>GYPC</i>	-0.44	0.001	0.027
<i>FOXD3</i>	-1.32	0.000	0.018	<i>HACD4</i>	-0.53	0.001	0.026
<i>FRMD6</i>	0.65	0.001	0.041	<i>HAPLN3</i>	1.06	0.000	0.005
<i>FRZB</i>	-2.75	0.000	0.000	<i>HCN2</i>	-0.86	0.000	0.015
<i>FST</i>	-1.33	0.000	0.001	<i>HDAC5</i>	-0.54	0.002	0.044
<i>FTHIP4</i>	-0.47	0.000	0.017	<i>HELZ2</i>	-0.46	0.001	0.024
<i>FUCA1</i>	-0.37	0.002	0.046	<i>HERC5</i>	-0.55	0.000	0.011
<i>FZD7</i>	-0.52	0.001	0.026	<i>HEXB</i>	-0.58	0.000	0.013
<i>GAA</i>	-0.37	0.002	0.046	<i>HEYL</i>	1.40	0.000	0.001
<i>GALNS</i>	-0.60	0.000	0.010	<i>HHIPL1</i>	0.66	0.002	0.042

Gene Symbol	logFC	p-value	FDR	Gene Symbol	logFC	p-value	FDR
<i>HJURP</i>	0.77	0.001	0.023	<i>JUP</i>	-0.48	0.000	0.017
<i>HLA-DOA</i>	2.36	0.000	0.002	<i>KANK1</i>	-0.54	0.001	0.034
<i>HLA-DQA1</i>	1.95	0.000	0.001	<i>KCNA3</i>	-1.69	0.001	0.040
<i>HLA-DQB1</i>	1.13	0.002	0.044	<i>KCNAB2</i>	-0.41	0.002	0.050
<i>HLA-F</i>	-0.57	0.001	0.039	<i>KCND2</i>	-0.68	0.001	0.031
<i>HLA-H</i>	-0.42	0.001	0.028	<i>KCNJ2</i>	-1.37	0.000	0.006
<i>HLX</i>	-1.24	0.000	0.013	<i>KCNK2</i>	1.35	0.000	0.006
<i>HPD</i>	1.86	0.000	0.016	<i>KCNK3</i>	-0.67	0.000	0.016
<i>HPSE</i>	-1.07	0.000	0.019	<i>KCNS1</i>	1.79	0.000	0.010
<i>HSPB6</i>	-0.59	0.000	0.017	<i>KCTD12</i>	0.90	0.000	0.014
<i>HSPB7</i>	0.53	0.001	0.034	<i>KIAA1324L</i>	2.25	0.000	0.001
<i>HTRA3</i>	0.66	0.000	0.007	<i>KIAA1549</i>	1.15	0.000	0.008
<i>HVCN1</i>	1.80	0.002	0.048	<i>KIAA1549L</i>	1.19	0.000	0.020
<i>ICAM1</i>	-0.74	0.000	0.005	<i>KIF18B</i>	0.73	0.001	0.033
<i>ID4</i>	1.31	0.000	0.002	<i>KIF21B</i>	2.75	0.001	0.037
<i>IFIT1</i>	-0.50	0.002	0.050	<i>KIF23</i>	0.56	0.001	0.036
<i>IFIT2</i>	-0.89	0.000	0.002	<i>KIF2C</i>	1.02	0.000	0.010
<i>IFITM9P</i>	-0.68	0.002	0.044	<i>KITLG</i>	0.85	0.000	0.002
<i>IFNLR1</i>	-1.15	0.001	0.036	<i>KLF7</i>	0.52	0.001	0.038
<i>IGDCC4</i>	-1.58	0.000	0.002	<i>KLHL13</i>	0.93	0.001	0.022
<i>IGFBP3</i>	0.62	0.000	0.006	<i>KLHL29</i>	0.76	0.000	0.019
<i>IGFBP6</i>	-0.75	0.001	0.025	<i>KLHL38</i>	-0.84	0.001	0.036
<i>IGFN1</i>	6.30	0.000	0.001	<i>KREMENT1</i>	-0.40	0.002	0.049
<i>IL12A</i>	1.52	0.002	0.043	<i>KRTAP2-3</i>	1.18	0.000	0.011
<i>IL6</i>	-0.85	0.000	0.006	<i>KYNU</i>	-2.20	0.000	0.000
<i>IL6R</i>	-0.80	0.000	0.005	<i>L3MBTL4</i>	-1.20	0.000	0.012
<i>IL7</i>	-1.35	0.000	0.006	<i>LAP3</i>	-0.47	0.001	0.034
<i>INA</i>	-1.92	0.000	0.000	<i>LAYN</i>	0.48	0.000	0.016
<i>INHBA</i>	0.80	0.000	0.002	<i>LBH</i>	-0.90	0.001	0.024
<i>INHBB</i>	-2.08	0.000	0.007	<i>LEP</i>	-3.12	0.000	0.006
<i>INKA2</i>	0.37	0.002	0.049	<i>LGALS9DP</i>	-1.22	0.001	0.031
<i>INPP4B</i>	-0.62	0.000	0.008	<i>LGR5</i>	-1.60	0.000	0.003
<i>IQCD</i>	-0.63	0.001	0.035	<i>LIMD2</i>	-0.59	0.001	0.025
<i>IQGAP3</i>	0.59	0.001	0.037	<i>LIN7A</i>	0.53	0.000	0.012
<i>IRAK3</i>	-0.60	0.000	0.010	<i>LINCO0310</i>	-1.86	0.000	0.005
<i>IRF2BPL</i>	-0.58	0.001	0.023	<i>LINCO0462</i>	-7.01	0.001	0.026
<i>IRF4</i>	-1.92	0.000	0.017	<i>LINCO0598</i>	-0.91	0.000	0.004
<i>IRF6</i>	-0.51	0.001	0.029	<i>LINCO0702</i>	-0.47	0.002	0.047
<i>IRF7</i>	-0.53	0.000	0.012	<i>LINCO0900</i>	0.85	0.000	0.013
<i>ITGA10</i>	-1.32	0.000	0.004	<i>LINCO0924</i>	-1.32	0.001	0.022
<i>ITGA8</i>	-1.74	0.000	0.016	<i>LINCO0941</i>	1.41	0.001	0.042
<i>ITGA9</i>	-1.74	0.000	0.007	<i>LINCO0942</i>	1.27	0.000	0.009
<i>JAM3</i>	-0.38	0.001	0.038	<i>LINCO0973</i>	2.14	0.001	0.024
<i>JUN</i>	1.01	0.000	0.011	<i>LINCO1091</i>	-2.03	0.000	0.017
<i>JUNB</i>	-0.51	0.000	0.018	<i>LINCO1173</i>	2.32	0.000	0.006

Gene Symbol	logFC	p-value	FDR	Gene Symbol	logFC	p-value	FDR
<i>LINC01410</i>	-1.40	0.000	0.007	<i>MPP7</i>	0.83	0.000	0.014
<i>LINC01444</i>	-4.17	0.000	0.009	<i>MRC2</i>	-0.65	0.000	0.007
<i>LINC01588</i>	0.96	0.000	0.014	<i>MRGPRF</i>	-1.54	0.000	0.011
<i>LINC02289</i>	-0.89	0.002	0.048	<i>MRV11</i>	1.74	0.000	0.001
<i>LINC02407</i>	1.14	0.001	0.033	<i>MS4A6E</i>	-1.30	0.000	0.000
<i>LMOD1</i>	1.44	0.000	0.001	<i>MSANTD3</i>	0.45	0.001	0.026
<i>LNPEP</i>	-0.41	0.001	0.031	<i>MSLN</i>	6.06	0.000	0.005
<i>LPAR1</i>	-0.64	0.000	0.021	<i>MST1</i>	-0.73	0.000	0.014
<i>LRP3</i>	0.86	0.001	0.027	<i>MX1</i>	-0.75	0.000	0.017
<i>LRP5</i>	-1.02	0.000	0.001	<i>MYBL2</i>	1.14	0.000	0.008
<i>LRRC3</i>	-1.31	0.000	0.014	<i>MYC</i>	0.63	0.000	0.007
<i>LRRC32</i>	2.97	0.000	0.000	<i>MYEOV</i>	1.43	0.000	0.000
<i>LRRN3</i>	-1.85	0.000	0.000	<i>MYLIP</i>	-0.84	0.000	0.004
<i>LTBP1</i>	-0.54	0.001	0.041	<i>MYLK</i>	0.96	0.000	0.003
<i>LTBP2</i>	-0.53	0.001	0.041	<i>MYLKPI</i>	1.09	0.001	0.026
<i>LUM</i>	3.07	0.000	0.001	<i>MYO1D</i>	0.77	0.000	0.004
<i>LY96</i>	1.89	0.000	0.005	<i>MYO1E</i>	0.40	0.002	0.046
<i>LYNX1-SLURP2</i>	-0.45	0.000	0.020	<i>NANOS1</i>	0.85	0.000	0.008
<i>LYPD6B</i>	2.45	0.000	0.004	<i>NAPIL3</i>	-1.33	0.000	0.018
<i>LZTS1</i>	1.35	0.000	0.000	<i>NCKAP5</i>	0.91	0.001	0.024
<i>MAD2L1</i>	0.63	0.002	0.046	<i>NEIL3</i>	1.08	0.002	0.044
<i>MAF</i>	1.57	0.000	0.006	<i>NEXN</i>	0.70	0.000	0.004
<i>MAL</i>	-2.02	0.000	0.017	<i>NFIX</i>	0.38	0.002	0.044
<i>MAML3</i>	-0.79	0.000	0.014	<i>NFKBIZ</i>	-0.47	0.000	0.021
<i>MAN1C1</i>	-1.48	0.000	0.004	<i>NGF</i>	1.54	0.000	0.003
<i>MAPK11</i>	-1.48	0.000	0.009	<i>NGF-AS1</i>	2.17	0.000	0.017
<i>MAPK13</i>	0.74	0.001	0.033	<i>NKIRAS2</i>	0.37	0.002	0.044
<i>MCM4</i>	0.43	0.002	0.049	<i>NLRC5</i>	-0.43	0.002	0.050
<i>MCOLN3</i>	-2.27	0.000	0.001	<i>NMNAT3</i>	-0.67	0.001	0.033
<i>MCTP2</i>	-1.90	0.000	0.006	<i>NOP56</i>	0.38	0.001	0.038
<i>MEDAG</i>	-0.66	0.000	0.015	<i>NR1H3</i>	-1.04	0.000	0.003
<i>MEF2A</i>	-0.74	0.000	0.006	<i>NR4A1</i>	-1.65	0.000	0.000
<i>MEGF10</i>	-0.76	0.000	0.010	<i>NR4A2</i>	-1.65	0.000	0.000
<i>MFAP4</i>	1.09	0.000	0.015	<i>NREP</i>	1.54	0.001	0.022
<i>MFSD12</i>	-0.39	0.002	0.044	<i>NRG1</i>	-2.27	0.000	0.002
<i>MFSD2A</i>	0.90	0.002	0.049	<i>NRP2</i>	-0.52	0.001	0.025
<i>MGAT5B</i>	-0.67	0.001	0.027	<i>NRXN2</i>	1.22	0.000	0.021
<i>MIR3142HG</i>	-0.83	0.000	0.004	<i>NSG1</i>	-1.90	0.001	0.038
<i>MKI67</i>	0.72	0.001	0.022	<i>NT5DC2</i>	0.54	0.000	0.017
<i>MLANA</i>	-2.17	0.000	0.004	<i>NTF3</i>	3.52	0.000	0.001
<i>MLPH</i>	0.77	0.000	0.005	<i>NTM</i>	-0.89	0.000	0.007
<i>MMP15</i>	-0.86	0.001	0.039	<i>NTN1</i>	-3.57	0.000	0.001
<i>MMP16</i>	1.85	0.002	0.048	<i>NUPR1</i>	1.72	0.000	0.010
<i>MMP25-AS1</i>	-0.77	0.001	0.033	<i>NXN</i>	1.21	0.000	0.010
<i>MOB3B</i>	1.09	0.002	0.049	<i>OAS1</i>	-0.50	0.001	0.032

Gene Symbol	logFC	p-value	FDR	Gene Symbol	logFC	p-value	FDR
<i>OASL</i>	-0.50	0.000	0.015	<i>PODN</i>	2.68	0.000	0.000
<i>OCA2</i>	-2.11	0.001	0.022	<i>POLA2</i>	0.60	0.000	0.013
<i>OLFML2B</i>	1.61	0.000	0.013	<i>POLH</i>	0.41	0.001	0.041
<i>OLFML3</i>	-1.42	0.000	0.006	<i>PPARGC1A</i>	-0.47	0.000	0.021
<i>OSBPL10</i>	-0.69	0.000	0.012	<i>PPEF1</i>	-2.27	0.000	0.009
<i>OSBPL8</i>	-0.50	0.001	0.033	<i>PPFIA2</i>	-0.82	0.002	0.046
<i>OSTN-AS1</i>	1.12	0.001	0.041	<i>PPFIBP2</i>	-0.88	0.000	0.013
<i>OXTR</i>	1.09	0.001	0.024	<i>PRC1</i>	0.37	0.002	0.047
<i>P3H2</i>	1.08	0.000	0.004	<i>PRKAR2B</i>	-1.16	0.000	0.009
<i>PAICS</i>	0.50	0.000	0.013	<i>PROB1</i>	-1.04	0.001	0.024
<i>PAMR1</i>	-1.13	0.000	0.018	<i>PRSS12</i>	1.02	0.000	0.021
<i>PARP15</i>	-2.47	0.000	0.006	<i>PRTFDC1</i>	-0.92	0.001	0.036
<i>PAX9</i>	-2.67	0.001	0.022	<i>PRXL2A</i>	-0.62	0.000	0.013
<i>PBK</i>	0.74	0.001	0.030	<i>PSG4</i>	2.90	0.000	0.012
<i>PBX1</i>	-0.47	0.001	0.026	<i>PSMD9</i>	0.49	0.001	0.038
<i>PCBP3</i>	0.66	0.001	0.037	<i>PTGFR</i>	-0.72	0.000	0.005
<i>PCDH1</i>	1.61	0.000	0.014	<i>PTGS2</i>	-1.91	0.000	0.000
<i>PCDH18</i>	-1.06	0.000	0.015	<i>PTP4A3</i>	2.23	0.000	0.001
<i>PDCD1LG2</i>	0.88	0.000	0.003	<i>PTPRD</i>	-3.44	0.000	0.002
<i>PDE1A</i>	-3.19	0.000	0.017	<i>PTPRE</i>	1.02	0.001	0.029
<i>PDE1C</i>	2.19	0.000	0.000	<i>PTPRQ</i>	0.87	0.000	0.007
<i>PDGFA</i>	0.50	0.001	0.026	<i>PTPRU</i>	-0.77	0.000	0.003
<i>PDGFB</i>	1.60	0.000	0.019	<i>PTX3</i>	0.54	0.001	0.023
<i>PDGFD</i>	-1.12	0.000	0.012	<i>PZP</i>	-0.84	0.001	0.032
<i>PDLIM4</i>	-0.48	0.002	0.043	<i>QPCT</i>	-1.13	0.000	0.000
<i>PEAR1</i>	-1.54	0.000	0.009	<i>RAB17</i>	-1.26	0.000	0.001
<i>PGF</i>	-1.10	0.000	0.004	<i>RAB3B</i>	0.65	0.000	0.006
<i>PHETA2</i>	0.56	0.001	0.024	<i>RAB31L1</i>	-1.04	0.000	0.011
<i>PHKG1</i>	-1.48	0.000	0.009	<i>RAC2</i>	0.79	0.000	0.012
<i>PIK3IP1</i>	-0.59	0.000	0.013	<i>RADIL</i>	1.96	0.000	0.018
<i>PIR</i>	-1.92	0.000	0.001	<i>RALGPS2</i>	0.77	0.000	0.008
<i>PITPNM3</i>	1.38	0.001	0.026	<i>RAP2A</i>	0.61	0.001	0.022
<i>PKMYT1</i>	0.86	0.002	0.047	<i>RARA</i>	-0.53	0.000	0.016
<i>PLA2G4A</i>	-0.97	0.000	0.001	<i>RARB</i>	-2.34	0.000	0.001
<i>PLCD4</i>	-0.97	0.000	0.003	<i>RASGRF2</i>	-0.91	0.000	0.021
<i>PLCE1-AS1</i>	2.21	0.002	0.045	<i>RASL10B</i>	-0.76	0.000	0.005
<i>PLEKHH3</i>	-0.55	0.000	0.011	<i>RCAN2</i>	-0.81	0.000	0.003
<i>PLK2</i>	0.62	0.001	0.036	<i>RCC1</i>	0.44	0.001	0.027
<i>PLP1</i>	-1.61	0.001	0.035	<i>RECK</i>	-0.37	0.002	0.049
<i>PLSCR1</i>	-0.53	0.000	0.020	<i>REV3L</i>	-0.61	0.001	0.024
<i>PLTP</i>	-0.45	0.001	0.026	<i>RGL2</i>	-0.36	0.002	0.048
<i>PLXDC1</i>	0.84	0.001	0.037	<i>RGMB</i>	0.71	0.000	0.011
<i>PLXNC1</i>	-1.80	0.000	0.000	<i>RGMB-AS1</i>	0.65	0.002	0.050
<i>PMEL</i>	-2.00	0.000	0.000	<i>RGS16</i>	-1.58	0.000	0.002
<i>PMP22</i>	0.68	0.001	0.028	<i>RHBDF2</i>	-0.43	0.001	0.037

Gene Symbol	logFC	p-value	FDR	Gene Symbol	logFC	p-value	FDR
<i>RHOBTB3</i>	-0.64	0.000	0.006	<i>SH3RF1</i>	0.75	0.000	0.003
<i>RHOU</i>	-1.44	0.001	0.035	<i>SH3RF3-AS1</i>	-0.65	0.001	0.026
<i>RIPK4</i>	0.56	0.002	0.044	<i>SHANK2</i>	1.39	0.002	0.043
<i>RNF13</i>	-0.40	0.001	0.041	<i>SHCBP1</i>	0.83	0.000	0.014
<i>RNF175</i>	-1.94	0.001	0.032	<i>SHROOM2</i>	-1.11	0.000	0.003
<i>RNPC3</i>	-0.42	0.001	0.030	<i>SIPA1L1</i>	0.94	0.000	0.001
<i>RPL22L1</i>	0.72	0.000	0.016	<i>SIX1</i>	-1.68	0.000	0.002
<i>RPTN</i>	2.30	0.001	0.028	<i>SIX2</i>	0.96	0.000	0.005
<i>RRAD</i>	-1.16	0.000	0.009	<i>SKA3</i>	0.90	0.001	0.032
<i>RRAS2</i>	0.80	0.000	0.004	<i>SLC15A3</i>	-1.22	0.000	0.002
<i>RRM2</i>	0.62	0.001	0.035	<i>SLC16A1</i>	0.43	0.001	0.028
<i>RSAD2</i>	-1.21	0.000	0.018	<i>SLC16A12</i>	1.06	0.000	0.018
<i>RTL5</i>	-0.64	0.001	0.022	<i>SLC16A2</i>	0.61	0.000	0.015
<i>RTN4RL1</i>	-0.88	0.001	0.038	<i>SLC16A6</i>	-0.60	0.001	0.022
<i>RWDD4</i>	0.44	0.002	0.047	<i>SLC1A4</i>	0.70	0.000	0.015
<i>S100B</i>	-1.69	0.001	0.039	<i>SLC22A18</i>	-0.45	0.001	0.038
<i>S1PR3</i>	-0.87	0.000	0.002	<i>SLC22A23</i>	1.19	0.000	0.006
<i>SALL1</i>	-0.81	0.000	0.008	<i>SLC27A2</i>	-2.30	0.001	0.026
<i>SALRNA1</i>	-1.98	0.000	0.011	<i>SLC2A4</i>	-1.53	0.000	0.003
<i>SAMD12</i>	0.93	0.001	0.039	<i>SLC35F5</i>	-0.48	0.001	0.038
<i>SAMD9</i>	-0.53	0.001	0.026	<i>SLC38A4</i>	-0.99	0.001	0.025
<i>SAMHD1</i>	-0.43	0.002	0.049	<i>SLC38A5</i>	2.22	0.000	0.005
<i>SASH1</i>	0.84	0.000	0.002	<i>SLC39A8</i>	-1.11	0.000	0.001
<i>SBSN</i>	2.13	0.002	0.046	<i>SLC44A1</i>	-0.44	0.001	0.029
<i>SCARA3</i>	1.34	0.002	0.045	<i>SLC47A1</i>	1.06	0.001	0.025
<i>SCG5</i>	1.22	0.002	0.049	<i>SLC7A1</i>	0.44	0.001	0.028
<i>SCO2</i>	-0.70	0.000	0.004	<i>SLC7A11</i>	1.06	0.000	0.001
<i>SCPEP1</i>	-0.43	0.002	0.045	<i>SLC7A14</i>	-0.63	0.000	0.011
<i>SDC2</i>	1.15	0.000	0.002	<i>SLC7A2</i>	-1.16	0.000	0.003
<i>SDC3</i>	-0.54	0.002	0.046	<i>SLC7A8</i>	-0.65	0.001	0.025
<i>SECTM1</i>	-0.67	0.000	0.007	<i>SLC8A1-AS1</i>	2.10	0.000	0.013
<i>SEL1L3</i>	2.40	0.000	0.002	<i>SLC9A7</i>	0.70	0.000	0.004
<i>SEMA5A</i>	-0.71	0.000	0.010	<i>SLFN11</i>	-0.51	0.000	0.021
<i>SEMA6B</i>	-0.54	0.000	0.019	<i>SLITRK5</i>	-1.61	0.000	0.002
<i>SEMA7A</i>	1.38	0.001	0.027	<i>SMO</i>	0.87	0.000	0.015
<i>SERPINB7</i>	2.65	0.000	0.006	<i>SMPD1</i>	-0.42	0.001	0.036
<i>SERPINB9</i>	1.75	0.000	0.001	<i>SMS</i>	0.54	0.000	0.012
<i>SERPING1</i>	-0.57	0.001	0.024	<i>SMURF1</i>	0.36	0.002	0.049
<i>SERPINI1</i>	-1.60	0.001	0.026	<i>SNAIL1</i>	-0.73	0.001	0.038
<i>SERTAD4</i>	-0.95	0.002	0.045	<i>SNAP25</i>	-0.75	0.000	0.009
<i>SESN3</i>	-0.44	0.002	0.042	<i>SNCA</i>	-0.85	0.001	0.026
<i>SFRP2</i>	-1.79	0.000	0.000	<i>SNHG26</i>	-0.62	0.000	0.020
<i>SFTA1P</i>	2.21	0.000	0.009	<i>SOD3</i>	-1.19	0.001	0.024
<i>SGMS1</i>	-0.65	0.000	0.014	<i>SORCS1</i>	-1.90	0.000	0.021
<i>SGPP2</i>	-1.59	0.000	0.015	<i>SOX10</i>	-1.44	0.001	0.025

Gene Symbol	logFC	p-value	FDR	Gene Symbol	logFC	p-value	FDR
<i>SOX11</i>	2.52	0.001	0.025	<i>TMEM119</i>	0.48	0.002	0.043
<i>SP110</i>	-0.42	0.001	0.029	<i>TMEM130</i>	-1.79	0.000	0.009
<i>SPDL1</i>	0.50	0.001	0.037	<i>TMEM132D</i>	3.97	0.002	0.047
<i>SPEG</i>	0.80	0.000	0.011	<i>TMEM173</i>	-0.43	0.001	0.029
<i>SPOCD1</i>	1.17	0.000	0.001	<i>TMEM178B</i>	0.41	0.001	0.041
<i>SPON1</i>	1.36	0.001	0.042	<i>TMEM200B</i>	-0.85	0.000	0.005
<i>SPON2</i>	0.98	0.002	0.049	<i>TMEM200C</i>	-1.18	0.001	0.042
<i>SPRY1</i>	-0.69	0.000	0.005	<i>TMEM35A</i>	1.63	0.000	0.012
<i>SRPX</i>	-0.66	0.000	0.008	<i>TMTC2</i>	-0.74	0.001	0.036
<i>SRRM3</i>	-0.90	0.001	0.039	<i>TMTC3</i>	0.47	0.000	0.018
<i>SSC5D</i>	-0.94	0.000	0.003	<i>TNC</i>	0.72	0.000	0.017
<i>ST3GAL5</i>	-0.76	0.000	0.015	<i>TNFAIP3</i>	-0.63	0.002	0.044
<i>STAC2</i>	0.89	0.001	0.023	<i>TNFAIP6</i>	-0.64	0.001	0.031
<i>STARD4</i>	0.73	0.001	0.041	<i>TNFAIP8</i>	-0.58	0.001	0.040
<i>STARD4-AS1</i>	1.15	0.000	0.020	<i>TNFRSF12A</i>	0.41	0.001	0.031
<i>STK17A</i>	0.69	0.000	0.004	<i>TNFSF13B</i>	-1.19	0.000	0.006
<i>STK38L</i>	-0.48	0.000	0.018	<i>TNFSF15</i>	-1.74	0.000	0.005
<i>STMN3</i>	-1.33	0.000	0.013	<i>TNFSF18</i>	1.70	0.001	0.035
<i>STS</i>	1.11	0.000	0.001	<i>TNK2</i>	-0.40	0.001	0.030
<i>STX12</i>	0.38	0.002	0.044	<i>TNNT1</i>	-2.24	0.000	0.010
<i>SULF2</i>	0.81	0.001	0.028	<i>TOB1</i>	-0.39	0.002	0.044
<i>SVEP1</i>	-0.83	0.000	0.006	<i>TOP2A</i>	0.42	0.001	0.026
<i>SVIL2P</i>	-0.69	0.002	0.048	<i>TOR4A</i>	-0.83	0.000	0.007
<i>SYNE3</i>	-0.43	0.001	0.025	<i>TP53I11</i>	1.44	0.000	0.021
<i>TAGLN</i>	1.90	0.002	0.044	<i>TPCN2</i>	-0.44	0.001	0.037
<i>TARS</i>	0.45	0.001	0.034	<i>TPX2</i>	0.72	0.000	0.012
<i>TBX18</i>	-1.81	0.000	0.006	<i>TRAF1</i>	-0.64	0.001	0.032
<i>TBX2-AS1</i>	-0.65	0.001	0.041	<i>TRIB1</i>	2.15	0.000	0.000
<i>TCF19</i>	0.88	0.000	0.017	<i>TRIM21</i>	-0.36	0.002	0.047
<i>TCF21</i>	-1.27	0.001	0.032	<i>TRPM3</i>	1.61	0.001	0.035
<i>TENM3</i>	0.39	0.002	0.047	<i>TRPM4</i>	-0.42	0.001	0.039
<i>TENM4</i>	0.76	0.000	0.013	<i>TRPM8</i>	1.97	0.000	0.004
<i>TENT5A</i>	-0.64	0.000	0.006	<i>TUBA4A</i>	0.71	0.000	0.011
<i>TEX11</i>	-1.72	0.002	0.043	<i>TVP23A</i>	1.28	0.001	0.038
<i>TFPI</i>	0.63	0.001	0.026	<i>TYR</i>	-2.07	0.000	0.004
<i>TGFBI</i>	1.24	0.000	0.013	<i>TYRL</i>	-2.74	0.000	0.021
<i>TGFBR2</i>	-0.60	0.000	0.021	<i>TYRPI</i>	-2.17	0.000	0.003
<i>TGFBR3</i>	-0.52	0.000	0.013	<i>UNC13A</i>	-2.07	0.000	0.014
<i>THEMIS2</i>	-0.45	0.001	0.026	<i>UNC5B</i>	1.73	0.001	0.033
<i>THY1</i>	3.54	0.000	0.021	<i>VASN</i>	-0.63	0.000	0.009
<i>TIMP4</i>	-0.91	0.000	0.002	<i>VATIL</i>	-2.37	0.000	0.001
<i>TLE2</i>	-1.16	0.000	0.013	<i>VGLL3</i>	0.71	0.000	0.007
<i>TLR2</i>	-1.48	0.000	0.001	<i>VSTM4</i>	2.34	0.000	0.000
<i>TMEFF2</i>	2.41	0.000	0.001	<i>WNT5B</i>	0.57	0.000	0.019
<i>TMEM100</i>	-0.78	0.000	0.006	<i>XYLT1</i>	-0.87	0.001	0.031

Gene Symbol	logFC	p-value	FDR
<i>YBX2</i>	-2.03	0.001	0.031
<i>ZBED6CL</i>	1.73	0.002	0.049
<i>ZC3H12A</i>	-0.55	0.000	0.013
<i>ZC3H12C</i>	-0.40	0.001	0.033
<i>ZEB1</i>	-1.10	0.001	0.033
<i>ZNF117</i>	-0.65	0.002	0.043
<i>ZNF204P</i>	-0.61	0.001	0.033
<i>ZNF385A</i>	-0.67	0.000	0.020
<i>ZNF423</i>	3.13	0.000	0.001
<i>ZNF469</i>	1.65	0.001	0.022
<i>ZNF503</i>	0.68	0.000	0.015
<i>ZNF667</i>	1.18	0.000	0.010
<i>ZNF667-AS1</i>	1.24	0.000	0.005
<i>ZNF704</i>	-0.90	0.000	0.019
<i>ZWINT</i>	0.63	0.002	0.050

ANNEX C

Data from *in silico* analysis from
the RNA sequencing data

Table S3. Enriched processes after RKIP silencing, specifying the False Discovery Rate for assignment and the list of genes for each one

Enriched term	FDR	Overlapping genes
Regulation of biological process	0.0479	<i>ACE,ADAMTS12,ADAPI,ANLN,ARHGAP26,ARHGEF28,ARHGEF6,ATP10A,AURKC,BCL3,BST2,CAPG,CCDC3,CCL13,CD302,CD4,CDC25B,CDON,CENPF,CFD,CHODL,CHRD1,CHRFAM7A,CLDN1,CLSTN2,CNTN4,COL8A1,CTCF,DIO2,EDA2R,EEF1A2,EFEMP1,EGLN3,EPHA3,EPHB6,EREG,EYA1,FBXO32,FMNL1,FRZB,GHR,GLP2R,GPR143,GPRC5A,GRIA3,GRID1,HCAR1,HDAC9,HOXA9,HOXB13,HOXD9,HSPB6,HSPB7,ID2,IGF2,IL17RE,IRF4,KCNA3,KCNK2,KIAA1549,KIF20A,KIT,KLF4,L3MBTL4,LANCL3,LINGO1,LRP5,LRRC32,LRRN3,LYPD6B,LZTS1,MAF,MAL,MCHRI,MCTP2,MFAP4,MGP,MID2,MKI67,MOK,MTSS1,MYCL,NAV3,NCEH1,NDRG4,NGFR,NOSIP,NTN1,NTRK2,NUPR1,NXP4,OLFM1,ORIE1,PAX9,PCBP3,PCDH17,PDE1C,PEAR1,PID1,PIM1,PIP,PODNL1,PPP1R1C,PROS1,PTGDS,PTP4A3,PTPRD,RAP2A,RARB,RARRES2,RCAN2,S100B,SEMA3F,SERPINB2,SHANK2,SIX2,SLC1A3,SLFN1,SORCS1,SOX11,SYNE2,TAC1,TDRD9,TEX11,THBS2,THY1,TLE2,TMEM132D,TMEM204,TNFSF15,TP53I11,TYRP1,UNC5B,ZEB1,ZNF558,ZNF560</i>
Developmental and differentiation process	0.0045	<i>ACE,ALPL,ANLN,ARHGAP26,ARHGEF28,AURKC,BCL3,BST2,CD4,CDC25B,CDO1,CDON,CENPF,CHODL,CHRD1,CLDN1,CNTN4,COL8A1,EDA2R,EFEMP1,EPHA3,EREG,EYA1,FLNC,FRZB,GREB1L,HDAC9,HOXA9,HOXB13,HOXD9,HSPB7,ID2,IGF2,IRF4,KCNK2,KIAA1217,KIT,KLF4,LINGO1,LRP5,MAF,MAL,MCOLN3,MCTP2,MGP,MME,MTSS1,MYCL,NDRG4,NGFR,NOSIP,NTN1,NTRK2,NUPR1,OLFM1,OLFML3,PAX9,PCDH17,PID1,PIM1,PRELP,PTPRD,RAP2A,RARB,RARRES2,S100B,SEMA3F,SHANK2,SIX2,SLC1A3,SOBP,SOX11,ST8SIA2,STEAP4,SYNE2,TDRD9,TEX11,THY1,TLE2,TMEM204,TYRP1,UNC5B,ZEB1</i>
Cell surface receptor signaling pathway	0.0451	<i>ADAPI,ARHGEF28,BST2,CCL13,CD4,CDON,CHRD1,EDA2R,EFEMP1,EPHA3,EPHB6,EREG,FRZB,GHR,GLP2R,GRIA3,GRID1,IGF2,IL17RE,IRF4,KIT,KLF4,LRP5,MCHRI,MTSS1,NGFR,NTRK2,PIM1,PODNL1,PTP4A3,PTPRD,SEMA3F,SERPINB2,THY1,TLE2,TNFSF15,UNC5B,ZEB1</i>
Regulation of cell population proliferation	0.0295	<i>ACE,CD4,CDC25B,CDON,EGLN3,EREG,EYA1,FRZB,GLP2R,ID2,IGF2,KCNK2,KIT,KLF4,LRP5,LRRC32,MTSS1,NDRG4,NGFR,NTN1,NTRK2,NUPR1,PID1,PIM1,RARB,S100B,SIX2,SOX11,TAC1,TP53I11,ZEB1</i>
Cellular response to cytokine stimulus	0.0443	<i>ADAMTS12,BST2,CCL13,CD4,CLDN1,EDA2R,EREG,GHR,IL17RE,IRF4,KIT,KLF4,MME,NGFR,PID1,PIM1,PODNL1,PTP4A3,SERPINB2,TNFSF15,ZEB1</i>
Behavior	0.0183	<i>GRID1,HOXD9,ID2,KCNK2,KIT,MCHRI,MCOLN3,NDRG4,NPTX2,NTRK2,PCDH17,S100B,SHANK2,SLC1A3,SOBP,TAC1</i>
Regulation of peptidyl-tyrosine phosphorylation	0.0443	<i>ACE,CD4,EREG,GHR,GPRC5A,IGF2,KIT,NTRK2,THY1</i>
Developmental pigmentation	0.0401	<i>GPR143,KIT,PMEL,TYRP1,MLANA</i>
Positive regulation of interleukin-10 biosynthetic process	0.0331	<i>BCL3,IRF4</i>

Table S4. Most enriched term analysis of differentially expressed gene in HEMn-LP after RKIP silencing, which are potentially targeted by NANOG transcription factor.

Enriched Term	FDR	Overlapping genes
positive regulation of nervous system development	0.014	<i>PTPRD;MME;SOX11</i>
skeletal system development	0.017	<i>KIAA1217;FRZB;IGF2;ALPL;SOX11;PRELP;HOXA9;HOXD9;HDAC9</i>
positive regulation of phosphorylation	0.018	<i>NTRK2;RAP2A;CD4;RARRES2;KIT;IGF2;EPHA3;ERE,UNC5B</i>
positive regulation of intracellular signal transduction	0.028	<i>BST2;NTRK2;CD4;UNC5B;KIT;IGF2;SOX11;NUPR1;S100B;EDA2R;EREG</i>
regulation of cell migration	0.032	<i>BST2;NGFR;RAP2A;ACE;KIT;SEMA3F;THY1;CLDN1;SYNE2;NDRG4;KLF4;HDAC9;</i>

Table S5. Genes related with development process, which are potentially targets of NANOG transcription factor.

Term description	FDR	Overlapping genes
Genes targeted by NANOG related to development	4.21E ⁻⁹	<i>ALPL,ANLN,ARHGAP26,AURKC,BCL3,BST2,CD4,CENPF,CLDN1,CNTN4,COL8A1,EDA2R,EPHA3,EREG,EYA1,FRZB,GREB1L,HOXA9,HOXB13,HSPB7,ID2,IGF2,UNC5B,KCNK2,KIAA1217,KIT,KLF4,MAL,MCOLN3,MME,MTS1,NDRG4,NGFR,NOSIP,NTN1,NTRK2,NUPR1,OLFM1,OLFML3,TLE2,THY1,TEX11,PAX9,PCDH17,PID1,PIM1,PRELP,PTPRD,RAP2A,RARB,SEMA3F,SHANK2,SLC1A3,SOBP,SOX11,ST8SIA2,STEAP4,SYNE2,TDRD9</i>

Table S6. Enriched processes after PIR silencing, specifying the False Discovery Rate for assignment and the list of genes for each one

Enriched term	FDR	Overlapping genes
regulation of cell proliferation	3.82E ⁻⁰²	'CXCL6', 'BNC1', 'PDGFB', 'PDGFA', 'FGF1', 'TOB1', 'ADGRG1', 'GPNMB', 'MYC', 'PDGFD', 'GPER1', 'NTF3', 'ZNF503', 'SPEG', 'TP53I11', 'TRPM4', 'CGREF1', 'JUN', 'JUP', 'IGFBP3', 'TNK2', 'DAB2IP', 'P3H2', 'SOX11', 'CDC6', 'INHBA', 'NGF', 'PODN', 'SHCBP1', 'AGT', 'FOSL1', 'DDAH1', 'PRC1', 'BHLHE40', 'CDH13'
cellular response to interferon-gamma	3.30E ⁻⁰²	'CCL13', 'CIITA', 'CCL8', 'OAS1', 'CCL7', 'IRF7', 'HLA-F', 'TRIM21', 'HLA-DQA1', 'OASL', 'HLA-DQB1'
positive regulation of cell motility	1.51E ⁻⁰²	'SEMA7A', 'WNT5B', 'PDGFB', 'PDGFA', 'FGF1', 'MYLK', 'CCL7', 'GPNMB', 'PDGFD', 'GPER1', 'NTF3', 'SNAI1', 'CDH13', 'DRD1', 'GTSE1'
extracellular matrix organization	7.64E ⁻⁰³	'COL13A1', 'LUM', 'PDGFB', 'TNC', 'PDGFA', 'ADAM19', 'ACAN', 'MMP16', 'COL4A2', 'COL4A1', 'COL8A1', 'COL10A1', 'TGFB1', 'A2M', 'GAS6', 'ADAMTS9', 'RECK', 'JAM3', 'ITGA9'
positive regulation of cell migration	7.64E ⁻⁰³	'TNFSF18', 'SEMA7A', 'WNT5B', 'PDGFB', 'DAB2IP', 'PDGFA', 'FGF1', 'MYLK', 'GPNMB', 'CCL7', 'PDGFD', 'GPER1', 'NTF3', 'SNAI1', 'ENPP2', 'CDH13', 'DRD1', 'GTSE1'
G1/S transition of mitotic cell cycle	7.64E ⁻⁰³	'DHFR', 'POLA2', 'RRM2', 'MYC', 'PLK2', 'EIF4EBP1', 'E2F1', 'RCC1', 'MCM4', 'INHBA', 'CDC6', 'BCAT1'
negative regulation of cell proliferation	7.64E ⁻⁰³	'CGREF1', 'IGFBP3', 'P3H2', 'DAB2IP', 'SOX11', 'CDC6', 'INHBA', 'PODN', 'NGF', 'TOB1', 'ADGRG1', 'ACVR1C', 'GPNMB', 'DDAH1', 'MYC', 'GPER1', 'BHLHE40', 'E2F1', 'SPEG', 'CDH13', 'ZNF503', 'IL12A', 'TRIB1', 'TP53I11'
regulation of cell migration	7.64E ⁻⁰³	'SEMA7A', 'WNT5B', 'PDGFB', 'PDGFA', 'NEXN', 'THY1', 'PODN', 'FGF1', 'MYLK', 'TMEFF2', 'GPNMB', 'CCL7', 'PDGFD', 'GPER1', 'NTF3', 'SNAI1', 'ENPP2', 'CDH13', 'DRD1', 'AMOTL1', 'GTSE1', 'RECK'
positive regulation of cell proliferation	6.16E ⁻⁰³	'PTGFR', 'CD81', 'CHR1', 'LRP5', 'TNFSF13B', 'DPP4', 'PDGFD', 'GPER1', 'S1PR3', 'IL6R', 'TRPM4', 'NRG1', 'AGT', 'PGF', 'ADRA2A', 'TGFB2', 'FOSL1', 'BMP4', 'TGFB3', 'BMP2', 'IL6', 'SFRP2', 'IL7', 'RARA', 'HPSE', 'GAS6'
cellular response to cytokine stimulus	3.26E ⁻⁰³	'CCL13', 'CEBPD', 'LRRC3', 'PTGS2', 'IFIT1', 'ICAM1', 'CCL8', 'CCL7', 'FLRT3', 'GPER1', 'DPYSL3', 'ZC3H12A', 'IL12A', 'CCR7', 'JUNB', 'IL6R', 'IFNLR1', 'IRAK3', 'BATF', 'MAPK11', 'IL6', 'ZEB1', 'RTN4RL1', 'IL7', 'IRF4', 'BCL2', 'RHOU', 'GAS6'
response to cytokine	2.70E ⁻⁰³	'GCH1', 'MX1', 'IFNLR1', 'IRAK3', 'PLSCR1', 'KYNU', 'DPYSL3', 'BCL2', 'CCR7', 'JUNB', 'IL6R', 'TRIM21', 'TIMP4', 'SNCA'
regulation of fat cell differentiation	8.16E ⁻⁰⁴	'BMP2', 'IL6', 'SFRP2', 'FRZB', 'GPER1', 'LEP', 'ZC3H12A', 'LRP5', 'ZNF385A', 'MEDAG', 'TRPM4'
cytokine-mediated signaling pathway	8.16E ⁻⁰⁴	'CCL13', 'CD40', 'CEBPD', 'LRRC3', 'PTGS2', 'IFIT1', 'SAMHD1', 'TNFSF13B', 'IFIT2', 'ICAM1', 'OASL', 'CCL8', 'CCL7', 'FLRT3', 'IL12A', 'JUNB', 'TRIM21', 'IL6R', 'RSAD2', 'TNFRSF12A', 'TNFSF15', 'MX1', 'IFNLR1', 'IRAK3', 'HLA-F', 'BATF', 'IL6', 'ZEB1', 'OAS1', 'RTN4RL1', 'IL7', 'IRF4', 'LEP', 'BCL2', 'IRF7', 'RHOU', 'IRF6'
positive regulation of cell differentiation	8.16E ⁻⁰⁴	'MEF2A', 'LRP5', 'AGT', 'MEDAG', 'TGFB2', 'BMP4', 'TMEM100', 'MAPK11', 'BMP2', 'IL6', 'SFRP2', 'FRZB', 'ZC3H12A', 'SNAI1', 'JUNB', 'IL6R', 'ZNF385A', 'TRPM4'
type I interferon signaling pathway	4.73E ⁻⁰⁴	'RSAD2', 'OAS1', 'IRF4', 'MX1', 'IRF7', 'IRF6', 'IFIT1', 'HLA-F', 'SAMHD1', 'IFIT2', 'OASL'
cellular response to type I interferon	4.73E ⁻⁰⁴	'RSAD2', 'OAS1', 'IRF4', 'MX1', 'IRF7', 'IRF6', 'IFIT1', 'HLA-F', 'SAMHD1', 'IFIT2', 'OASL'

Table S7. Most enriched term analysis of differentially expressed gene in HEMn-LP after PIR silencing, which are potentially targeted by JARID1B transcriptional regulator.

Enriched term	FDR	Overlapping genes
transcription, DNA-templated	2.94E ⁻⁰²	AR, ATOH8, BCOR, BHLHE22, BNC1, COL4A2, EGR3, EYA4, FLI1, FOXD3, GLIS1, HEYL, HLX, JUN, MAF, MAML3, NFIX, NR4A2, PAX9, RARA, SIX1, SIX2, SOX10, SOX11, TBX18, TCF21
regulation of cell population proliferation	9.96E ⁻⁰⁵	ADRA2A, AR, ATOH8, AVPR1A, BCL2, BMP2, BNC1, CDH13, EGR3, E2F1, FRZB, HLX, JUN, KCNK2, MYC, NGF, NRP2, NTF3, NTN1, PODN, PTPRU, RARA, SIX1, SIX2, SOX10, SOX11, SPEG, TGFB3
regulation of biosynthetic process	3.32E ⁻⁰²	AGAP2, AR, ATOH8, AVPR1A, BCL2, BCOR, BHLHE22, BMP2, BNC1, CDH13, EGR3, EYA4, FLI1, FOXD3, FST, GLIS1, HEYL, HLX, INHBB, JUN, KCNK2, MAF, MAML3, NFIX, NR4A2, PAX9, PTX3, RARA, RGM, RIPK4, SIX1, SIX2, SOX10, SOX11, TBX18, TCF21, TGFB3, TMEFF2
anatomical structure morphogenesis	1.00E ⁻⁰⁸	AR, ATOH8, BCL2, BCOR, BMP2, CDH13, COL4A1, COL4A2, DSP, EGR3, EYA4, FJX1, FLI1, FOXD3, FRZB, GFRA1, GREB1L, HEYL, HLX, JUN, MMP15, NGF, NR4A2, NRP2, NTF3, NTN1, PAX9, RARA, RIPK4, SEMA7A, SIX1, SIX2, SLITRK5, SOX10, SOX11, TCF21, TGFB3, TMEFF2, UNC5B
regulation of cell communication	1.18E ⁻⁰²	ADRA2A, AR, AVPR1A, BCL2, BICC1, BMP2, CDH13, CXXC4, EYA4, FRZB, FST, HEYL, INHBB, JUN, LUM, LYPD6B, MAML3, NGF, NR4A2, NSG1, NTF3, OXTR, PLK2, PODN, PTPRE, RARA, RTN4RL1, SEMA7A, SOX11, TBX18, TCF21, TGFB3, THY1, UNC5B, WNT5B
cell differentiation	8.54E ⁻⁰⁷	AR, ATOH8, AVPR1A, BCL2, BHLHE22, BMP2, BNC1, COL4A1, COL4A2, DSP, EYA4, FLI1, FLNC, FOXD3, FRZB, FST, GFRA1, HEYL, HLX, INHBB, JUN, LUM, MAF, MFSD2A, MMP15, NEXN, NGF, NR4A2, NRP2, NTF3, NTN1, PLK2, PLXNC1, PTPRD, PTPRU, RARA, RTN4RL1, SEMA7A, SIX1, SIX2, SLITRK5, SOX10, SOX11, SPEG, TCF21, TGFB3, THY1, UNC5B, WNT5B

